Hysteresis in Magnetocaloric Materials

An experimental and modelling approach

von Moos, Lars

Publication date:
2014

Document Version
Publisher's PDF, also known as Version of record

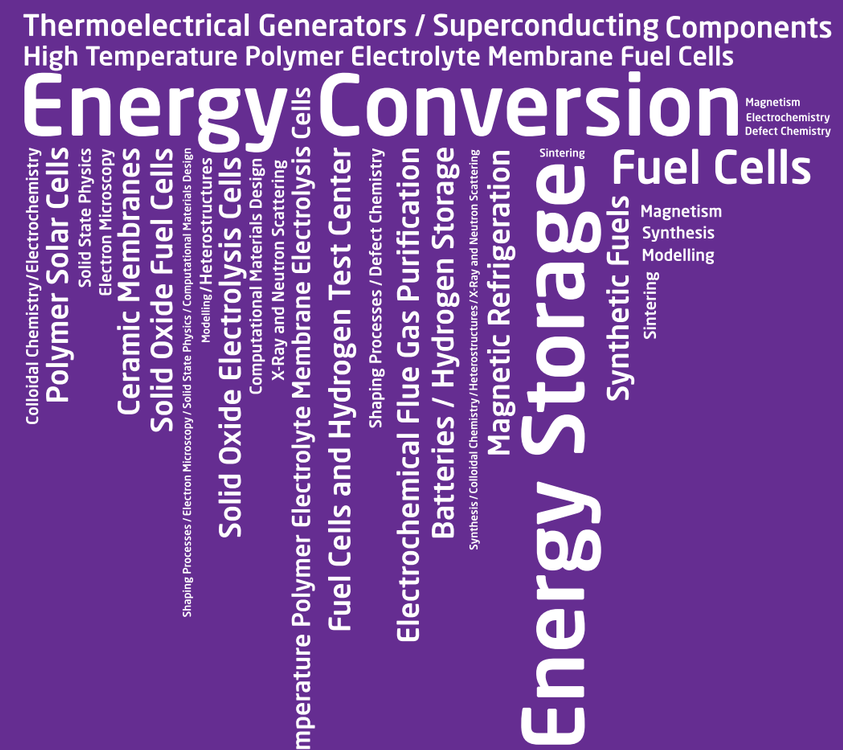

Department of Energy Conversion and Storage
Technical University of Denmark
Risø Campus
Frederiksborgvej 399
4000 Roskilde
Denmark
www.ecs.dtu.dk

ISBN 978-87-92986-28-3

Hysteresis in Magnetocaloric Materials

September 2014

Technical University of Denmark

DTU

Hysteresis in Magnetocaloric Materials

Lars von Moos
Department of Energy Conversion and Storage
Ph.D. Thesis, September 2014

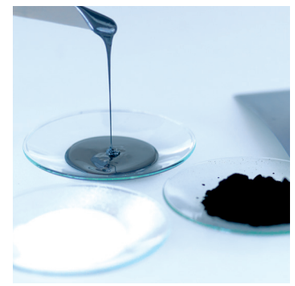

DTU Energy
Department of Energy Conversion and Storage

Hysteresis in magnetocaloric materials

An experimental and modelling approach

Lars von Moos

PhD-2014-
Supervised by: Christian Bahl, Kaspar Nielsen and Kurt Engelbrecht

Technical University of Denmark
Department of Energy Conversion and Storage
DTU Risø Campus, Frederiksborgvej 399,
4000 Roskilde, Denmark
Phone +45 4677 5800
info@ecs.dtu.dk
www.ecs.dtu.dk PhD-2014-

Summary

In this thesis the effects of hysteresis on magnetocaloric material properties and their performance in magnetic refrigeration devices are investigated. This is done through an experimental and model study of first order magnetocaloric materials MnFe(P,As) and $Gd_5Si_2Ge_2$.

The experimental characterization of the magnetocaloric effect (MCE) in these materials is done through conventional indirect magnetometric and calorimetric methods, as well as newly developed direct methods. The determination of the MCE due to a magnetic field change is in principle given by the isofield material entropy curves, obtained at the initial low and final high field. However, in first order materials thermal entropy hysteresis loops are obtained through characterization, corresponding to measurements done in an increasing and a decreasing temperature mode. Indirectly determining the MCE through the use of the Maxwell relation or calorimetric measurements done only in a heating or cooling mode, estimate the MCE as the reversible difference between the set isofield heating-heating or cooling-cooling entropy curves. Here it is shown that direct measurements suggest that the real MCE is given by the difference between the low field heating and high field cooling entropy curves, which can reduce the MCE estimate significantly.

The experimental data obtained through the material characterization is used as a foundation for Preisach type models. This type of model is suited to handle the non-equilibrium nature of first order materials, taking the magnetic and thermal history dependence of material properties into account, as well as the heat production due to hysteretic losses. MnFe(P,As) and $Gd_5Si_2Ge_2$ compounds are modelled and it is found that the Preisach approach is suitable to reproduce material behavior in both cases. The $Gd_5Si_2Ge_2$ model is based on detailed first order reversal curve data, taking both reversible and irreversible properties into account, and is able to reproduce a series of independent experimental results. The Preisach models are applied to simulate material behavior under realistic application conditions in AMR-type cycles. The findings support those of the direct MCE measurements, namely that under AMR-type conditions the available MCE is bound by low field heating and high field cooling entropy curves. The heat production due to hysteresis in an AMR-type cycle initiated at a given temperature is found to be equal to that of the corresponding isothermal magnetization hysteresis loop. Furthermore the MCE is seen to be correlated to the hysteresis. This allows for relatively simple implementation of magnetic hysteresis losses in numerical AMR system models: either from measured isothermal magnetization curves or simply by adding heat production in the form of a suitably scaled MCE.

Due to the history dependence of hysteretic materials, experimental procedures

need careful analysis. It is demonstrated that magnetization measurements can suffer from unintended effects due uncareful change of the magnetic field and temperature. Too high magnetic field ramps in isothermal magnetization experiments can induce extrinsic hysteresis effects due to the MCE destroying the isothermal conditions, even at relatively low ramp rates. Aggressive temperature control can lead to oscillations around temperature set points, which is demonstrated to induce partial hysteresis loop behavior that will generally underestimate thermal hysteresis. Furthermore it is shown that care should be taken in non-isofield type experiments, as is the case for direct MCE experiments. Measuring the temperature dependence of the MCE can yield different results in heating or cooling modes. Cooling mode measurements will tend to be overestimated, whereas the heating mode results are representative of the realistic MCE available in application conditions.

Resumé

I denne afhandling behandles effekten af hysterese på magnetokaloriske materialers egenskaber samt dens indflydelse på ydeevnen i magnetiske kølingsapparater. Dette gøres gennem et kombineret eksperimentelt og modelleringsstudie af de to første ordens magnetokaloriske materialer MnFe(P,As) og $Gd_5Si_2Ge_2$.

Den eksperimentelle karakterisering af den magnetokaloriske effekt (MCE) i disse materialer er udført ved brug af konventionelle indirekte metoder, baseret på magnetometri og kalorimetri, samt nyudviklede direkte metoder. Bestemmelsen af MCE'en ved en ændring af magnetfeltet er i princippet givet ved materialets temperaturafhængige isofelt entropikurver, bestemt ved det lave startfelt og det høje slutfelt. Men i første ordens materialer opnås termiske entropi hysteresekurver gennem karakteriseringen, svarende til målinger udført under øgning og sænkning af temperaturen. Indirekte metoder til bestemmelse af MCE'en, så som Maxwell relationen eller kalorimetriske målinger udført kun ved enten opvarmning eller nedkølning, estimerer MCE'en som den reversible forskel mellem de to isofelt opvarmningskurver eller nedkølningskurver. Her vises det, at direkte målemetoder angiver at den korrekte MCE er givet ved forskellen mellem opvarmningskurven ved lavt felt og nedkølningskurven ved højt felt, hvilket kan reducere den estimerede MCE betragteligt.

Data fra materialekarakteriseringen bruges som fundament til modeller af Preisach typen. Disse modeller er velegnede til at håndtere de ude-af-ligevægtsforhold der eksisterer i første ordens materialer, ved at tage højde for materialeegenskabernes afhængighed af den termiske og magnetiske historie, samt varmeudvikling i forbindelse med hysterestab. Både MnFe(P,As) og $Gd_5Si_2Ge_2$ modelleres og det ses at Preisach-tilgangen er anvendelig til at kunne genskabe materialernes

opførsel. Modellen af $Gd_5Si_2Ge_2$ er baseret på detaljerede first order reversal curves, der tager højde for både reversible og irreversible egenskaber. Det illustreres at modellen kan reproducere en serie af uafhængigt udførte eksperimenter. Preisach modellerne anvendes til at simulere materialernes opførsel under realistiske anvendelsesforhold i AMR-lignende cyklusser. Resultaterne af dette bekræfter observationerne fra de direkte eksperimenter, at under AMR lignende forhold er den tilgængelige MCE bundet af det minimale areal i entropi-temperatur rummet; rummet mellem minimumfeltets opvarmningskurve og maksimumfeltets nedkølningskurve. Varmeudviklingen forårsaget af hysterese i en AMR-lignende cyklus sat i gang ved en given temperature demonstreres at være lig den tilsvarende isoterme magnetiserings hysteresekurve. Derudover ses det, at MCE'en er tæt korreleret med hysteresen. Dette åbner op for en relativ simpel implementering af magnetisk hysteresetab i numeriske AMR systemmodeller: enten ved brug af data fra målte isoterme hysteresekurver eller endnu simplere ved at tilføje en varmeproduktion der er skaleret efter den kendte MCE.

På grund af historieafhængigheden i materialer med hysterese, skal eksperimentelle procedurer grundigt analyseres. Her demonstreres det, at magnetiseringsmålinger kan lide af uforudsete effekter, på grund af uvarsomme ændringer af magnetfelt og temperature. For høje magnetfeltramper inducerer kunstige hystereseeffekter på grund af MCE'en, selv ved lave ramperater. Aggressiv temperaturkontrol kan føre til oscillationer omkring sættemperaturer. Dette kan føre til partielle hysteresekurver, hvilket generelt vil underestimere den målte termiske hysterese. Derudover illustreres det, at man skal være varsom ved udførslen af målinger der foregår ved ikke konstante felter, som er tilfældet i direkte målinger af MCE'en. Ved bestemmelse af den temperaturafhængige MCE kan forskellige resultater opnås ved målinger foretaget under opvarmning og nedkølning. Nedkølningsmetoden vil generelt bevirke at resultaterne er overestimerede, hvorimod resultater opnået ved opvarmningsmetoden er repræsentativ for MCE i realistiske anvendelsesforhold.

Acknowledgements

When I started at DTU in the magnetic refrigeration group I had little knowledge about magnetocalorics. Now, three years have swiftly passed and I am putting the final touches on my thesis. It has been quite the journey and one I could not have completed without the vast amounts of guidance and active participation from my supervisors Christian Bahl, Kaspar Nielsen and Kurt Engelbrecht. Countless knocks on supervisor doors, discussion at the coffee machine and calls from the lab has made this work possible. The vast amount of knowledge contained in these guys is both amazing and a little intimidating. Despite that, Christian, Kaspar and Kurt have all made me feel more like a colleague than a student. For all of this I am ever grateful.

It has been a great experience to be part of a research group that does it all: producing materials, modelling magnets, regenerators and seemingly everything else, with all the separate parts coming together in the building of working magnetic refrigeration devices. Not only does the group gather in the scientific work space, but also socially in the daily lunch club and at private events. It has been great to be part of this.

During my studies I spent 3 months in Italy at Istituto nazionale di ricerca metrologica, working with Vittorio Basso. The time spend there has been of tremendous help to me and has really accelerated the modelling part of my thesis. I am very grateful for all the time spent helping me with both experiments and modelling during my time there. Thank you Vittorio.

Furthermore I would like to thank the Copenhagen Cleantech Cluster organization for financing part of my project. Lastly, I would like to extend my thanks to both BASF and Profs. K.A. Gschneidner Jr. and V. Pecharsky from Ames Laboratory for providing the samples investigated in this thesis.

Lars von Moos, September 2014

List of publications

K. K. Nielsen, C. R. H. Bahl, H. N. Bez, R. Bjørk, L. von Moos, and D. Eriksen. Direct measurements of the magnetocaloric effect. In *6th IIF-IIR International Conference on Magnetic Refrigeration*, 2014.

L. von Moos, C. R. H. Bahl, K. K. Nielsen, and K. Engelbrecht. The influence of hysteresis on the determination of the magnetocaloric effect in $Gd_5Si_2Ge_2$. *Journal of Physics D: Applied Physics*, In print, 2014a.

L. von Moos, C. R. H. Bahl, K. K. Nielsen, and K. Engelbrecht. Quantification of the effect of hysteresis on the magnetocaloric effect in first order $Gd_5Si_2Ge_2$. In *6th IIF-IIR International Conference on Magnetic Refrigeration*, 2014b.

L. von Moos, C. R. H. Bahl, K. K. Nielsen, K. Engelbrecht, M. Küpferling, and V. Basso. A preisach approach to modeling partial phase transitions in the first order magnetocaloric material MnFe(P,As). *Physica B: Condensed Matter*, 435(0):144 – 147, 2014c. URL `http://www.sciencedirect.com/science/article/pii/S0921452613006054`.

L. von Moos, K. K. Nielsen, K. Engelbrecht, and C. R. H. Bahl. Experimental investigation of the effect of thermal hysteresis in first order material MnFe(P,As) applied in an AMR device. *International Journal of Refrigeration*, 37(0):303 – 306, 2014d. URL `http://www.sciencedirect.com/science/article/pii/S0140700713001163`.

Contents

I Introduction and theory **1**

1 Introduction **3**

1.1 Thesis composition 4

2 Theory **7**

2.1 Magnetocalorics 7

2.2 A Preisach approach to first order transitions 19

2.3 Summary 28

II Experimental equipment and procedures **29**

3 Calorimetric characterization **31**

3.1 The DTU DSC 31

3.2 The PerkinElmer DSC 41

3.3 Characterizing the transition 42

3.4 Direct MCE measurements 44

3.5 Summary 46

4 Magnetization measurement procedures **47**

4.1 Stability and precision of measurements 48

4.2 Measuring isofield magnetization - Temperature control 48

4.3 Measuring isothermal magnetization 54
4.4 Procedures for isothermal magnetization measurements 58
4.5 Obtaining the isothermal entropy change 61
4.6 Summary 64

III Material characterization 65

5 Characterization of $Gd_5Si_2Ge_2$ 67
5.1 Magnetometry 69
5.2 Calorimetry 76
5.3 Discussion and summary 86

6 Characterization of MnFe(P,As) 89
6.1 Low hysteresis MnFe(P,As) 91
6.2 High hysteresis MnFe(P,As) 101
6.3 Summary 114

IV Preisach modelling 115

7 Preisach modelling of $Gd_5Si_2Ge_2$ and MnFe(P,As) 117
7.1 Parameter estimation 119
7.2 MnFe(P,As) - Compound 1, high hysteresis 124
7.3 MnFe(P,As) - Compound 2, low hysteresis 130
7.4 Modelling $Gd_5Si_2Ge_2$ 135
7.5 Measuring first order materials in a cooling mode 141
7.6 Summary and discussion 144

V Summary and publications 149

8 Summary and outlook 151
8.1 Future considerations 153

A Experimental investigation of the effect of thermal hysteresis in first order material MnFe(P,As) applied in an AMR device 157

B A Preisach approach to modeling partial phase transitions in the first order magnetocaloric material MnFe(P,As) 163

C The influence of hysteresis on the determination of the magnetocaloric effect in $Gd_5Si_2Ge_2$ 169

D Quantification of the effect of hysteresis on the magnetocaloric effect in first order $Gd_5Si_2Ge_2$ 179

E Direct measurements of the magnetocaloric effect 183

F Delft Days 2013 187

G Pure phase parameters 189

Bibliography 193

Part I

Introduction and theory

Chapter 1

Introduction

The work presented in this thesis aims to provide insight into the properties of hysteresis in magnetocaloric materials (MCMs) and the influence it has on their performance in magnetic refrigeration devices. Magnetic refrigeration utilizes the magnetocaloric effect (MCE), which causes a reversible temperature change in magnetic materials by changing an external magnetic field. This concept is not new and has been applied for low temperature cooling applications since the 1930s. However, with the discovery of high performing near room-temperature MCMs and the focus on efficient cooling technologies, the field of magnetocalorics has seen a great increase in popularity in recent years.

Many of these new materials with a large MCE have the adverse property of exhibiting hysteresis, which introduces a series of challenges. Hysteresis in magnetic materials is seen from two main effects: hysteresis losses in terms of internal heat production in the material during magnetic field changes and thermal and magnetic history dependence of material properties. So why is this a problem? As magnetic refrigeration relies on utilizing thermodynamic cycles to move heat between thermal reservoirs, irreversible heat production will inadvertently reduce the effectiveness since this extra heat needs to be removed somehow. The introduction of thermal and magnetic history dependence of materials properties makes characterization of the materials non-trivial. Conventionally the MCE is characterized indirectly through measurements of the magnetization or the heat capacity, as function of temperature and magnetic field. This works well for

MCMs not exhibiting hysteresis, since every material property can be described by single valued functions of the intensive variables. However, for hysteretic materials all parameters become dependent on the conditions under which they were measured and are no longer uniquely defined at a given temperature and field.

As hysteresis is a non-equilibrium phenomenon, this makes the thermodynamic framework often used to characterize the MCE principally invalid. The heat production is not accounted for and the history dependence of material properties makes them ambiguous. The standard way of circumventing these problems is to ignore the heat production and measure the material properties under controlled and standardized conditions. This generally provides two distinct material parameter curves, on which the equilibrium framework is applied to deduce the MCE. This introduces a new set of problems. i) What are the effects of the ignored heat production? ii) Given two different MCE curves, each representing the same property, what is then the correct value in a given situation? iii) The MCE curves are deduced on the basis of a standard characterization procedure, but how do these relate to actual refrigeration conditions where thermal and magnetic profiles are certainly different?

These properties make it difficult to quantify the real MCE and compare different materials. Furthermore, it makes material property data implementation in numerical models suffer from the same problems as stated above. Numerical models of refrigeration systems are crucial to understand the interplay between the different elements. But the model output is only as good as its input, so a procedure for taking the hysteretic properties of MCMs into account is important to realistically simulate refrigeration performance and understand the direct effects of hysteresis.

The aim of this work is to illuminate these problems and provide tools to handle them.

1.1 Thesis composition

The work presented in this thesis revolves around the properties of hysteresis. These properties have been investigated within three different but coupled areas: experimental equipment and procedures, hysteretic material characterization and modelling of hysteretic materials. The thesis is divided into separate parts, concerning the separate areas.

Part I The thesis work is introduced and the underlying theoretical concepts are presented in chapters 1 and 2. No new knowledge is presented in these chapters. They are meant as a short introduction to the field of

magnetocalorics and its conventions and definitions.

Part II The experimental equipment used in this work is presented. The procedures used to characterize the materials are described and the pitfalls of measuring on hysteretic materials are experimentally investigated and discussed. Calorimetric and magnetometric procedures are described in chapters 3 and 4, respectively. A discussion of the potential problems related to direct measurements of the MCE in hysteretic materials is also presented in section 7.5 in relation to a material model.

Part III The experimental characterizations performed on two types of first order magnetocaloric compounds, $Gd_5Si_2Ge_2$ and MnFe(P,As), are presented in chapters 5 and 6, respectively. Material characterization includes magnetization, heat capacity and direct measurements of the MCE on newly developed devices at DTU. These characterizations are carried out as described in Part II and the detailed discussions concerning experimental procedures are omitted in the material chapters themselves, where just the results are presented.

Part IV The application of the non-equilibrium Preisach model approach to hysteretic materials is presented. In chapter 7 the model is applied to describe the non-equilibrium behavior of both MnFe(P,As) and $Gd_5Si_2Ge_2$ in application like conditions. The model results are used in addition to the experimental data to predict how first order materials behave during realistic refrigeration cycles. The basic theoretical concepts of this approach are presented in section 2.2.

Part V A brief summary of the entire thesis work is presented in chapter 8, along with a discussion of future consideration that can be inferred from this work. In the following appendices the publications related to this work are presented. This includes two publications in peer reviewed international journals, one publication currently under review and two peer-reviewed conference proceedings papers. These are also listed before the table of contents. The relevant papers are referenced in the sections where the published results are presented. The information contained in the papers is also presented in the thesis. However, the papers generally contain results from several parts of the thesis and can perhaps give a more collective presentation of all the relevant material.

Chapter 2

Theory

2.1 Magnetocalorics

In the following section the basic concepts of magnetocalorics are introduced: the magnetocaloric effect(MCE), the application for magnetic refrigeration and magnetocaloric materials (MCMs). This is meant as a brief introduction and no new information is introduced here. A more in depth overview of the field in general, with extensive literature references to the specific areas, can be found in the review paper by Smith et al. [2012].

The magnetocaloric effect and magnetic refrigeration

The magnetocaloric effect was experimentally discovered in 1918 by Weiss and Piccard, when they showed that when a nickel sample was magnetized and demagnetized around the Curie temperature, the sample temperature would reversibly increase and decrease, respectively [Smith et al., 2012]. Some years later it was demonstrated that this effect could be used for refrigeration purposes. At this time it was only possible to utilize in low temperature conditions. However, in 1976 it was demonstrated by Brown [1976] that the ferromagnetic material gadolinium (Gd) could be used for refrigeration purposes in near room temperature conditions. In 1997 a new, near room temperature MCM, $Gd_5Si_2Ge_2$, was introduced, which

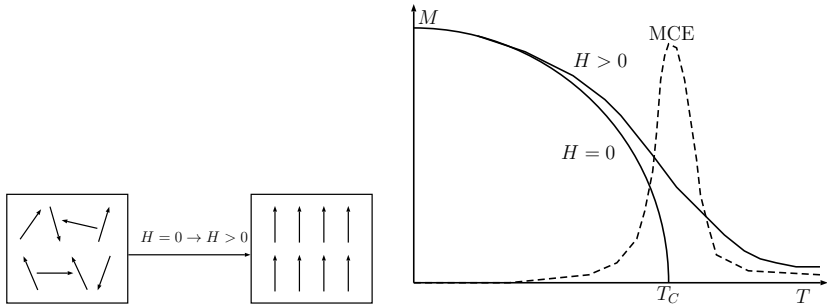

(a) Adiabatic magnetization cause a temperature increase in magnetic materials.

(b) The correspondence between the magnetocaloric effect (MCE) and the magnetization.

Figure 2.1

seemingly greatly outperformed Gd and other known MCMs [Pecharsky and Gschneidner, 1997]. Coupled with the focus on new environmentally friendly technologies during those years, the field of magnetic refrigeration saw a great increase in research and development.

The explanation of the MCE lies in the coupling between magnetic spin and the crystal lattice. When a ferro- or paramagnetic material is magnetized there will be some ordering of the magnetic spins, forcing them towards the direction of the applied field, as illustrated in Fig. 2.1a. If this is done isothermally, this will lower the material's magnetic entropy by the isothermal entropy change ΔS. However, if the magnetization is done adiabatically, with no thermal transfer to the ambient, the total sample entropy remains constant and the decrease in magnetic entropy is countered by an increase in lattice and electron entropy. This causes a heating of the material and a temperature increase given by the adiabatic temperature change ΔT_{ad}. The inverse procedure also applies: under adiabatic demagnetization the magnetic entropy increases, causing a decrease in lattice vibrations and by that a temperature decrease. This conventional MCE is the focus of this thesis work and all the results pertain to this. However, it is noted that an inverse MCE has been shown to exist in Heusler alloys, in which the entropy increases upon magnetization, leading to a cooling effect Krenke et al. [2005].

For ferromagnetic materials the magnetization only changes significantly around the Curie temperature T_C, which is the temperature at which the spontaneous magnetization goes to 0. This means that the MCE is largest around this temperature, as shown in Fig. 2.1b.

As ΔT_{ad} is of the order of a couple of degrees for magnetic field changes from 0 T to 1-2 T, it is insufficient to drive any cooling process by itself. To overcome this, the MCM is used as the active component of a regenerative magnetic cycle, the active magnetic regenerator (AMR) cycle as introduced by Barclay and Steyert [1982]. The basic idea of the AMR cycle is illustrated in Fig. 2.2a, where steps are as follows

1. Adiabatic magnetization from initial field H_i to a larger final field H_f at temperature T_i, increasing the material temperature by $\Delta T_{\mathrm{ad}}(H_i; H_f, T_i)$.

2. Heat rejection of Q_h from the MCM to a hot side heat exchanger, which ideally reduces the temperature back to T_i at constant field H_f.

3. Adiabatic demagnetization from initial high field H_f to the low field H_i at temperature T_i, decreasing the temperature by $\Delta T_{\mathrm{ad}}(H_f; H_i, T_i)$.

4. Heat absorption of Q_c from a cold side heat exchanger to the MCM, increasing the temperature back to T_i at constant field H_i.

This process allows for a continuous and cyclic use of the MCE, which allows for a temperature span between the hot and cold side many times larger than ΔT_{ad}.

Both ΔT_{ad} and ΔS are required to fully characterize the performance of materials in the AMR cycle. The ΔT_{ad} value provides information about the temperature gradient under which Q_h and Q_c can be transferred. However, it does not contain any information about the available thermal energy that can be transferred, as this depends on the heat capacity of the material. This is given by the ΔS value, which gives a measure of the available thermal energy $Q \sim \Delta S T$. The MCE is reversible upon magnetization and demagnetization between fields H_i and H_f in the case of second order phase transitions, meaning that

$$0 = \Delta S(H_i; H_f, T_i) + \Delta S(H_f; H_i, T_i)\,, \tag{2.1}$$

$$0 = \Delta T_{\mathrm{ad}}(H_i; H_f, T_i) + \Delta T_{\mathrm{ad}}(H_f; H_i, T_i + \Delta T_{\mathrm{ad}}(H_i; H_f, T_i))\,. \tag{2.2}$$

It is important to note that the magnitude of ΔT_{ad} during magnetization at temperature T_i does not equal the magnitude of ΔT_{ad} during demagnetization at T_i, which is stated both in the above expression and illustrated in Fig. 2.2b.

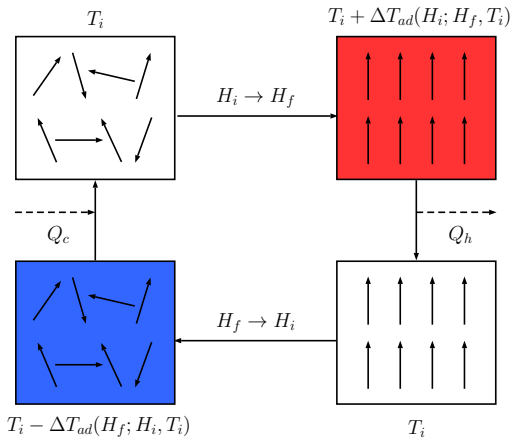

(a) Schematic illustration of the AMR cycle initiated at T_i: 1) adiabatic magnetization from H_i to H_f, 2) heat rejection at H_f, 3) adiabatic demagnetization from H_f to H_i, and 4) heat absorption at H_i.

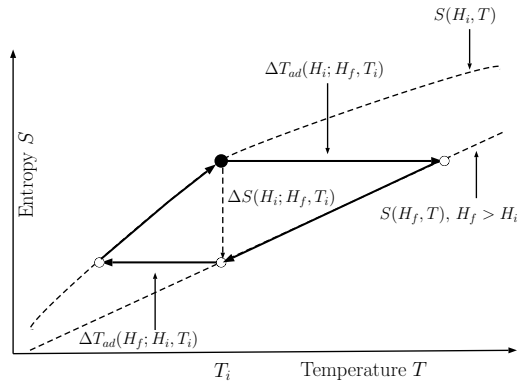

(b) The magnetocaloric effect in terms of the adiabatic temperature change ΔT_{ad} and the isothermal entropy change ΔS as defined by the material entropy S.

Figure 2.2: Illustrations of the AMR cycle.

Thermodynamics of the reversible MCE

In the following the basic thermodynamics of the magnetocaloric effect are presented. This is done under the assumption of reversibility, meaning that there is no entropy production involved and the entropy constitutes a material state function, unless stated otherwise. This is only correct for reversible second order phase transitions and does not hold for irreversible hysteretic first order materials. However, this approach does illustrate why materials are characterized the way they are. Furthermore parts of this equilibrium framework is used in the non-equilibrium model described in section 2.2. The discussion of the effects of hysteresis is provided in section 2.1.

The determination of the MCE follows from the first and second laws of thermodynamics,

$$dU = \delta W + \delta Q \tag{2.3}$$

where the internal energy change is given by the work done on the system δW and the heat added to the system δQ. Here δw is only the magnetic work done by the magnetic field H

$$\delta W = \mu_0 H dM \tag{2.4}$$

as pressure and volume are assumed constant. In this work this is always assumed, which is often the case in standard magnetic refrigeration applications even though that use of pressure has been suggested [Liu et al., 2012]. The added heat follows from the second law

$$dS \geq \frac{\delta Q}{T} \tag{2.5}$$

where the inequality is general and the equality holds only for reversible processes. As the relevant experimentally determined variables in magnetocalorics are the temperature and the applied magnetic field, the relevant thermodynamic potential is the Gibbs free energy

$$G = U - ST - \mu_0 MH\,, \tag{2.6}$$

which in differential form is given as

$$dG = -SdT - \mu_0 MdH\,. \tag{2.7}$$

If reversibility is assumed, the Maxwell relation for a magnetic material can be derived from Eq. (2.7)

$$\left(\frac{\partial S}{\partial H}\right)_T = \mu_0 \left(\frac{\partial M}{\partial T}\right)_H\,, \tag{2.8}$$

which relates the entropy change upon a magnetic field change to the material magnetization dependence on temperature. Application of Eq. (2.8) is the most common method for estimating ΔS, as it follows directly from integration

$$\Delta S(H_i; H_f, T) = \mu_0 \int_{H_i}^{H_f} \left(\frac{\partial M}{\partial T}\right)_H dH\,. \tag{2.9}$$

having experimentally measured the magnetization $M(H,T)$. However, this can be prone to large errors if this is applied on hysteretic materials as will be discussed in section 4.5.

Another approach to determine the MCE, is to consider the entropy as a state function. The total material entropy contains contributions from the electrons, the lattice and the magnetic spins,

$$S = S_E + S_L + S_H \tag{2.10}$$

where the electron and lattice contribution can generally be considered as independent of magnetic field [Pecharsky et al., 2001]. The total entropy differential $dS(H,T)$ is given by

$$dS = \left(\frac{\partial S}{\partial T}\right)_H dT + \left(\frac{\partial S}{\partial H}\right)_T dH\,. \tag{2.11}$$

The entropy derivative with respect to temperature is directly coupled to the heat capacity C through Eq. (2.5)

$$\left(\frac{\partial S}{\partial T}\right)_H = \frac{C_H(H,T)}{T}\,. \tag{2.12}$$

The isothermal entropy change between magnetic fields H_i and H_f at temperature T is defined as

$$\Delta S(H_i; H_f, T) = S(H_f, T) - S(H_i, T) \tag{2.13}$$

which can be stated in terms of the heat capacity using Eq. (2.12)

$$\Delta S(H_i; H_f, T_i) = \int_0^{T_i} \frac{C_H(H_f,T) - C_H(H_i,T)}{T} dT\,. \tag{2.14}$$

In adiabatic conditions it is required that $dS = 0$ in the reversible case, which can be stated as

$$S(H_i, T_i) = S(H_f, T_i + \Delta T_{\mathrm{ad}}(H_i; H_f, T_i))\,. \tag{2.15}$$

The adiabatic temperature change can be found implicitly from the entropy curves obtained from the heat capacity, Eq. (2.12). The expressions stated in Eq. (2.14) and Eq. (2.15) make it clear why calorimetric heat capacity measurements are commonly used as a tool to estimate both ΔS and ΔT_{ad}.

The connection between the various material properties and ΔT_{ad} can be directly illustrated by applying the Maxwell relation in Eq. (2.11),

$$dT = -\mu_0 \frac{T}{C_H(H,T)} \left(\frac{\partial M}{\partial T}\right)_H dH \tag{2.16}$$

This can in principle be integrated along the constant entropy isentrope γ to give the total adiabatic temperature change ΔT_{ad} from initial temperature T_i undergoing a magnetic field change from H_i to H_f

$$\Delta T_{\mathrm{ad}}(H_i; H_f, T_i) = -\mu_0 \int_\gamma \frac{T}{C_H(H,T)} \left(\frac{\partial M}{\partial T}\right)_H dH\,. \tag{2.17}$$

As discussed in detail in Smith et al. [2012] it is important to note that in the above integral the temperature becomes a function of the field, which makes practical application of this formula non-trivial. However, it does illustrate the important features of ΔT_{ad}, namely that it is largest around the Curie temperature, where the magnetization gradient is large, and greater magnetic field changes provide larger MCE.

Hysteresis and first order transitions

In magnetocalorics, one of the main areas of interest is to find materials that have a large MCE. These materials are generally put into two groups: materials undergoing either a first or second order magnetic phase transition. In second order transitions, the magnetization changes continuously. In first order transition the magnetization changes discontinuously at the transition and is connected with latent heat. The distinction is not always completely clear and some materials experience characteristics that can be attributed to both types. This can be caused by impurities and defects in the materials that can lead to a distribution of transition temperatures broadening what should in principle be a discontinuous transition [Bahl et al., 2012].

As mentioned in the introduction, the recent surge in popularity in magnetic cooling near room temperature was spurred by the discovery of $Gd_5Si_2Ge_2$, experiencing a "giant" MCE. This material undergoes a first order transition, due to a coupling between the magnetic transition and a structural first order transition. The structural transition involves a small volume change that is both the cause of the sought giant MCE, but also irreversible hysteretic properties, which are not desired, as discussed in the following. These magneto-structural transitions are general for the first order materials considered in this work, namely $Gd_5Si_2Ge_2$ and MnFe(P,As) [Wang, 2012].

The equilibrium thermodynamic framework stated in the previous section works nicely for reversible second order MCMs. However, in first order materials that experience hysteresis, irreversibility cause the equations to be principally invalid. In the following sections the concept of hysteresis is introduced along with its relation to first order MCMs and the problems it involves.

Conventional hysteresis

In the following the conceptual idea of hysteresis is presented as it relates to magnetic materials. The origin of hysteresis is complex as it is the result of many different phenomena. Here a brief introduction of the main mechanisms is given. These concepts are mentioned in most textbooks on magnetism, but for a more in depth discussion Bertotti [1998] is recommended.

Hysteresis is a well known phenomenon that occurs in various contexts. The word is adopted from Greek and means "to lag behind". In the context of magnetics, the conventional illustration of hysteresis is shown in Fig. 2.3a. A ferromagnetic material is initially completely demagnetized with magnetization $M = 0$ with no external field H present. An external magnetic field is then applied, which induces a net magnetization in the material that increases with increasing field, as shown by the dashed line. When a critical field H_s is reached, all magnetic

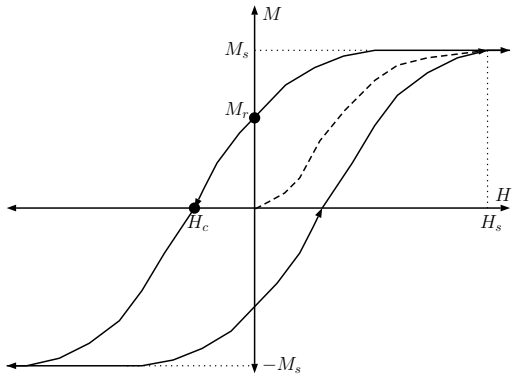

(a) Hysteresis loop originating from magnetic field cycling of a hard ferromagnet.

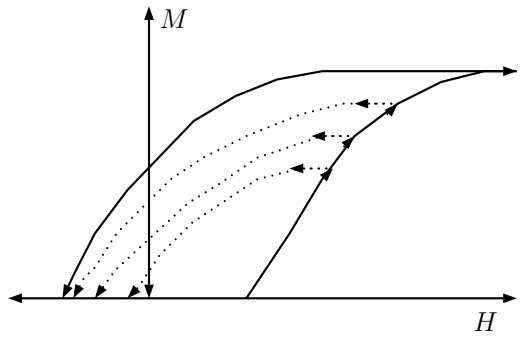

(b) Minor/partial hysteresis loops upon field reversal prior to saturation.

Figure 2.3

moments point along the external field direction and the material has obtained its maximum saturated magnetization M_s. Upon demagnetization, removal of the field, the material magnetization tends to remain more magnetic than upon magnetization at a given field; it lags behind in some sense. When the external field has returned to 0, a net remanence magnetization M_r still remains in the material. Not until the external field direction is reversed to the coercive field H_c is the net magnetization of the material again 0. Further reversal of the external field will saturate the material with the moments pointing in the opposite direction, $-M_s$. Upon cycling of the magnetic field between $\pm H_s$, the process is repeated and the hysteresis loop shown in solid lines is traced during each cycle. The initial magnetization curve from the demagnetized state is history independent and is called the anhysteretic curve. It cannot be realized again until the material's memory of its magnetic history is reset by heating it up enough to become completely demagnetized again.

This means that the material magnetization is not unique, given the external field. It depends on the magnetic and thermal history of the material. As might be suggested from Fig. 2.3a, there are three possible values for M at a given field. However, the magnetization can actually lie anywhere between the two solid magnetization and demagnetization curves at a given field. This is illustrated in Fig. 2.3b, where the field is now reversed prior to the material reaching saturation. Doing this introduces partial/minor hysteresis loops, though here just shown for the first quadrant.

The explanation of this irreversible behavior is complicated and can be at-

tributed to a series of phenomena that are connected to anisotropy in the material and the formation of magnetic domains: separate regions with individual uniform magnetic moments. Domains arise as a result of minimizing the total energy of the magnetic system, to which several competing interactions contribute

- Exchange interactions - Neighboring spins will tend to align in the same direction (for ferromagnets).
- Crystal anisotropy - The crystal lattice structure can induce favored directions of the magnetic spins. The preferred directions are called the easy-axes.
- External magnetic field - An application of an external magnetic field will tend to align spins in its direction.
- Shape anisotropy - Due to the demagnetization field, the shape of the material and the domains themselves affect the magnetostatic energy, introducing additional preferred spin directions.

All these contributions determine the domain structure in order to minimize the energy under given conditions. An illustration is given in Fig. 2.4. The configurations shown here correspond to the initial magnetization curve shown in Fig. 2.3a. With no external field present it is favorable to have no net magnetization, since this minimizes the magnetostatic energy by eliminating the stray field outside the material (or minimizes the demagnetization field inside). This is why some ferromagnets show no net magnetization below the Curie temperature when no external field is present. However, as an external field is applied, the spins are forced towards the direction of the field. The now favorable domains will grow at the cost of the less energetically favored. Upon reaching the saturation field H_s all magnetic moments are forced in the direction of the external field and just one domain remains. Upon removal of the field, domains will be created again as the energy balance changes.

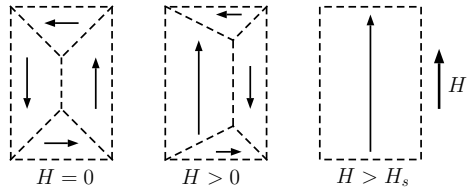

Figure 2.4: Domains in a ferromagnetic material created to minimize self-energy. At $H = 0$ no net magnetization is observed. Upon application of a magnetic field the favorable domain grows until the sample is saturated.

Hysteresis generally depends on the particular domain structure, but it can also occur in single domain anisotropic materials, as demonstrated in the Stoner-Wohlfart model [Stoner and Wohlfarth, 1948]. Here a miss-alignment between the applied field and the crystal easy-axis introduce a metastable energy landscape. With no external field the magnetic moment can point in either of the directions along the easy-axis. As the external field is applied the moment will tend towards to direction of the field in competition with the anisotropy, making one state stable and the other metastable. At some point, the external field will be so large that the moment points along its direction, leaving only one stable state.

However, in realistic bulk materials were domains come into play, the problem becomes more complicated. As an external field is applied, the domain structure undergoes changes, which can happen both reversible and irreversibly. The movement of domains is closely connected to the particular crystal structure of the material. Real materials always show some kind of structural disorder; defects in the lattice structure, polycrystalline features where anisotropy changes locally, small variations in material composition etc.. This introduces local anisotropy and changes in the magnetostatic forces that can pin particular domains in place, creating energy barriers. When such domains are eventually changed or annihilated under the influence of large fields, it is accompanied by irreversible internal friction. The dissipated energy due to the irreversibility upon an isothermal magnetization cycle is given by the area of the hysteresis loop

$$Q_{hyst} = \mu_0 \oint H dM = \oint T \delta S_i \,, \tag{2.18}$$

which corresponds to the irreversible entropy production δS_i [Bertotti, 1998]. There is a subtle problem involved with this determination of the heat production. It is only possible to characterize it during a complete cycle. This means that one can easily measure the magnetization during application and removal of an applied field, calculate the hysteresis loop area to obtain the magnetic loss. However, this

only provides information about that particular cycle, at the given temperature and field profile. There is no way of knowing how much entropy is produced at any given part of the transformation.

All these mechanisms introduce a complicated material energy landscape, where a huge number of metastable states exist and the global energy minimum state is not accessible. The metastability can cause a phase coexistence, in which both the PM and FM phases are present within the sample. The material becomes dependent on its own intrinsic properties as well as the thermal and magnetic history.

Hysteresis in magnetocalorics

Hysteretic properties can be very useful. It is the presence of remanence magnetization and high coercive fields that make it possible to have permanent magnets, which have uses as just that, magnets, but also in many data storage technologies. However, they are generally prohibitive in other applications, which also apply for magnetic refrigeration.

There exist some differences between hysteresis in MCMs and the brief conventional introduction given above. The classic hysteresis loop illustration of Fig. 2.3a shows the behavior of a hard magnetic material characterized by high remanence magnetization and a high coercive field. MCMs are generally soft ferromagnets that have a high saturation magnetization, but practically no remanence magnetization. However, they still possess some degree of hysteresis, both magnetic and thermal, as shown in Fig. 2.5.

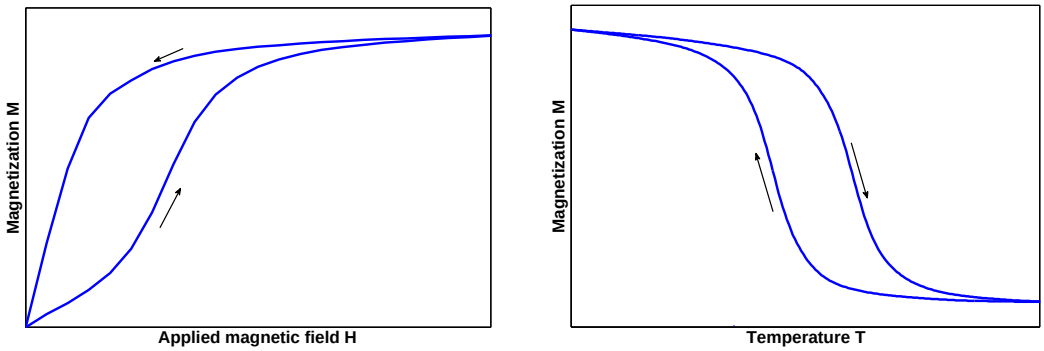

(a) Magnetic hysteresis loop for a soft magnetocaloric material. Heat corresponding to the area of the loop is dissipated during the magnetization cycle.

(b) Thermal hysteresis loop for a soft magnetocaloric material.

Figure 2.5

Both the thermal and magnetic hysteresis have consequences when analyzing the MCE:

- History dependence - The fact that the thermal and magnetic history becomes an influential part in material characterization is a problem. Parameters such as magnetization and heat capacity now become non-single valued functions of temperature and field. This makes the entire equilibrium thermodynamic framework described in the previous section principally invalid, as neither C_H nor M are uniquely defined. Furthermore it makes experimental procedures and comparison between different experiments troublesome. Since the thermal and magnetic history can determine the material behaviour, results from experiments can depend on the particular procedure applied. This also requires experiments to be carried out under identical conditions to be comparable.

- Energy dissipation - Heat is dissipated during the magnetization process, which is never wanted in a refrigeration application. The dissipation adds heat to the system, which by some means needs to be removed. This will inherently lower the performance of any type of cooling device. Furthermore it changes the temperature of the material slightly, increasing the complexity of the thermal history of the material. However, the hysteretic heat production could perhaps be utilized in heat pump applications where.

As hysteresis is an inherent non-equilibrium phenomenon, a non-equilibrium thermodynamic approach is needed to investigate how the irreversibility affects the MCMs undergoing AMR cycles.

2.2 A Preisach approach to first order transitions

In this chapter the Preisach approach to the non-equilibrium first order phase transition in magnetocaloric materials is presented.

In 1935 F. Preisach introduced an intuitive phenomenological model to simulate what happens in bulk magnetic materials experiencing hysteresis [Preisach, 1935, Mayergoyz, 2003]. The model had its origin in magnetism and is still widely used within this field. However, the model was generalized from the 1970s and upwards to decouple it from magnetism and put it into a more strict and general mathematical setting, primarily by Krasnosel'skii and Pokrovskii [1983] and Mayergoyz [1985]. When the interest for room temperature magnetic cooling spurred with the discovery of the giant MCE coupled to a first order hysteretic phase transition, it was relevant to study the effects of hysteresis on the MCE. This work was pioneered in the field of magnetocalorics by Basso et al. [2005] and LoBue et al. [2005]. The work presented in this thesis is a further development of these early works, basing the model on much more detailed data and including reversible effects as well as irreversible hysteretic behavior.

In the following a Preisach approach to first order transitions in magnetocaloric materials is presented. This is based on the general descriptions found in Mayergoyz [2003], Bertotti [1998]. These both treat the Preisach model in detail and in general terms and are highly recommended for an introduction to Preisach modelling. The application to magnetocalorics is introduced in LoBue et al. [2005], Basso et al. [2005, 2007b].

The bistable unit

The basis of the Preisach model approach is to build up a macroscopic system using a superposition of simple and individual hysteretic units. Such a bistable unit is illustrated in Fig. 2.6a. A unit can be in two different phases, denoted by $x = 0, 1$, which here refers to the paramagnetic (PM) and ferromagnetic (FM) phases, respectively. Each unit is characterized by two parameters describing the stored energy, g_u, and the dissipated energy, $g_c \geq 0$, during a transition between the two phases. Having a given set of unit parameters (g_u, g_c), the current phase is determined by a generalized field Z driving the transition,

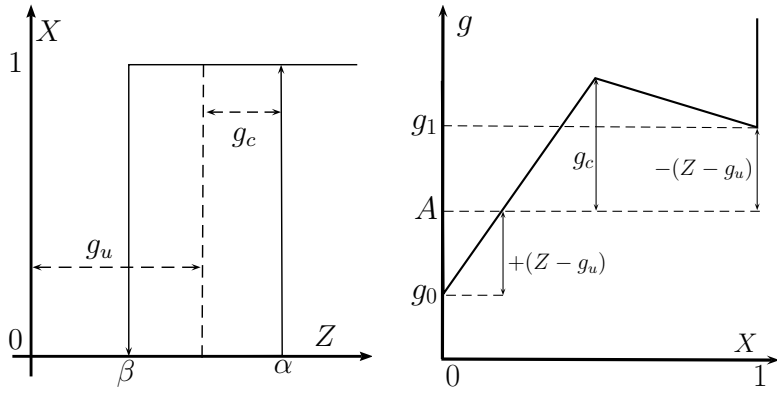

(a) A two-phase bistable unit, with phase switching fields $\alpha_{0\to1} = g_u + g_c$ and $\beta_{1\to0} = g_u - g_c$.

(b) The energy of a bistable unit under the influence of field Z.

Figure 2.6

- For fields above the threshold $Z \geq g_u + g_c$, the unit is always in phase $x = 1$.
- For fields below the threshold $Z \leq g_u - g_c$, the unit is always in phase $x = 0$.
- For fields in the intermediate range $g_u - g_c < Z < g_u + g_c$, the unit is in a metastable state and remains in its current phase.

The metastability of the unit in the intermediate field region introduces the history dependence into the system. It is noted that some authors use the equivalent switching field parameters instead

$$\alpha_{0\to1} = g_u + g_c\,, \quad \beta_{1\to0} = g_u - g_c\,. \tag{2.19}$$

However, this is not used in this work in order to keep nomenclature consistent with previous works in this field.

The current phase and the transition between the phases is governed by the Gibbs free energy of the unit. Each phase has a corresponding Gibbs free energy $g_x(H,T)$, where the subscript x refers to either phase 0 or 1. The free energy depends on the intensive variables, which here is the magnetic field H and the temperature T. The transition is driven by the difference in free energy between the two phases, from which the Z field is defined as

$$Z = \frac{g_0 - g_1}{2}\,. \tag{2.20}$$

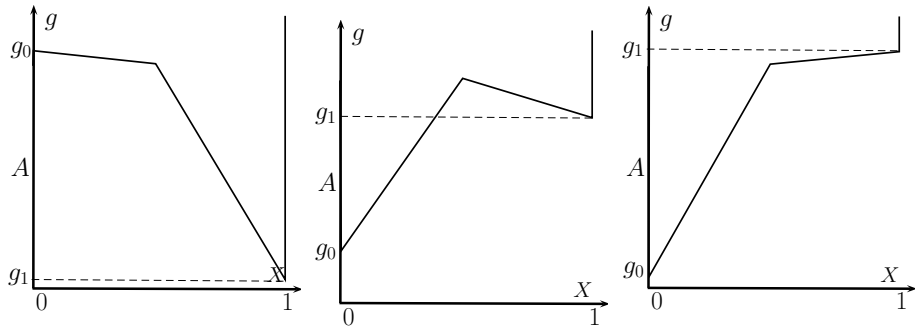

(a) Stable phase 1, $Z \geq g_u + g_c$.

(b) Metastable phase 1, $g_u - g_c < Z < g_u + g_c$

(c) Stable phase 0, $Z \leq g_u - g_c$.

Figure 2.7: Stability of the phases.

The Z-field leads to equal magnitude changes of the free energy of each phase,

$$g_0 = A + (Z - g_u)\,, \quad g_1 = A - (Z - g_u) \tag{2.21}$$

where the mean average free energy of the phases is

$$A = \frac{g_0 + g_1}{2}\,. \tag{2.22}$$

An illustration of the unit's energy landscape is shown in Fig. 2.6b, from where the meaning of the energy terms can be visualized. The stability of the two phases is shown in Fig. 2.7. Fig. 2.7a shows a situation where the FM(1) phase is stable and represent the global energy minimum of the unit. As Z is decreased to an intermediate value, by increasing temperature or lowering the magnetic field, the PM(0) phase represents a global energy minimum, but due to the hysteresis the unit remains in the FM phase, as shown in Fig. 2.7b. When the Z field is decreased sufficiently, the unit is forced to the PM state which now represent the only energy minimum, as shown in Fig. 2.7c.

The Preisach distribution

A single bistable unit is not representative of any real material behavior. In the Preisach approach this is accommodated by considering a distribution of individual bistable units. A distribution of g_u allows for a gradual transition, which is not perfectly first order, as is the case with many real materials. It can in principle represent a distribution of Curie temperatures and/or differences in

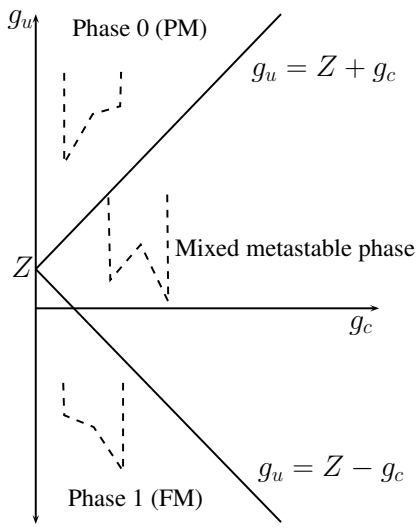

(a) Bistable units and their phase stability in the (g_u, g_c)-Preisach plane

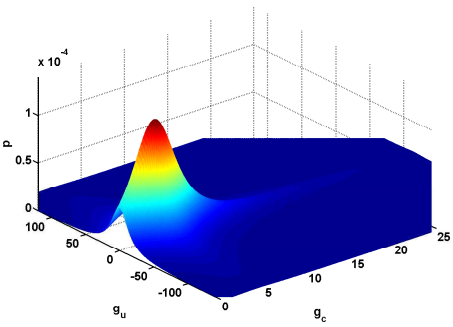

(b) Example of a Preisach distribution

Figure 2.8: Illustration of the Preisach plane.

internal magnetic fields within the material. The distribution of g_c allows for the hysteretic properties being dependent on the intensive variables, i.e. only existing in a region around the transition, as is the case in MCMs.

The distribution of units, each with individual (g_u, g_c)-values, is called the Preisach distribution and is denoted $p(g_u, g_c)$. As illustrated in Fig. 2.8a the individual units now exist in the (g_u, g_c)-plane and their phase is determined by the stability criteria listed in the previous section,

- All units below the FM-phase line $g_u \leq Z - g_c$ are stable in the FM phase, $x = 1$.
- All units above the PM-phase line $g_u \geq Z + g_c$ are stable in the PM phase, $x = 0$.
- All units in the intermediate cone-region remain in their current metastable phase.

To illustrate the hysteretic properties of this approach, the evolution of the Preisach plane with varying Z-values is shown in Fig. 2.9. Consider a material completely reset in the PM phase, here meaning that Z takes its lowest possible

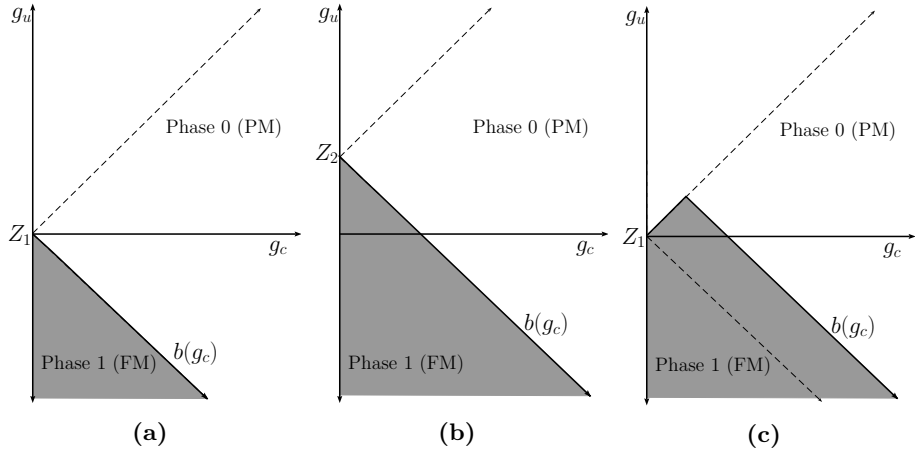

Figure 2.9: The evolution of the Preisach plane during a cyclic change in Z. The end state in (c) is different from the initial state in (a).

value. Now Z is increased up to some value Z_1, corresponding to cooling the material, as shown in Fig. 2.9a, transforming the units below the FM-phase line to the FM phase (grey area). The material has now undergone a partial transition, where it exhibits a mixed state. Z is now increased to the value Z_2 by further cooling, Fig. 2.9b, increasing the amount of units in the FM state. The material is now heated back up, decreasing Z back to Z_1, as shown in Fig. 2.9c. Now it is the PM-phase line that forces units above it back to the PM state, where units in the cone-region remain in their metastable state. Comparing Fig. 2.9a and Fig. 2.9c, the Z-field is the same but the fraction of units in the FM/PM states is not. The material remains partly in the FM phase upon reheating, giving rise to thermal hysteresis. The variation of Z introduces a history dependent state line $b(g_c)$ that separates the two phases.

A Preisach model experiences a wipe-out property, meaning that at very high and low values of Z, the history of previous variations will be erased [Mayergoyz, 1985]. This can be visualized from Fig. 2.9c considering Z being lowered to the minimum, which would completely erase the history of the state line $b(g_c)$. This property is required of the system being modelled, which is the case with magnetic materials. Upon sufficient cooling or heating, the material will either be completely in the FM or PM phase and thus erasing any previous magnetic and thermal history. This also means that in magnetic materials, the Preisach plane is of finite size, meaning that at some temperature and magnetic field the material is magnetically saturated and completely in the FM-phase. Likewise,

when heated enough the material will be completely in the PM phase.

There is another requirement for a Preisach model to be applicable for a system, which is the minor hysteresis loop congruency property [Mayergoyz, 1985]. This means that the minor hysteresis loops traversed by equal field cycles are congruent. This can also be visualized from Fig. 2.9. During continuous cycling, the area of the Preisach plane undergoing changes is given by the difference in shaded area between (b) and (c). Considering the case where the system is initiated in the complete FM state (everything is initially grey), the absolute phase state of the system changes but the hysteretic region swept out by $Z_1 \rightarrow Z_2 \rightarrow Z_1$ does not. Thus the minor hysteresis loops are offset from each other, but congruent.

Distribution functions

The determination of the distribution of bistable units is practically done by fitting it to experimental data. It turns out that many magnetic materials can be described sufficiently by multivariate normal, Lorentzian/Cauchy or log-normal distribution functions. The best choice of distribution functions depends on the specific material, as discussed by Pruksanubal et al. [2006]. In all previous works by Basso et al., only normal distributions have been used. The findings are here that Lorentzian functions provide a much better description of the investigated materials.

Through trial and error, the best fit to experimental data in this work comes from using Lorentzian distribution functions of the form

$$p(X) = \frac{A}{1 + \left(\frac{X-\mu}{\sigma}\right)^2} \tag{2.23}$$

where X is the distributed variable, μ the mean/offset, σ the standard deviation/spread and A the appropriate normalization. In the case of bistable units with two parameters, the distribution function is multivariate in the independently distributed parameters g_u and g_c

$$p_i(g_u, g_c) \propto \frac{1}{\left[1 + \left(\frac{g_u - g_{u,0}}{\sigma_u}\right)^2\right] \cdot \left[1 + \left(\frac{g_c - g_{c,0}}{\sigma_c}\right)^2\right]} \,. \tag{2.24}$$

In practice there is no need for an offset in $g_{u,0}$, since this will just shift the reversible energy scale of the distribution, which is taken care of by other modelling parameters to be described later. This distribution primarily represents the irreversible part p_i of the material as only units with $g_c = 0$ are completely reversible. To allow for part of the transition being reversible, a reversible contribution p_r is

added to the distribution, which has not been done in magnetocalorics before this work[1],

$$p(g_u, g_c) \propto p_i + p_r \tag{2.25}$$

$$p(g_u, g_c) \propto \frac{1 - f_r}{\left[1 + \left(\frac{g_u - g_{u,0}}{\sigma_u}\right)^2\right] \cdot \left[1 + \left(\frac{g_c - g_{c,0}}{\sigma_c}\right)^2\right]} + \delta(g_c) \frac{f_r}{1 + \left(\frac{g_u}{\sigma_{u,r}}\right)^2} \tag{2.26}$$

where the distribution is normalized such that f_r represent the reversible fraction of the contribution and δ is the delta function.

Determination of the distribution of bistable units can be done experimentally, as suggested by Mayergoyz [1985]. This approach requires a lot of experimental data and good resolution in both temperature and field to be applicable. This method is not used in this work.

Determining material properties

The Preisach model keeps track of the history dependent mixed phase state of the material through the state transition line $b(g_c)$. When the state transition line is known, the fraction of the material being in the FM-phase X is

$$X = \int_0^\infty dg_c \int_{-\infty}^{b(g_c)} p(g_u, g_c) dg_u \,. \tag{2.27}$$

The assumption is now that the fraction of the material in the FM phase behaves like a pure FM material and the remaining fraction in the PM phase behaves like a pure PM material. The bulk behavior of the mixed phase state then follows as

$$Y(Z) = XY_1 + (1 - X)Y_0 \tag{2.28}$$

where Y represents some phase dependent material property, such as entropy or magnetization. The subscripts 0 and 1 represent the material property in the pure PM and FM phase, which both have to be known in order to apply the model. In the case of MCMs, this is done experimentally. Characterization through magnetometry and calorimetry in the low temperature FM range and high temperature PM range provides the information required.

Entropy production

The Preisach approach gives a straight forward way of characterizing the heat generation (or entropy production) during transformations of any kind. This is

[1] The first results using this approach are published in von Moos et al. [2014a].

not in general a trivial problem. As described previously, the hysteretic losses are described as the enclosed area within a closed isothermal hysteresis loop. This only provides information about the loss in this particular isothermal cycle. However, in an AMR type cycle there is no isothermal transformations, but both adiabatic and isofield transformations in field and temperature. It is not obvious how these are related. This problem is handled by the individual bistable units used in the Preisach model.

Considering the bistable unit in Fig. 2.6a, a cyclic variation of the field Z, tracing the whole hysteresis loop, encloses the area

$$Q^1_{cycle} = \alpha^1 - \beta^1 = 2g^1_c \tag{2.29}$$

with the superscript representing that we are dealing with just one unit with a specific g_c value. Assuming that a phase transition from either phase to the other is symmetric[Mayergoyz, 2003], the dissipated energy during a single phase switch is

$$Q^1_{switch} = g^1_c \,. \tag{2.30}$$

This means that under any transformation, the energy dissipated as heat is the sum from each bistable unit that switched phase, weighted by the distribution function

$$Q_h = \iint_S p(g_u, g_c)\, g_c \, dg_u \, dg_c \tag{2.31}$$

where S is the region of switched units. Fig. 2.10 illustrates the switching of units and change of the state line due to the change from $Z_2 \to Z_1$. The (g_u, g_c) space S of switched units is marked by red and the state line $b(g_c)$ is seen to change from completely straight to having a kink between two linear segments. By keeping track of the region S during a variation of Z, the dissipated heat can be calculated from Eq. (2.31) with no need of imposing cyclic loop behavior.

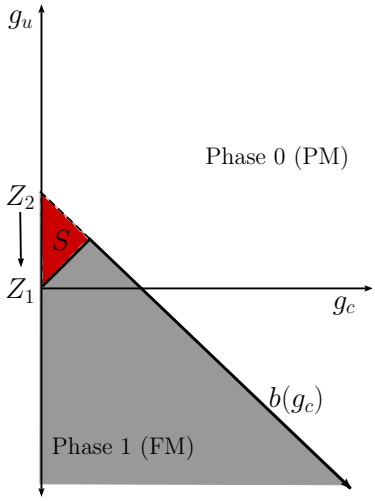

Figure 2.10: The part of the Preisach plane containing bistable units that switched phase during a change from Z_2 to Z_1, causing hysteretic heat production.

Adiabatic transformations

When modelling MCMs undergoing AMR-like cycles one of the purposes is to determine the adiabatic temperature change ΔT_{ad}. For second order materials the equilibrium thermodynamic framework can be used. However, for first order materials with hysteresis this is no longer the case. In the following this calculation process within the Preisach modelling framework is described, following a similar approach as described in Basso et al. [2006a].

The entropy $S = S_H + S_T$ of a material is assumed to consist of a contribution related to the magnetic properties $S_H(H,T)$ and a strictly temperature dependent part $S_T(T)$. If the system undergoes a change, the total entropy change dS is

$$dS = dS_e + dS_i \tag{2.32}$$

where dS_e is the exchange with the environment and dS_i the internal entropy production due to dissipation, which is always positive. During the magnetization or demagnetization step in an AMR-cycle the material temperature changes, under conditions which are here assumed completely adiabatic for the duration of the magnetic field change. This means that $dS_e = 0$ and there is an entropy

exchange between the thermal and magnetic parts that needs to fulfill

$$dS = \frac{\partial S}{\partial H} dH + \frac{\partial S}{\partial T} dT = dS_i \,. \tag{2.33}$$

The entropy dependence on field and temperature are inferred from experiments and by applying Eq. (2.27) and Eq. (2.28). The entropy production term from any transformation dS_i follows from Eq. (2.31) and depends on the temperature, the field and the changes in both.

It is important to note that when the above transformation is carried out in practice due to a change in H and T, the corresponding change in Z should happen monotonically [Basso et al., 2008c]. Non-monotonic change in Z during a single transformation would induce non-physical partial loop behavior in the material.

2.3 Summary

In this chapter the fundamental concepts of the conventional magnetocaloric effect were presented. This was done on the standard foundation of equilibrium thermodynamics to illustrate the general approach to describing the MCE. It was demonstrated that in the presence of hysteresis in first order materials, a non-equilibrium approach is needed to sufficiently describe the transformations taking place in an AMR type cycle. Such an approach was presented through a Preisach type model that can handle any kind of irreversible and reversible transformations related to the application of magnetocaloric materials.

Part II

Experimental equipment and procedures

Chapter 3

Calorimetric characterization

In the following chapter the equipment used for all calorimetric measurements in this work will be presented. The focus here is to discuss the applied experimental procedures in general and not to present experimental results, as they are presented in the dedicated material chapters 5 and 6. The primary focus is the differential scanning calorimeter (DSC) custom build at DTU Energy, which has been used for most of the calorimetric experimental work. The different procedures for calibration of the device and data analysis are described and a simple thermal model is presented to give a more direct understanding of the thermal properties of the DSC and how they affect the data analysis. The second part of this chapter describes other instruments used for calorimetric measurements: a commercial DSC used for a small series of measurements and devices to directly measure the isothermal entropy change Δs and adiabatic temperature change ΔT_{ad} following an applied magnetic field change.

3.1 The DTU DSC

One of the standard ways of characterizing magnetocaloric materials (MCMs) is by determining the heat capacity. Through this the entropy can be calculated and the magnetocaloric effect (MCE) indirectly estimated, as described in section 2.1. There exists a variety of different calorimeters, but they generally measure the

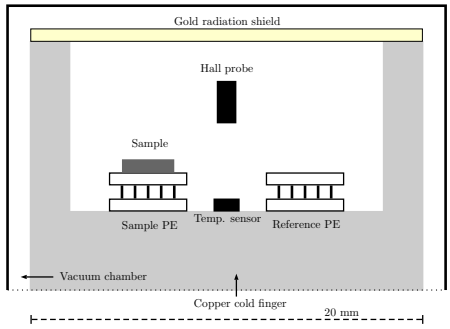

(a) Illustrated side view. Not to scale.

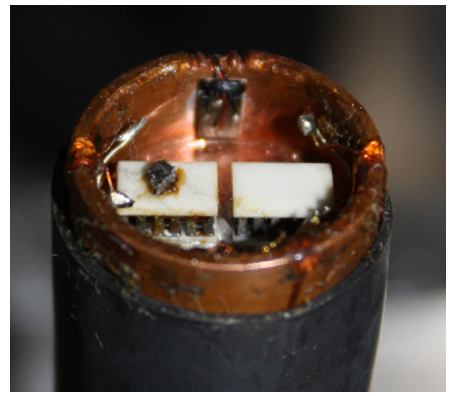

(b) Picture of the DSC, without the radiation shield and vacuum cover.

Figure 3.1: The custom build DSC

heat flux $\dot{Q}$ (in watts) to or from a sample under dynamic conditions, from which the heat capacity can be deduced. Knowing $\dot{Q}$, the heat capacity C follows as

$$C_x = \left(\frac{\delta Q}{dT}\right)_x = \left(\frac{\delta Q/dt}{dT/dt}\right)_x = \left(\frac{\dot{Q}}{R}\right)_x \tag{3.1}$$

given that the rate of change of the temperature $R = dT/dt$ is known. This is the case in scanning calorimeters where the temperature of the system is scanned in either a cooling or heating mode with a known rate. The subscript x signifies which intensive variables are constant. In this work experiments are always done under constant pressure and magnetic field conditions.

The DSC used in this work is a heat flux calorimeter, utilizing Peltier elements (PE) as heat flux sensors, that was custom build as part of a PhD project in 2008. The original documentation can be found in Jeppesen [2008, Ch. 5] and Jeppesen et al. [2008]. The current instrument is functioning as the original, but both PEs and temperature sensors have since been changed. The specifications are given in the following, along with an overview of the instrument and the data analysis procedure.

The sample area of the instrument is shown in Fig. 3.1. Two separate PEs are mounted with thermal adhesive on a copper surface in the sample chamber. The properties of the heat flux PEs are given in Table 3.1. The copper chamber acts as a cold finger, which can be temperature controlled by a large PE (not shown in the figure) in a range between 230-320 K. The temperature controlling PE is coupled to a Julabo CF40 thermal bath, which cycles a coolant at around -20C to

the PE cold side. When experiments are carried out, the whole system is enclosed in a vacuum with pressure $p < 10^{-5}$ mbar, which is low enough the eliminate conductive and convective heat transfer to the air in the sample chamber (see section 3.1). A Pt100 thermoresistor and a Hall probe are installed on the copper base along with the PEs, to measure the chamber temperature and magnetic field, respectively. The magnetic field is controlled by two concentric, cylindrical Halbach permanent magnets, placed around the cold finger. This setup can provide an applied magnetic field between 0 and 1.5 T, which can be gradually controlled [Bjørk et al., 2010a]. The sample is mounted on the sample PE with a small amount of Apiezon H-grease to ensure good thermal contact. Sample sizes generally range between 10-60 mg.

When the thermoelectric material in a PE is submitted to a temperature difference ΔT, a voltage drop U is induced across the hot and cold side

$$U = S\Delta T \tag{3.2}$$

with S being the intrinsic Seebeck coefficient. During an experiment the system temperature is changed at a constant rate R, which is user controlled. This leads to a thermal energy transfer $\dot{Q}$ through the PE, on top of which the sample is located. Since the experiments are carried out in a vacuum the temperature profile through the PE is governed by conduction (ignoring radiative losses)

$$\dot{Q} = -Ak_p \frac{\partial T}{\partial x} \tag{3.3}$$

where A is the heat transfer area and k_p the thermal conduction coefficient of the PE. If a steady and linear temperature profile is assumed, this can be approximated by

$$\dot{Q} \approx -\underbrace{\frac{Ak_p}{H_p}}_{\kappa} \Delta T \tag{3.4}$$

where κ is the absolute thermal conductance and H_p the height of the PE. Applying Eq. (3.2) and (3.4) to (3.1), the heat capacity of the sample and PE system is

PE type	PELTIER OT08,11,F1,0305,11,W2.25
Dimensions, LxWxH	4.88mm x 3.25mm x 2.44mm
$\dot{Q}\text{max}@T_h$	0.6W @ 25°C
$\Delta T_{\text{max}}@T_h$	67°C @ 25°C
Ohmic resistance	1.43 Ω @ 25°C
Thermal conductance ($\kappa = \dot{Q}\text{max}/\Delta T_{\text{max}}$)	$9 \cdot 10^{-3}$ W/K

Table 3.1: Peltier element specifications

given as

$$C(T) = \frac{\kappa}{S}\frac{U}{R} \tag{3.5}$$

where the PE parameters need to be determined from calibration measurements.

Calibration

In order to obtain experimental data with correct values, a series of calibration procedures are required. For this particular device the PE parameters (S and κ) and thus the heat flux need to be calibrated to a known sample in order to obtain absolute heat capacity values. Furthermore the temperature scale needs to be calibrated, since the thermoresistor and the sample are not located at the same position in the sample chamber. The following two sections will describe these procedures as they were carried out in this project.

Heat flux calibration

To obtain the actual heat capacity of an unknown sample, a 3-step procedure is employed, where the investigated sample, a known reference sample and an empty PE signal are measured. This is a standard method and it is described detail in Höhne et al. [2003].

As in all DSCs, the relevant measured signal is the difference between the signal from the sample PE, U_s, and the empty reference PE, U_r, hence the name differential calorimetry. The voltage difference $\delta U_s = U_s - U_r$ then only shows a sample-related signal with the influence of the PE subtracted. In principle, this also eliminates potential thermal disturbances in the system since they would influence both PEs equally. However, this relies on perfect thermal symmetry, which cannot be assumed. To correct for any asymmetries, a measurement of the voltage difference between the reference PE and the sample PE, δU_0, where no sample but only a small amount of thermal grease is placed. This procedure modifies Eq. (3.5) to

$$C(T) = \frac{\kappa}{S}\frac{\delta U_s}{R} - \frac{\kappa}{S}\frac{\delta U_0}{R}\,. \tag{3.6}$$

In order to eliminate the unknown PE parameter S and the temperature dependence of κ, a known reference sample is measured. Here a high purity 99.999%(trace metal basis) Cu sample is used, where the temperature dependent heat capacity is well documented in literature [White and Collocott, 1984]. By measuring the reference Cu sample voltage δU_r at a temperature rate R, the unknown parameters can be obtained from Eq. (3.6) and the reference table

values c_r

$$c_r(T) = \frac{1}{m_r}\frac{\kappa}{S}\left(\frac{\delta U_r(T)}{R} - \frac{\delta U_0(T)}{R}\right)$$
$$\frac{\kappa}{S} = c_r(T)\frac{m_r\, R}{\delta U_r(T) - \delta U_0(T)} \tag{3.7}$$

where m_r is the reference sample mass. The specific heat capacity of an unknown sample c with mass m_s is then obtained by applying Eq. (3.6) and Eq. (3.7)

$$c(H,T) = \frac{m_r}{m_s}\frac{\delta U_s(H,T) - \delta U_0(T)}{\delta U_r(T) - \delta U_0(T)}c_r(T) \tag{3.8}$$

where H is the constant applied magnetic field. The reference measurements are independent of the magnetic field and the temperature rate is assumed equal in all measurements.

Temperature calibration

The temperature of the system is measured by the sensor located directly on the copper base in the sample chamber, as shown in Fig. 3.1. Since we are interested in the temperature at the sample position, on top of the PE, a temperature calibration is required. The temperature experienced by the sample is expected to be different from the measured temperature due to several reasons:

- Thermal lag - when the temperature of the copper is changed it takes some time before this change is seen by the sample due to the conduction time and thermal mass of the PE.
- Thermal contact resistance - Both the temperature sensor and the PE are mounted on the copper with thermally conductive adhesive. The sample itself is also mounted on the PE with thermal grease, however there will always be some thermal contact resistance between the interfaces.
- Thermal asymmetry - As the thermoresistor and the PE/sample are not placed at the same position there will be temperature variation due to temperature gradients in the system and different thermal losses.

The calibration procedure used here is outlined in detail in Höhne et al. [2003]. The principle is to use a substance with a well defined solid to liquid phase transition temperature T_t. The measured rate dependent transition temperature $T_e(R)$ can then be compared to the actual transition temperature T_t. A high purity 99.99999% (trace metal basis) gallium (Ga) sample is used, which has a

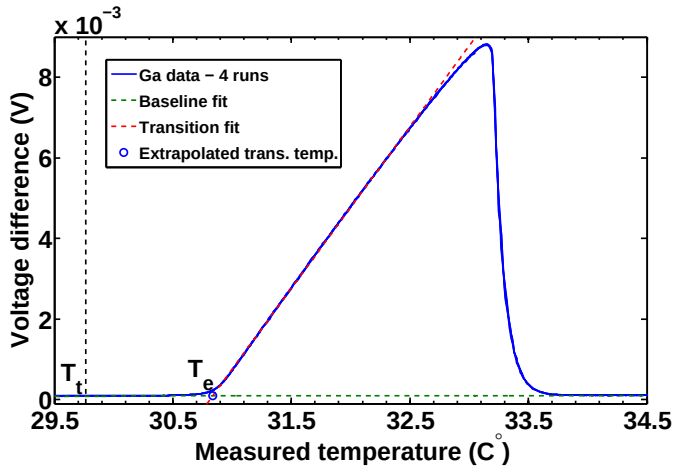

Figure 3.2: Four consecutive 1 K/min heating scans of the melting of high purity gallium (Ga). The onset of the measured transition temperature T_e is defined as the intersection between the linear fits of the baseline and transition signals. The real transition temperature T_t is shown as a vertical line.

well defined melting point at $T_t = 29.74$°C. Unfortunately Ga supercools and the solidification temperature is not well defined. This means that the calibration can only be done in a heating mode and a symmetric cooling calibration has to be assumed. It is optimal to calibrate with several different materials that cover the entire temperature range of the DSC, but Ga is the only suitable substance in our given range. Water unfortunately experiences the same problem in terms of potential supercooling, depending on the purity. Furthermore there is inherent problems with carrying out experiments with water in vacuum conditions. Measurements could of course be done under ambient pressure, but this will alter the conditions between calibration and sample experiments.

Fig. 3.2 shows a series of 4 consecutive heating scans from 0 to 40°C at $R = 1$ K/min. The onset temperature of the phase transition T_e is extrapolated from the intersection of linear line fits to the baseline voltage and the transition slope. The actual transition temperature is shown as a vertical line. It is important to note that this extrapolated transition onset temperature is generally a good way to define the transition temperature when applicable. Both the peak top and the transition end temperatures dependent on the thermal properties of the sample: thermal conductivity and thermal mass.

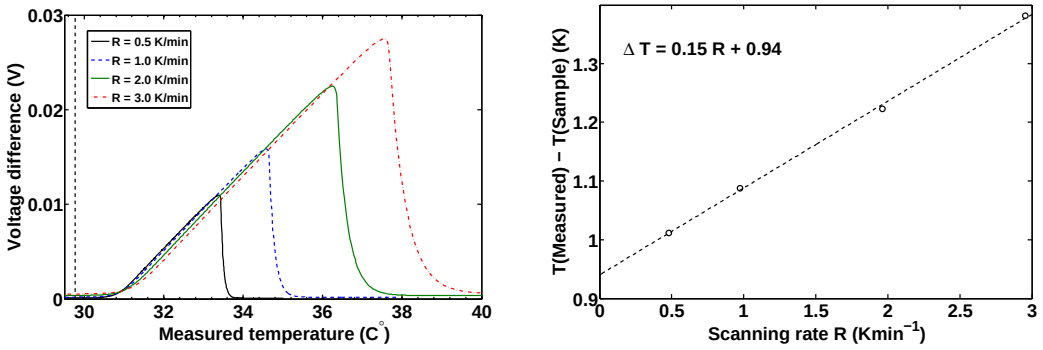

(a) (b)

Figure 3.3: (a) Measurement of the melting of Ga at different temperature scanning rates. (b) A linear fit to the rate dependent temperature offset.

This experiment was carried out at rates 0.5, 1, 2, and 3 K/min and T_e determined at each rate. These results are shown in Fig. 3.3. The measured transition temperature T_e is approximately linear in the rate R

$$T_e(R) = T_e(0) + \frac{dT_e}{dR} R \,. \tag{3.9}$$

The system temperature correction is found by linear regression, as shown in Fig. 3.3

$$\begin{aligned} \Delta T_c(R) = T_e(R) - T_t &= (30.71^\circ\mathrm{C} + 0.15\mathrm{s}\, R) - 29.76^\circ\mathrm{C} \\ &= 0.94^\circ\mathrm{C} + 0.15\mathrm{s}\, R \,. \end{aligned} \tag{3.10}$$

This leads to a rate correction between the measured temperature T_m at rate R and the actual sample temperature T_s,

$$T_s = T_m - \Delta T_c(R) = T_m - 0.94\mathrm{K} - 0.15\mathrm{s}\, R \,. \tag{3.11}$$

In equilibrium, the extrapolation suggests that the sample is approximately 1 K cooler than the copper base. At 30°C this makes sense, since the surroundings will be colder than the copper base. A decreasing thermal gradient is created along the height of the cold finger, resulting in a thermal loss from the sample to the surroundings. However, the absolute offset will probably change sign when moving from warmer to colder temperatures, where the copper base becomes cooler than the surroundings. This was not investigated further during this work, but should

be considered in the future. In practice it means that the temperature scale can be 1-2 K offset in the positive direction in the low temperature range. This can come into play, when comparing material characterizations between instruments. In terms of characterizing thermal hysteresis it does not matter since only the temperature differences are relevant and the thermal losses are not expected to vary significantly over the thermal hysteresis range (around 1-5 K).

Eliminating conductive losses

The main heat leak from the sample would be through conduction and convection to the surrounding air, which is why experiments are carried out in a vacuum. The critical pressure to eliminate these effects depends on the system geometry. In the continuum gas regime, the thermal conductivity of a gas is independent of pressure, since the number density of molecules increases linearly with pressure, but the mean free path decreases inversely with pressure [Reif, 1965]. Thus the thermal transfer through molecular collisions is unchanged. However, by decreasing the pressure enough, the mean free path will be limited by the length scale of the instrument and further pressure decrease will only decrease the molecular density and by that the thermal conductivity. Figure 3.4 shows the measured thermal equilibrium voltage at different pressures. The results show that at pressures below 10^{-4} mbar, convective and conductive thermal losses are eliminated. As experiments are carried out in pressures between 10^{-5} to 10^{-6} mbar, these losses can be ignored.

A thermal DSC model

The thermal coupling between the measured PE voltage and the thermal properties of the sample is discussed in a bit more detail in this section through solving the heat equation. This approach perhaps provides a more straightforward understanding of the system.

To discuss the coupling between the thermal properties of the sample and the DSC signal the 1D heat equation can be considered,

$$\rho c \frac{\partial T}{\partial t} = \frac{\partial}{\partial x}\left(k(x,T)\frac{\partial T}{\partial x}\right), \tag{3.12}$$

where ρ, c and k are the density, heat capacity and thermal conductivity, respectively. When a temperature scan is initiated, the system will set up a temperature profile. We are assuming a system with no heat generating sources(so ignoring any MCE that might occur), which then must imply that the system settles at a constant temperature profile shape. This means that all parts of the system

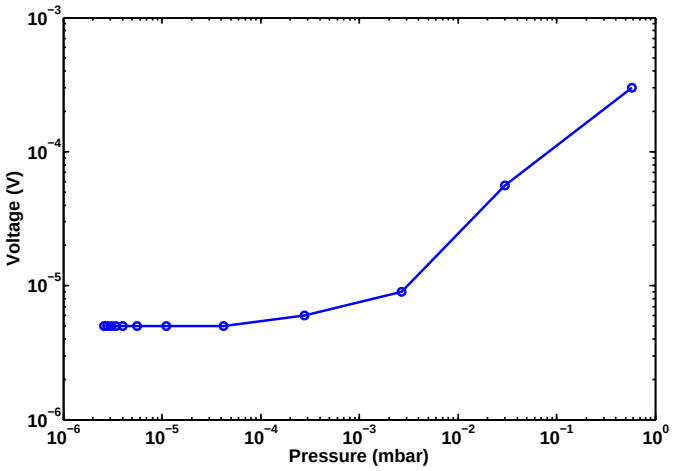

Figure 3.4: The voltage across the sample Peltier element with varying sample chamber pressure, measured at 20°C.

have to change temperature at the same rate R when the steady state is reached. Applying this condition to the heat equation and assuming constant conductivity one gets

$$\frac{\partial^2 T}{\partial x^2} = \underbrace{\frac{\rho c R}{k}}_{B} . \tag{3.13}$$

For a single homogeneous material, the solution is obtained by direct integration as

$$T(x) = \frac{B}{2}x^2 + C_1 x + C_2 \,, \tag{3.14}$$

where the constants C_1 and C_2 are determined by boundary conditions.

The DSC is a composite system consisting of the PE and the sample. The material parameters $\rho(x)$, $c(x)$ and $k(x)$ become position dependent in a stepwise manner and therefore Eq. (3.14) needs to be solved for 2 different cases,

$$T_p(x) = \frac{B_p}{2}x^2 + C_{p1}x + C_{p2} \,, \qquad 0 \le x \le H_p \tag{3.15}$$

$$T_s(x) = \frac{B_s}{2}(x - H_p)^2 + C_{s1}(x - H_p) + C_{s2} \,, \qquad H_p \le x \le H_p + H_s \tag{3.16}$$

where the subscripts p/s represent the constants related to the PE and sample, respectively, and H_p and H_s are the PE and sample heights, respectively. It

should be noted that this is not strictly correct, since k is no longer constant with x. However, the extra term one gets from the product derivative can be seen a thermal contact resistance, which is included below. The coefficients are determined by the external boundary conditions

$$T_p(0) = T_c\,, \qquad 0 = k_s \frac{dT_s}{dx}\bigg|_{H_p+H_s} \tag{3.17}$$

stating that the bottom of the PE has the same temperature as the copper bath T_c (no thermal contact resistance at the base) and there are no heat losses from the top of the sample to the surroundings. Assuming a thermal contact resistance R_t between the top of the PE and the sample, conservation of the heat flux requires

$$-k_p \frac{dT_p}{dx}\bigg|_{H_p} = -\frac{T_s(H_p) - T_p(H_p)}{R_{tc}}\,, \qquad k_p \frac{dT_p}{dx}\bigg|_{H_p} = k_s \frac{dT_s}{dx}\bigg|_{H_p}\,. \tag{3.18}$$

The coefficients can be shown to be

$$C_{p2} = T_c \tag{3.19}$$

$$C_{s1} = -B_s H_s \tag{3.20}$$

$$C_{p1} = \frac{k_s}{k_p} C_{s1} - B_p H_p = -\frac{k_s}{k_p} B_s H_s - B_p H_p \tag{3.21}$$

$$C_{s2} = R_t k_p (B_p H_p + C_{p1}) + \frac{1}{2} B_p H_p^2 + C_{p1} H_p + C_{p2} \tag{3.22}$$

It follows from the coefficients that the temperature difference between the copper base and the bottom of the sample is $\Delta T_s = T_s(H_p) - T_c$

$$\Delta T_s = -\underbrace{\frac{\rho_p c_p H_p^2}{2k_p}}_{\tau_p} R - \underbrace{\frac{R_{tc}}{A_s}}_{R_i} \overbrace{A_s H_s \rho_s}^{m_s} c_s R - \underbrace{\frac{H_p}{A_s k_p}}_{R_p} A_s H_s \rho_s c_s R \tag{3.23}$$

$$= -\tau_p R - m_s c_s R_p R - m_s c_s R_i R \tag{3.24}$$

where τ_p, R_i and $R_p = 1/\kappa$ denote the characteristic conduction time, the absolute thermal resistance of the PE/sample interface and the absolute thermal resistance of the PE. This expression shows that the temperature seen by the sample lags behind the copper base due to i) the thermal mass and finite conduction time of the PE (first term), ii) the thermal resistance of the PE (second term), iii) and the thermal contact resistance between the sample and the PE surface (third term). The temperature lag is linear with the temperature scanning rate R.

The above expression should be compared to the temperature difference seen by the PE, $\Delta T_p = T_p(H_p) - T_c$, which will be represented by the measured voltage.

This difference will only have the two first terms of Eq. (3.24), meaning that the sample temperature is different from the that of the corresponding PE signal. When a differential signal is considered, the first term is eliminated. Through the heat flux calibration the unknown constants are eliminated and through the temperature calibration, the offset between the PE and sample temperature is corrected. In the end one obtains an expression equivalent to the original approach leading to Eq. (3.8).

3.2 The PerkinElmer DSC

As part of this work, a series of DSC experiments were carried out at INRIM in Torino, Italy. The device used for this work is a commercial PerkinElmer Diamond DSC. This device is a power compensation calorimeter that utilizes furnaces to maintain a given temperature in the sample and reference chambers. The heat flux to a sample is measured directly as the electrical power needed to maintain a certain temperature in the furnace. A thermometer is placed right below the furnace bottom, directly underneath the sample holder, which gives the approximate sample temperature. The sample is placed in an aluminum pan with an aluminum lid. An empty pan with lid is placed in the reference chamber. The heat capacity of a sample is then calculated from the differential heat flux between the sample and reference chambers. This can either be done by continuous scanning a temperature range at a given rate, or by step scanning where the heat capacity is measured at a certain temperature from the dynamic response to a fast and small step wise temperature change. The step scan procedure is rate independent, but is also very time consuming due to the complete thermal relaxation that needs to take place between each temperature step. Besides the way of obtaining the heat flux to the sample, the general procedure for calculating the heat capacity is the same as outlined in the introduction of this chapter.

Thermal contact resistance

When the sample chamber receives the heat flux $\dot{Q}$ at some chamber temperature T_0, the sample will have slightly different temperature, due to the thermometer being placed beneath the sample and non-perfect thermal contact between chamber/sample-pan and sample-pan/sample. The contact resistance can be estimated through Fourier's law, Eq. (3.4), applied across the thermal contact interface

$$T_s - T_0 = -\underbrace{\frac{\delta x}{k\,A}}_{R_{th}}\,\dot{Q} \tag{3.25}$$

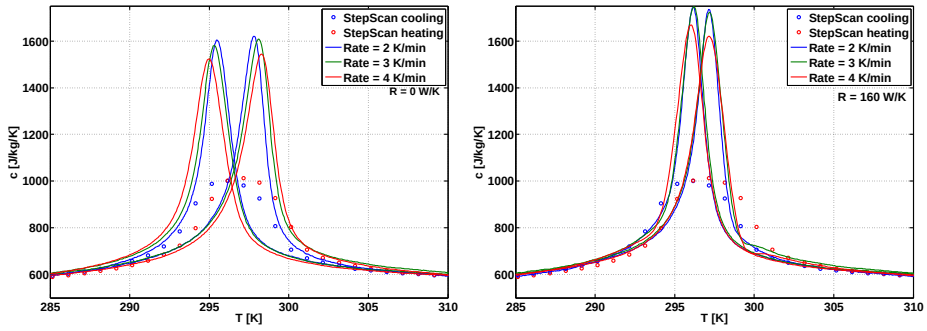

Figure 3.5: Determination of thermal contact resistance R through measurements of MnFe(P,As) at rates of 2, 3 and 4 K/min.

where R_{th} represent a thermal resistance and T_s and T_0 the sample and chamber temperatures, respectively. The corrected rate-independent calculation of heat capacity is then

$$c_p(T_s) = \frac{1}{m}\frac{\dot{Q}}{\dot{T}_s} = \frac{1}{m}\frac{\dot{Q}}{R - R_{th}\,\ddot{Q}}\,. \tag{3.26}$$

The fact that there is practically no thermal mass between the sample and the thermometer, but only a thermal contact resistance, makes the thermal analysis much simpler than that of the DTU DSC, described in section 3.1.

The determination of the thermal resistance is done by measuring a material at different rates. In Fig. 3.5 an example is shown for a sample of MnFe(P,As), a first order magnetocaloric material, which is discussed in further detail in chapter 6. The solid lines show the scanning experiments at the different rates of 2, 3 and 4 K/min. The dots show data points for a step-scan procedure, which are rate independent. With a fitted thermal contact resistance of 160 W/K all curves collapse onto each other making the results approximately rate independent.

3.3 Characterizing the transition

In many DSCs, as the ones used in this work, the measured heat flux curves will depend not only on the heat capacity of the sample, but also the sample mass and thermal conductivity. The characteristic conduction time through a sample with height H, thermal mass $m\,c$, thermal conductivity k ans thermal contact area A is $\tau \propto mcH/(Ak)$ (see section 3.1). Having a low thermal conductivity or high mass will require more time to complete a transition, resulting in an apparent broadening of the transition temperature range in a continuous scanning

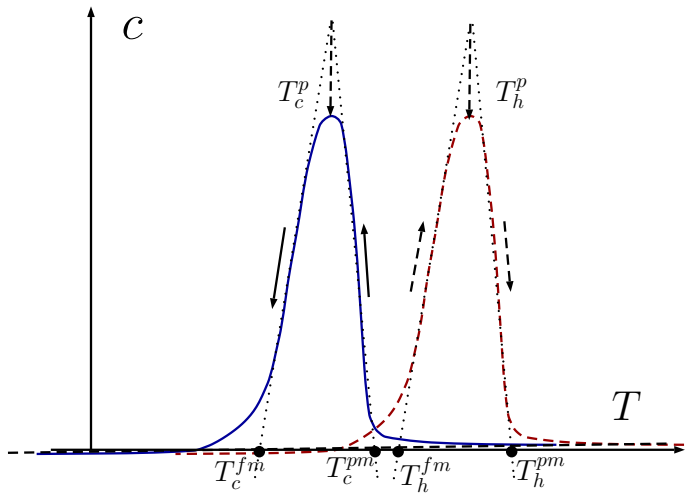

Figure 3.6: Illustration of a set of heat capacity curves obtained during heating and cooling modes on a hysterestic first order material.

mode. The actual width of the transition due to the intrinsic material properties is then convoluted with these experimental effects. For both first and second order materials this can also cause a separation of the heating and cooling mode curves, showing an apparent thermal hysteresis that might not exist.

In Fig. 3.6 an illustration of a heat capacity measurement on a hysteretic first order material is shown. Here a transition between a low temperature FM state and a high temperature PM state is considered in the presence of thermal hysteresis. The two curves represent the measured heat capacity in a heating (red) and cooling (blue) mode. The transition can be characterized by three temperatures, in both the heating and cooling mode: the transition onset temperature (T_h^{fm}/T_c^{pm}), the transition end temperature (T_h^{pm}/T_c^{fm}), and the peak maximum temperature (T_h^p/T_c^p). In the figure these temperatures are shown for both curves, with the superscript fm and pm referring to the current phase, p to the peak temperature and the subscripts h/c the heating or cooling modes, respectively.

In an ideal scenario where all sample and experimental properties are filtered from the resulting heat capacity curves (mass, thermal conductivity, scanning rate

etc.), the thermal hysteresis is given by any of the three temperature differences,

$$\Delta T_{\text{hyst}} = T_h^{fm} - T_c^{fm} = T_h^{pm} - T_c^{pm} = T_h^{p} - T_c^{p} \tag{3.27}$$

In practice it can be difficult to obtain values for any of these sets of temperatures that are independent of experimental conditions. Both a large sample mass and a high scanning rate will not influence the onset temperatures much, but will separate both the peak and end-of-transition temperatures further, meaning that Eq. (3.27) will generally overestimate the thermal hysteresis. Ideally, one would want to use the lowest possible rate and mass when using the DSC method on first order materials. However, this will increase the noise and the measuring time significantly. As was illustrated in Fig. 3.5 these effects are present even for the relatively low scanning rates used in this work.

In practice, the determination of the onset and end of transition temperatures might not be so obvious, depending on the shape of the peak. If it is possible, one can determine the transition onset temperatures in both the heating and cooling mode T_c^{pm}/T_h^{fm}, which are relatively independent of sample properties and can be calibrated to be independent of rate (sec. 3.1). However, the two onset temperatures do by themselves not provide information about the thermal hysteresis. The corresponding transition end-temperatures are required as well, but they both depend on the particular sample used, making Eq. (3.27) prone to error. Often the peak temperatures T_h^p/T_c^p are used to characterize the transition temperature, since the peak maximum is straight forward to define. One should just note that both the temperature scanning rate and the sample's thermal properties will influence the peak temperature position. This will generally lead to an artificially large observed thermal hysteresis, as all these effects push the peaks apart.

3.4 Direct MCE measurements

Direct measurements of the MCE have been more utilized in recent years due to developments in equipment. They offer a direct way of characterizing both the adiabatic temperature change ΔT_{ad} and the isothermal entropy change Δs, without having to rely on estimates deduced indirectly from magnetization or heat capacity data. In the following two instruments currently under development are described.

Direct isothermal entropy measurements

The DTU DSC device described in section 3.1 can be utilized to measure the isothermal entropy change directly. The procedure and the application is briefly

described in Nielsen et al. [2014] (This paper is coauthored by the thesis author and is provided in appendix E) and a detailed description of a similar instrument can be found in Basso et al. [2008a].

The basic idea is to use the PE of the DSC to measure the total heat flux to/from a sample when changing the applied magnetic field. The system temperature is kept constant under these experiments, as opposed to the scanning mode of the DSC experiments. The magnetic field is changed and the temperature change induced in the sample results in a heat flux from the sample through the PE. A time integration of the heat flux is then a measure of the total thermal energy released by the sample

$$Q(H_i; H_f, T) = \int_0^t \dot{Q} dt' \tag{3.28}$$

where H_i and H_f are the initial and final applied magnetic fields. The isothermal entropy change per sample mass m is found "directly" as

$$\Delta s(H_i; H_f, T) = \frac{1}{m} \frac{Q}{T} . \tag{3.29}$$

Of course these are not perfect isothermal conditions, by definition. However, as the sample temperature changes upon magnetization is of the order of degrees, the deviation is negligible as measurements are done around room temperature. The advantage of this approach is that the total thermal energy produced is measured, including hysteretic energy production.

Direct adiabatic temperature change measurements

A series of experiments were performed on a custom build direct ΔT_{ad} measurement device, under development at the time of this work. It is designed to measure the temperature of the sample through an IR sensor, thus limiting thermal contact and thermal resistance through attached thermocouples. However, the full capability of the device was not available at the time these experiments were done, requiring the use of thermocouples to measure the sample temperature.

Figure 3.7 shows a picture of the experimental setup. The sample is placed in a cup-shaped brass sample holder, in which the bottom is covered by isolating material to ensure that the sample is not in direct contact with the brass. The sample holder is connected to a copper cold-finger, which is connected to a user controlled Julabo CF40 thermal bath. The whole setup is placed in a high vacuum chamber, $p < 10^{-4}$ mbar, where convective and conductive thermal transfer through the air surrounding the sample is removed. The sample is thermally connected to the system through contact with the isolating material, which is needed to control the sample temperature in a reasonable time frame.

Figure 3.7: Picture of the ΔT_{ad} device. A thermocouple is sandwiched between two sample pieces. The sample is placed on an isolating material in the sample holder, measuring approx. 1 cm across. Under experimental conditions the sample system is enclosed in a vacuum.

The sample temperature is monitored by a directly attached E-type thermocouple. The thermocouple is sandwiched between two solid pieces of material, using a small amount of Arctic Silver thermal adhesive made with 99.8% pure micronized silver. The thermal mass of the sample is much larger than that of the thermocouple and the thermal adhesive. The magnetic field is controlled by two concentric, cylindrical Halback permanent magnets, placed around the cold finger [Bjørk et al., 2010a]. This setup can provide an applied magnetic field between 0 and 1.5 T, which can be gradually controlled.

3.5 Summary

In this chapter the calorimetric methods used in this thesis were discussed. The DSC devices used and their respective procedures for calibration and data analysis were presented, along with a thermal model to illustrate the thermal lag properties of the system and how they affect measurements. The objective determination of the transition range relating to the phase transition can be non-trivial and can lead to an apparent thermal hysteresis that overestimates the intrinsic material hysteresis. Furthermore two new devices under development were presented. These are used to directly measure the adiabatic temperature change and the isothermal entropy change, which can be compared to often used indirect methods.

Chapter 4

Magnetization measurement procedures

The purpose of this chapter is to discuss the different methods of characterizing magnetocaloric materials (MCMs) through magnetometry. Both isothermal magnetic field scans and isofield temperature scans are often used to characterize the phase transition and the corresponding magnetocaloric effect (MCE), which is also the case in this work. When measuring hysteretic materials, one needs to keep track of the thermal and magnetic history in order to know what exactly has been measured. If these conditions are not taken care off, one can end up measuring magnetic states that do not correspond to the desired ones and comparison of data and estimates of the MCE become complicated. Measuring magnetization is often done on standard equipment with standard procedures that might not be suitable for measuring hysteretic MCMs by default. Here it is illustrated that especially rates of ramping temperature and magnetic field can cause problems in measurements due to both the MCE and the history dependence of hysteretic materials.

In this work a LakeShore 7407 Vibrating Sample Magnetotometer (VSM) is used. The basic principle of a VSM is that a magnetic sample is placed in a uniform magnetic field, which will magnetize the sample. The sample is vibrated vertically, creating a changing magnetic flux in the vicinity of the sample due to its induced magnetic moment. This change in magnetic flux induces a voltage in

two pickup coils located close to the sample, from which the sample's magnetic moment can be deduced. This particular system uses an electromagnet that can create a magnetic field up to 1.6 T (tesla) when used with a cryostat. The sample environment is cooled by a flow of nitrogen gas that is temperature controlled by a coupled heater.

4.1 Stability and precision of measurements

In order to check the temperature fluctuations in the cryostat and how they affect the magnetization of the sample, the magnetization of a $Gd_5Si_2Ge_2$ sample was measured 2200 times over the duration of 1 hour. The measurements were carried out at a cryostat temperature of 270 K with a constant applied magnetic field of 1 T. Under these conditions the material is in the middle of the first order transition and is sensitive to temperature changes.

Both temperature and magnetization data has been centered and normalized around the time averaged mean, i.e.

$$\tilde{M} = \frac{M(t) - \bar{M}}{\bar{M}}, \quad \bar{M} = \frac{1}{\tau}\int_0^\tau M(t)dt \tag{4.1}$$

and are plotted in figure 4.1 as probability densities, along with the 95% confidence intervals. The temperature is known with 95% confidence to be within $\pm 0.04\%$ around the mean, corresponding to absolute temperature fluctuations of ± 0.1 K.

The temperature dependent magnetization is seen to fluctuate correspondingly little around the mean value. The measured magnetization fluctuates with $\pm 0.07\%$, or ± 0.06 Am^2/kg, around the mean. These small fluctuations are not relevant for this work, and they show that even though the cryostat temperature fluctuates with 0.1 K, the magnetization measurements are not affected.

4.2 Measuring isofield magnetization - Temperature control

This section will describe the problems that can be encountered when changing material temperature through simple thermal considerations and experimental data. The cryostat used in this experimental setup is the Lakeshore 74018. Gas from liquid nitrogen flows past the sample, where the gas temperature is controlled by a heater. The heater power is governed by a standard Proportional-Integral-Derivative controller (PID), which is used for temperature control in many devices.

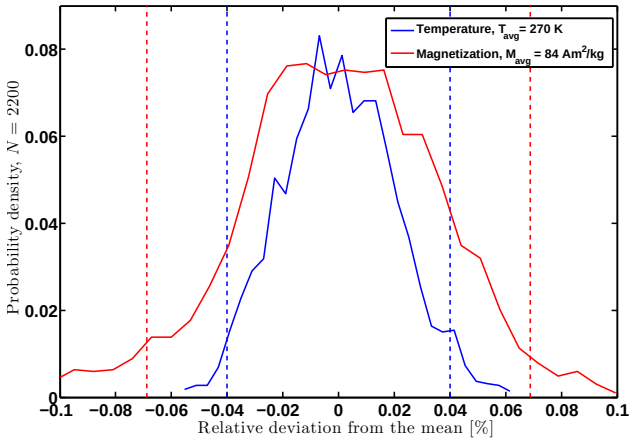

Figure 4.1: Stability and precision of temperature and magnetization measurements on the VSM. The solid lines show the probability distribution of values around their mean, given on a relative scale. The dashed lines represent the 95% confidence interval. Data is taken at constant set temperature over the duration of an hour, corresponding to 2200 data points.

A PID controller manipulates a given variable in order to converge to some set point value (SP). Here, the set point is the desired temperature and the manipulated variable is the heater power, which controls the temperature. The correctional output to the heater $u(t)$ of the PID controller is given by

$$u(t) = k_p E(t) + k_i \int_0^t E(t')dt' + k_d \frac{dE(t)}{dt} . \tag{4.2}$$

The error is the difference between the set point and the present value (PV), $E(t) = SP - PV$, and the parameters k_p, k_i and k_d are the proportional, integral and derivative gains, respectively. Together these determine the path from the present value to the set point. The path, speed and the general precision will depend on the magnitude of each parameter.

An example of a temperature signal is shown in Fig. 4.2, where temperature data obtained from the VSM is used. The default PID settings for this system, $\{k_p, k_i, k_d\} = \{20, 15, 0\}$, are shown as the dashed red line, where a custom and less aggressive control, $\{k_p, k_i, k_d\} = \{4, 1, 0\}$, is shown in solid blue. The dashed black lines show the set points. When the PID control is optimized for speed, one

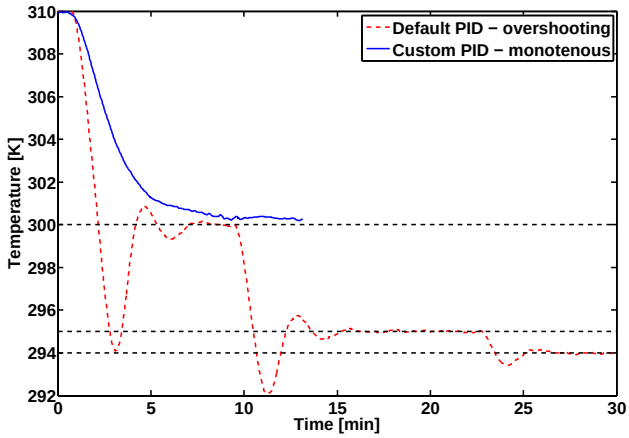

Figure 4.2: Temperature data from the sample environment of the VSM. Oscillations and overshooting are illustrated by the red dashed lines that try to converge to the set points, the horizontal lines. The solid blue curve shows a monotonous convergence towards the set point, with no oscillations or overshooting.

pays with oscillations around the set point and some degree of overshooting[1]. It is noted that the specific temporal temperature profile will vary from system to system and the relevance of overshooting with the specific task.

As hysteretic materials are dependent on both magnetic and thermal history, one has to take care when ramping the temperature and magnetic field in measurements. An illustration of the overshooting problem is shown in Fig. 4.3. The dashed lines represent the ideal magnetization curve at constant field as a function of temperature. Here temperature is increased/decreased monotonously and the phase transition is crossed in a controlled and repeatable way. This procedure characterizes the full thermal hysteresis loop, undergoing a full transition between the PM and FM state. If the temperature control is too aggressive however, one can end up in a situation illustrated by the solid lines. The magnetization is wanted at the set point temperature T_{sp}, but a temperature overshoot of ΔT_s in the sample takes place. Due to the irreversibility of the material, the descending magnetization return branch will generally not coincide with the ascending branch. The material will have been pushed further in to the transition, becoming

[1]The term overshooting will be used for both temperatures that go below and above the set point, depending on the ramping direction, and will refer to the first peak of the oscillation (i.e. Fig. 4.2, between time 0-5 min).

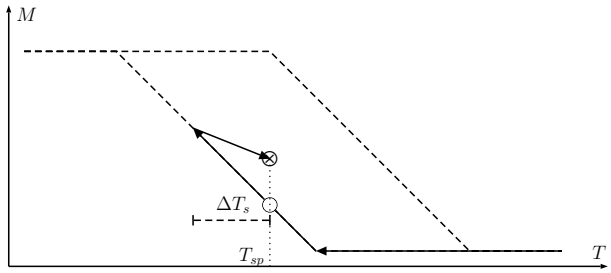

Figure 4.3: Illustration of a magnetization measurement as a function of temperature, at constant applied field. The dashed curves show the complete thermal hysteresis loop, and the solid line show the deviation in magnetization due to overshooting.

more ferromagnetic and one will measure an "artificially" high magnetization (the crossed circle). This will underestimate the thermal hysteresis and destroy the intended thermal history of the material.

It should be noted that similar effects can occur if the magnetic field overshoots during changes. However, magnetic fields are usually more promptly controlled, either through applied currents in electromagnets or by mechanically changing the arrangement of permanent magnets, which will generally not give rise to overshooting. This should of course be checked for any given system.

A simple thermal model

The sample is never in perfect thermal contact with the surroundings, hence it is useful to consider how the actual sample temperature responds to temperature oscillations in the sample environment. Here a simple thermal model is set up to show the general characteristics of the sample response overshooting.

A lumped capacity approach, where any heat transferred is instantly distributed throughout the whole sample, is assumed. The temperature difference between the sample and the surroundings is assumed to be small enough that the heat transfer rate is proportional to the temperature difference,

$$\dot{Q}(t) = C\dot{T}_s(t) = -h(T_s(t) - T_c(t))\,. \tag{4.3}$$

where C is the sample heat capacity, h the total heat transfer coefficient, T_s and T_c the sample and chamber temperatures, respectively. The chamber temperature is time averaged over the duration of the first overshoot τ_o,

$$\bar{T_c} = \frac{1}{\tau_o}\int_0^{\tau_o} T_c(t)dt \tag{4.4}$$

giving the sample temperature

$$T_s(\tau_o) = \bar{T_c} + (T_s(0) - \bar{T_c}) \exp\left(-\frac{\tau_o}{\tau}\right), \quad \tau = \frac{C}{h}. \tag{4.5}$$

The system ramps the temperature at an approximately constant speed $R = \dot{\bar{T}}_c = \dot{T}_s$ towards the set point. This means that the sample temperature at time $t = 0$, where the chamber temperature begins to overshoot, is given by $T_s(0) - T_c(0) = -R\tau$. The sample temperature overshoot after time $t = \tau_o$, where the main overshoot has taken place in the chamber, follows as

$$\Delta T_s \approx \Delta T_c - (\tau R + \Delta T_c) \exp\left(-\frac{\tau_o}{\tau}\right) \tag{4.6}$$

where $\Delta T_s = T_s - T_{sp}$ and $\Delta T_c = \bar{T_c} - T_{sp}$ are the sample and chamber overshoots, respectively.

Here we consider the case of a negative cooling ramp, $R < 0$, and a negative overshoot $\Delta\bar{T_c} < 0$, which is completely analogous to the case of heating. The ideal case is represented by $\Delta T_s = 0$, which occurs when no overshooting is present and the thermal relaxation time (τ_0) is long enough for the sample to monotonously reach thermal equilibrium with the chamber temperature. If $\Delta T_s \geq 0$ the overshoot time is very short or the sample and chamber are so thermally decoupled that there will be no temperature overshooting in the sample itself. However, thermal decoupling leads to thermal lag in the sample and the system needs to relax before any measurements are done. Even in cases where no overshooting occurs, oscillations in the sample temperature are not desired, since the thermal history will be convoluted. When $\Delta T_s < 0$ the sample temperature will overshoot and oscillate until it reaches the set point within the given system bounds. Here one has not only ruined the sample thermal history, but also thermally forced the sample further into the phase transition than the actual set point temperature merits. This will cause hysteresis effects to be underestimated, as was shown in Fig. 4.3.

The actual conditions of the thermal system will vary greatly between different experimental setups and samples. The system specific parameters, the overshooting period τ_o, temperature ramp rate R and the actual overshoot ΔT_c can often be controlled by the PID parameters. The characteristic heat transfer time τ will depend on the thermal conditions of the system, along with sample parameters such as size, heat capacity and thermal conductivity. When using small samples, with low thermal masses, one should be very careful if aggressive non-monotonous temperature controls are used.

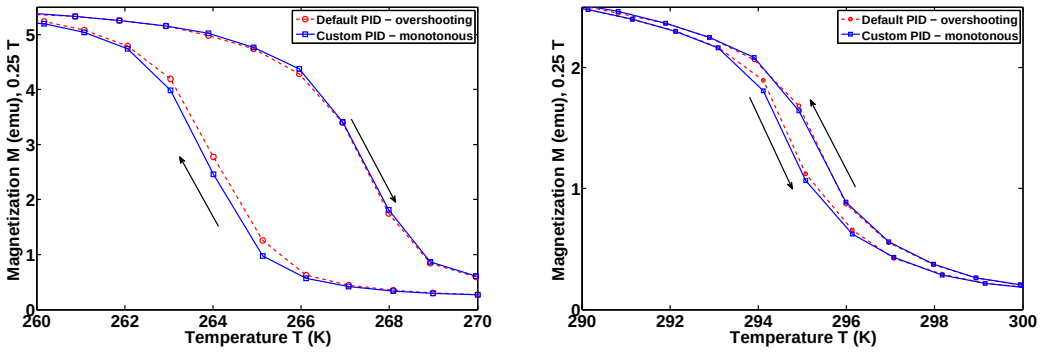

Figure 4.4: Magnetization of $Gd_5Si_2Ge_2$ (a) and MnFe(P,As) (b), measured from the high temperature PM phase to the low temperature FM phase and back again. This is done with two different PID control settings, the VSM default setting and custom, non-overshooting setting. Thermal hysteresis is underestimated about 10-15% using the default setting.

The effect of non-monotonous temperature control in $Gd_5Si_2Ge_2$ and MnFe(P,As)

In this section a series of magnetization measurements done on the first order MCMs $Gd_5Si_2Ge_2$ and MnFe(P,As) are presented. The results show a clear underestimation of thermal hysteresis when applying non-monotonous temperature scans.

The measurements were carried out in a point-by-point temperature scan at a constant applied field of 0.25 T. $Gd_5Si_2Ge_2$ was measured from 310 K to 230 K and back to 310 K. MnFe(P,As) was done in the other direction from 250 K to 320 K and back to 250 K. The PID parameters used for both materials were the default values in the LakeShore software, $\{k_p, k_i, k_d\} = \{20, 15, 0\}$, and a custom set of values, $\{k_p, k_i, k_d\} = \{4, 1, 0\}$. It is noted that these absolute values will probably not have any relevance for other cryostat solutions than the one used here. As was shown in Fig. 4.2, the default settings cause a temperature overshoot of about 3 K at 5 K steps and 0.5 K at 1 K steps. In the literature, most reported isofield measurements use a temperature resolution between these two step sizes. Here a step size of 1 K is used around the transition where overshooting is relevant. This is a relatively small step and the effects will be correspondingly larger for larger step sizes.

The results of the material measurements are shown in Fig. 4.4. Both materials show an underestimated thermal hysteresis using the setting where the temperature overshoots between measurement points. Hysteresis is underestimated by 10% in the case of $Gd_5Si_2Ge_2$ and 15% in MnFe(P,As). It seems that the underestimation only occurs during the cooling mode. The reason for this is most likely that the temperature control is not symmetric during heating and cooling modes. For this particular system, the time integrated temperature overshoot is about 20% larger when cooling, compared to heating. The underestimation of the hysteresis would be twice as large in the case of equal overshooting in each direction.

These results confirm that temperature control should be considered and investigated when measuring hysteretic materials. Only under perfect conditions will the hysteresis be correctly characterized; in all other cases it will be underestimated. This is especially relevant in the field of magnetocalorics where the characterization of hysteresis is important in order to evaluate material performance. In the case presented here, the samples are relatively large (40 and 60 mg, respectively), both with thermal masses around 0.02 J/K and the overshoot is only about a maximum of 0.5 K, in a duration of about 1.5 min. This leads to errors of the order of 10%. The severity of the underestimation will be very sample and system dependent,

- The larger the overshoot temperature and overshooting time duration, the larger the error.
- Good thermal transfer conditions between sample and sample chamber will increase the error. Too low thermal transfer can on the other hand lead to too large thermal lag in the sample, causing the sample temperature to never be in thermal equilibrium with the sample chamber.
- Lower thermal sample mass will increase the error.

It is difficult to compare the temperature control between systems. The conditions should be checked for every system and sample. The thermal transfer condition of the system will often not be customizable, but the temperature overshoot can generally be managed by PID settings and limiting the ramp rate of the temperature. The sample properties are given, so care has to be taken when measuring samples with low thermal mass and high thermal conductivity.

4.3 Measuring isothermal magnetization

Measuring the isothermal magnetization primarily has one advantage over doing it in constant field, which is time. Changing temperature and reaching equilibrium

and doing so correctly (as discussed in the previous section) takes a lot of time. Each data point easily takes between 5-15 min. Changing the applied magnetic field at a constant temperature can practically be done instantly. However, as will be discussed in the following, one has to be aware of too high magnetic field ramps used with magnetic field changes as they can possibly ruin the isothermal conditions due to the effects of the MCE.

Avoiding the magnetocaloric effect

When the isothermal magnetization is measured, the applied magnetic field is changed with some chosen ramp rate in both continuous scans and point-by-point scans, between data points. If the field is changed in large steps or too rapidly, the magnetocaloric heating/cooling will destroy the isothermal condition. This results in an erroneous magnetization curve and an overestimation of the magnetic hysteresis. Furthermore, the thermal history of the sample is compromised.

The model developed in section 4.2, Eq. (4.5), can be restated in another form to illustrate the problem. The time evolution of the sample temperature T, with thermal mass C can be approximated by

$$T(t) = T_c + \Delta T_{\mathrm{ad}}(H_i; H_f, T) \exp\left(-\frac{t}{\tau}\right), \quad \tau = \frac{C}{h}. \tag{4.7}$$

where h is the total heat transfer coefficient, T_c and ΔT_{ad} the isothermal chamber temperature and the material adiabatic temperature change, respectively. From this follows that,

- A large MCE will increase the error. It is noted that the MCE not only depends on the relative field change, but also on the absolute field. This results in a skewed erroneous magnetization curve.
- Magnetization, where $T > T_c$, results in a too low magnetization. Demagnetization, where $T < T_c$, results in a too high magnetization. This causes a doubling of the error during a cycle, overestimating the hysteresis loop.
- The characteristic relaxation time τ depends both on the thermal transfer conditions between system and sample and the thermal mass of the sample. Bad heat transfer and large thermal masses can increase the error.

The effects and potential problems will vary with sample and experimental setup and should therefore be investigated on every setup.

The fact that the magnetocaloric effect plays a role in standard magnetization measurements has been reported before by Moore et al. [2009], Hansen et al.

[2010]. However, it is an issue that is rarely commented on in publications when explaining experimental procedures.

The issue was initially brought up by Moore et al. [2009], who named the effect extrinsic hysteresis. They show that for the first order material $La(Fe_{1-x-y}Co_xSi_y)_{13}$ the "isothermal" magnetization is field rate dependent. The magnetic hysteresis is significantly more than doubled at high scan rates, 12 mT/s, compared to very slow rates of 0.3 mT/s. A Pt100 sensor was placed on the sample, registering the real-time sample temperature during the magnetic sweep. For their VSM system, the characteristic relaxation time($1/e$'th of initial) of the sample temperature was about 15 s.

Hansen et al. [2010] showed that the effect is relevant for both first and second order materials, $Gd_5Si_2Ge_2$ and $La(Fe_{0.945}Co_{0.055})_{11.9}Si_{1.1}$. This study was done on the same setup as was used in this thesis, a LakeShore 7407 VSM. It is shown that second order material LFCS exhibits an artificial magnetization/demagnetization curve separation, giving the impression of hysteresis at too high ramp rates, which disappears at sufficiently low rates. For $Gd_5Si_2Ge_2$ there is an intrinsic hysteresis curve, but at too high ramp rates both the curve shape and hysteresis area are significantly altered compared to the true isothermal curve. Estimating the entropy change from such measurements is found to cause a higher and more narrow peak.

Experimental determination of correct ramp rates

Here experimental results for isothermal magnetization measurements at different rates for both $Gd_5Si_2Ge_2$ and MnFe(P,As) are presented. In the VSM setup used for this work, the standard setting for measuring isothermal magnetization M is using a point-by-point scan, where the magnetization is averaged over 10 s after each field increment. The measurements were done at constant cryostat temperature of 270 K and 300 K, for $Gd_5Si_2Ge_2$ and MnFe(P,As) respectively.

In Fig. 4.5 the time dependent magnetization is shown, measured directly after different field increments, ramped at 67 mT/s. The values are normalized to the maximum magnetization value. The characteristic equilibrium times found from fitting Eq. (4.7) range from 20-40 s, depending on the field increment. Another way of stating the results is that for the magnetization to be within 5% of its true isothermal value, one needs to wait at least between 30-90 s, depending on the field increment, before the magnetization is measured. This can be restated in an effective field ramp rate of between 3-1 mT/s. If one follows the default experimental settings, it is seen that for realistic field increments of 0.1 T and 0.05 T (red and yellow curves), one would measure magnetization values that are around 20% and 10% too low, respectively.

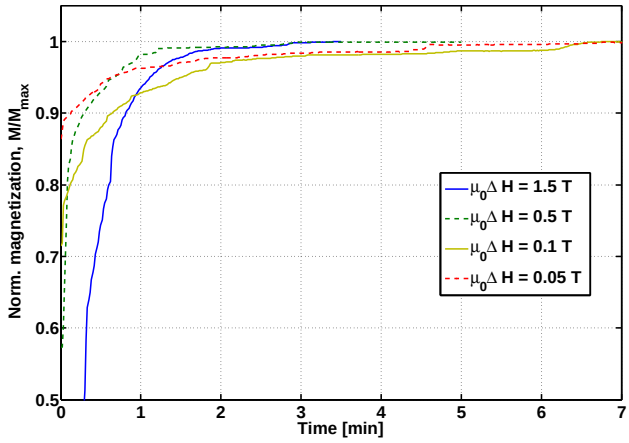

Figure 4.5: The normalized magnetization of $Gd_5Si_2Ge_2$ at 270 K, measured directly after different field increments.

The effect of ramp rates on the actual magnetization curves is shown in Fig. 4.6. The ramp rates are given in both ramping time between each increment and an effective ramp rate, because these measurements are not continuous but done point-by-point. For both materials it is clear that the default settings of the VSM greatly overestimate the hysteresis and skews the hysteresis loop. There is a clear give-away of the problem in the fastest $Gd_5Si_2Ge_2$ ramp; the magnetization after ramping to the highest field, is lower than the magnetization after the following demagnetization step. This is clearly not correct in a thermal equilibrium state. The hysteresis is overestimated about 25% in the case of $Gd_5Si_2Ge_2$ and 120% in MnFe(P,As) . In both cases, the curves approximately collapse to the steady isothermal curve at ramp rates between 1.7 and 0.8 mT/s.

The conclusion for this system is that a maximum effective ramp rate of about 1 mT/s (0.06 T/min) is necessary to avoid problems with the MCE. This is in stark contrast to the default system settings of 67 mT/s. The non-isothermal conditions do not only cause a wrong magnetization curve, but also induce a non-monotonous thermal history.

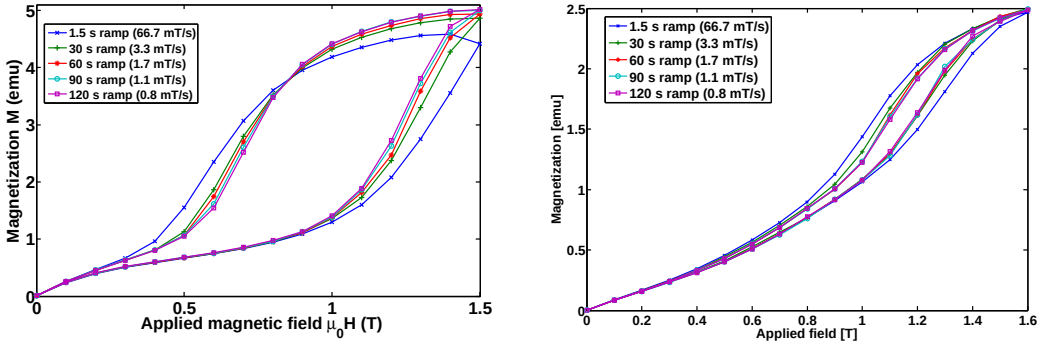

(a) $Gd_5Si_2Ge_2$ at 270 K.

(b) MnFe(P,As) at 300 K.

Figure 4.6: Isothermal magnetization curves measured at different field ramp rates.

4.4 Procedures for isothermal magnetization measurements

The previous sections have dealt with the technicalities of measuring magnetization, taking the limitations of the equipment and samples into account. This section will discuss a more fundamental problem in measuring isothermal magnetization in first order materials. There is an inherent problem in characterizing history dependent materials; that it depends on the specific experimental procedure. Generally, data that has been obtained through different procedures cannot be directly compared. Furthermore, it is crucial for material modelling that the exact procedure is known. Otherwise one might end up modelling material behavior that does not correspond to the conditions under which it was obtained.

In literature generally only two procedures have been discussed and employed to obtain a map of $M(H,T)$ through isothermal field scans,

The standard procedure This procedure has been and is still probably the most widely used

- The sample is cooled to the lowest temperature of interest, T_{min}, and the magnetization is measured while scanning the applied field from 0 to H_{max} and back to 0.
- The temperature is increased by a chosen temperature step ΔT, to $T_{min} + \Delta T$. The magnetization is again measured while scanning the field, as described in step 1.

- The procedure is repeated until the maximum temperature T_{max} is reached.

The loop procedure The procedure was suggested by Caron et al. [2009], in order to avoid problems when using the Maxwell relation. The procedure resets the sample to a paramagnetic state before each magnetization measurements. The procedure is as follows,

- The sample is heated up to a pure paramagnetic phase state temperature T_{pm}.
- The sample is cooled down to lowest wanted temperature T_{min} and the magnetization is measured under increasing magnetic field after which the field is set back to 0.
- The sample temperature is again brought up to T_{pm}, and then back down to the next temperature $T_{min} + \Delta T$, where magnetization is recorded as in step 2.
- This is repeated until the maximum temperature is reached.

As will be discussed in the following these procedures each have their rightful place, depending on the application.

Magnetic field cycling

In the area of magnetocaloric materials, the interest lies in knowing the material behavior under cyclic field application, at various temperatures. It is practically impossible to achieve data that corresponds exactly to the conditions of an AMR system, since there is no simple way of knowing how temperatures change in such a system. The conditions can however be approximated, if the right procedure is chosen.

Intuitively, the standard procedure approximately corresponds to a realistic AMR scenario, since the material here undergoes a monotonous temperature change and the field is cycled in each isothermal state. The loop procedure however, does not. Here the sample is reset to a pure PM-state between each isotherm, introducing an artificially high PM phase fraction. The first magnetization will cause a large switch from PM to FM states, where subsequent demagnetization and magnetization will affect the material much less. This scenario is illustrated in Fig. 4.7. A sample of $Gd_5Si_2Ge_2$ is brought both from a high temperature PM state and a low temperature FM state to the desired set temperature, without overshooting. In each case the magnetic field is scanned three consecutive times, from 0 to 1.5 T and back to 0. This was done in steps of 0.1 T, with a ramp of 0.8 mT/s. This was done for two set temperatures of 265 K and 270 K.

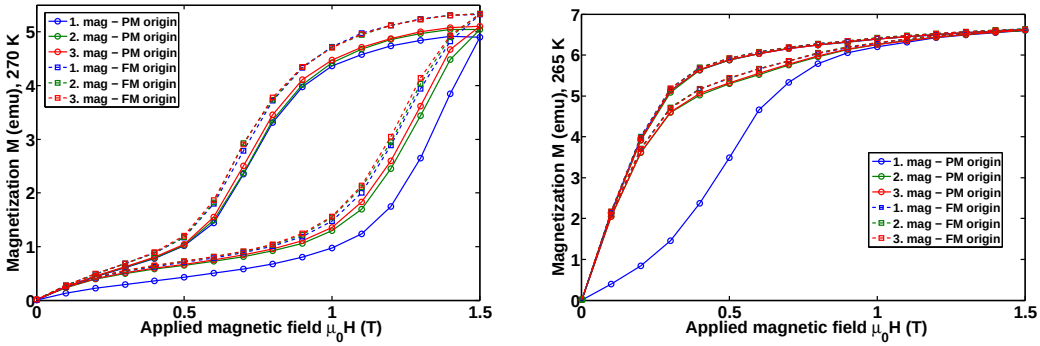

(a) 270 K. **(b)** 265 K.

Figure 4.7: Triple magnetization cycles of $Gd_5Si_2Ge_2$ carried out with the sample being initially reset in both the FM and PM state

In both magnetic isotherms, the curves corresponding to the loop procedure (solid, blue circle curves) are significantly different than the rest. It is clear that this is an unstable state, as the subsequent cycles collapse to a single stable state. The dashed curves represent the standard procedure and are seen to be stable and independent of the number of magnetic cycles. In the low temperature case, all curves collapse to just one single curve after the initial magnetization, regardless of the initial thermal reset. This is due to the field being large enough to saturate the FM state. At 270 K, the materials remain in a minor magnetic loop cycle and thermal hysteresis persists through the magnetization cycles. This illustrates that lower fields that cannot complete the transition at the given temperature, material behavior will depend on whether the sample was ever in a pure FM or PM state.

If the goal is to illustrate material characteristics, such as magnetization, under practical AMR conditions, the loop procedure is misleading. The initial magnetic cycle is the result of an unstable state that will underestimate the magnetization and greatly overestimate the magnetic hysteresis loop area. The standard procedure provides a stable magnetization curve that will approximately correspond to the cyclic conditions in an AMR scenario. However, this procedure can lead to problems when deducing the entropy change from the Maxwell relation, as will be discussed in the following.

4.5 Obtaining the isothermal entropy change

The general approach to calculating the isothermal entropy change ΔS from magnetization measurements is to apply the Maxwell relation

$$\Delta S(H_i; H_f, T) = \mu_0 \int_{H_i}^{H_f} \left(\frac{\partial M}{\partial T} \right)_H dH \,. \tag{4.8}$$

This expression assumes thermodynamic equilibrium, which is correct when applying it to second order MCMs. Here the entire $M(H,T)$ surface can be mapped out by either isofield temperature scans or isothermal field scans, since M is a state function, independent of path. There is no implication of taking the derivative, other than the resolution of the numerical differentiation itself. In first order MCMs however, this is in general no longer the case as M is no longer a state variable, but now depends on the path due to the coexistence of phases. The phase mixing can be described by the FM phase fraction X, which plays the role of a hidden internal material variable. Applying the approach given in Tocado et al. [2009], Eq. (2.8) can be rewritten by writing the magnetization as a FM(1) and PM(0) contribution mixed by X

$$\begin{aligned} \Delta S &= \mu_0 \int_{H_i}^{H_f} \left(\frac{\partial (X M_1 + (1-X) M_0)}{\partial T} \right)_H dH \\ \Delta S &= \mu_0 \int_{H_i}^{H_f} \left(\frac{\partial X}{\partial T}(M_1 - M_0) + X \frac{\partial M_1}{\partial T} + (1-X) \frac{\partial M_0}{\partial T} \right)_H dH \,. \end{aligned} \tag{4.9}$$

The phase fraction derivative is the cause of problems in using this approach in first order materials.

In Fig. 4.8 an illustration of a characteristic first order phase diagram is shown. The solid blue and red lines represent the phase transition lines between the PM and FM states in a cooling and heating mode, respectively. The accompanying dashed lines show the width of the transition. The three horizontal lines represent isothermal magnetic field scans between 0 and $H_{\max}$ at temperatures $T_1 < T_2 < T_3$ and the two vertical lines the isofield temperature scans at fields $H_1 < H_2$.

To illustrate the difference between the isofield and isothermal procedures, consider the isothermal entropy change induced by the field change $H_2 - H_1$ at temperature T_3, as shown in Fig. 4.8. In the isofield procedure, data points are obtained by moving vertically along the dotted line in the phase diagram at each field. The applied magnetic field is constant during the temperature scan and the magnetization derivative between data points $M(H_1, T_3)$ and $M(H_1, T_2)$ is well defined

$$\frac{M(H_1, T_3) - M(H_1, T_2)}{T_3 - T_2} \,.$$

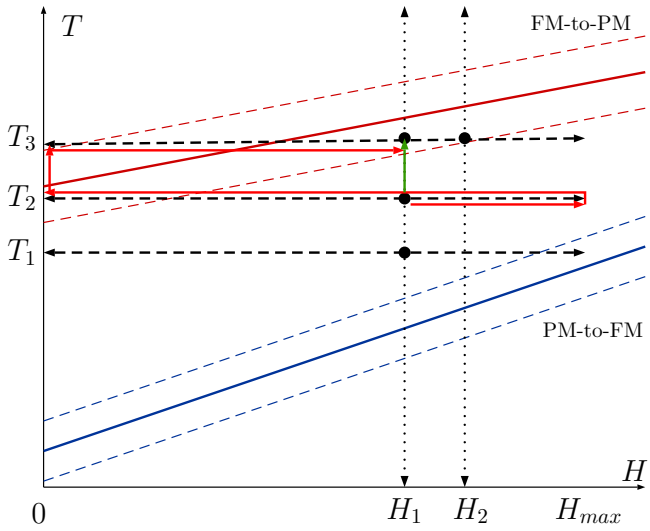

Figure 4.8: An illustration of a hysteretic phase diagram. The transition lines between the PM and FM phases are shown in solid red and blue, corresponding to a heating and cooling mode, respectively. The colored dashed lines reflect the width of the transition. The horizontal and vertical lines show the paths of isothermal and isofield magnetization measurements, respectively.

The path between these two points is shown with a green line arrow in the figure. As the transition region is crossed monotonically during a temperature scan, there is no abrupt change in the phase fraction X between consecutive data points. This means that the contribution of $\partial X/\partial T$ in Eq. (4.9) is minimized. The contribution of course depends on the temperature steps used, as large steps will increase the change in X. The step size should be significantly smaller than the transition width.

However, in the isothermal procedure, following the horizontal dashed lines, this is not generally the case. Considering the same two points, $M(H_1, T_2)$ and $M(H_1, T_3)$, the path taken between them is now rather complex, as illustrated by the red arrow-line. Where the isofield procedure only introduced the change $T_2 \to T_3$ between the data points used in the magnetization derivative, the isothermal procedure introduces the following changes,

$$H_1 \to H_{max} \to 0\,, \quad T_2 \to T_3\,, \quad 0 \to H_1.$$

Not only has the magnetic history become convoluted between data points, but

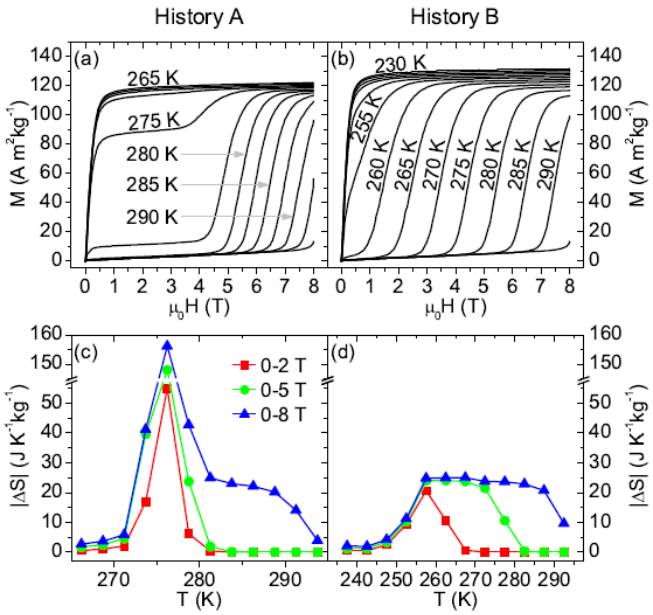

Figure 4.9: Illustration of the "colossal" MCE - spike effect. Adopted from Bratko et al. [2012]

the transition line is crossed in one measurement but not the other. This can introduce a large change in X, regardless of the temperature step size, resulting in a wrongfully large contribution to the calculated entropy change.

Correcting the wrongfully calculated entropy change by using specific experimental procedures or correctional terms in calculations has been subject for debate since the introduction of first order materials showing a "colossal" MCE, as illustrated in figure Fig. 4.9 on the left side. There are several papers that discuss this in detail, supported by thermodynamics and experimental data. Among the initial contributors are Liu et al. [2007], Caron et al. [2009], Tocado et al. [2009], Das et al. [2010], who all discuss experimental procedures and corrections for wrongful use of the Maxwell relation. For a thorough discussion of all the results, see the thesis by Wang [2012, ch. 4].

If one wants to use isothermal measurements, a way to solve the problem is by employing the loop procedure as described by Caron et al. [2009]. By heating the sample to the high temperature PM state and then cooling it to the isothermal temperature between each field scan, the change in X is minimized between data points. The standard and loop isothermal procedures are shown in Fig. 4.9 as

history A and B, respectively. Here the path dependence is clearly seen in the different magnetization values and ΔS values. The spike effect is clearly seen in history A, due to the uneven phase mixing between data points.

Using the loop procedure, the situation in Fig. 4.8 would not see any problems, since both data points would remain in the PM phase. However, the corresponding isotherms, shifted to the blue PM-FM transition line, could still see some problems if two following isotherms are on separate sides of the line. This will still cause some change in X, but it would be minimized compared to the standard procedure. It should be noted, that a precise temperature control is very important here. Any kind of overshooting around the transition band will destroy equal path idea. As discussed in section 4.2 the overshooting can be significant even at small temperature steps. In this case, steps could be of the order of 10-50 K between each reset, which could cause huge overshoots.

It is important to note that using the Maxwell relation on either isofield or isothermal magnetization data does not takes any kind of hysteresis effects into account. The discussion stated above illustrates how to avoid implementing direct errors in the numerical differentiation, nothing more. The calculated MCE still only reflects a reversible estimate. This will be further discussed in chapter 7.

4.6 Summary

In this chapter the experimental procedures for obtaining magnetization data were described. As isothermal and isofield procedures for magnetization measurements are both used in this thesis work, the related problems were discussed:

- The importance of having a controlled and monotonous temperature variation during isofield measurements, as temperature oscillations and overshooting cause partial hysteresis loop behavior and can underestimate thermal hysteresis.
- The importance of using a low magnetic field ramp in isothermal measurements, due to the magnetocaloric effect otherwise ruining the isothermal conditions in the material.
- The application of the Maxwell equation on first order materials and the problems it can lead to when applied on standard isothermal magnetization data.

Part III

Material characterization

Chapter 5

Characterization of $Gd_5Si_2Ge_2$

This chapter presents a series of experimental characterizations of the magnetocaloric effect (MCE) in the first order material $Gd_5Si_2Ge_2$. The standard indirect characterization methods of calorimetric and magnetization measurements are employed and supplemented by direct measurements of the isothermal entropy Δs and adiabatic temperature change ΔT_{ad}. This chapter is primarily meant as a presentation of results and does not contain detailed explanations and discussions of experimental methods and procedures. These can be found in the calorimetry chapter 3 and the magnetometry chapter 4.

$Gd_5Si_2Ge_2$ was the first magnetocaloric material (MCM) reported with a giant MCE around room temperature [Pecharsky and Gschneidner, 1997]. It exhibits a coupled crystallographic and magnetic transition, from a low temperature ferromagnetic (FM) phase to a high temperature paramagnetic (PM) phase [Gschneidner Jr. and Pecharsky, 2000]. As its discovery constituted a breakthrough in room temperature application of MCMs, it has been investigated thoroughly in various contexts in the last 15 years. So why this extensive experimental study if this material? There are two main reasons for this. Firstly to do a range of independent and both overlapping and supplementary measurements on the *same* sample. These Gd-Si-Ge compounds experience relatively large variation in material characteristics depending on both small variation in stoichiometry and preparation methods [Pecharsky et al., 2003]. Furthermore, the precise methods used to measure first order materials are important in order to keep track of

the magnetic and thermal history, allowing for comparison between experiments. This is not always so well documented in literature. Performing a large range of experiments on the same sample allows for a more direct comparison of methods and their derived results, such as Δs. Secondly, many of these experiments are used as a foundation for the Preisach model, described in section 7.4. Here, the exact experimental procedure is also crucial to obtain meaningful results.

When characterizing hysteretic MCMs, the deduced entropy curves are not single valued functions as is the case with second order materials, making estimation of the MCE ambiguous. There are four possibilities of choosing the low and high magnetic field entropy curves, from which one can estimate both ΔT_{ad} and Δs,

1. Low field cooling, high field cooling
2. Low field heating, high field heating
3. Low field cooling, high field heating
4. Low field heating, high field cooling

Number 1 and 2 often represent the results of indirect magnetization and heat capacity methods, as will be shown in this chapter. Number 3 represents the most optimistic case, but in an AMR-like scenario it would seem unrealistic. As the magnetization step always follows a heating step, the low field cooling curve is practically never applicable. Number 4 represents the most pessimistic case, but as all the results in this chapter suggest, it seems to be the correct representation, as has also been suggested through other methods in Engelbrecht et al. [2013], Skokov et al. [2013].

The results of each experiment are presented individually in the following, where after the important points are compared and summarized.

Samples of $Gd_5Si_2Ge_2$

The samples used for all of the following experiments are provided by Profs. Gschneidner and Pecharsky from AMES lab. The general production details can be found in Pecharsky et al. [2003]. This specific sample is made of high purity Gd and was annealed at 1300° for 1 hour. It is not the exact same sample characterized in the different experiments, however, the different small samples are all taken from the same larger sample. This is unfortunate since the main goal is to compare the different methods and demagnetization effects can play a significant role between samples with different geometry. But due to the brittleness of these compounds, they simply break apart after some period of time. The problem of

demagnetization is ignored in this section, due to the complexity of correcting all of the experiments and the need of extensive data sets.

5.1 Magnetometry

In the following two subsections the results of both isofield and isothermal magnetization measurements are presented. The sample used for these measurements is an approximately rectangular cuboid, with dimensions $(L, W, H) = (3.5, 1.9, 1.35)$ mm and a sample mass of 60 mg. Utilizing the method described in Aharoni [1998], the demagnetization factor along the length L, in which the field is applied, is approximately $N_L \approx 0.23$. It should be noted that during the isofield measurements, which were carried out first, the sample deteriorated and small pieces broke off. The remaining part of the sample used for the isothermal measurements weighs about 5 mg less with a much more jagged surface structure. The magnetization values does therefore not match exactly between the two experimental series. All measurements are done on a LakeShore 7407 vibrating sample magnetometer. The technical details concerning the instrument and the procedures are discussed in chapter 4.

Isofield measurements

This series of isofield magnetization measurement will be the basis of a Preisach model (chapter 7.4). The experimental data has a good resolution in both temperature and magnetic field variation, allowing for detailed modelling. The standard full temperature scan measurements, spanning from the high to low temperature states, are supplemented by a set of first order reversal curves, providing useful material information about partial transformations. The main results of this section are published in von Moos et al. [2014b] (appendix C), along with corresponding Preisach model.

This series of measurements were carried out following a standard cooling and heating procedure:

1. Heating to the maximum temperature, 310 K
2. Application of a constant applied magnetic field $\mu_0 H = 0.05$ T
3. Measurement of the magnetization M at 310 K
4. Steady and monotonic[1] temperature decrease to the new setpoint temperature T_i

[1] The monotonic temperature change is important for first order materials, see section 4.2.

5. Thermal relaxation of the sample for 5 min
6. Measurement of the magnetization at T_i
7. Repetition of steps 4-6 until the lowest temperature of 230 K is reached
8. Repetition of steps 4-6 in a heating mode where the temperature is monotonically increased between 230-310 K
9. Repetition of steps 1-8 for the different magnetic fields of $\mu_0 H = (0.05, 0.10, 0.25, 0.50, 0.75, 1.00, 1.20, 1.40, 1.60)$ T

The results are shown in Fig. 5.1. Each isofield temperature scan is shown in separately colored lines, with the solid and dashed lines illustrating the cooling and heating modes, respectively. The measurements done at 0.25 T are shown with circular symbols to illustrate the temperature stepsize, which is constant for all experiments. In Fig. 5.2 the transition temperature T_t is shown as a function of the applied magnetic field. The transition temperature is here defined as the point of inflection on the magnetization curve. In this field range the shift of the transition temperature is approximately linear with the applied field, with a gradient of about 6 K/T. The thermal hysteresis between the heating and cooling mode is roughly 3.9 K across the entire field range.

The isothermal entropy change Δs is estimated through the Maxwell relation (see sec. 4.5 for a discussion of this)

$$\Delta s(H_i; H_f, T) = \mu_0 \int_{H_i}^{H_f} \left(\frac{\partial M}{\partial T} \right)_H dH \,. \tag{5.1}$$

In Fig. 5.3 the calculated values of Δs are shown for the cooling and heating mode, depicted by solid and dashed lines, respectively. The values between 1.4 T and 1.6 T, which is used later for comparison with other experiments, is about 17 J/kg/K, which is similar to previous reports of the MCE in this compound [Pecharsky and Gschneidner, 1997, Pecharsky et al., 2003, Basso et al., 2006a]. The maximum Δs and full-width-at-half-maximum (FWHM) values for each peak are shown in Fig. 5.4. The maximum peak values are not very sensitive to increasing the applied magnetic field when above 0.75 T, where domain effects are mostly eliminated. The width of the Δs peaks scale approximately linearly with the applied field, which is known to be the case with both Gd-Si-Ge and Mn-Fe based first order materials [Basso et al., 2006a, Wada and Tanabe, 2001].

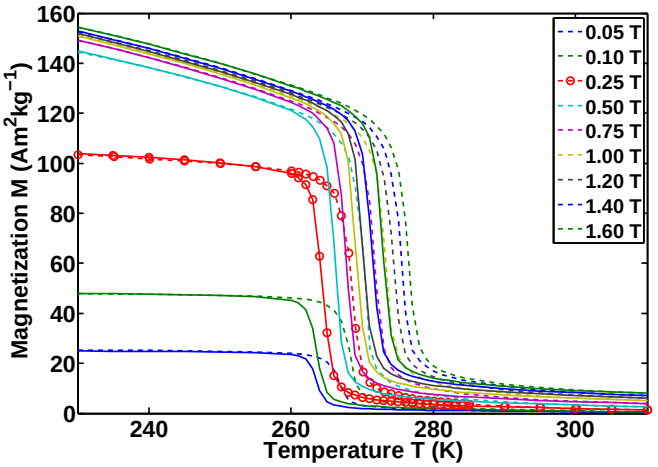

Figure 5.1: Magnetization of a $Gd_5Si_2Ge_2$ sample, measured under the application of constant applied magnetic fields. Solid and dashed lines represent cooling and heating, respectively, and the symbols the temperature stepsize.

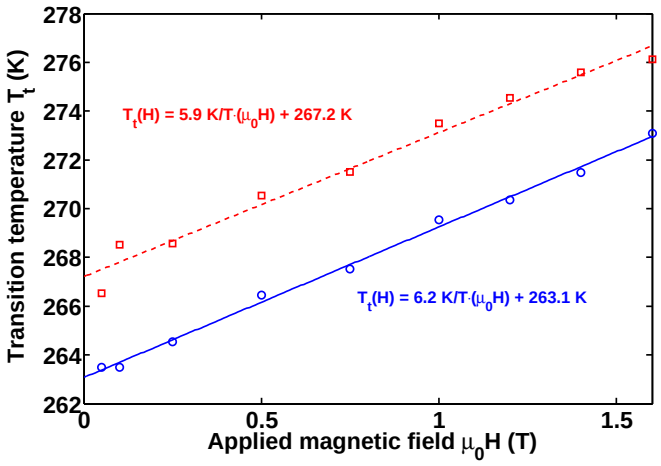

Figure 5.2: The transition temperature (symbols) defined as the point of inflection on each magnetization curve, along with linear fits.

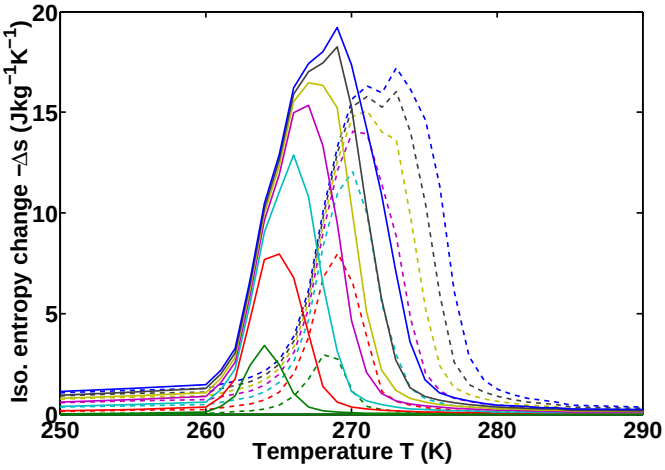

Figure 5.3: The isothermal entropy change, obtained from the Maxwell relation for both heating(dashed) and cooling (solid), shown for increasing applied magnetic field changes of $\mu_0 H = (0.10, 0.25, 0.50, 0.75, 1.00, 1.20, 1.40, 1.60)$ T.

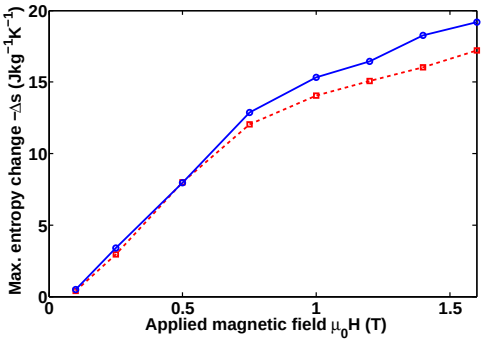

(a) The maximum entropy change obtained from Fig. 5.3.

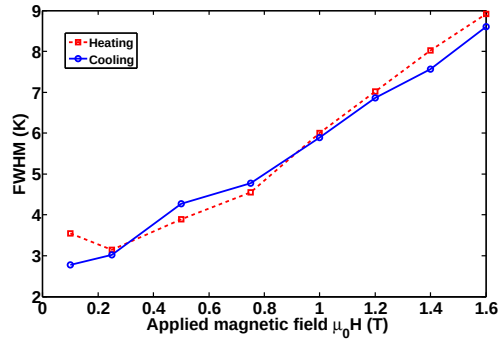

(b) The full width at half maximum of the Δs peak obtained from Fig. 5.3.

Figure 5.4

First order reversal curves

First order reversal curves (FORC) are often employed in general Preisach modelling, as they can in principle determine model parameters. However, in magne-

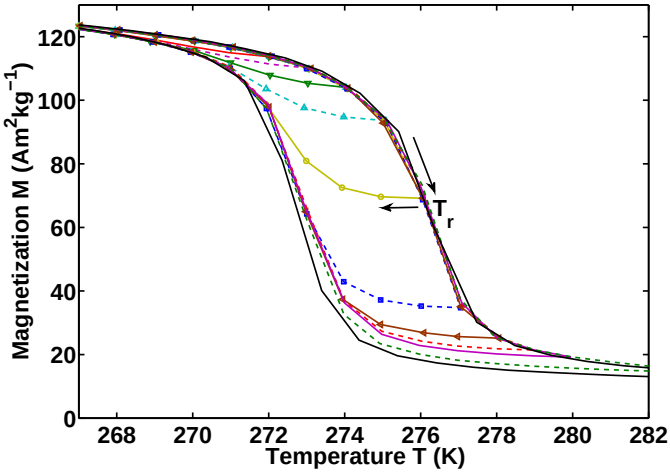

Figure 5.5: First order reversal curves, measured in an initial heating mode until a reversal temperature T_r is reached, whereafter a cooling mode is applied. The measurements are done in an applied magnetic field of 1.6 T.

tocaloric Preisach modelling they are rarely seen. They illustrate the material behavior under partial phase transformations. This is crucial to correctly model the material, since partial transformations partly determine the reversibility of the transformation.

Here a series of reversal curves are carried out in an applied magnetic field of 1.6 T. Each reversal curve is done similarly to the heating and cooling modes, described in the previous section. However, here the switch between the two modes is not at a constant high temperature, but at a variable reversal temperature T_r. The magnetization is measured in an initial heating mode, until T_r is reached, whereafter the magnetization is measured in a cooling mode. This is repeated for a series of T_r-values around the transition. The results are shown in Fig. 5.5. The different FORCs are shown in varying color, some with symbols to illustrate the temperature steps. The importance of these curves lies in the return branch, which gives information about the reversibility of the transformation.

Isothermal measurements

These measurements were carried out by employing the standard method of isothermal characterization:

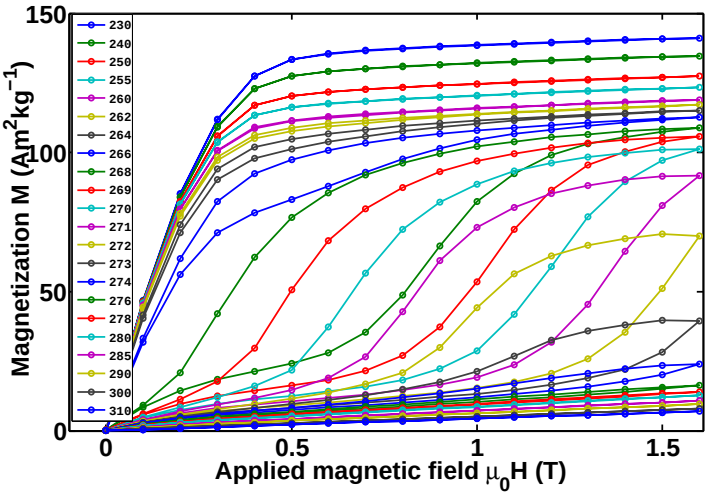

Figure 5.6: Isothermal magnetization curves for during magnetization and demagnetization between 0 and 1.6 T applied magnetic field.

1. The sample is cooled to 230 K
2. A magnetic field is step wise applied to the sample, from 0 T to 1.6 T in steps of 0.1 T. The measurements are done point-by-point and the magnetic field is changed with a rate of 0.067 T/min between measurements[2]
3. The magnetic field is removed in the same step wise manner
4. The sample temperature is increased to the new set point and steps 2-3 are repeated

The results are shown in Fig. 5.6. It is noted that even though care was taken to ramp the magnetic field very slowly, the MCE still affects the magnetization around the transition temperature. This is most evident from the 272 K magnetization curve, where the magnetization at 1.6 T is lower than the value at 1.4 T, during demagnetization. As this should not be the case, it is clear that the MCE changes the actual sample temperature and by that shifts the magnetization.

In Fig. 5.7a Δs is calculated from the Maxwell equation for an applied magnetic field change between 0 and 1.6 T and shown along with the corresponding calculation from the isofield measurements. Here the erroneously large peak from

[2]See section 4.3 for a discussion about the importance of low field ramps in MCMs

the isothermal measurements become evident, as discussed in sec. 4.5. The effect is here relatively small, but will be much more pronounced at larger fields [Caron et al., 2009]. The Δs curves from isofield cooling and isothermal magnetization coincide nicely, ignoring the spike in the peak. This is not the case for the heating and demagnetization curves. The demagnetization curves around the transition are return branches of partial transitions, due to the low magnetic field and does by that not represent the same states as obtained from the isofield measurements. A consequence of this is that isothermal measurements provide less usefull information for calculation of the MCE in magnetic field too small to force a complete PM-FM transition.

In Fig. 5.7b show the hysteretic loss during each magnetization cycle, calculated as the magnetization loop area. The hysteresis peak is centered around the maximum Δs values, which was also reported by [Hansen et al., 2010]. The maximum hysteretic loss is about 40 J/kg during a magnetization and demagnetization cycle between 0 and 1.6 T. This corresponds to an entropy production of roughly $\sim 40/270 = 0.1$ J/kg/K. Only half of this value is produced during the magnetization/demagnetization step, corresponding to less than 1% of the reversible isothermal entropy change of about 17 J/kg/K.

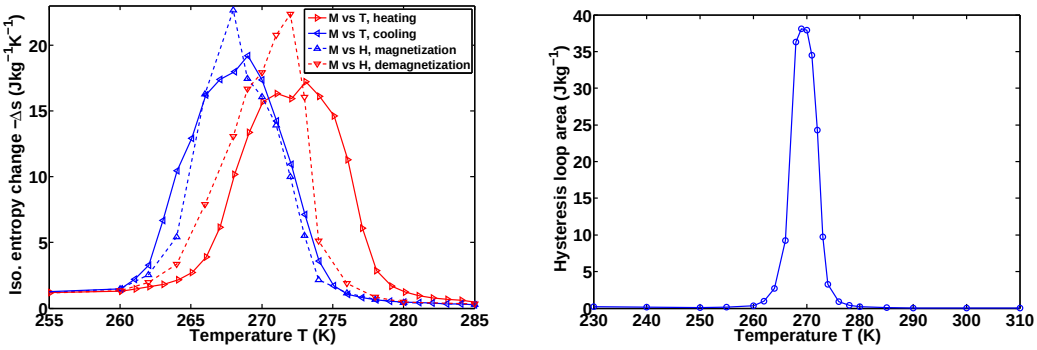

(a) The isothermal entropy change Δs, calculated from the Maxwell relation for an applied magnetic field change between 0 and 1.6 T.

(b) The hysteretic loss in each isothermal magnetization cycle.

Figure 5.7

5.2 Calorimetry

A small sample of 6.5 mg was mounted in a heat flux differential scanning calorimeter, utilizing Peltier elements as heat flux sensors (see chapter 3 and [Jeppesen et al., 2008]). The measurements were carried out in both heating and cooling modes, using a temperature scanning rate of $R = \pm 1$ K/min, respectively. Each cooling and heating scan was carried out under the constant applied magnetic fields of $\mu_0 H = (1.5, 1.0, 0.5, 0)$ T. These results are shown in Fig. 5.8 in the temperature range 255 K to 285 K.

At the time of these measurements only this sample was available, which is unfortunately close to being too small for this instrument. This makes the signal to noise ratio too large, as seen by the jaggedness of the data. The small sample size also makes measurements susceptible to thermal disturbances, due to the low thermal mass. As the sample was removed after this approximately 12 hour experiment series it broke apart, suggesting that the material suffered mechanical failure at some points during the experiments.

From Fig. 5.8 the transition temperature T_t can be calculated, as shown

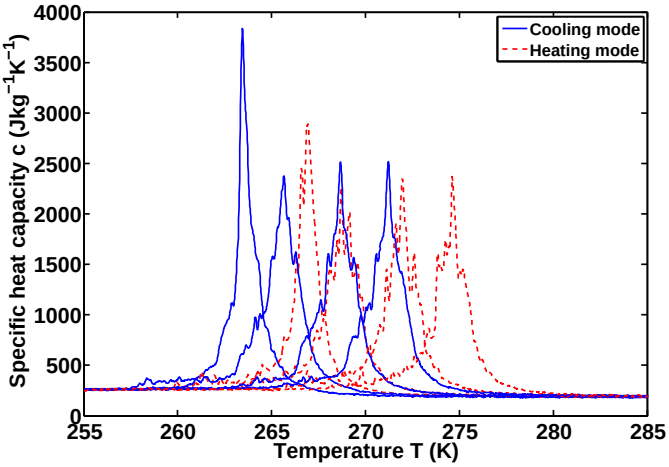

Figure 5.8: The specific heat capacity of a 6.5 mg $Gd_5Si_2Ge_2$ sample measured on a DSC. The blue solid lines and red dashed lines show the cooling and heating modes, respectively. The peaks, from left to the right, are done under constant applied magnetic fields of $\mu_0 H = (0, 0.5, 1.0, 1.5)$ T.

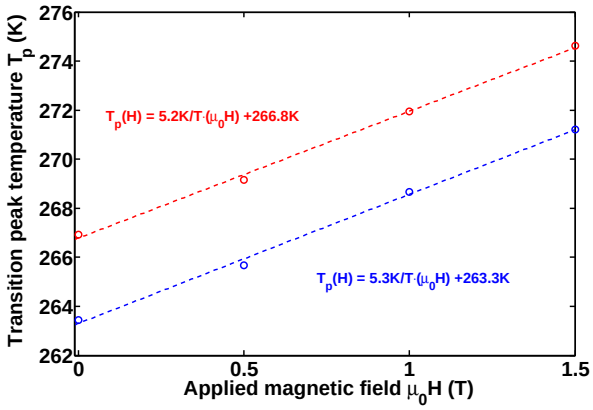

Figure 5.9: Transition temperature variation with magnetic field.

in Fig. 5.9. The transition temperature is here defined as the temperature at which the heat capacity peaks. As discussed in section 3.3, the peak temperature depend on the thermal mass of the sample. However, since it is small it should not lead to a significant artificial increase of the apparent thermal hysteresis. The thermal hysteresis in this field range is constant with a value of 3.5 K and the transition temperature is shifted about 5.2 K/T with increasing magnetic field. This can be compared to the results of the magnetization measurements (Fig. 5.2), from which a thermal hysteresis of 3.9 K and a 6 K/T transition temperature shift. These differences are attributed to demagnetization effects due to the geometrical variation between the two samples used. The heat of the transformation increases with decreasing magnetic field, ranging from 4300-4700 J/kg. The average value corresponds approximately to a total entropy change of the transition $\Delta S_t \sim 4500/270 = 17$ J/kg/K, matching the Δs value calculated from magnetization measurements.

In order to characterize the MCE, the heat capacity can be integrated to calculate the entropy,

$$s_H(T') - s_0(T_0) = \int_{T_0}^{T'} \frac{c_H(T)}{T} dT \,. \tag{5.2}$$

Setting $T_0 = 300$ K and $s_0(T_0) = 0$, the results for $\mu_0 H = 0$ and $\mu_0 H = 1.5$ T are shown in Fig. 5.10a.

The general question, regarding the MCE deduced from heat capacity measurements, is which set of low and high field entropy curves should be used for

estimating the entropy change. The different representations are shown in Fig. 5.10b, along with a direct Δs measurement, utilizing the same DSC device on the same sample (sec. 3.4). As this measurement solely represents the heat flux from the sample during magnetization, it illustrates the most direct measure of Δs. It is seen that the estimate from the low field heating and high field cooling curves coincide closely with the direct measurements, strongly suggesting that this is indeed the curves that should be used to realistically estimate the MCE from heat capacity measurements.

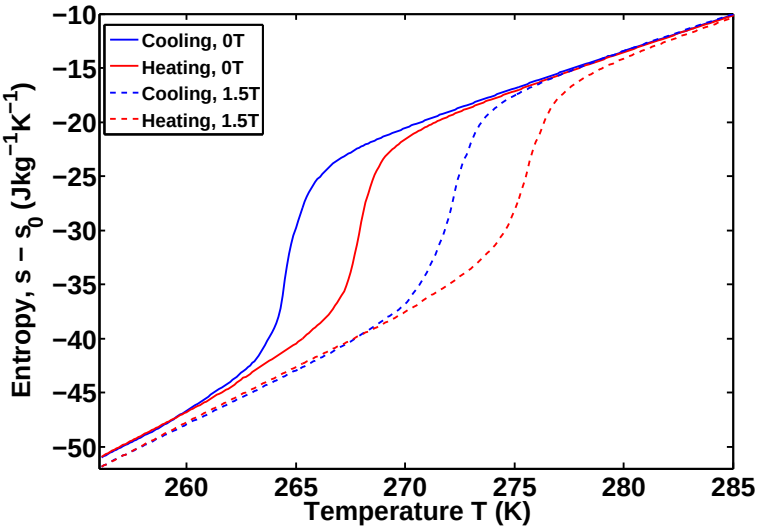

(a) Entropy deduced from the heat capacity measurements, shown for 0 and 1.5 T applied magnetic field.

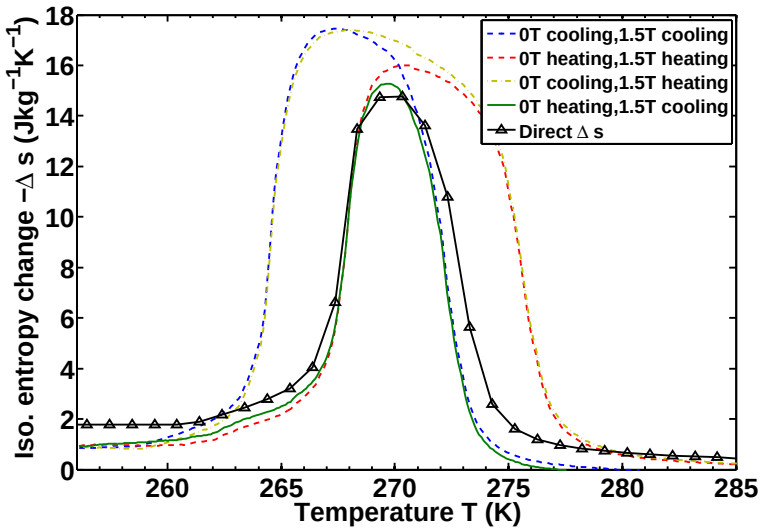

(b) Different ways of calculating the isothermal entropy change from the entropy curves in Fig. 5.10a, along with a direct measurement of the entropy change.

Figure 5.10

Direct adiabatic temperature change measurements

The direct adiabatic temperature (ΔT_{ad}) measurements were performed on an instrument currently under development at DTU Energy Conversion. At the time of this work nothing has yet been published on the instrument, but the experimental setup is briefly discussed in section 3.4. The sample temperature is here measured by a type-E thermocouple, sandwiched between two pieces of $Gd_5Si_2Ge_2$, with a total sample mass of approximately 120 mg. The measurements are carried out in a vacuum chamber ($p < 10^{-5}$ mbar) with the sample shielded from the sample holder by pads of insulation. Most of the results in this section have been published in von Moos et al. [2014b] (see appendix C).

Stepwise magnetization

In this section measurements of ΔT_{ad} are carried out, applying the magnetic field changes in discrete steps. This will show how adiabatic the experimental conditions are and demonstrate how ΔT_{ad} behaves as a function of both initial field and field increments.

In Fig. 5.11 the raw time series data for one experiment is shown. Here the sample has been i) reset in the PM state by heating it to 320 K, ii) cooled to 267 K, and iii) magnetized by an applied magnetic field between 0 and 1.5 T in steps of 0.25 T. During the 5 s wait time between each field increment the temperature stays fairly constant, showing that the conditions are approximately adiabatic within this time frame.

This procedure has been repeated with different magnetic field step sizes and with the sample being reset in the FM state by cooling it to 240 K prior to heating it to 267 K. As will be discussed later this is a more accurate representation of realistic application performance. In Fig. 5.12a the individual ΔT_{ad} values are shown in the format $\Delta T_{ad}(H_{i-1} + \Delta H, T)$, where H_{i-1} is the initial field and ΔH the given field increment. In Fig. 5.12b the cumulative sum of each step is shown. The ΔT_{ad} value at each increment is defined as the temperature difference between two constant field plateaus, as seen in Fig. 5.11. The primary interest lies in the 0.25 step curves, shown for both the PM/FM reset experiments. The PM curve show much larger ΔT_{ad} values compared to the FM curve, but as will be shown in the following, these values are unstable during cyclic magnetization and hence under real application conditions. The MCE scaling with field can here be observed for relatively low fields in the permanent magnet range. There is a clear threshold around 0.5 T at this temperature, below which the MCE is insignificant. However, at field above 0.5 T the MCE increases approximately linearly with the field, providing about 2 K/T and 4 K/T in the FM/PM cases, respectively. The final temperature change in the FM case is largely independent

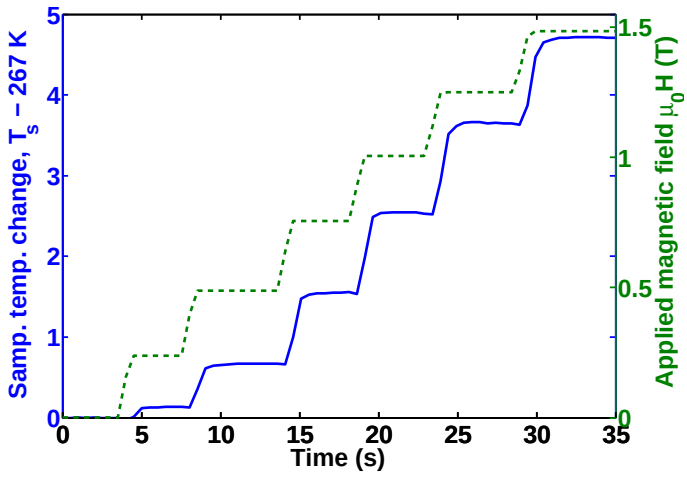

Figure 5.11: The adiabatic temperature change of a 120 mg sample of $Gd_5Si_2Ge_2$. The magnetic field is applied in steps of 0.25 T and the corresponding sample temperature change is recorded. The sample has been thermally reset in the paramagnetic state prior to this measurement.

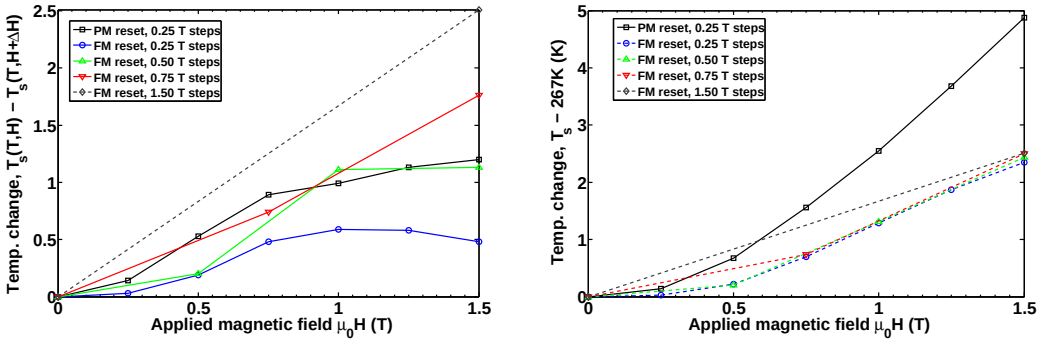

(a) The adiabatic temperature change as a function of field and field increments.

(b) The cumulatative sum of the ΔT_{ad} values in Fig. 5.12a.

Figure 5.12

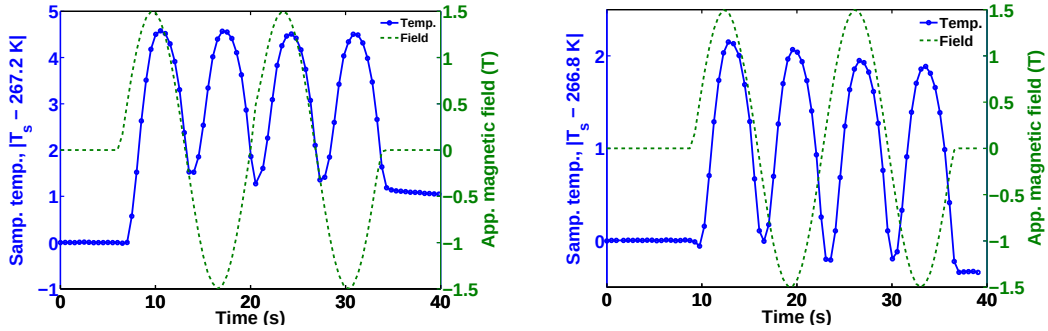

(a) PM reset **(b)** FM reset

Figure 5.13: Directly measured ΔT_{ad} during continuous magnetic field cycling between ± 1.5 T, shown for both a PM(a) and FM(b) sample reset.

of the field increment history. They all end up at approximately 2.5 K at 1.5 T with a small decrease with increasing numbers of steps, which is simply due to thermal losses since each step increases the measuring time about 5 s.

Magnetic field cycling

In order to address the issue of the cyclic stability of the MCE in first order materials and how preparation of the sample can affect the measured results, this section presents a series of cyclic measurements of ΔT_{ad}. It is shown that the large value obtained from an initial magnetization of a PM reset sample is misleading and should not be used for characterization.

In these experiments the sample undergoes a triple cycle of magnetization and demagnetization, initiated around 267 K. The field is continuously changed with a rate of 0.4 T/s. The cycling has been done both on a PM and FM reset sample, as shown in Fig. 5.13 (a) and (b), respectively. The figures show the absolute sample temperature T_s relative to the initial temperature of approximately 267 K.

As seen in the PM-reset cycle, there is an initial large temperature change of 4.5 K. However, the subsequent cycles settle at a constant value of approximately 3 K under both magnetization and demagnetization. In the case of the FM-reset, there is no initial anomalous ΔT_{ad} value; it remains constant at 2 K through all cycles. This behavior has been previously reported by Liu et al. [2012], Skokov et al. [2013] for other MCMs. It is noted that the initial temperatures in the

experiments are not equal. There is a difference of about 0.4 K, which can explain the difference in ΔT_{ad} between the experiments. As 267 K is right in the transition area, where the magnetization gradient with temperature is large, 0.5 K can easily change the MCE significantly.

It is important to note that there is no significant difference in ΔT_{ad} between magnetization and demagnetization. This suggests that the heat generation due to hysteresis loss is minimal compared to ΔT_{ad}, and the MCE is close to reversible. As seen from both figures, there is a steady drop in temperature with time due to thermal losses. This makes it non-trivial to estimate any differences in ΔT_{ad} between the different peaks, except that it is relatively small.

Magnetic field cycling - an AMR simulation

The results presented in the previous section show how $Gd_5Si_2Ge_2$ behaves under magnetic field cycling in a continuous manner. However, this is not what a material would experience in a cooling application where it would undergo an AMR-like cycle (section 2.1). In this section an experimental simulation of such a cycle is presented. The experiments are carried out in the following way

1. The system is either reset in the PM/FM state by heating or cooling to temperature of 240/320 K, respectively.
2. The system temperature is set to 267 K.
3. An applied magnetic field is applied from 0 to 1.5 T, with a rate of 0.4 T/s and the temperature change recorded.
4. The sample is thermally relaxed back to 267 K, corresponding to the heat removal step in the AMR cycle.
5. The magnetic field is removed, at a rate of 0.4 T/s and the temperature change recorded.
6. The sample is thermally relaxed back up to 267 K, representing the heat absorption step in the AMR cycle.
7. Steps 3-6 are repeated 3 times.

This procedure has also been carried out where steps 1-2 are done under a 1.5 T applied magnetic field, with the cycles initiated with the demagnetization step. In this case, the set temperature is 272 K. All these results are shown in Table 5.1.

	ΔT_{ad} (K), cooled to 267 K		ΔT_{ad} (K), heated to 267 K	
Cycle	Mag.	Demag.	Mag.	Demag.
1	4.51	-1.68	2.41	-1.69
2	2.31	-1.74	2.40	-1.69
3	2.35	-1.73	2.40	-1.67

	ΔT_{ad} (K), cooled to 272 K		ΔT_{ad} (K), heated to 272 K	
	Demag.	Mag.	Demag.	Mag.
1	-2.07	1.25	-4.14	1.35
2	-2.13	1.28	-2.87	1.38
3	-2.12	1.29	-2.87	1.34

Table 5.1: Measured adiabatic temperature change during a triple magnetization cycle with an applied magnetic field of 1.5 T, in both a heating and cooling mode. The field cycling has been done both with initial magnetization and demagnetization, shown in the top and bottom part of the table, respectively.

In the top table rows, the magnetization-demagnetization cycling is shown. The results show the same tendency as the previous section. The initially large PM-reset values are unstable and settle at lower and constant values in subsequent cycles. The FM reset values closely reproduce the stable PM reset values. The bottom table rows show the demagnetization-magnetization cycling. If the sample does indeed follow the isofield heating and cooling entropy curves these measurements should be antisymmetric compared to the magnetization-demagnetization cycling. Here one would expect the initial demagnetization after a FM reset to be large, where after it should settle at a lower constant value. This is exactly what is seen here and is also an effect seen elsewhere Küpferling et al. [2008].

The reason for not having equal initial temperatures in the two experiments is that the ΔT_{ad} values under magnetization and demagnetization at the same temperature are shifted, such that

$$\Delta T_{ad}(H_i; H_f, T) = -\Delta T_{ad}(H_f; H_i, T + \Delta T_{ad}(H_i; H_f, T)) \tag{5.3}$$

which is why the demagnetization cycling is set to 272 K.

ΔT_{ad} under application conditions

This section presents the measured temperature dependence of ΔT_{ad}. These measurements are carried out following the same AMR-like procedure as outlined in the previous section:

1. The wanted set point temperature T_i is set.
2. The sample is magnetized with an applied field of 1.5 T, at a rate of 0.4 K/s and the temperature change recorded.
3. The sample is thermally relaxed back to T_i.
4. The sample is demagnetized by removing the magnetic field and the temperature change recorded
5. The sample is thermally relaxed back to T_i
6. The system is cooled to a new set point T_{i+1} and steps 2-5 repeated until the lowest temperature is reached

The absolute values of the ΔT_{ad} measurements for both magnetization and demagnetization are shown in Fig. 5.14. A maximum ΔT_{ad} value of about 3.5 K in a 1.5 T applied magnetic field is in agreement with other published results [Giguère et al., 1999]. The two curves show similar shapes with a shift in the peak center (see Eq. (5.3)), as expected. However, it is noted that the magnetization curve is systematically higher around the peak compared to the demagnetization curve. This can be explained by the way the experiment is carried out. When changing the set point temperature, it goes from a heating mode, directly into a cooling mode (steps 5-6), which results in a movement in the (s, T)-plane from the zero field heating curve, to the zero field cooling curve. This corresponds to a partial PM-reset, as discussed in the previous section, and hence the ΔT_{ad} value is a bit larger than expected.

In hindsight, this experimentally procedure is not optimal, since the thermal and magnetic history become convoluted. Future measurements should be done in a heating mode or in a FM-reset mode, where the sample is thermally reset to a low temperature between each measurement. This would make the thermal and magnetic history of each measurement clear and the ΔT_{ad} values representative of realistic application conditions, opposed to a PM reset method, where all magnetization values would be artificially inflated.

In Fig. 5.14 the ΔT_{ad} values obtained from the DSC deduced entropy curves (Fig. 5.10a) are also shown. They are obtained as the temperature difference between the zero field heating and high field cooling curves at constant entropy,

$$s_{\mathrm{cool}}(1.5\mathrm{T}, T + \Delta T_{\mathrm{ad}}) - s_{\mathrm{heat}}(0\mathrm{T}, T) = 0\,, \tag{5.4}$$

for both magnetization and demagnetization. These estimates coincide approximately with the directly measured values. The estimated values are generally higher, which is expected from the lack of complete adiabatic conditions in the direct ΔT_{ad} measurements.

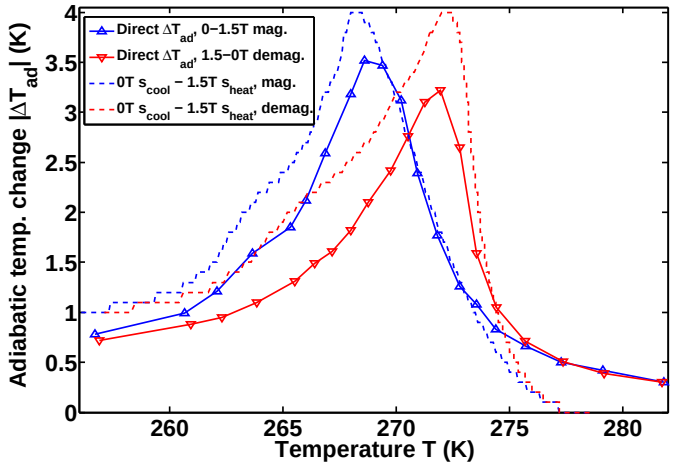

Figure 5.14: The absolute values of the adiabatic temperature change, measured under the application and removal of a 1.5 T applied magnetic field (symbols). The dashed lines show the estimated ΔT_{ad} obtained from the DSC deduced entropy curves in Fig. 5.10a.

5.3 Discussion and summary

In this chapter a series of different characterizations of the first order material $Gd_5Si_2Ge_2$ were carried out. All experiments were performed on samples taken from the same sample batch, though not all on the exact same sample. This allows for a more direct comparison of results obtained by various means.

The isothermal entropy change Δs was estimated through using the Maxwell relation on magnetization measurements, integration of the heat capacity measured on a DSC device and a more direct measurement, employing the DSC device to measure the heat released during magnetization. These different approaches are all shown in Fig. 5.15. The magnetometry estimates from isofield heating and cooling measurements coincide nicely with those of the corresponding calorimetric estimates. The isothermal magnetization and demagnetization estimates are here omitted, since they approximately coincide with the isofield measurements. Furthermore, the demagnetization curves are not comparable with the heating mode measurements due the partial transformations they represent due to the magnetic field being too small to complete the transformation.

The main point of Fig. 5.15 is that the most direct measurement of Δs corresponds to the (s, T)-space bounded by the low field heating and high field

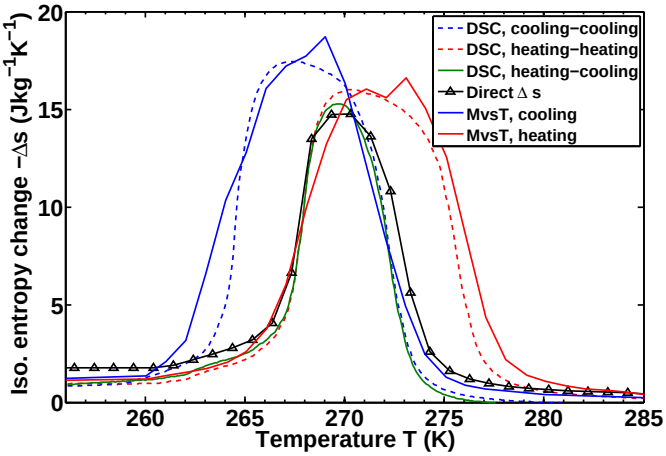

Figure 5.15: Comparison of Δs estimates from magnetometric (Maxwell relation), calorimetric (heat capacity) and direct measurements. The first and second DSC term represent low and high magnetic field curves.

cooling entropy curves. As seen from the figure, this space is well approximated by the minimum of the heating and cooling curves, through both magnetometry and calorimetry. This suggests a simple way to realistically estimate the MCE from the Maxwell relation, with no need of further measurements: the overlapping area between heating/cooling or magnetization/demagnetization modes reflect the available (s, T)-space under application conditions.

The idea that the available (s, T)-space is bounded by the low field heating and high field cooling entropy curves is also supported by the ΔT_{ad} measurements, especially Fig. 5.14. Here estimated ΔT_{ad} -values obtained from the entropy curves approximately match the directly measured values. Furthermore, the magnetic field cycling show that the sample can be prepared to be on the low field cooling or high field heating curves, prior to an initial magnetization and demagnetization, respectively, which leads to initial large ΔT_{ad} values. However, subsequent cycling of the field leads to significantly smaller but constant ΔT_{ad} values, which suggests that the material enters a bound metastable region. As will be shown in chapter 7.4, this is also supported by Preisach simulations of $Gd_5Si_2Ge_2$.

Chapter 6

Characterization of MnFe(P,As)

In the following chapter a series of experimental characterizations of two different compounds of the first order material MnFe(P,As) will be presented. The purpose of this chapter is to present a broad range of experimental investigations that give a characterization of the hysteretic properties, some of which can be used for modelling later on. The primary results based on the experimental data presented in section 6.2 has been published in von Moos et al. [2014d](see appendix A) and von Moos et al. [2014a] (see appendix B).

The experimental characterization presented here is not as extensive and naturally coherent as for the $Gd_5Si_2Ge_2$ material, due to the availability of samples and experimental equipment at the time this work was carried out. However, the conclusion of the chapter reinforce those observed for $Gd_5Si_2Ge_2$ in chapter 5. Here the material properties are also investigated though both application in a real magnetic refrigeration device and through Mössbauer spectroscopy.

The two compounds are characterized individually and treated in their own respective sections. Both samples were provided by *BASF - The Chemical Company*, which due to the commercial nature of the material production means that there is no specific information available in regards to the exact stoichiometry and preparation methods. As the purpose of this work is not to evaluate performance and design new materials, the materials are just considered as different examples

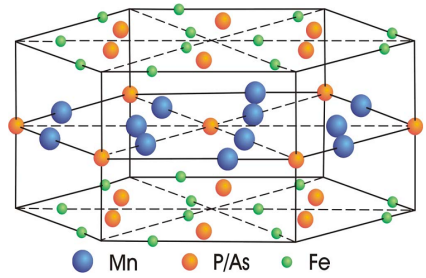

Figure 6.1: Crystal structure of MnFe(P,As) [Bacmann et al., 1994].

of first order hysteretic compounds with different characteristics that can be sought to be captured by a general modelling approach. This chapter is primarily meant as a presentation of results and does not contain detailed explanations and discussions of experimental methods and procedures. Descriptions and discussion regarding standard characterization methods of magnetometry and calorimetry can be found in chapter 4 and 3, respectively.

Manganese based materials have been known to have a significant magnetocaloric effect (MCE) across broad temperature ranges, depending on the composition [Belov et al., 1974]. A large room temperature MCE was presented by Wada and Tanabe [2001] in Mn(As,Sb) compounds and shortly after in MnFe(P,As) compounds by Tegus et al. [2002]. The MnFe(P,As) compounds have been studied in recent years due to their potential efficient use in magnetic refrigeration. MnFe(P,As) is a first order magnetocaloric material that has a coupled magnetic and structural phase transition. The transition temperature T_t can be tuned by varying the ratio between P and As [Tegus et al., 2002]. As is generally the case with first order materials, the transition is accompanied by hysteresis, the severity depending on the specific composition. The material has a hexagonal Fe_2P crystal structure, as shown in Fig. 6.1 [Bacmann et al., 1994]. Each Fe-site has four P/As neighbors. P and As atoms are randomly distributed at these sites, leading to 5 different Fe-neighborhoods, with between 0-4 P/As atoms. Several other Mn-based compounds has recently also been studied, in order to eliminate potential toxic elements such as As, maximize the MCE and minimize hysteresis. A large study of different Mn-type compounds can be found in Dung [2012], Wang [2012].

6.1 Low hysteresis MnFe(P,As)

The standard indirect characterization methods of calorimetric and magnetization measurements are employed and supplemented by direct measurements of the adiabatic temperature change ΔT_{ad}. All measurements are carried out on the same sample, allowing for direct comparison. The isothermal magnetization measurements presented here are also used for modelling purposes in sec. 7.3. The sample used in this study was prepared by BASF and the actual P/As-ratio is not known. The composition was chosen such that the transition temperature is around 293 K. The sample used for these measurements is an approximately rectangular cuboid, with dimensions $(L, W, H) = (3.35, 1.95, 1.05)$ mm and a sample mass of 37 mg. Following the approach given by Aharoni [1998], this leads to an approximate demagnetization factor along the length L of $N_L \approx 0.2$. However, in the following demagnetization effects are not compensated, since the same sample is used for all measurements, with the exception of the ΔT_{ad} measurements. These were carried out prior to this thesis work was started and the sample dimensions are not currently known.

Magnetometry

In the following sections the results of both isofield and isothermal magnetization measurements are presented. All measurements are done on a LakeShore 7407 vibrating sample magnetometer. The technical details concerning the instrument and the procedures are discussed in chapter 4. This series of measurements will be the basis of a Preisach model (sec. 7.3), as the experimental data has a good resolution in both temperature and magnetic field variation, allowing for detailed modelling.

Isofield measurements

This series of measurements were carried out following a standard cooling and heating procedure:

1. Heating to the maximum temperature, 350 K
2. Application of a constant applied magnetic field $\mu_0 H = 0.02$ T
3. Measurement of the magnetization M at 350 K
4. Steady and monotonic[1] temperature decrease to the new setpoint temperature T_i

[1] The monotonic temperature change is important for first order materials, see section 4.2.

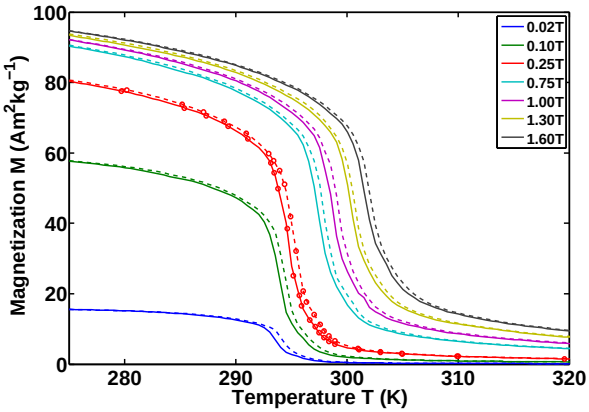

Figure 6.2: Magnetization of a MnFe(P,As) sample, measured under the application of constant applied magnetic fields. Solid and dashed lines represent the cooling and heating, respectively, and the symbols the temperature step size.

5. Thermal relaxation of the sample for 5 min
6. Measurement of the magnetization at T_i
7. Repetition of steps 4-6 until the lowest temperature of 250 K is reached
8. Repetition of steps 4-6 in a heating mode where the temperature is monotonically increased between 250-350 K
9. Repetition of steps 1-8 for the different magnetic fields of $\mu_0 H = (0.02, 0.10, 0.25, 0.75, 1.00, 1.30, 1.60)$ T

The results are shown in Fig. 6.2, in the temperature range 275-320 K where the transition takes place. Each isofield temperature scan is shown in separately colored lines, with the solid and dashed lines illustrating the heating and cooling modes, respectively. The measurements done at 0.25 T are shown with circular symbols to illustrate the small temperature step size. In Fig. 6.3 the transition temperature T_t is shown as a function of the applied magnetic field. The transition temperature is here defined as the point of inflection on the magnetization curve. In this field range the shift of the transition temperature is approximately linear with the applied field, with a gradient of about 5.2 K/T. A relatively small 0.6 K thermal hysteresis is present between the heating and cooling modes across the entire field range.

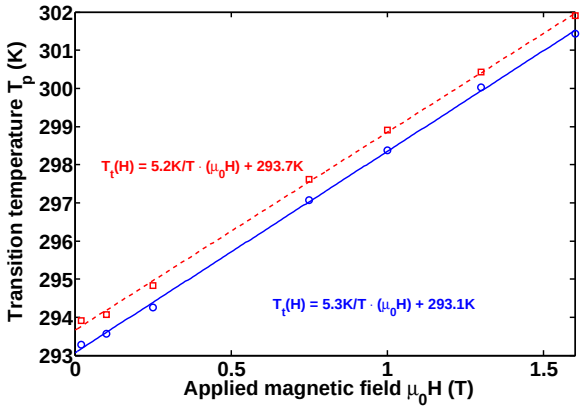

Figure 6.3: The transition temperature (symbols), defined as the point of inflection on each magnetization curve, along with linear fits.

In Fig. 6.4 the values of Δs are calculated using the Maxwell relation (Eq. (2.8)) and are shown for the cooling and heating mode, depicted by solid and dashed lines, respectively. From this plot it is clear that the magnetization does not vary smoothly across the transition, giving rise to two separate peaks in both the heating and cooling modes. This can be caused by the inherent properties of the material itself, becoming apparent due to the fine temperature resolution. It can also be relaxation effects, since the sample spends a long time right at the transition, and the hysteresis is relatively small. The values between 1.3 T and 1.6 T, which is used later for comparison with other experiments, is about 12 J/kg/K. The maximum Δs and full-width-at-half-maximum (FWHM) values for each peak are shown in Fig. 6.5. The maximum peak values become less sensitive to increasing the applied magnetic field as the field increases. The width of the Δs peaks scale approximately linearly with the applied field, which is known to be the case with both Gd-Si-Ge and Mn-Fe based first order materials [Basso et al., 2006a, Wada and Tanabe, 2001].

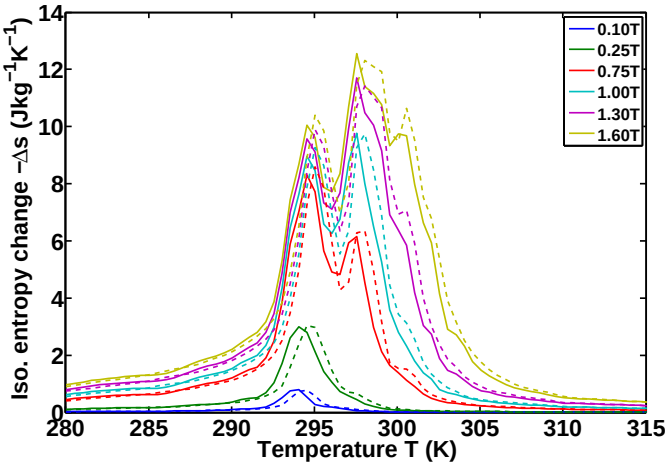

Figure 6.4: The isothermal entropy change, obtained from the Maxwell relation for both heating(dashed) and cooling (solid) modes, shown for increasing applied magnetic fields of $\mu_0 H = (0.10, 0.25, 0.75, 1.30, 1.60)$ T.

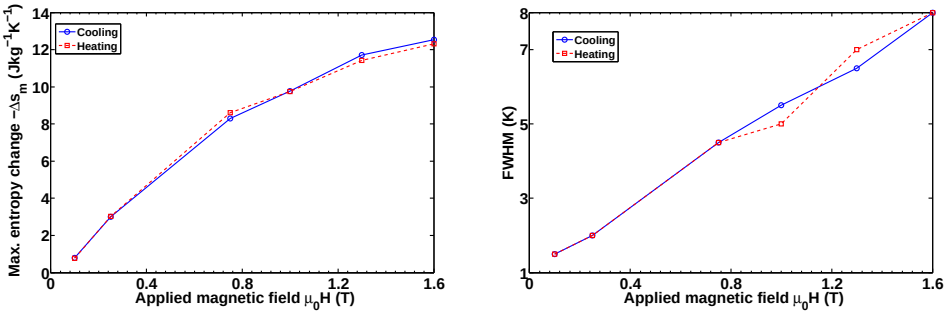

(a) The maximum entropy change from Fig. 6.4.

(b) The full width at half maximum of the Δs-peak obtained from Fig. 6.4

Figure 6.5

Isothermal measurements

These measurements were carried out by measuring the isothermal sample magnetization during application and removal of an applied magnetic field between 0

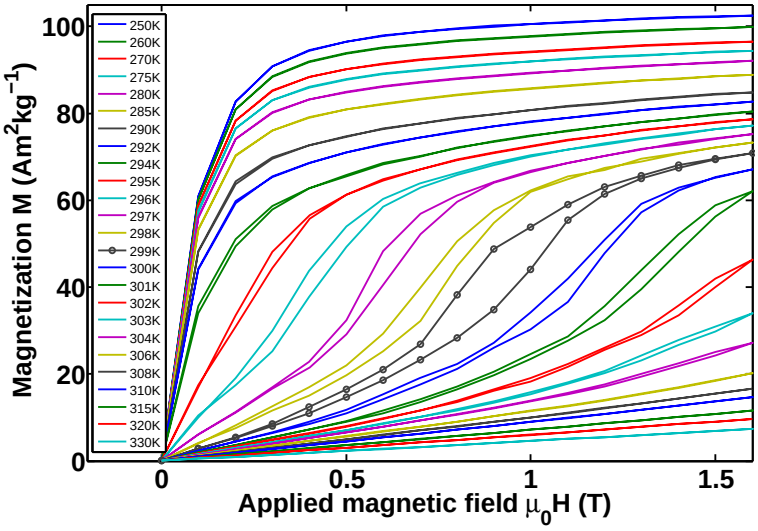

Figure 6.6: Magnetization of MnFe(P,As) measured during isothermal mag- and demagnetization between an applied magnetic field of 0 and 1.6 T

and 1.6 T in steps of 0.1 T:

1. The sample is cooled to 250 K
2. A magnetic field is stepwise applied to the sample, from 0 T to 1.6 T in steps of 0.1 T. The measurements are done point-by-point and the magnetic field is changed with a rate of 0.067 T/min between measurements[2]
3. The magnetic field is removed in the same stepwise manner
4. The sample temperature is increased to the new setpoint and steps 2-3 are repeated

The entire set of results are shown in Fig. 6.6, showing each isotherm with varying colored lines. The scan at 299 K is marked with symbols to illustrate the field resolution.

In Fig. 6.7a Δs is calculated from the Maxwell relation for an applied magnetic field change from 0 to 1.6 T and shown with the corresponding calculation from the isofield measurements. Since the hysteresis is so small in this material, there

[2]See section 4.3 for a discussion about the importance of low field ramps in MCMs

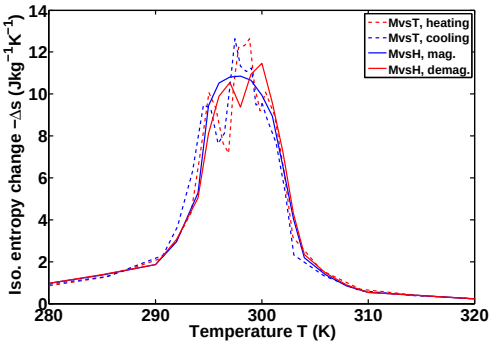

(a) The isothermal entropy change Δs of MnFe(P,As) , calculated from the Maxwell relation from a magnetic field change from 0 to 1.6 T.

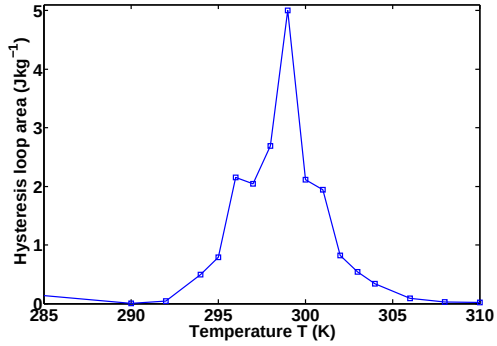

(b) The hysteretic loss in each magnetization cycle between 0 and 1.6 T.

Figure 6.7

is little mixing of the PM and FM states, resulting in approximately coinciding curves. There is no clear problems with not employing the reset-method as discussed in section 4.5. Any possible difference between the two methods is below the numerical precision, which is also noted to obscure most of the thermal hysteresis.

In Fig. 6.7b the hysteretic loss during each magnetization cycle is shown, calculated as the magnetization loop area. The hysteresis peak is centered around the maximum Δs values, which was also reported by [Hansen et al., 2010]. The maximum hysteretic loss is about 5 J/kg during a magnetization and demagnetization cycle between 0 and 1.6 T. This corresponds to an entropy production of roughly $\sim 5/300 = 0.02$ J/kg/K. Only half of this value is produced during the magnetization/demagnetization step, corresponding to approximately 0.1% of the estimated reversible isothermal entropy change of 12 J/kg/K.

Calorimetry

In this section a series of heat capacity measurements are presented. These measurements were carried out by Kaspar Nielsen before this PhD work was started, however the data analysis is done by the thesis author. The measurements were done on the DSC described in 3, in both heating and cooling modes between 240-315 K, using a temperature scanning rate of $R = \pm 1$ K/min, respectively. Each cooling and heating scan was carried out under the constant applied magnetic

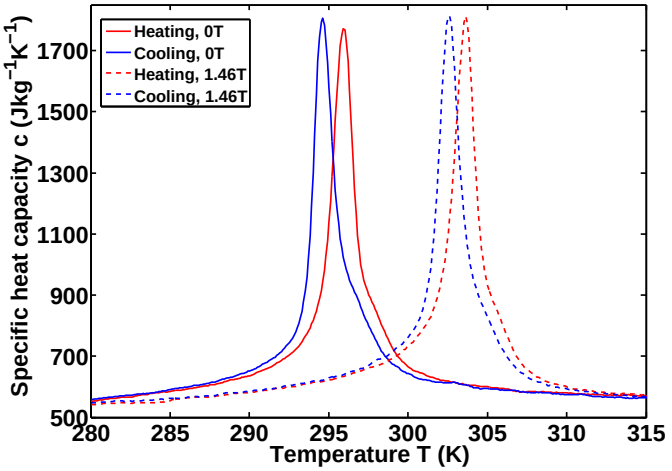

Figure 6.8: The specific heat capacity of a MnFe(P,As) sample measured with DSC.

fields of 0 T and 1.5 T using a permanent magnet setup at a pressure below 10^{-5} mbar. These results are shown in Fig. 6.8 in the temperature range 280 K to 315 K.

The heat capacity is roughly constant at 550 J/kg/K in this temperature range, away from the transition, and peaks at 1800 J/kg/K at the transition. A thermal hysteresis of about 1 K is seen between the two peaks. As discussed in sec. 3.3, it can be non-trivial to correctly determine the thermal hysteresis from DSC measurements, due to the peak's dependence of sample properties. Using the peak temperatures will overestimate the thermal hysteresis, which is in line with the 0.6 K thermal hysteresis measured through magnetometry.

The heat capacity can be integrated to calculate the entropy,

$$s_H(T') - s_0(T_0) = \int_{T'}^{T_0} \frac{c_H(T)}{T} dT \,. \tag{6.1}$$

Setting $T_0 = 315$ K and $s_0(T_0) = 0$, the results for $\mu_0 H = 0$ and $\mu_0 H = 1.5$ T are shown in Fig. 6.9a. The isothermal entropy change can be estimated from the difference in the 0 and high field entropy curves. This is shown in Fig. 6.9b, where the three relevant combinations of curve differences are shown along with the Maxwell estimates from the isothermal magnetization measurements. As hysteresis effects are almost completely screened by numerical noise in the magnetization measurements, there is no clear direct comparison between the

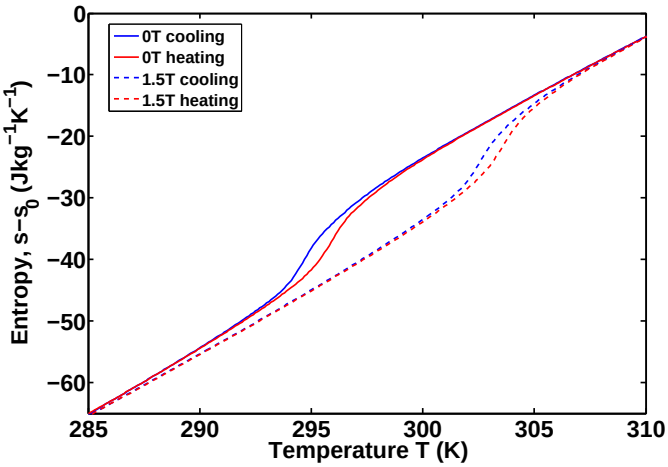

(a) Entropy deduced from the heat capacity measurements.

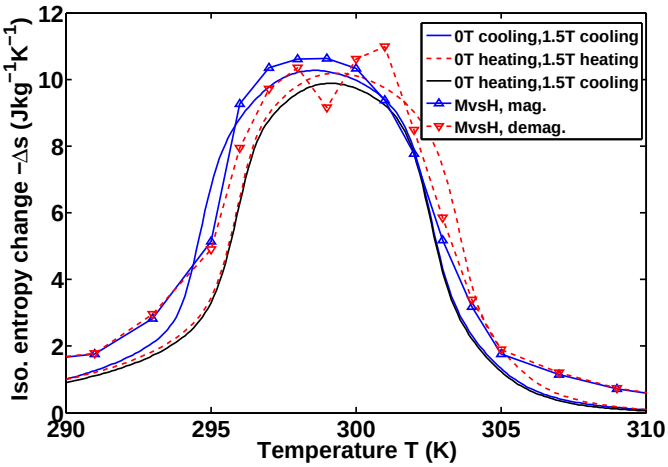

(b) Different ways of calculating the isothermal entropy change.

Figure 6.9

corresponding cooling/magnetization and heating/demagnetization estimates of Δs, other than the curves approximately coincide.

Direct ΔT_{ad} measurements

A series of direct adiabatic temperature change measurements were done under application and removal of a magnetic field of 1.5 T. This was carried out in an older setup, where a thermocouple is sandwiched between to sample pieces. The sample is placed on the end of a rod, connected to a motor. The sample end is then continuously dropped and raised into the bore of a permanent, Hallback magnet. The whole system is located inside a freezer at an initially low temperature. As the experiment runs, the freezer is slowly heated by a 40 W heat source inside. This means that the experiments are carried out under ambient pressure in a heating mode, with little thermal relaxation time between magnetization and demagnetization measurements. This equipment in described in further detail in [Bjørk et al., 2010b]. The results are shown in Fig. 6.10, along with the estimated values from Fig. 6.9a obtained as the temperature difference between the different zero field and high field entropy curves such that

$$s_{h,c}(0\mathrm{T}, T) = -s_{h,c}(1.5\mathrm{T}, T + \Delta T_{\mathrm{ad}}(0; 1.5\mathrm{T}, T)) \,. \tag{6.2}$$

These results suggest that using the low field heating and high field cooling entropy curves to estimate the real MCE provides the best correspondence with direct measurements. This result has also been observed for other Mn-based compounds in Tocado et al. [2006]. The indirect method overestimates the ΔT_{ad} values compared to the direct estimates, which is expected due to the lack of adiabatic conditions in the direct measurements. The width and centering of the peaks do however fit nicely, whereas using low and high field cooling or heating curves will shift the estimates to too low and high temperatures, respectively.

To illustrate the reversibility of the MCE observed, the values obtained during demagnetization can be compared to shifted values obtained during magnetization. In the completely reversible case, where no heat is generated due to hysteresis, the demagnetization curve should follow as

$$\Delta T_{\mathrm{ad}}(H_f; H_i, T + \Delta T_{\mathrm{ad}}(H_i; H_f, T)) = -\Delta T_{\mathrm{ad}}(H_i; H_f, T) \,. \tag{6.3}$$

If hysteretic heat production is present, the measured demagnetization curve is expected to be lower. This comparison is shown in Fig. 6.11, where Eq. (6.3) is seen to hold within the uncertainty of these experiments. This is not to say that no hysteresis losses are present, but to note that they are small compared to the MCE.

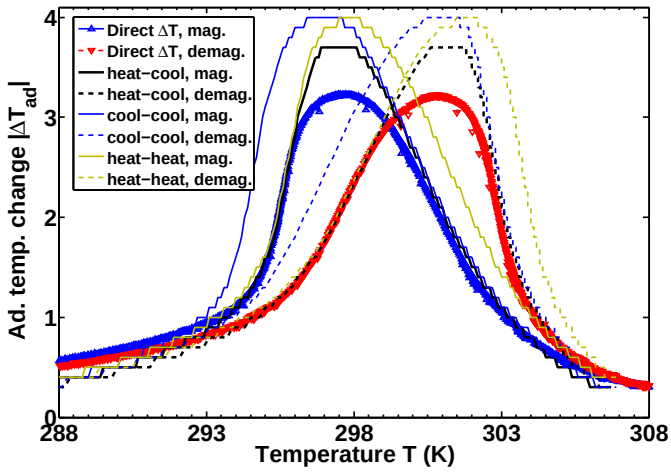

Figure 6.10: Comparison of ΔT_{ad} estimates from heat capacity and direct measurements. The first and second DSC terms in the legend represent low and high magnetic field entropy curves.

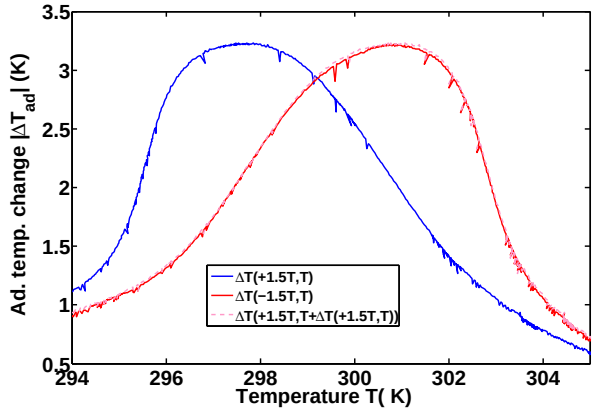

Figure 6.11: Comparison between the directly measured ΔT_{ad} demagnetization curve and one inferred from the ΔT_{ad} magnetization curve.

6.2 High hysteresis MnFe(P,As)

Like the MnFe(P,As) sample discussed in the previous section, this sample was provided by BASF, with unknown stoichiometry and preparation methods. As will be presented in the following, the compound characterized here is very different in its hysteretic properties compared to the other sample.

In this section a series of isofield magnetization measurements are presented. As this material was available in large quantities, in the form of flat plates it allowed for testing in a working magnetic cooling device located at DTU Energy Conversion. These results are published in von Moos et al. [2014d] (appendix A). In corporation with Vittorio Basso a series of calorimetric measurements were carried out by the thesis author at Istituto Nazionale di Ricerca Metrologica in Torino, Italy. These measurements enable characterization of partial phase transitions, which is of general relevance in hysteretic materials. These results along with the corresponding Preisach model of the material are published in von Moos et al. [2014a](appendix B) and were presented at the Delft Days 2013 conference in poster format (appendix F).

Lastly, a short section presents the results of Mössbauer measurements done as part of a side project. They illustrate the clear coexistence of the FM and PM phase in the material around the transition.

Isofield magnetization

This series of measurements were carried out following a standard cooling and heating procedure:

1. Heating to the maximum temperature, 320 K
2. Application of a constant applied magnetic field $\mu_0 H = 0.05$ T
3. Measurement of the magnetization M at 320 K
4. Temperature decrease to the new setpoint temperature T_i
5. Thermal relaxation of the sample for 5 min
6. Measurement of the magnetization at T_i
7. Repetition of steps 4-6 until the lowest temperature of 275 K is reached
8. Repetition of steps 4-6 in a heating mode where the temperature is between 275-320 K

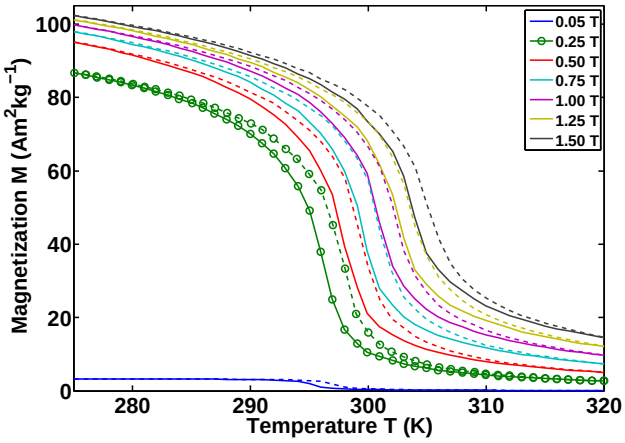

Figure 6.12: Magnetization as a function of temperature at constant external magnetic field with solid and dashed curves show cooling and heating, respectively. The symbols illustrate the temperature resolution for all isofield scans.

9. Repetition of steps 1-8 for the different magnetic fields of $\mu_0 H = (0.25, 0.50, 0.75, 1.00, 1.25, 1.50)$ T

The results are shown in Fig. 6.12. Each isofield temperature scan is shown in separately colored lines, with the solid and dashed lines illustrating the heating and cooling modes, respectively. The measurements done at 0.25 T are shown with circular symbols, to illustrate the temperature step size. In Fig. 6.13 the transition temperature T_t is shown as a function of the applied magnetic field. The transition temperature is here defined as the point of inflection on the magnetization curve. In this magnetic field range the shift of the transition temperature is approximately linear with the applied field. However, there is a clear difference in the FM-to-PM and PM-to-FM transitions line gradients; the hysteresis is visibly reduced at higher fields. This is the only material treated in this work were this behavior is evident at magnetic field below 1.6 T. The mean shift in transition temperature with applied magnetic field is about 6 K/T. The thermal hysteresis is at low fields between 2-1.5 K and then reduces to just about 1 K at higher fields.

In Fig. 6.14 the values of Δs are calculated using the Maxwell relation (Eq. (2.8)) and are shown for the cooling and heating mode, depicted by solid and dashed lines, respectively. The maximum value obtained is 9 J/kg/K at an applied

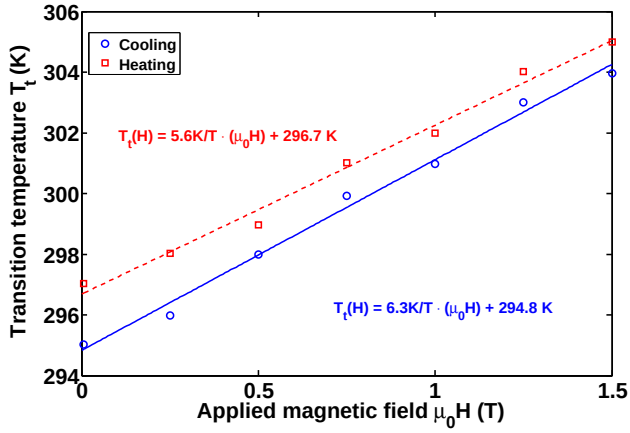

Figure 6.13: The transition temperature, defined as the point of inflection on each magnetization curve.

magnetic field change from 0 to 1.5 T. The maximum Δs and full-width-at-half-maximum (FWHM) values for each peak are shown in Fig. 6.15a and Fig. 6.15b, respectively. The maximum peak values become less sensitive to increasing the applied magnetic field as the field increases and the width of the Δs peaks scale approximately linearly with the applied field.

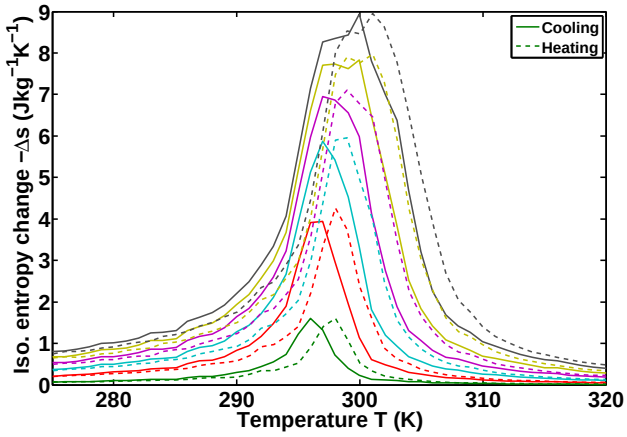

Figure 6.14: The isothermal entropy change calculated from applying the Maxwell relation to Fig. 6.12 for magnetic field changes from 0 to $\mu_0 H = \{0.25, 0.50, 0.75, 1.00, 1.25, 1.50\}$ T.

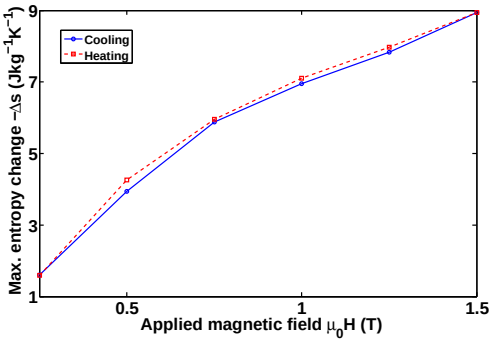

(a) The maximum Δs values as function of applied magnetic field in Fig. 6.14.

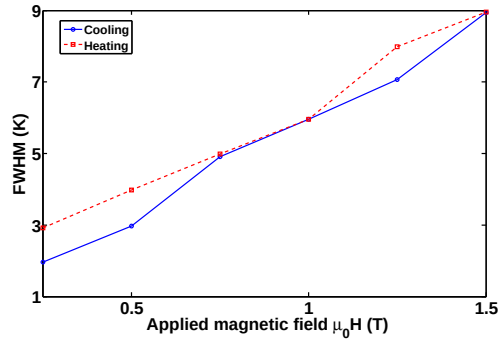

(b) The full width at half maximum of the entropy change peaks in Fig. 6.14.

Figure 6.15

Calorimetry

This section presents the results of a series of calorimetric measurements, carried out at INRIM in Torino Italy, in corporation with Vittorio Basso. The purpose of these measurements is to characterize the material behavior during partial phase

transitions. This is of general interest in first order MCMs, since they do not always undergo complete phase transition under real application conditions. This especially applies to situations where only smaller magnetic fields are available. If they are insufficient to force a complete transition, the material will only go through minor hysteresis loops under magnetization and demagnetization. The data presented here is used in a Preisach model, with the purpose of capturing the partial transition behavior. This is described in section 7.2.

The measurements are carried out on a commercial Perkin-Elmer diamond DSC (see section 3.2). The measurements are done in zero field, since this setup does not allow for any external magnetic field. These measurements are the calorimetric equivalent to the first order reversal magnetization curves (FORC) done on $Gd_5Si_2Ge_2$, as described in 5.1. The following procedure was used

1. The system is cooled to 275 K
2. The temperature is ramped with $R = +2$ K/min while measuring the heat flux to/from the sample.
3. The temperature is ramped until the chosen reversal temperature is reached, whereafter the ramp is immediately reversed to $R = -2$ K/min.
4. Steps 1-3 are repeated for a series of increasing reversal temperatures.

An example of a reversal scan is shown in Fig. 6.16a. Here the reversal temperature is 308 K, which allows for a complete phase transition. It is noted that the data is not presented as heat capacity, but as heat flux. These are related, approximately as $c \approx q/R$, where $R = (2/60)$ K/s. This is done to make the data easier visualize compared to a positive heat capacity scale. The heat capacity is approximately 600 J/kg/K away from the transition and peaks around 1800 J/kg/K. There is a thermal hysteresis of approximately 1.4 K, which is similar to what was found through the magnetization measurements.

The entropy is calculated from the heat flux

$$s(T) - s(T_0) = \frac{1}{m} \int_{T_0}^{T} \frac{q(T)}{\dot{T}\, T} dT \tag{6.4}$$

where m is the sample mass and $s(T_0) = s(275\text{K}) = 0$. The entropy curve corresponding to Fig. 6.16a is shown in Fig. 6.16b. The temperature dependence of the entropy in both the low temperature FM phase and high temperature PM phase is approximately linear

$$s_1(T) = \alpha(T - T_0)\,, \qquad s_0(T) = s_1(T) + \delta s \tag{6.5}$$

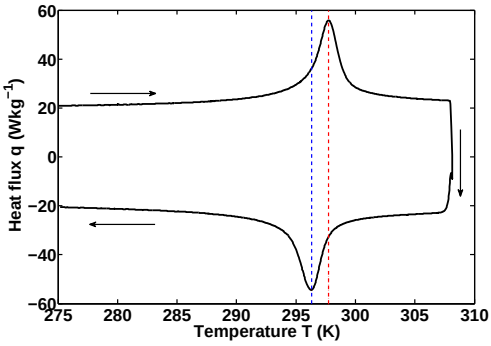

(a) Experimentally measured heat flux to a MnFe(P,As) sample during a temperature scan with rate ±2 K/min.

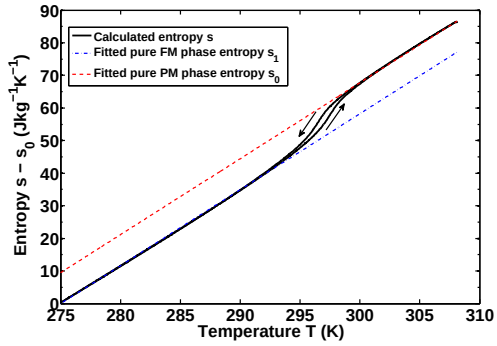

(b) The entropy derived from the heat flux measurements, along with linear fits of the high and low temperature phases.

Figure 6.16

with $\alpha = 2.3$ J/kg/K and $\delta s = 10.7$ J/kg/K. These pure phase expressions are used along with the actual entropy s to estimate the current material FM phase fraction X

$$X = \frac{s - s_0}{s_0 - s_1}\,. \tag{6.6}$$

This approach was used on a series of FORC measurements with varying reversal temperatures. The heat flux data is shown in Fig. 6.17a, where alternating solid and dashed lines and coloring has been introduced to make separation of the curves easier. In Fig. 6.17b the estimated FM phase fraction is shown for a selection of the heat flux measurements. These are obtained through the procedure outlined above. At each reversal point there is a small oscillation in the heat flux, which is assumed to be related to the PID control of the DSC heater. This is not related to the material itself and has been filtered out when possible in the estimated phase fraction calculations.

The phase fraction estimates in Fig. 6.17b illustrate an important feature of the material during partial phase transitions, namely the gradient of X with temperature right after the reversal point. This gives information about the reversibility of the transition. In the completely reversible case the ascending returnbranch would follow the initial descending curve, where in a very irreversible case it would be completely horizontal. This is further discussed in the modelling section 7.2.

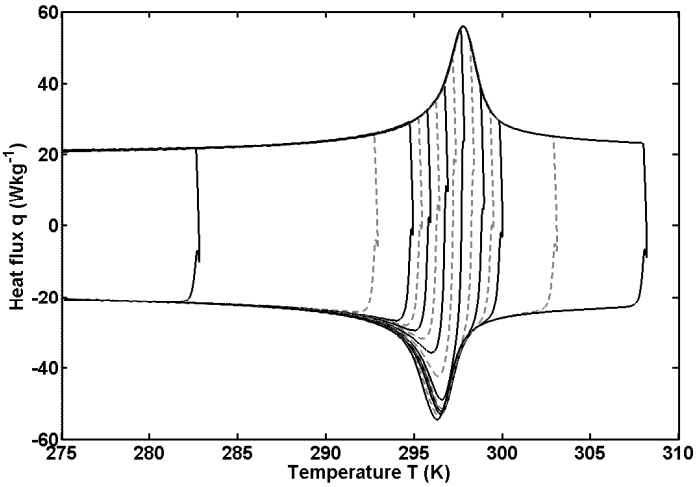

(a) Measured heat flux supplied to a MnFe(P,As) sample during a ±2 K/min temperature scan.

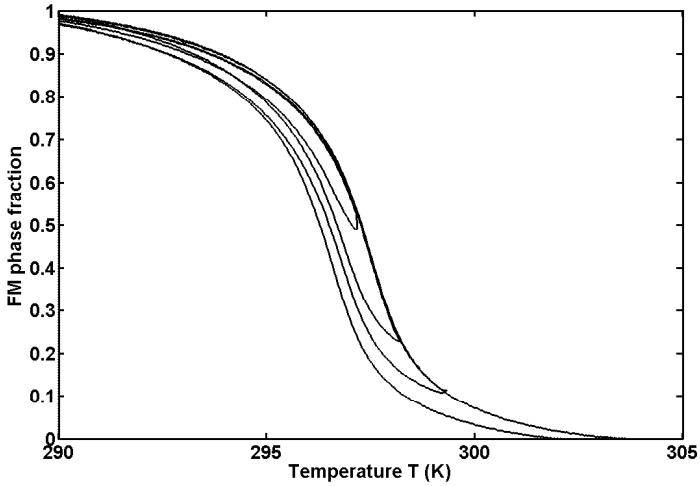

(b) Estimated FM phase fraction of the material.

Figure 6.17

Material application in a magnetic cooling device

As this MnFe(P,As) -compound was produced and available in large quantities of flat plates, it could be tested as a refrigerant in an actual magnetic cooling device.

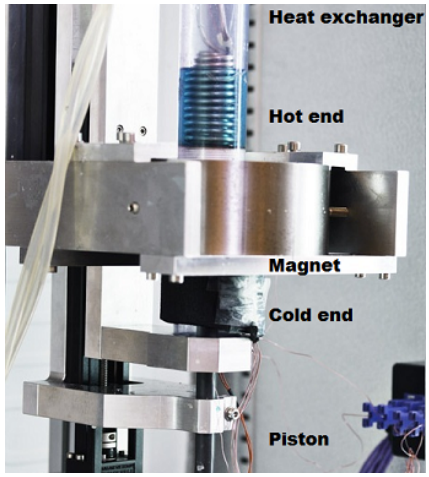

(a) The magnetic refrigeration device.

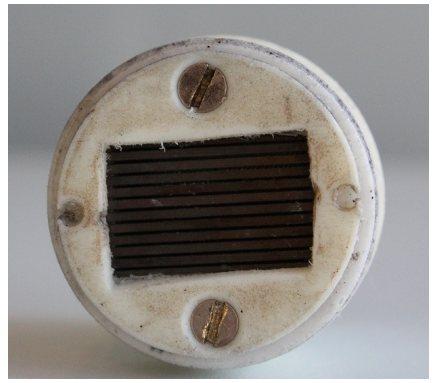

(b) The regenerator housing approximately 63 g of MnFe(P,As) in the form of flat plates.

Figure 6.18

The magnetic refrigeration device used for these experiments is briefly described in the following. Further details can be found in Bahl et al. [2008].

The magnetic refrigeration device is shown in Fig. 6.18 along with the MnFe(P,As) flat-plate regenerator. The material within the regenerator is moved in and out of a magnetic field of 1 T, provided by a cylindrical permanent magnet. After material magnetization, part of the heat produced is transferred to an inter-plate liquid, which is then pushed to the hot side by a piston. By moving the regenerator out of the field, the material is cooled and heat is absorbed from the liquid, which is then pulled to the cold end by the piston. This active magnetic regenerator (AMR) cycle is then run continuously until a steady temperature difference is build up between the hot and cold ends. The system runs such a cycle with a frequency of about 0.2 Hz. The hot side of the regenerator is kept at constant temperature through a heat bath at a controlled temperature.

A series of measurements of the temperature span between the hot and cold side temperatures were done for a range of hot side temperatures between 314 - 294 K. The measurements carried out in both a cooling and heating mode. The temperature span at each hot end temperature was measured when the system had completely settled thermally after about 1 hour, corresponding to about 700 AMR cycles. In Fig. 6.19 the results are shown. The maximum temperature span is just below 5.5 K for both series of measurements and the peak performance temperature is about 302.5 K and 303.5 K when cooling and heating, respectively.

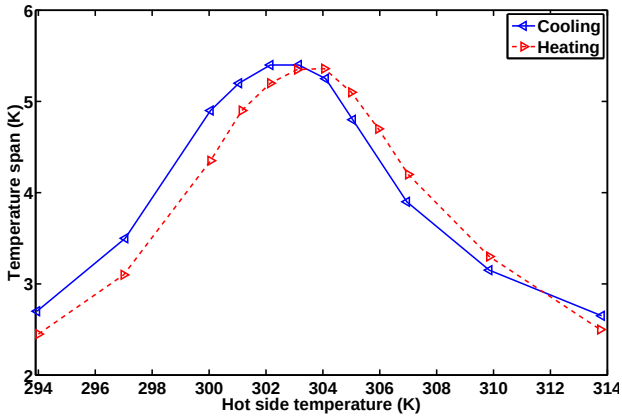

Figure 6.19: The measured temperature span between the hot and cold side of the refrigeration device. A stack of 12 flat plates of MnFe(P,As) , totaling 63 g, was used as a regenerator, cycling between 0 and 1 T magnetic field with a frequency of 0.2 Hz.

These temperatures are slightly higher than the peak temperature of the Δs curves measured by magnetometry. This is due to the material experiencing a thermal gradient along its length. A thermal hysteresis of about 1 K is observed, matching the values previously established through magnetization measurements. This illustrates that thermal hysteresis remains present in a real refrigeration device and that it is sustained through thousands of AMR cycles. The reason that the thermal hysteresis is sustained through all these cycles is due to the relatively small magnetic field. It is insufficient to wipe out the thermal history of the sample. Due to the long thermal equilibrium time between each measurement, these hysteresis effects are not caused by thermal lag in the system. It is noted that the temperature span for the cooling curve at 314 K is relatively high. However, this is the first measured point in the series of experiments. The regenerator was not heated up above 314 K prior to this measurement and the actual thermal history is unknown.

Mössbauer spectroscopy

As part of a side project, the MnFe(P,As) compound was characterized by Mössbauer spectroscopy. This method allows for a probing of the Zeeman effect and hyperfine energy splitting in magnetic materials. These results are somewhat

Transition	Δm	Angular dependence	Random orientations	$\phi = \pi/2$
$+3/2 \rightarrow +1/2$	-1	$\frac{9}{4}(1+\cos^2\phi)$	3	3
$-3/2 \rightarrow -1/2$	$+1$	$\frac{9}{4}(1+\cos^2\phi)$	3	3
$+1/2 \rightarrow +1/2$	0	$3\sin^2\phi$	2	4
$-1/2 \rightarrow -1/2$	0	$3\sin^2\phi$	2	4
$-1/2 \rightarrow +1/2$	$+1$	$\frac{3}{4}(1+\cos^2\phi)$	1	1
$+1/2 \rightarrow -1/2$	-1	$\frac{3}{4}(1+\cos^2\phi)$	1	1

Table 6.1: Transition probabilities as a function of the angle ϕ between gamma-rays and nuclear spin. The relative intensities are given for random and perpendicular orientations [Mørup, 2004].

decoupled from the rest of this chapter, but they give a quantitative illustration of the coexistence of phases in the material. No background information is here given on the Mössbauer method and just the results are presented. For an introduction, see [Mørup, 2004].

A sample was prepared by grounding the MnFe(P,As) material and fixing it in a flat plastic container. The container was mounted in an evacuated chamber that was connected to a Nitrogen cryostat and a Co^{57} source was used. For data analysis the freeware program *mfit* was used. It fits Lorentzians to the obtained resonance lines under given restrictions. When fitting the data, one doublet and one sextet is used. Furthermore, the relative intensities of the resonance lines (see table 6.1) are forced onto the fit and each line pair is forced to be identical. As there are 5 different Fe-sites in this compound one should fit 5 sextets. This is not done here, since it will complicate things enormously. This was done by Brück et al. [2005] on a similar compound.

Three different temperatures were measured; 285 K, 296 K and 305 K, where the magnetic transition temperature is around 296 K. The sample was measured at these temperatures both originating from the ferromagnetic phase, being cooled to 80 K prior to the measurements and originating from the paramagnetic phase, being heated up to around 330 K. This was all done with no external magnetic field. These results are shown in Fig. 6.20. It is noted that the two plots at 305 K are the same. That temperature was only measured once, with the sample originating from the ferromagnetic phase. Since it was completely paramagnetic at this temperature there was no reason to measure it again. The blue dots show the data points, the green dashed line the FM sextet part of the fit, the red dashed line the PM doublet part of the fit and the blue solid line the resulting fit.

The measurements were redone with an external magnetic field of 0.6 T, all with the material originating in the ferromagnetic phase. These results are shown

			δ [mm/s]		ϵ [mm/s]	
T [K]	F [%]	B [T]	s	d	s	d
Ferromagnetic origin, $B = 0$ T						
285	93.8	13.34	0.42	0.40	-0.039	0.22
296	74.6	11.41	0.41	0.40	-0.038	0.19
305	0	-	-	0.39	-	0.18
Paramagnetic origin, $B = 0$ T						
285	93.6	13.31	0.42	0.40	-0.036	0.22
296	71.0	11.40	0.41	0.40	-0.034	0.17
305	0	-	-	0.39	-	0.18
Ferromagnetic origin, $B = 0.6$ T						
80	100	17.61	0.53	-	-0.025	-
285	93.3	13.01	0.42	0.42	-0.017	0.36
296	85.4	11.63	0.42	0.40	-0.014	0.27
305	0	-	-	0.40	-	0.23

Table 6.2: Fitted parameters. F is the ferromagnetic fraction of the fit, s the sextet part of the fit and d the doublet part

.

in Fig. 6.21, compared with the measurements in no external field.

Using just one sextet and one doublet fits the data very well, even though it should in principle be 5 sextets. The fitted parameters for all these measurements are shown in table 6.2. Here just the FM phase fraction parameter F is discussed. Comparing measurements of the two different phase origins at the same temperature, it is seen that the material prefers to remain in its originating phase. At 305 K the material is 100 % paramagnetic regardless of the thermal history. At lower temperatures the ferromagnetic phase fraction is higher when the material originated from the ferromagnetic phase due to thermal hysteresis. This effect is amplified by an external field which keeps the material in the ferromagnetic phase at higher temperatures, shifting the transition temperature upwards.

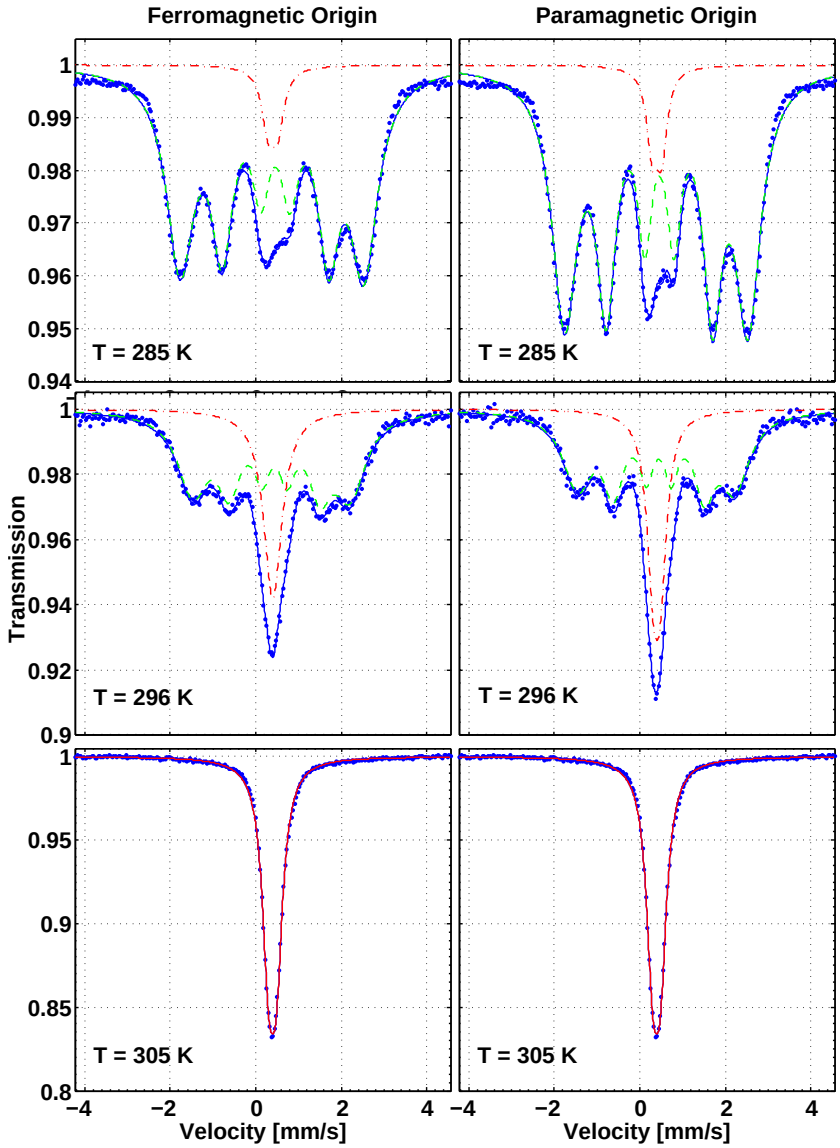

Figure 6.20: MnFe(P,As) spectra with no external magnetic field. The blue dots show the data points, green dashed lines the FM sextet part of the fit, red dashed lines the PM doublet part of the fit and the blue solid lines the resulting fit.

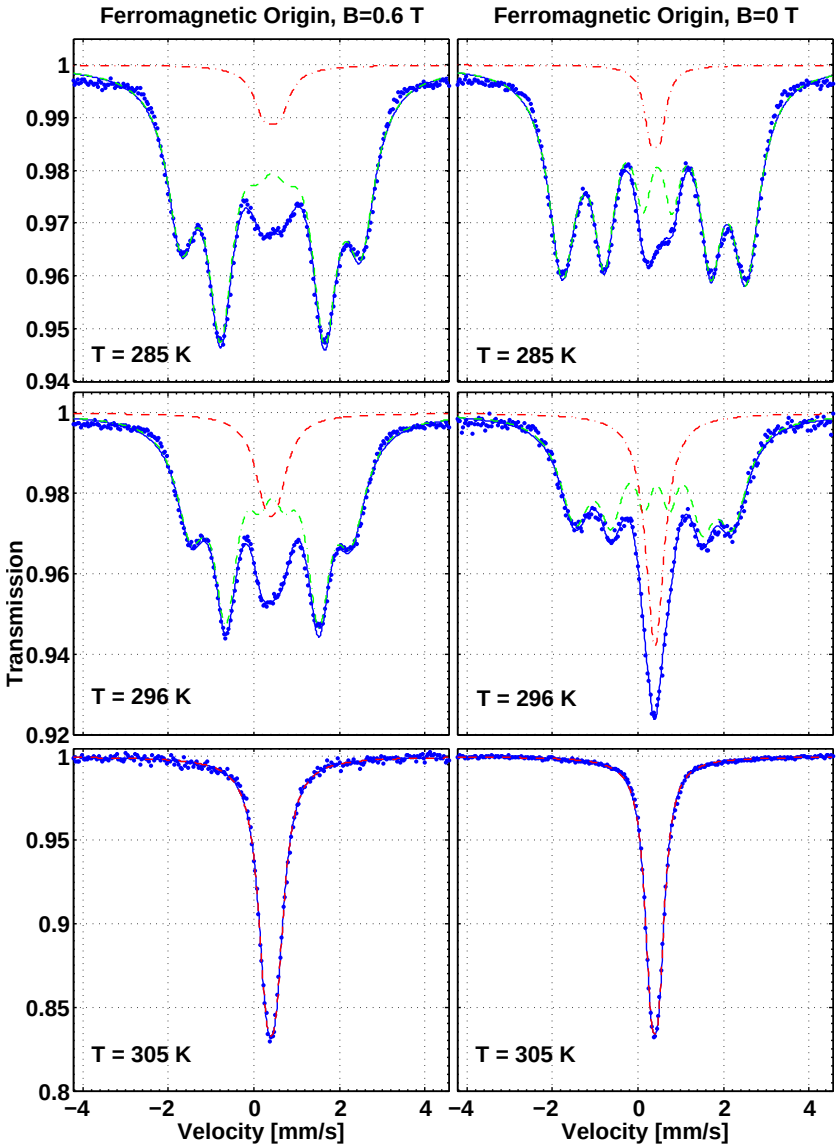

Figure 6.21: MnFe(P,As) spectra with 0.6 T external magnetic field shown along side spectra with no external magnetic field. The blue dots show the data points, green dashed lines the FM sextet part of the fit, red dashed lines the PM doublet part of the fit and the blue solid lines the resulting fit.

6.3 Summary

In this chapter two different compounds of MnFe(P,As) experiencing a thermal hysteresis between 0.5 K and 1 K, respectively, were investigated. They were both characterized by a series of experimental measurements, including isofield magnetization, isothermal magnetization, heat capacity and direct measurements of ΔT_{ad} and were seen to show very similar behavior, with the exception of the reduced hysteresis. The experimental investigations provided the following main results,

- The magnetization and calorimetric data present detailed characterization of the material behavior under different conditions, which are used for modelling purposes in chapter 7.
- When comparing the indirect methods of estimating Δs, it is seen that the Maxwell relation estimates coincide with the corresponding values obtained from the set of isofield entropy curves, obtained in either a cooling or heating mode through DSC measurements.
- Inferring ΔT_{ad} from the deduced entropy curves and comparing the values to directly measured ΔT_{ad} data, suggest that using the set of either cooling or heating isofield entropy curves will lead to overestimation. Instead the low field heating and high field cooling entropy curves should be used for estimating the MCE.
- A series of calorimetric measurements allowed for investigation of partial transition behavior, which can help describe the reversible properties of the transition. Partial transitions are rarely studied and this data is used as the basis of a Preisach type model in section 7.2.
- The MnFe(P,As) material experiencing 1 K thermal hysteresis was tested in an actual magnetic refrigeration device. Here the thermal hysteresis was observed in real application conditions, undergoing thousands of AMR cycles. The applied magnetic field of 1 T was not enough to erase initial thermal preparations of the sample. The thermal hysteresis was not seen to lower performance, but shift the optimal working temperature.

Part IV

Preisach modelling

Chapter 7

Preisach modelling of $Gd_5Si_2Ge_2$ and MnFe(P,As)

In the following chapter the procedures and results of applying the non-equilibrium Preisach approach to first order materials MnFe(P,As) and $Gd_5Si_2Ge_2$ are presented. The first section describes the general approach to experimentally determining the material properties in the high temperature paramagnetic (PM) and low temperature ferromagnetic (FM) phases. Furthermore the procedure for fitting the Preisach model parameters is described. The subsequent sections present the model as it is applied to the three materials considered in this work: the two MnFe(P,As) compounds and $Gd_5Si_2Ge_2$, characterized in chapters 6 and 5 respectively. A final section contains a discussion of problems concerning temperature scanning experiments under non-isofield conditions and how this affects measurements of first order materials. This is based on experimental data coupled with a model interpretation.

The modelling results are presented in chronological order, which means that the first sections concerning MnFe(P,As) show initial modelling approaches touching upon different aspects of the process. The results regarding modelling partial phase transitions have been published in von Moos et al. [2014a] (see appendix B). The section describing $Gd_5Si_2Ge_2$ represents the most complete model, utilizing the experience and procedures obtained from the MnFe(P,As) modelling. It is furthermore based on more detailed experimental data and a series

of independent experiments have been done, which can be directly compared to model predictions. The primary results are published in von Moos et al. [2014b] (see appendix C).

Before introducing the modelling sections, a couple of definitions of procedures and wording are given:

Simulating experiments In the material modelling sections the experimental data, on which the model is based, is shown along with model simulations of those very experiments. This means that given the model, the experimental conditions and procedures have been replicated using the same temperature and magnetic field profiles. When an experiment is simulated, the model material undergoes the same thermal and magnetic history as the experimental sample material.

Estimating entropy change As the usual way of estimating the isothermal entropy change Δs is through the Maxwell relation,

$$\Delta s(H_i; H_f, T) = \mu_0 \int_{H_i}^{H_f} \left(\frac{\partial M(H,T)}{\partial T} \right)_H dH \,,$$

these calculations are applied and shown for the experimental data. The calculations are also carried out on the simulated experimental data. This illustrates the precision of the model, avoids numerical derivative resolution problems and makes comparison between the Maxwell equilibrium and the non-equilibrium model estimates of Δs directly comparable.

Non-equilibrium estimates Estimates of the magnetocaloric effect (MCE) through Δs and ΔT_{ad} from the non-equilibrium model are presented such that they represent values that are stable under continuous field cycling and are independent of how the material was initiated thermally. These estimates include entropy/heat production due to hysteresis, as well as the thermal hysteresis. It should be noted that it is generally not possible to detect the entropy production in the plots, since it is comparably much less than Δs.

Ideal AMR cycles The non-equilibrium model is used to simulate the material properties under working conditions, through an ideal AMR-type cycle. The cycle consists of four steps: i) completely adiabatic magnetization (0 heat loss to the ambient) at temperature T, ii) isofield cooling with ideal heat transfer to a thermal bath back to T, iii) completely adiabatic demagnetization, iv) isofield heating with ideal heat transfer back to T. When these cycles are represented in $s - T$ diagrams, the actual material entropy is shown as the cycle is traced. These cycles are always shown

with two full entropy curves, showing a full temperature scan at 0 field and the maximum applied field. These represent the standard curves obtained through calorimetry.

The different material modelling results are presented in their respective sections. However, the more detailed discussion of the overall results is presented in the last summary section.

7.1 Parameter estimation

The three materials considered in this work all experience similar qualitative behavior when in their respective pure phases; the high temperature PM and low temperature FM phase. The pure phase magnetization and entropy properties can as a consequence be modelled in a similar manner, which is described in the following sections.

The output of the Preisach model is the thermal and magnetic history dependent FM phase fraction X, which depends on the Preisach distribution. The properties of a material in a non-equilibrium mixed phase state follow from its pure phase properties and X,

$$M(H,T) = XM_1(H,T) + (1-X)M_0(H,T)\,,$$
$$s(H,T) = Xs_1(H,T) + (1-X)s_0(H,T)\,,$$

with the subscripts 0 and 1 representing the PM and FM states, respectively. The pure phase properties are determined directly from experimental data and are thus closely bound by this. The Preisach distribution parameters are more subtly determined, since they individually do not relate to any direct measurements. The distribution as a whole determines the hysteretic behavior, which can lead to parameter correlation. This is sought to be avoided here by the procedures described in the following. No formal analysis of parameter correlation has been done in this work, but it is certainly an area that could be looked into more rigorously.

It should be noted that when the pure phase properties are known and the distribution function determined, the model framework is in a sense complete. Any kind of transformation relating to the properties determinable by the model can be simulated with no further information needed. This is of course the whole point: the model based on standard procedure magnetization and heat capacity measurements can provide insight in the non-standard transformations relevant in an AMR cycle.

Magnetization

Magnetization measurements are often used to characterize magnetocaloric materials (MCMs) and from them deduce the MCE. In this work a series of magnetization measurements were done on MnFe(P,As) and $Gd_5Si_2Ge_2$. In the following the field and temperature ranges where the materials exhibit pure phase behavior are defined as the ranges away from the transition where no hysteresis is present. A series of isothermal magnetization measurements done on MnFe(P,As) is shown in Fig. 7.1a. The FM and PM phases are determined by the sets of low temperature curves(blue) and high temperature curves(red), respectively, which show no magnetic hysteresis in the measured field range. In the same manner this is applied to isofield measurements, where the high temperature range (higher than the red dashed line) and the low temperature range (lower than the dashed blue line) represent the PM and FM phases, respectively. This is illustrated in Fig. 7.1b for $Gd_5Si_2Ge_2$. This approach is used for all considered materials since they all experience this characteristic behavior.

In the case of isofield measurements, the magnetization of each phase M_x is approximated as linear in temperature with magnetic field dependent coefficients

$$M_x(H,T) = \left.\frac{\delta M_x}{\delta T}\right|_H (H)\,(T - T_{0,x}) + M_{0,x}(H)\,. \tag{7.1}$$

where the subscript $x = \{0,1\}$ represents the PM and FM phase, respectively.

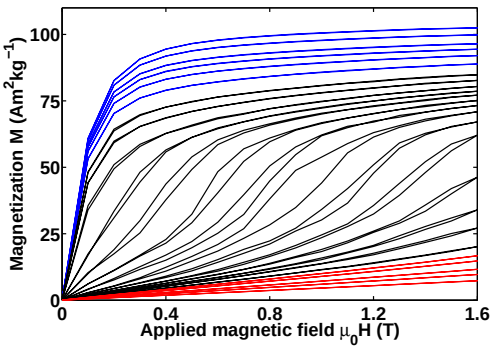

(a) Isothermal magnetization of MnFe(P,As): FM and PM pure phases are determined by the reversible blue and red curves, respectively.

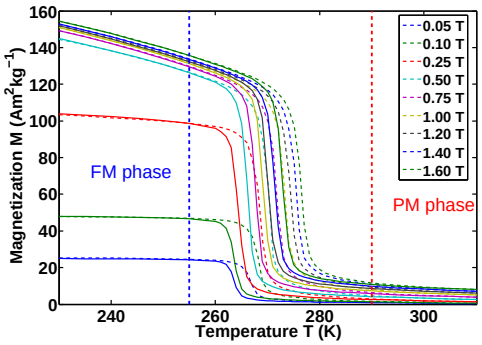

(b) Isofield magnetization of $Gd_5Si_2Ge_2$: FM and PM pure phases are determined by the reversible low and high temperature ranges, bound by dashed lines.

Figure 7.1: Determination of pure phase magnetization behavior

The field dependent reference magnetization $M_{0,x}$ at temperature $T_{0,x}$ is given by

$$\begin{aligned} M_{0,1}(H) &= M_s \tanh(\gamma\,\mu_0 H) + \chi_1\,\mu_0 H \quad \text{and} \\ M_{0,0}(H) &= \chi_0\,\mu_0 H\,, \end{aligned} \tag{7.2}$$

where the constant coefficients M_s, γ, χ_1 and χ_0 are all obtained by fitting to the experimental data. The applied magnetic field is written as $\mu_0 H$ as the input is given in units of tesla. The magnetization gradients with respect to temperature vary between materials and the fitting is described in appendix G.

In the case of isothermal measurements, the field dependent pure phase magnetization is approximated using the expressions given in Eq. (7.2), with temperature dependent coefficients

$$M_1(H,T) = M_s(T)\,\tanh\big(\gamma(T)\,\mu_0 H\big) + \chi_1(T)\,\mu_0 H \quad \text{and} \tag{7.3}$$

$$M_0(H,T) = \chi_0(T)\,\mu_0 H\,. \tag{7.4}$$

The fitting of the temperature dependence of the coefficients is described in appendix G.

Entropy and Gibbs free energy

The pure phase entropy of the materials is assumed to consist of a magnetic contribution and a purely thermal contribution

$$s_x(H,T) = s_{T,x}(T) + s_{H,x}(H,T)\,. \tag{7.5}$$

The thermal contribution is deduced from heat capacity measurements. As characterized in the material chapters, the heat capacity is approximately constant on either side of the phase transition, within the temperature ranges relevant here. Assuming a constant heat capacity $\bar{c}$, the thermal part of the entropy is logarithmic in temperature

$$\bar{c} = T\frac{\partial s_{T,x}}{\partial T} \Rightarrow s_{T,x}(T) - s_{T,x}(T_0) = \int_{T_0}^{T} \frac{\bar{c}}{T'} dT' = \bar{c}\log\left(\frac{T}{T_0}\right) \tag{7.6}$$

where T_0 is a chosen reference temperature. In the relatively narrow temperature range of interest here, the argument of the log-function is close to 1 and the entropy function can be linearly expanded as

$$s_{T,x}(T) \approx \alpha\,(T - T_0) + s_{T,x}(T_0)\,, \quad \alpha = \frac{\bar{c}}{T_0}\,. \tag{7.7}$$

The parameter α determines the temperature scaling of the entropy and is approximately given by heat capacity measurements. The absolute entropy scale

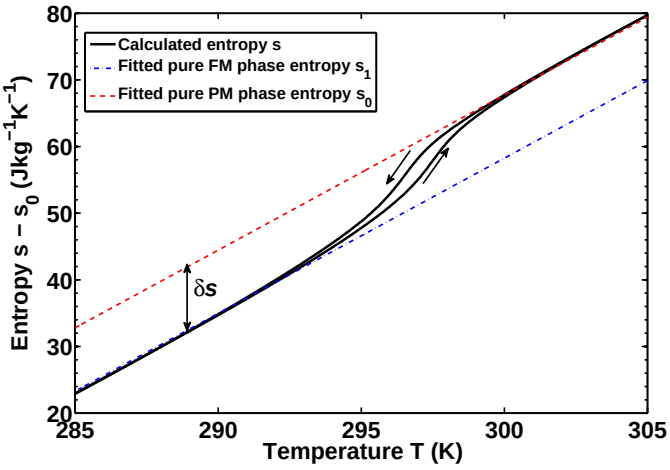

Figure 7.2: The pure phase behavior of entropy shown for MnFe(P,As) . The black solid lines show the entropy obtained from heat capacity measurements and the dashed lines the linear pure phase approximations.

does not matter, so the FM phase entropy scale is defined such that $s_{T,1}(T_0) = 0$. The phase transition is assumed to be associated with a constant entropy change, requiring $s_{T,0}(T_0) = \delta s$. This leads to the following approximations for the thermal contribution to the pure phase entropies

$$s_{T,1}(T) = \alpha(T - T_0)\,, \qquad s_{T,0}(T) = s_{T,1}(T) + \delta s\,. \tag{7.8}$$

This approximation scheme is illustrated for MnFe(P,As) in Fig. 7.2.

An applied magnetic field provides an additional contribution to the entropy, given as

$$s_{H,x}(H_i; H_f, T) = \mu_0 \int_{H_i}^{H_f} \left(\frac{\partial M_x}{\partial T}\right)_H dH\,, \tag{7.9}$$

which added to the thermal contribution gives the total pure phase entropy.

The Gibbs free energy of the pure phases determine the thermodynamic field Z driving the phase transition. The Gibbs free energy follows from the pure phase

entropy $dg_x/dT = -s_x$,

$$g_x(H_i; H_f, T) = g_x(0, T_0) - \int_{T_0}^{T} \left[\alpha(T' - T_0) + s_{T,x}(T_0)\right] dT' - \mu_0 \int_{H_i}^{H_f} M_x(H, T) dH, . \tag{7.10}$$

As Z is defined as, (chapter 2.2, Eq. (2.20)),

$$Z = \frac{g_1 - g_0}{2} \tag{7.11}$$

the interest lies in the difference in Gibbs free energy between the pure phases,

$$2Z(H_i; H_f, T) = \underbrace{(g_1(0, T_0) - g_0(0, T_0))}_{\epsilon} + \delta s(T - T_0) - \mu_0 \int_{H_i}^{H_f} \Big(M_1(H, T) - M_0(H, T)\Big) dH \,. \tag{7.12}$$

The parameters $\bar{c}$, T_0 and δs are all found through heat capacity experiments. The constant heat capacity value is directly obtainable from the measurements. The reference temperature T_0 is usually defined as the lowest temperature of interest. The entropy change follows approximately from the measured heat of the transformation Q_t, such that $\delta s \approx Q_t/T_p$, where T_p is the transition temperature. Thus the only unknown material parameter is ϵ, which is used as a model fitting parameter with the purpose of shifting the transition temperature.

The Preisach distribution

As described in section 2.2 the Preisach distribution used for all these materials is approximated by Lorentzian functions

$$p(g_u, g_c) \propto \frac{1 - f_r}{\left[1 + \left(\frac{g_u - g_{u,0}}{\sigma_u}\right)^2\right] \cdot \left[1 + \left(\frac{g_c - g_{c,0}}{\sigma_c}\right)^2\right]} + \delta(g_c) \frac{f_r}{1 + \left(\frac{g_u}{\sigma_{u,r}}\right)^2} \,. \tag{7.13}$$

This introduces the five model parameters $\{\sigma_u, g_{c,0}, \sigma_c, \sigma_{u,r}, f_r\}$, which all need to be fitted from the experimental data. Opposed to the pure phase modelling considering only data away from the transition, the distribution parameters are determined from the intermediate mixed phase range, in either field or temperature. The distribution is assumed to be independent of the intensive variables, temperature and field.

Material	δs (J/kg/K)	σ_u (J/kg)	σ_c (J/kg)	$g_{0,c}$ (J/kg)	f_r	$\sigma_{u,r}$ (J/kg)
MnFe(P,As)[1]	11.0	10.0	4.0	4.0	-	-
MnFe(P,As)[1]	11.0	4.3	1.5	2.3	0.30	4.3
MnFe(P,As)[2]	10.3	4.0	4.0	-1.0	0.73	6.8
$Gd_5Si_2Ge_2$	18.6	6.9	4.2	19.2	0.06	9.1

Table 7.1: Parameters determining the Preisach distribution of the three materials. Superscript 1 and 2 refer to the 1 K and 0.5 K thermal hysteresis MnFe(P,As) compounds, respectively.

When possible this is done in several steps, in order to obtain meaningful parameters were correlation is reduced. Initially the completely reversible contribution is determined from approximated anhysteretic magnetization curves. In the case of isofield measurements these are assumed to be described by the mean magnetization between the heating and cooling curves. Similarly, the anhysteretic curves are determined from the mean magnetization value between the magnetization and demagnetization branches in the isothermal case. This procedure determines $\sigma_{u,r}$ and ϵ, using $f_r = 1$. Secondly the reversible parameters are locked and the rest of the parameters, σ_u, $g_{c,0}$, σ_c and f_r are determined from the actual hysteretic data.

As observed hysteretic properties per definition depend on the specific experimental procedure used, it is crucial to know exactly how the experimental data was obtained. The determination of the parameters is done by using the Preisach model to simulate the actual experiments. Through this the model material undergoes the same thermal and magnetic history as the real sample measured in the experiment. The parameters are fitted through Matlab's "fminsearch" function, which is set to minimize the total squared error between the experimental and simulated data sets.

All Preisach distribution parameters obtained from the three considered materials are given in Table 7.1. Also provided in the table is the experimentally determined δs.

7.2 MnFe(P,As) - Compound 1, high hysteresis

This section presents the initial Preisach model approach, applied to the MnFe(P,As) compound characterized in sec. 6.2, experiencing a thermal hysteresis of about 1 K. The model is based on a series of isofield magnetization measurements. No form of experimental first order reversal curves are used and the Preisach

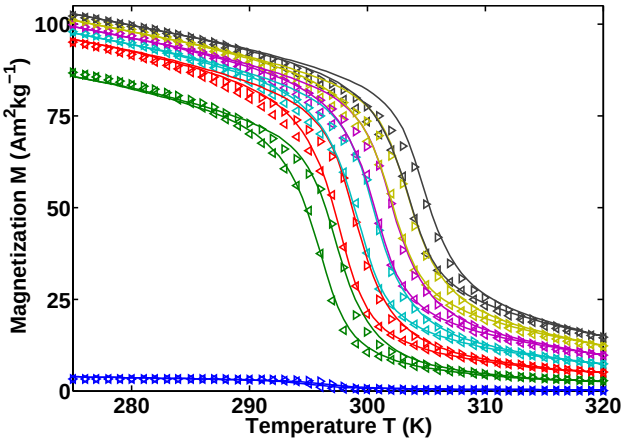

Figure 7.3: Simulation of MnFe(P,As) isofield magnetization experiments at $\mu_0 H = (0.05, 0.25, 0.50, 0.75, 1.00, 1.25, 1.50)$ T. The symbols represent the data and the solid lines the model simulation.

distribution does not contain any separate purely reversible contribution. The material dependent fitting functions and the estimated parameters are given in appendix G.

In Fig. 7.3 the model simulation of the isofield magnetization experiment is shown for applied magnetic fields of $\mu_0 H = (0.05, 0.25, 0.50, 0.75, 1.00, 1.25, 1.50)$ T. The experimental data is denoted by symbols and the simulation by solid lines. The model reproduces the material behavior well. As shown in the data section, the thermal hysteresis decrease with increasing field. Since the Preisach distribution is assumed independent of the intensive variables the thermal hysteresis is slightly overestimated at higher fields. It is noted that the model overestimates the magnetization at the low temperature part of the transition. This is due to the symmetric nature of the chosen Preisach distribution function, which do not capture the slight asymmetry of the transition.

In Fig. 7.4 the estimation of the isothermal entropy change Δs is shown, determined in five different ways. The symbols represent Δs calculated from experimental data using the Maxwell relation on either the heating or cooling curves. The solid red and blue curves show the same Maxwell calculations used on simulated data obtained from model experiment simulations. The solid black central line shows the non-equilibrium model estimate of the entropy change. The model reproduction of the Maxwell estimate overlaps nicely with the data values, except around 290 K due to the asymmetry of the transition as stated above.

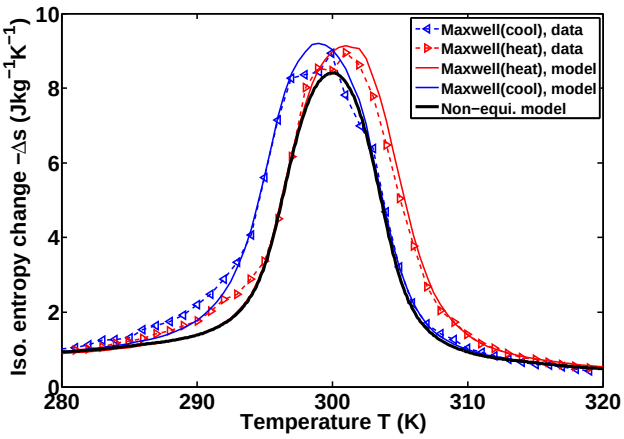

Figure 7.4: Estimation of the isothermal entropy change Δs through the Maxwell relation and the Preisach model with a field change from 0 to 1.5 T. The Maxwell estimates are calculated from experimental data (symbols) and simulated data(solid lines). The non-equilibrium model result is shown as the solid black line.

The available entropy change, when accounting for both magnetic and thermal hysteresis, is practically bound by the minimum value between the Maxwell estimates obtained from heating and cooling modes. This is equivalent to stating that the available entropy is bound by the low field heating and high field cooling entropy curves.

AMR cycles and magnetic hysteresis

The model is used to simulate how the material entropy changes during an ideal AMR cycle, with a magnetic field change between 0 and 1.5 T. Four such cycles are shown in Fig. 7.5 along with the 0 and 1.5 T entropy curves. The entropy production is so small that it is not visible in the plot. These results show the material behavior under working type conditions and it is clear that the available $s - T$ space is bound by the low field heating and high field cooling entropy curve.

The heat production due to hysteresis when going through the AMR cycle is given by the model, which is shown in Fig. 7.6. The maximum heat generated is about 10 J/kg when going through a full AMR cycle initiated at 300 K, between 0 and 1.5 T. This coincides with the hysteresis loss calculated from the area of the isothermal hysteresis loop at the same initial temperature. In terms of

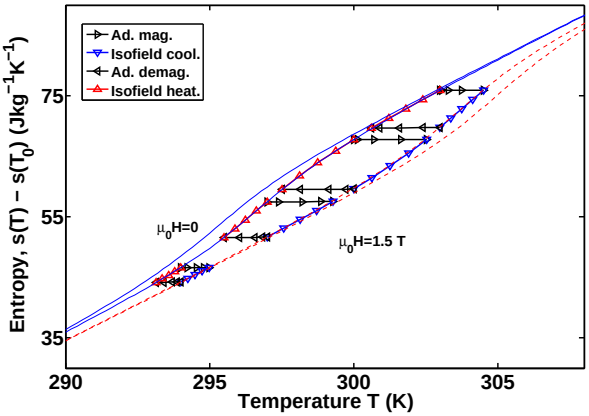

Figure 7.5: MnFe(P,As) undergoing AMR cycles at four different temperatures, between 0 T and 1.5 T. The material's entropy is traced by the symbols during the AMR transformations. The characteristic full entropy curves are shown for 0 and 1.5 T.

entropy production, the stated heat production values should be divided by temperature. This puts the irreversible entropy production in the order of 0.03 J/kg/K, corresponding to about 0.5% of Δs. The Δs curve is rescaled to the maximum hysteresis value and shown in the figure. This illustrates the close correlation between the hysteretic heat production and MCE properties, which can be of use in more pragmatic models considering magnetic hysteresis.

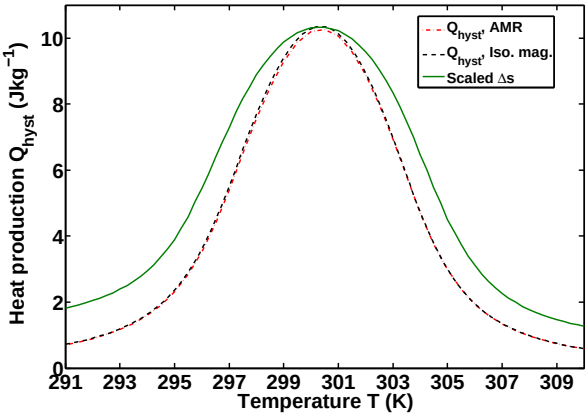

Figure 7.6: The heat production due to magnetic hysteresis in MnFe(P,As). The generated heat during a full AMR cycle coincide with the heat generated in the corresponding isothermal hysteresis loop. Δs has been scaled to $\max(Q_{\text{hyst}})$ and is seen to correlate with the magnitude of the heat production.

Partial phase transitions in MnFe(P,As)

This section presents the modelling results concerning the material behavior of MnFe(P,As) during partial phase transitions. The model is based on calorimetric measurements done with no magnetic field, as presented in section 6.2. The purpose of this modelling is to investigate how well the Preisach model can capture partial phase transitions in a first order material, which is something that is rarely done.

When such materials are characterized it is through standard characterization methods that give information about the hysteretic properties in the most extreme case of a complete phase transition. This applies to both DSC and isofield magnetization measurements, where the phase transition is completed by scanning large temperatures ranges. The same is often true for isothermal magnetization measurements done in fields high enough to saturate the magnetization. However, this is not necessarily indicative of what a material actually experiences in AMR type working conditions. Often permanent magnets are used, which provide fields of the order of 1 T. For many materials, including the ones described here, this is often insufficient to drive a full phase transition. This means that under working conditions, the material undergoes only partial transitions. Therefore, if a model is only based on saturation-type characterization data, it is not given that it also

captures partial transformations as well. The results presented in this section are published in von Moos et al. [2014a] (see appendix B).

In these experiments the heat capacity was measured, though here given equivalently as heat flux q needed to maintain a steady temperature ramp rate of ± 2 K/min. The experiments were done in a temperature scanning mode, where the temperature rate changes sign when a given setpoint temperature is reached. The entropy is calculated from the heat flux data and the experimentally determined FM phase fraction is estimated by

$$X_{\text{est}} = \frac{s - s_0}{s_1 - s_0}\,, \tag{7.14}$$

where s_0 and s_1 are the estimated pure phase entropy functions.

The Preisach distribution is fitted to the data, including a purely reversible contribution of about 30% of the total distribution, as shown in Table 7.1. The model simulation of the experiment is shown in Fig. 7.7 and the corresponding model estimation of the FM phase fraction is shown in Fig. 7.8. The data is illustrated by solid red lines, whereas the model results are given in black dashed lines. The heat flux is seen to oscillate around the temperature reversal point due to the PID control of the DSC. This signal has been eliminated when possible in calculating the phase fraction.

The model generally captures the qualitative partial transition behavior seen in the experiment. The paths of the return branches following reversal points provide unique information about the reversibility of the partial transitions, which is not present in full saturation characterization. This model approach illustrates that it is indeed possible to capture the properties of partial transitions, which will be applied in the following section to the other materials.

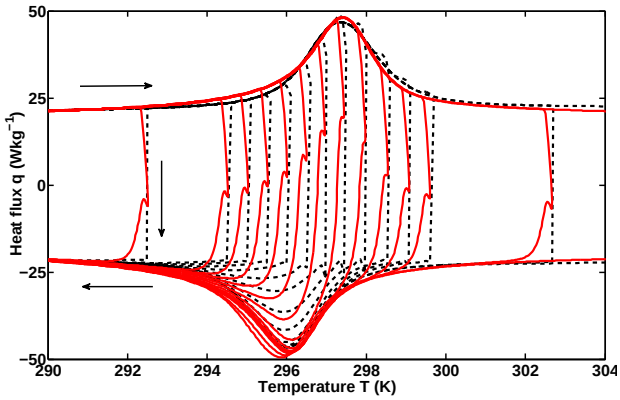

Figure 7.7: Experimental calorimetric data measured on a MnFe(P,As) sample (solid curves) and the corresponding model simulation of the same experiment (dashed curves).

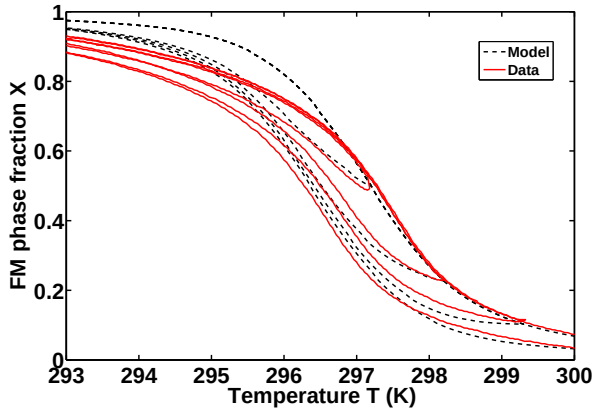

Figure 7.8: The FM phase fraction estimated from DSC measurements and simulated by the Preisach model during partial phase transitions.

7.3 MnFe(P,As) - Compound 2, low hysteresis

In this section a model of the MnFe(P,As) compound with a relatively low thermal hysteresis of 0.5 K, described in section 6.1, is presented. The validity of the

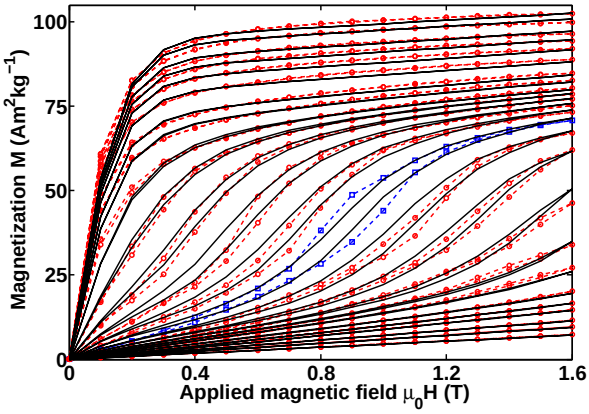

Figure 7.9: Simulation of MnFe(P,As) isothermal magnetization experiments between 250 K and 330 K. The symbols show the experimental data and the solid lines the corresponding model simulation.

model is investigated through comparison with independent experiments carried out under different conditions than those under which the model is based. Here isothermal magnetization measurements are used to estimate model parameters. The main idea behind using these, as opposed to isofield measurements, is that they to some extend provide information about partial transition behavior due to the relatively low field applied. Under these conditions, the field will be insufficient to complete the transition in a region around the transition temperature.

In Fig. 7.9 the experimental data is shown in the temperature range from 250 K to 330 K, with temperature steps 1 K around the transition. The blue symbols show the $T = 299$ K measurement. The solid black lines show the model simulation of the experiment. The model reproduces the data very well across the whole temperature and field range. The hysteresis loop at 299 K is significantly larger than at any other temperatures, which the model cannot capture.

The model is used to simulate a series of isofield magnetization experiments on the same sample, carried out independently of the isothermal measurements. The experiments were done in an applied field of $\mu_0 H = \{0.02, 0.10, 0.25, 0.75, 1.0, 1.30, 1.60\}$ T. The results are shown in Fig. 7.10, with symbols showing the data and solid lines the simulated model data. The general qualitative behavior of the material is captured by the model. Two primary discrepancies are observed: i) the low temperature region is underestimated at low fields, and ii) the shift of the transition temperature with increasing field is a bit too large. Both of these effects are actually also present in the isothermal simulation, however not so

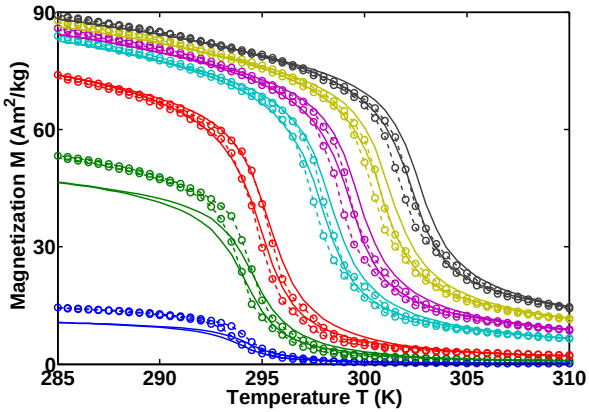

Figure 7.10: Simulation of MnFe(P,As) isofield magnetization experiments at $\mu_0 H = \{0.02, 0.10, 0.25, 0.75, 1.0, 1.30, 1.60\}$ T. The symbols show the experimental data and the solid lines the corresponding model simulation.

visible. This implies that the model can capture material behavior under different conditions and it is consistent.

The model is applied to simulate a large series of both isothermal and isofield experiments, on which the Maxwell relation can be applied to estimate the reversible Δs. These results are shown in Fig. 7.11a, along with the non-equilibrium model estimate. First it is noted that the estimates from the Maxwell relation differ between isofield and isothermal experiments. This is the effect of the erroneous "colossal" MCE, discussed in section 4.5, that arises when the thermal and magnetic history variance between isotherms become too large. This can according to Caron et al. [2009], be avoided by resetting the sample in the PM state between each isotherm. If this is simulated, it is indeed found that the isothermal magnetization Δs curve collapse to the isofield cooling curve. It is noted that in order for the demagnetization Δs curve to collapse to the isofield heating curve, the sample needs to be reset in the FM state under the maximum applied field.

The results here support the findings for the first MnFe(P,As) compound: the available Δs, taking into account the thermal and magnetic hysteresis, is bound by the minimum of the two Maxwell relation estimates based on the heating and cooling data.

The direct ΔT_{ad} measurements carried out on this material were simulated

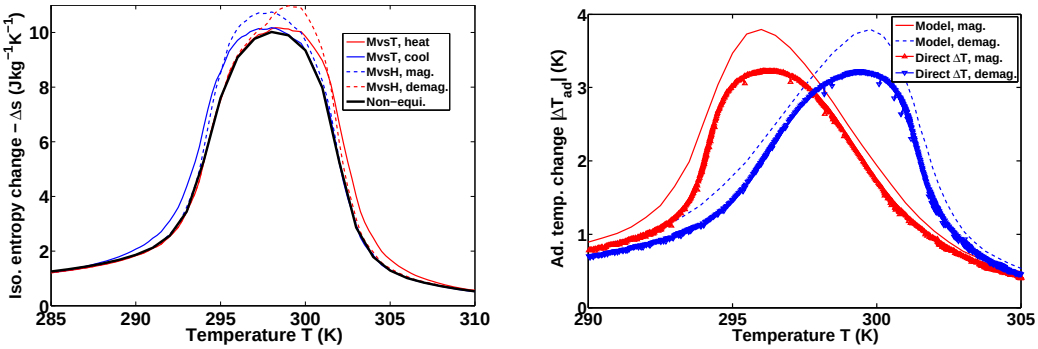

(a) Estimation of Δs through the non-equi. model(black curve) and the Maxwell Eq. used on simulated isofield and isothermal data(red and blue curves).

(b) Directly measured ΔT_{ad} (symbols) along with the corresponding simulation of the experiment (lines).

Figure 7.11: Simulation of the MCE.

and the results shown in Fig. 7.11b. The qualitative behavior is well described by the model, however with a systematic overestimation of ΔT_{ad} at all temperatures. The reason most likely lies in the fact that different samples were used for the magnetization and ΔT_{ad} measurements, as well as two different permanent magnet assemblies. This can give rise to variation in the intrinsic sample properties, as well as differences in the internal magnetic field due to demagnetization effects. Furthermore it is noticed that the overestimation is larger at low temperatures. This is most likely a consequence of the experimental data, on which the model is based, has not been corrected for demagnetization.

AMR cycles and magnetic hysteresis

The model is used to simulate how the material entropy changes during an ideal AMR cycle, with a magnetic field change between 0 and 1.5 T. Three cycles are shown in Fig. 7.12 along with the 0 and 1.5 T entropy curves, where the symbols show the direction of movement in the $s - T$ plane by the material. The entropy production is so small that it is not visible in the plot. These results show the material behavior under working type conditions and it is found that the available $s - T$ space is bound by the low field heating and high field cooling entropy curve.

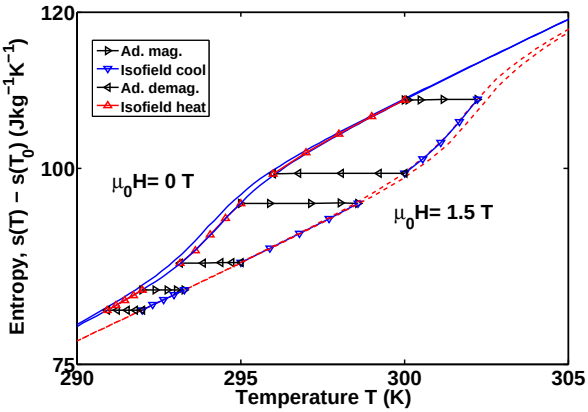

Figure 7.12: Simulated material entropy during AMR cycles at three different temperatures, bewteen 0-1.5 T. Symbols show the direction of the transformations. The full transition entropy curves are shown for 0 T and 1.5 T.

The heat production due to hysteresis when going through the AMR cycle is shown in Fig. 7.13a. The maximum heat generated is about 4 J/kg when going through a full AMR cycle initiated at 299 K, between 0 and 1.5 T. This coincides with the hysteresis loss calculated from the area of the isothermal hysteresis loop at the same initial temperature. This puts the irreversible entropy production in the order of 0.01 J/kg/K, corresponding to about 0.1% of Δs. The Δs curve has been rescaled to the maximum hysteresis value and is seen to approximately have the same profile as the hysteresis curve.

To compare the predicted thermal hysteresis between the model and the experimental data, Fig. 7.13b shows the total thermal hysteresis area calculated from isofield magnetization curves. It is noted that the thermal hysteresis goes to zero at small fields due to domains. This effect is also present in the model, since it is directly based on the experimental data. The model systematically underestimates the thermal hysteresis, even though the magnetic hysteresis is well described. The explanation lies in two subtle points. i) The simple distribution functions used here cannot capture all transformations equally well. Furthermore, the spread (σ) parameters used are only determined in the orthogonal g_u and g_c directions of the Preisach plane, even though there is no reason that this should be the case in reality. ii) When the applied magnetic field is so small that it does not saturate the sample magnetization around the transition, where hysteresis is at a maximum, then the obtained data will show partial hysteresis loops. This

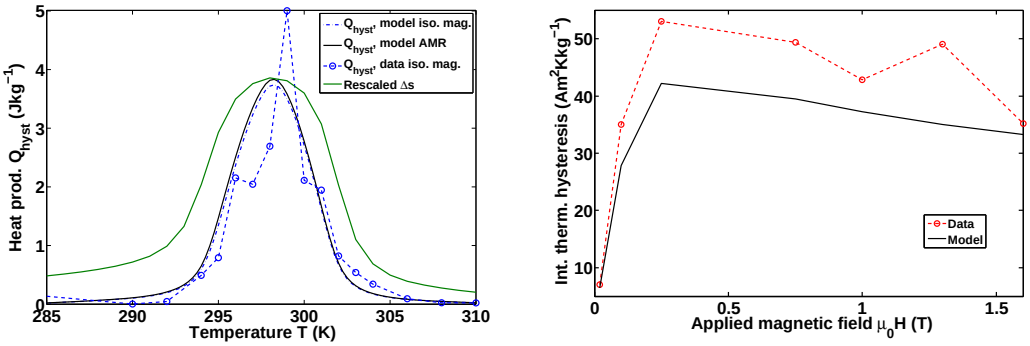

(a) The hysteretic heat production shown for both data and model, along with Δs rescaled to the maximum hysteresis value.

(b) Integrated thermal hysteresis calculated from data and model.

Figure 7.13: Hysteresis comparison between model and experiments.

was the idea behind using isothermal measurements in the first place, but it also introduces the risk of underestimating the hysteresis parameters, since the maximum hysteresis is not apparent from the data.

7.4 Modelling $Gd_5Si_2Ge_2$

In this section the ideas from the two previous sections are applied to model the first order material $Gd_5Si_2Ge_2$, described in chapter 5. The model is based on isofield magnetization data, so that the maximum hysteresis properties are obtainable. The partial phase transition behavior is given by a series of first order reversal curves (FORC), done at an applied magnetic field of 1.6 T. Here the sample is heated from 230 K up to a set of reversal point temperatures, after which the sample is cooled again. This is doable with good resolution in temperature on this material due to the large thermal hysteresis of 4 K. The Preisach distribution is fitted to both these data sets with the parameters given in Table 7.1. The results of this section are published in von Moos et al. [2014b] (see appendix C).

Applying the model to simulate both the standard isofield and the FORC measurements yields the results shown in Fig. 7.14 and Fig. 7.15, respectively. Experimental data is denoted by symbols and the model by solid curves. Only a selection of isofield curves are shown, since they all overlap due to the high thermal hysteresis. The simulated isofield curves generally capture the qualitative properties of the experimental data. More importantly, the model captures the

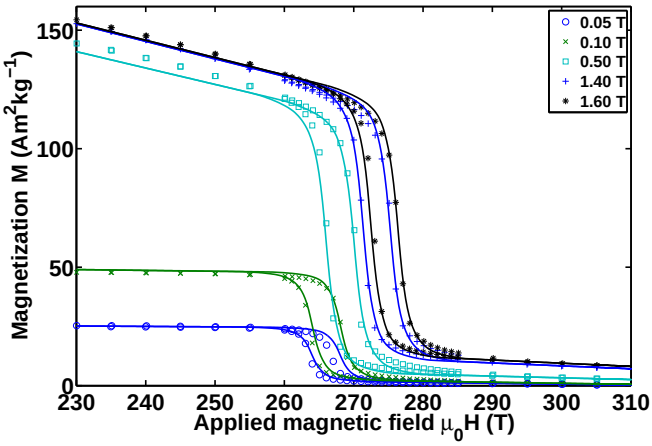

Figure 7.14: Simulation of $Gd_5Si_2Ge_2$ isofield magnetization experiments for a selection of magnetic fields. The symbols represent the data and the solid lines the model simulation.

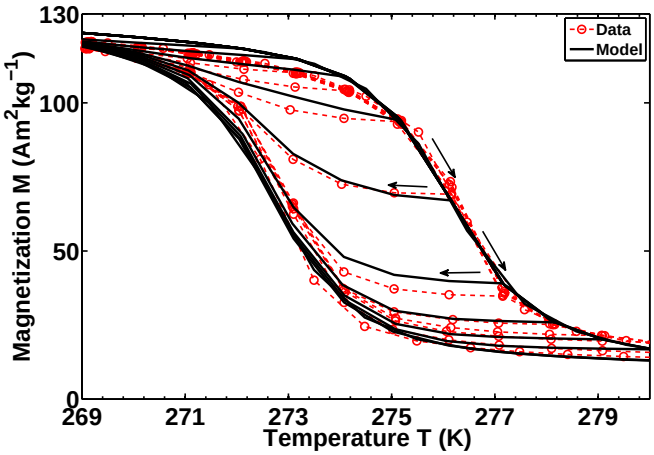

Figure 7.15: Simulation of $Gd_5Si_2Ge_2$ isofield FORC magnetization experiments at 1.6 T. The symbols represent the data and the solid lines the model simulation.

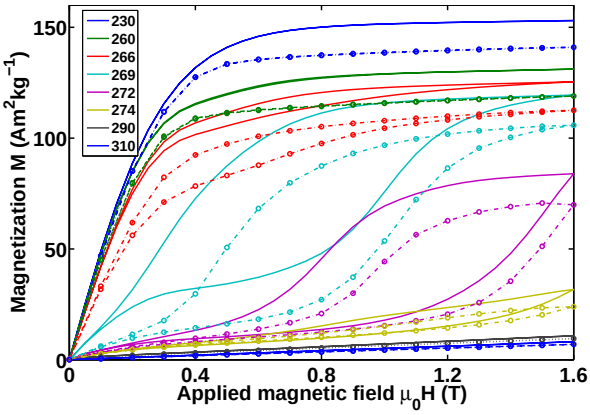

Figure 7.16: Simulation of $Gd_5Si_2Ge_2$ isothermal magnetization experiments for a selection of temperatures. The symbols represent the data and the solid lines the model simulation.

FORC measurements very well. The fact that the model captures the behavior of the return branches illustrate that the model not only can reproduce full transition hysteresis loops, but also partial loops that can be more relevant for estimating material performance under realistic working conditions.

To investigate the model behavior under different conditions than those on which it is based, a series of isothermal magnetization measurements are simulated, as shown in Fig. 7.16. Here a clear offset is observed between the experimental and simulated magnetization values. It is noted that this is related to differences in the two experiments and not due to the model. As discussed in the materials chapter, the sample suffered from mechanical stress during the isothermal experimental series, causing cracks and small parts breaking off. This caused a change in the sample properties, which resulted in an offset in the experimental data between the two experiments. The change in magnetization is directly observed in the experimental data when comparing Fig. 7.14 and Fig. 7.16, considering for example the magnetization in 1.6 T at 230 K being 150 and 140 Am^2/kg in the isofield and isothermal measurements, respectively. The important observation here is that the qualitative properties of the model are very similar to the experiment.

Estimating the Δs upon magnetization including the hysteretic properties produce results agreeing with those of the previous sections, as shown in Fig. 7.17a for a field change of 0 T to 1.5 T. Here the non-equilibrium model (solid black line) approximately traces the minimum of the Maxwell relation estimates

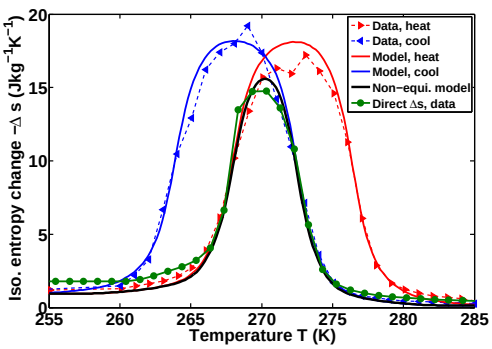

(a) Estimates of Δs using the non-equlibrium model, the Maxwell relation on isofield measurements and direct measurements.

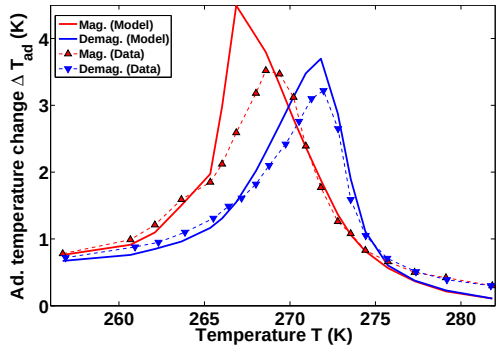

(b) Comparison bewteen ΔT_{ad} estimates obtained from the non-equilibrium model and direct measurements.

Figure 7.17: Comparison of model and experimental MCE.

used on the heating and cooling curves. In the figure the results of a direct Δs experiment are also shown, as circular symbols. These coincide with the model predictions.

In Fig. 7.17b the model estimates of ΔT_{ad} during magnetization and demagnetization between 0 T and 1.5 T are shown, along with directly measured ΔT_{ad} values. The model generally overestimates the ΔT_{ad} values, as is expected due to the lack of perfect adiabatic conditions in the experiment. Furthermore, the sample used in the ΔT_{ad} measurements is not the same as was used in the magnetization experiments. This leads to a change in the demagnetization effects which changes the effective internal field. It is noted that both experiment and simulation show higher values for magnetization, compared to demagnetization. This is not due to hysteretic heat production. This is due to the way that the experiment was carried out using a cooling procedure, which one should be very careful using, as discussed in section 7.5.

AMR type conditions

Here the material behavior undergoing AMR cycles is investigated in further detail than the two previous sections. The model is used to simulate the triple AMR cycle experiments, described in sec. 5.2, and investigate the properties depending on the sample's thermal history.

The material is brought to the near transition temperature $T = 267$ K where

Table 7.2: Measured and modelled adiabatic temperature change during triple AMR-type cycles with an applied magnetic field of 1.5 T, in both a heating and cooling mode. One cycle is given by i) magnetization(M) at T, ii) thermal relaxation to T, iii) demagnetization (DM) at T, iv) thermal relaxation to T, and is illustrated in Fig. 7.18a and Fig. 7.18b.

Cycle	Exp. ΔT_{ad} (K)		Model ΔT_{ad} (K)		Exp. ΔT_{ad} (K)		Model ΔT_{ad} (K)	
	Cooled to 267 K				Heated to 267 K			
	M	DM	M	DM	M	DM	M	DM
1	4.5	-1.7	5.2	-1.6	2.4	-1.7	3.0	-1.6
2	2.3	-1.7	3.0	-1.6	2.4	-1.7	3.0	-1.6
3	2.3	-1.7	3.0	-1.6	2.4	-1.7	3.0	-1.6
	Cooled to 272 K				Heated to 272 K			
	DM	M	DM	M	DM	M	DM	M
1	-2.1	1.3	-3.7	1.7	-4.1	1.4	-4.7	1.7
2	-2.1	1.3	-3.7	1.7	-2.9	1.4	-3.7	1.7
3	-2.1	1.3	-3.7	1.7	-2.9	1.4	-3.7	1.7

it undergoes an AMR cycle three consecutive times, with a maximum field of 1.5 T. This is carried out using two thermal histories, where the material is thermally reset in the high temperature PM and the low temperature FM phases. The experimentally measured ΔT_{ad} values along with the corresponding model simulation are listed in the top part of Table 7.2. The simulated material position in the $(s-T)$-space is shown in Fig. 7.18a as it changes during the transformations.

When the sample is initiated in the high temperature PM state, an initially large ΔT_{ad} is available during the first magnetization. However, in subsequent cycles it settles at a lower and constant value, while the demagnetization values remain constant in all three cycles. When the same experiment and simulation are carried out with the material thermally reset in the low temperature FM state, this is not observed. The ΔT_{ad} values are constant between all cycles, matching the stable values from the PM-reset experiment. The model captures both of these properties, as seen in Fig. 7.18a and from the numerical values presented in Table 7.2. It should be noted that the figure actually shows six individual AMR cycles, three from both the PM and FM resets. However, the stable, closed loop cycles are all equal.

A symmetric demagnetization experiment was carried out and simulated. Here the material is reset in both the PM and FM states as previously described, but in an applied field of 1.5 T, resulting in the cycling being initiated with a

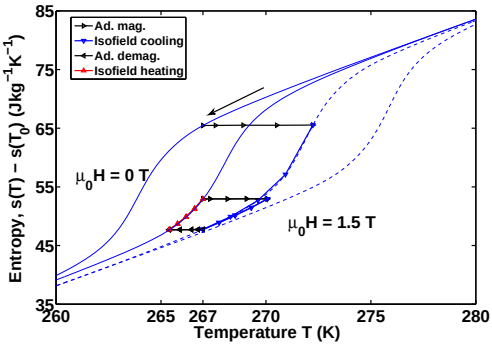

(a) Triple AMR cycle initiated with magnetization step. The material is both reset thermally in the pure PM and FM state prior to the cycling at 267 K.

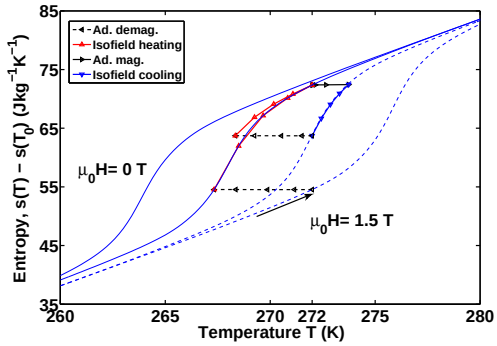

(b) Triple AMR-like cycle initiated with a demagnetization step. The material is both reset thermally in the pure PM and FM state prior to the cycling at 272 K.

Figure 7.18

demagnetization step. This is illustrated in Fig. 7.18b, with the experimental and simulated ΔT_{ad} values given in the bottom part of Table 7.2. When the sample has been heated from the FM phase the initial ΔT_{ad} during demagnetization is high, but the subsequent cycles settle at a constant value. The ΔT_{ad} values obtained from the field cycling after the PM reset are constant and stable.

This illustrates the main point, that regardless of the material's thermal history, it will settle in a metastable state during AMR like conditions. This state is approximately bound by the low field heating and high field cooling entropy curves. Similar behavior has been reported for other materials, however under continuous magnetization cycles without any thermal relaxation [Skokov et al., 2013, Liu et al., 2012].

The heat production due to hysteresis when going through the AMR cycle is shown in Fig. 7.19. The maximum heat generated is about 50 J/kg when going through a full AMR cycle initiated at 270 K, between 0 and 1.5 T. This coincides with the hysteresis loss calculated from the area of the isothermal hysteresis loop at the same initial temperature. In terms of entropy production, the stated heat production values should be divided by temperature. This puts the irreversible entropy production in the order of 0.2 J/kg/K, corresponding to about 1% of Δs. It is illustrated that Δs correlates with the hysteresis, as was also the case with MnFe(P,As).

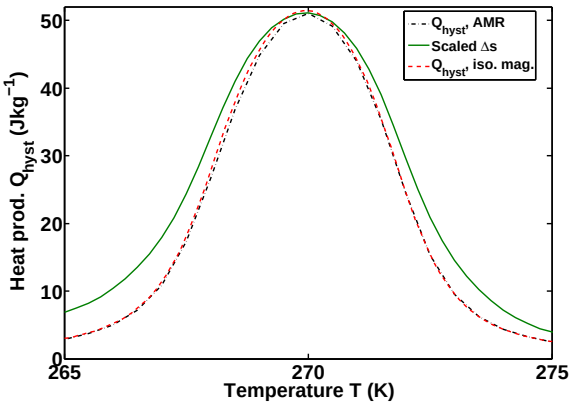

Figure 7.19: The hysteretic heat production shown for both data and model for $Gd_5Si_2Ge_2$, along with Δs rescaled to the maximum hysteresis values.

7.5 Measuring first order materials in a cooling mode

The following section presents results related to experimental procedures on hysteretic materials. As material properties depend on both thermal and magnetic history it is important to make certain that one is in control of both magnetic field and temperature, especially during variations in either. This was discussed in chapter 4 in regards to varying temperature and magnetic field between magnetization measurements, where non-monotonic changes cause overshooting and induce partial loop behavior in the material. Here it is shown that even though completely monotonic temperature changes are provided, measurements done in a non-isofield temperature cooling mode will generally be overestimated.

Two experiments fulfilling these conditions are direct measurements of ΔT_{ad} and Δs, where the magnetic field is applied and removed again at every temperature set point. In Fig. 7.20a experimental Δs data obtained from $Gd_5Si_2Ge_2$ is shown for both a heating and cooling mode scan of the temperature range. Here it is clear that the values obtained through the cooling procedure is systematically higher than those obtained from a heating procedure. This is reproduced by the model. In experiments measuring ΔT_{ad}, the magnetization curve is systematically higher than the demagnetization curve, when done in a cooling mode as shown in Fig. 7.20b (Re-illustration of Fig. 7.17b). This effect is also captured by the model.

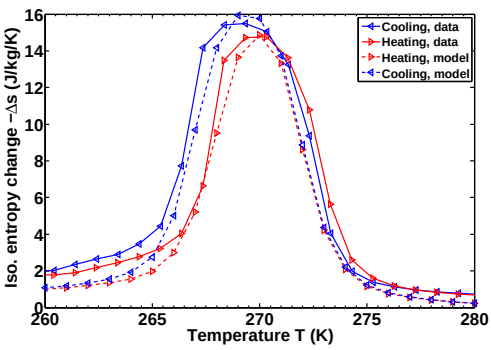

(a) Comparison of experimentally measured and model simulated Δs, during both heating and cooling.

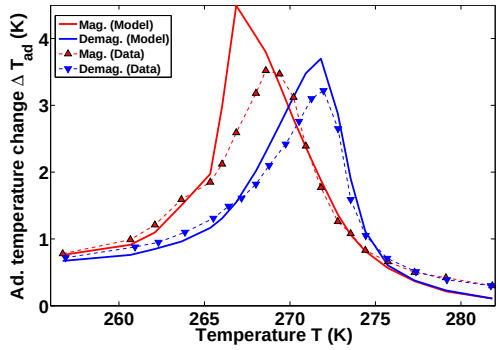

(b) Comparison of experimentally measured and model simulated ΔT_{ad} during magnetization and demagnetization, carried out in a cooling mode.

Figure 7.20: Inconsistency of MCE measurements between cooling and heating procedures.

This can be explained if the general model results are correct: the available $s-T$ space of a first order material is bound by the low field heating and high field cooling entropy curves in cyclic application. Assuming this, the systematically higher cooling mode values are understood from Fig. 7.21. After a magnetization and demagnetization procedure at temperature T^c_{i-1}, the material entropy is given as a point on the 0-field heating curve (hollow circle symbol). Now the sample temperature is cooled to the next set point temperature T_i. However, as the material is cooled a principal first order reversal is induced as the entropy moves towards the 0-field cooling curve. The mixed material state is now somewhere inside the thermal hysteresis region, denoted by the x-symbol. Upon the initial magnetization one thus measures a larger value of either ΔT_{ad} or Δs, compared to the demagnetization value as this will only return the material entropy state to the 0-field heating curve (Solid black circle). One is measuring a value of the MCE that lies somewhere between the reversible and irreversible values during magnetization, and the real irreversible value during demagnetization. These effects do not occur in a heating mode, as illustrated in the figure. When heating from T^h_{i-1} to T_i the material remains on the 0-field heating curve and ends up in the correct state.

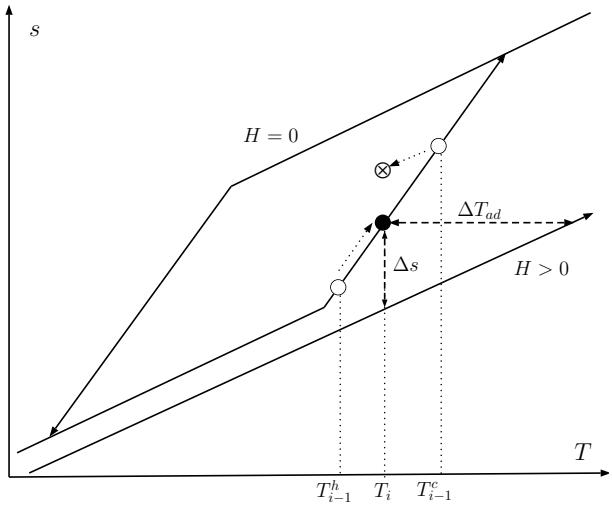

Figure 7.21: Illustration of the difference in the material entropy due to irreversible behavior. During a cooling mode the material enters the thermal hysteresis region, resulting in overestimates of the MCE upon magnetization. During a heating mode the irreversible MCE is always measured correctly.

The severity of this induced reversal behavior will depend on the magnitude of the thermal hysteresis, but also on the temperature step size used in the experiment. This property can be investigated in the model. In Fig. 7.22a the direct Δs experiment is simulated at three different temperature stepsizes in both a heating and cooling mode. The magnitude of Δs is independent of step size in a heating mode, where it increases with increasing step size in a cooling mode. When the step size is sufficiently small, the heating and cooling curves collapse onto a single curve.

The same effect is in Fig. 7.22b, showing a simulation of the direct ΔT_{ad} experiments. Here the heating mode curves are shown in solid and dashed blue lines, representing magnetization and demagnetization. These do not change with temperature step size. The red and green curves represent magnetization and demagnetization in a cooling mode, respectively. The ΔT_{ad} values obtained during magnetization increase with step size, whereas the demagnetization values remain constant. At sufficiently small temperature step size the heating and cooling curves collapse. It is noted that the cooling magnetization and demagnetization curves collapse with the heating curves, which is why only six curves are seen in the figure.

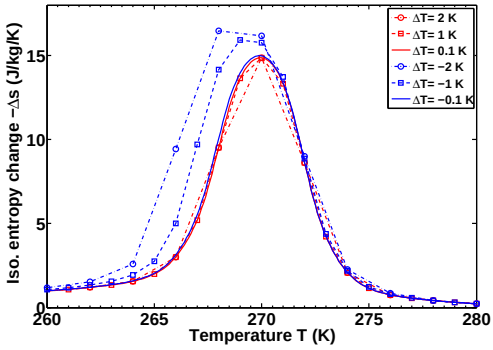

(a) Temperature step size dependence of directly measured Δs during magnetization, illustrated by experiment simulations.

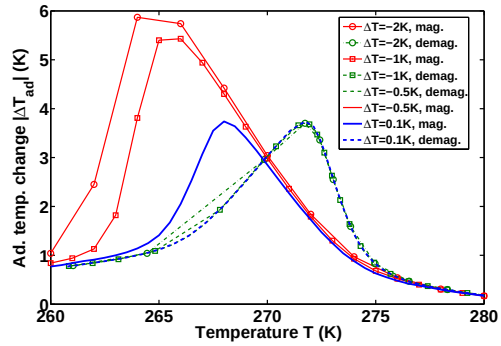

(b) Temperature step size dependence of directly measured ΔT_{ad} during magnetization and demagnetization, illustrated by experiment simulations

Figure 7.22: Measuring the MCE in a cooling mode depends on the temperature resolution.

7.6 Summary and discussion

Applicability of the Preisach approach In this chapter it was demonstrated that the Preisach approach captures first order magnetocaloric material behaviour under various conditions. Previous works have related the model to a single experimental series on which the model itself is based, primarily considering very high magnetic fields fully completing the phase transition [Basso et al., 2006a, 2007a, 2008b]. The findings in this chapter support the validity of this modelling approach, by comparing model predictions of material behavior under widely different conditions to data from independent experiments. As the Preisach model is a phenomenological and semi-empirical approach, it is not known a priori that this should be the case. The model captures the general qualitative behavior of first order MCMs in all the experimentally investigated conditions, including partial transitions, which heightens the confidence in applying the model to AMR-like conditions.

Realistic performance versus equilibrium estimates The conclusion seen for each material modelled in this chapter is that the Maxwell relation overestimates the realistically available Δs, when the materials are applied in AMR working type conditions. The results suggest that the available $(s, T)-$space is bounded by the low field heating and high field cooling entropy curves. Calcula-

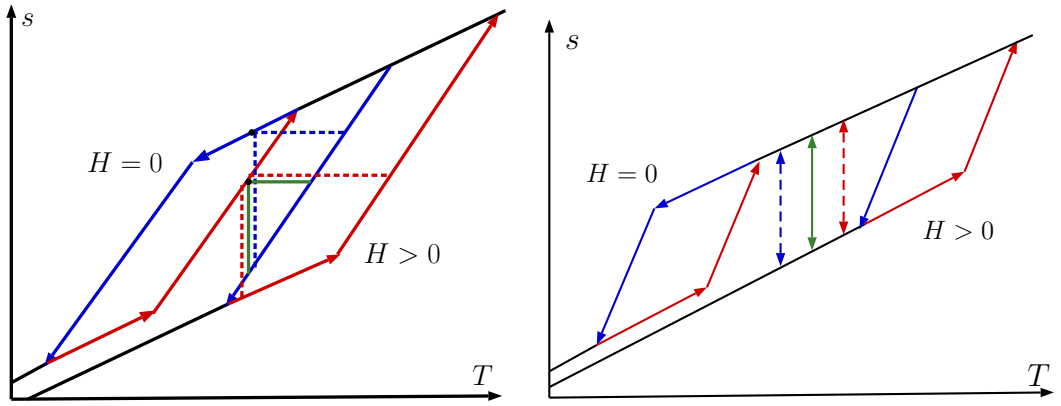

(a) Magnetic field too low to complete the phase transition.

(b) Magnetic field large enough to complete the phase transition.

Figure 7.23: The MCE obtained indirectly from the set of heating(red) or cooling(blue) entropy curves, compared to what is cyclically available in an AMR(green).

tions of Δs using the Maxwell equation represent either the $(s,T)-$space between the zero and high field heating or cooling curves. It is only the overlapping area that is realizable in an application scenario for a given magnetic field change, as illustrated in Fig. 7.23a. This means that the realistically available Δs^* is at best bounded by the minimum of the two Maxwell estimates (from either isofield heating and cooling curves or isothermal magnetization and demagnetization curves)

$$\Delta s^* \leq \min\left(\Delta s^{\text{cool/mag}}, \Delta s^{\text{heat/demag}}\right) . \tag{7.15}$$

The equality only applies under conditions where the magnetic field is large enough to traverse shift the transition temperature across the width of the transition, including the thermal hysteresis gap, as illustrated in Fig. 7.23b. This means if the field is high enough, the maximum Δs values obtained through the Maxwell relation is still realizable. However the width of the Δs^*-curve is always reduced by the thermal hysteresis ΔT_{hyst} compared to either of the Maxwell curves. The realistically achievable ΔT_{ad} is approximately given as the indirectly estimated reversible value during heating, subtracted the thermal hysteresis ΔT_{hyst}

$$\Delta T^*_{\text{ad}} \approx \Delta T^{\text{heat}}_{\text{ad}} - \Delta T_{\text{hyst}} . \tag{7.16}$$

As was illustrated in the various AMR cycle simulations, the material stays within the zero field heating and high field cooling curves. This implies two things:

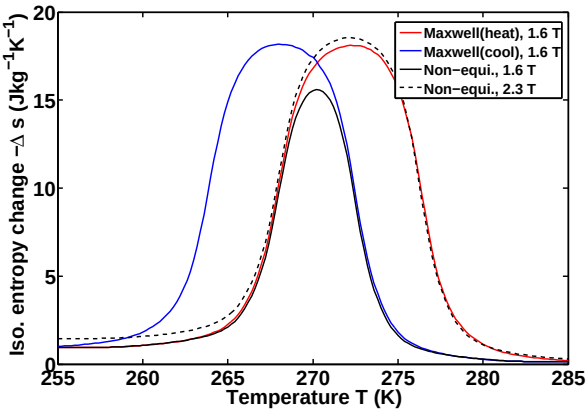

Figure 7.24: The Maxwell relation provides information about realistic performance at a higher field than than at which is was measured.

i) the $(s,T)-$space bounded by the low field thermal hysteresis region is practically never available under working conditions. However, the $(s,T)-$space bounded by the high field thermal hysteresis region is available, at a higher magnetic field. The magnetic field needs to be increased by an amount corresponding to shifting the transition temperature by the thermal hysteresis. Another way of stating this is to note that the Δs values calculated from data obtained at field H is in reality only available at a larger field

$$H^* \approx H + \frac{\delta H_c}{\delta T_p}\Delta T_{\text{hyst}} \tag{7.17}$$

where $(\delta H_c/\delta T_p)^{-1}$ is the change in transition temperature with magnetic field. In the case of $Gd_5Si_2Ge_2$, where $\Delta T_{\text{hyst}} \approx 4$ K and $(\delta H_c/\delta T_p)^{-1} \approx 6$ K/T[1], a magnetic field of 2.3 T would be needed to practically realize the Δs values obtained at 1.6 T using the Maxwell relation. This is illustrated in Fig. 7.24.

This means that when utilizing the Maxwell relations without further considerations, the width of the Δs curve till be approximately ΔT_{hyst} too wide and the maximum value will only be obtainable at high magnetic fields.

Accounting for magnetic hysteresis For all three materials it was observed that the irreversible entropy/heat production due to magnetic hysteresis during

[1]See section 7.4

an AMR cycle was equal to that of the isothermal magnetization hysteresis loop area at the same starting temperature.

This is a nice feature that allows for simple inclusion of heat generation in complete AMR system models. The AMR cycle modelling done here only provides information about the effects of hysteresis at one specific temperature, in response to a specific magnetic field change. In real systems the MCM regenerator has a given size, over which both temperature and magnetic profile changes in time and space, in principle giving rise to an infinite number of individual local AMR cycles within the system. System models seek to describe actual refrigeration performance of a whole system, including the effects position and time dependent magnetic field and temperature in the MCM matrix, thermal transfer between the MCM and thermal transfer fluid, thermal losses to the ambient etc. Not much work has been done on including hysteretic heat production in such models until a recent paper by Brey et al. [2014]. Here the magnetic hysteresis is modelled on the assumption that the hysteretic heat production during field changes can be directly related to isothermal hysteresis loops. This assumption is supported to some extend by the results of this chapter. Their direct implementation is that a given field change will cause a heat production corresponding to the fraction it represent out of a full hysteresis loop. As thermal hysteresis is not accounted for, this approximation is only valid in the case where the magnetic field is larger enough to complete the full hysteresis loop. If the model is used to model scenarios in which the field is so small that the material traces only partial hysteresis loops, the hysteresis will be overestimated. It is worth noting that the heat production not only happens during magnetization and demagnetization, but also during material temperature changes induced by heat rejection or absorption. This might influence the thermal balance in the model.

As was seen for all materials in this work, the MCE close correlates with the magnetic hysteresis. This suggests an even more simple, but of course not as accurate, model implementation of magnetic hysteresis in AMR system models. If one wants to include a varying magnitude of heat production, it can be done by simply adding the heat to the material during the transformations, but scaling it with the known MCE

$$Q_{\mathrm{hyst}}(H_i; H_f, T) \approx \frac{\Delta s(H_i; H_f, T)}{\max(\Delta s)} Q_{\max}\,, \tag{7.18}$$

stating that if no MCE is present, there is no heat production either.

Cooling mode direct MCE experiments With a coupling between experimental data of directly measured Δs and ΔT_{ad} and the model, it was shown that these values can depend on the chosen experimental procedure. When non-isofield

experiments are carried out the measured MCE will generally be larger during a cooling mode compared to a heating mode. This is due to the introduction of first order reversal behavior in the material entropy (Fig. 7.21). In a cooling mode an intermediate value between the completely reversible and the more appropriate irreversible MCE is measured, while just the irreversible MCE is measured during a heating mode. As the temperature stepsize between measurements is reduced this effect disappears.

In general experimental procedures should be carefully analyzed in order to avoid introducing any partial loop type behavior.

Part V

Summary and publications

Chapter 8

Summary and outlook

The work done in this thesis has consisted of both experimental and modelling approaches to illuminate the effects of hysteresis on the performance and characterization of magnetocaloric materials (MCMs). This has led to results concerning both the technicalities of experimental procedures and the estimation of the magnetocaloric effect (MCE) through standard equilibrium methods, such as deriving entropy curves from calorimetric measurements or using the Maxwell relation on magnetization data. Below the main conclusions are listed.

Temperature control It was demonstrated that unintended temperature oscillations and overshooting can occur during isofield magnetization measurements if care is not taken. If the temperature change between two temperature set points is not monotonic, partial hysteresis loop behavior can be induced. This will introduce a complex thermal history, which is reflected in the data. In isofield magnetization measurements this causes an underestimation of the thermal hysteresis. This effect is very system dependent as it is governed by the particular temperature control employed and the heat transfer conditions between the system and the sample. Good thermal contact between sample and system environment and a small sample thermal mass will generally increase the effect. These effects should be investigated in any equipment used to characterize first order MCMs. In the particular system used here, thermal hysteresis was underestimated by 10% in a response to a maximum

0.5 K overshoot in the sample chamber temperature, with a duration of approximately 1 min.

Magnetic field ramp rate If the magnetic field is changed too quickly in isothermal magnetization measurements, the induced temperature change due to the MCE, will invalidate the isothermal conditions. It was shown that very low magnetic field ramp rates are required for the particular system used in this work. The sufficiently low ramp rate depends on MCE and thermal mass of the sample as well as the thermal contact to the system. This effect has been reported before by Moore et al. [2009], Hansen et al. [2010], however it is an issue that is rarely commented on in publications when describing experimental procedures.

Direct MCE measuring methods It was demonstrated experimentally that using direct methods to measure the temperature dependence of the MCE in first order materials during magnetization can yield different results when done in a heating or cooling mode. The results were interpreted through a Preisach type model: in a heating mode the more appropriate cyclically available MCE is measured, whereas in a cooling mode an overestimated and partly reversible value is measured. This effect increases with increasing thermal hysteresis and temperature step size between temperature set points.

Detailed Preisach models Preisach type models were applied to three different first order materials of the type MnFe(P,As) and $Gd_5Si_2Ge_2$. The Preisach approach was shown to be applicable in all three cases. Furthermore, the detailed experimental data, including first order reversal curves, allowed for models that could capture material behavior in varying conditions, different from those from which the models were based. Such detailed comparison between Preisach model predictions and independent experiments has not previously been done. The close correspondence increases the confidence in the modelling framework as being representative of a real material.

Estimating the MCE through equilibrium methods The MCE available in realistic application conditions is not accurately represented by the standard equilibrium methods often employed in publications. This is suggested both by experimental data, as well as simulations of material behavior during AMR-type cycles. It is found that under these conditions, the material can only access the entropy space bound by the low field heating and high field cooling entropy curves. In practice this means that if the MCE is indirectly determined through heat capacity measurements, the low field heating and high field cooling curves should be used. Using the Maxwell relation will overestimate the available $(s-T)$ space, as it determines either the space between the two isofield cooling curves or the two isofield heating

curves. Only the overlapping area between the two Δs curves obtained under heating and cooling should be considered.

Magnetic hysteresis and heat production The Preisach models were used to investigate the heat production during AMR-type cycles. The heat produced in an AMR-type cycle initiated at a given temperature was found to coincide with that of the corresponding isothermal magnetization hysteresis loop area at the same temperature.

8.1 Future considerations

The results of this thesis are relevant for both experimental and modelling research. It is clear that both approaches are needed to move the field of magnetocalorics forward. It is the experimental characterization that allows for realistic material implementation in the models.

The experimental and model results presented here show a connection between the realistically available MCE in application conditions and conventional estimates of the reversible MCE through the Maxwell relation or DSC measurements. This allows for a quantification of the effect of thermal hysteresis, which makes comparison between different materials more straight forward. Furthermore it provides a simple and approximate implementation of thermal hysteresis in models, using the fact the MCE is bound by the low field heating and high field cooling entropy curves. However, the more complicated effects of partial hysteresis loop behavior and the effect of magnetic hysteresis is still not accounted for.

There has been a general advancement of the experimental technologies involved in characterization of MCMs in recent years. Equipment for direct measurements of ΔT_{ad} and Δs is being developed by several different groups, which is a great advancement. This avoids the problems with using equilibrium theory to indirectly estimate inherent non-equilibrium quantities. However, direct methods are also susceptible to experimental procedure dependent results. Even though the MCE is in some sense measured directly at a given field change and temperature, this does not ensure that it is actually representative of the MCE in an AMR-type cycle. It is crucial that a thorough analysis is done on each particular setup and on each applied experimental procedure, to avoid unintended variations in the thermal and magnetic history of the material. In Table 8.1 different direct MCE procedures are outlined. This illustrates that depending on the procedure chosen, one might end up measuring some value of the MCE that reflects the complete or partly reversible value, which is not available in cyclic application. It is worth to note that if the high temperature PM-reset method is used, one will overestimate the MCE. This is in complete contrast to the indirect isothermal magnetization

Table 8.1: Generalized direct MCE experimental procedures, where the MCE is measured during magnetization and demagnetization at each temperature. Cooling/heating refer to experiments where the temperature range is monotonically scanned in the given direction. Thermal reset refers to the sample being heated or cooled between each magnetization/demagnetization. The MCE is denoted irreversible if it reflects the realistically appropriate value, and reversible if it reflects an overstimated and cyclically unstable value. Intermediate means that it is somewhere in between the irreversible and reversible values.

Method	Temp. reset	H_i	H_f	MCE, $H_i \rightarrow H_f$	MCE, $H_f \rightarrow H_i$
Cooling	No	0	H_{max}	**Intermediate**	Irreversible
Heating	No	0	H_{max}	Irreversible	Irreversible
Cooling	No	H_{max}	0	Irreversible	Irreversible
Heating	No	H_{max}	0	Irreversible.	**Intermediate**
PM reset	Yes, high T	0	H_{max}	**Reversible**	Irreversible
FM reset	Yes, low T	0	H_{max}	Irreversible.	Irreversible
PM reset	Yes, high T	H_{max}	0	Irreversible	Irreversible
FM reset	Yes, low T	H_{max}	0	Irreversible	**Reversible**

procedure where this exact reset method is used to eliminate erroneous Δs values obtained by the Maxwell relation [Caron et al., 2009]. Both are correct in their respective application, but it underlines that analysis of the thermal and magnetic history is needed for each setup, for each procedure.

The characterization of magnetic hysteresis and the corresponding heat production during magnetic field cycling is not necessarily solved by direct methods. In principle, the heat production can be derived from both direct ΔT_{ad} and Δs measurements, as the heat production appears in both. This means that ΔT_{ad} and Δs should be larger during magnetization compared to demagnetization. However, this can in practice be difficult to measure accurately. The irreversible entropy production was found to be less than 1% of the MCE for the materials considered here. As small samples are generally used for experiments, the absolute difference between magnetization and demagnetization values can be small and very precise equipment is needed.

From an application viewpoint it is the interplay between the refrigeration system as a whole and the material properties that is of crucial importance. The material behavior during application type conditions is described here, absent the system itself. Here a single and isolated volume element of a material undergoing a unique AMR cycle is investigated. In a real MCM regenerator matrix each volume

element sees a different magnetic field and temperature. There is no unique AMR cycle, but in principle infinitely many. This leads to thermal interactions between different part of the regenerator, as well as the remaining system as well.

Full AMR system model describing these interactions have existed for several years. Material properties such as magnetization, heat capacity and the MCE are used as input in the system models through some kind of lookup tables or single valued functions of field and temperature. This approach completely ignores any hysteresis effects. As stated above, thermal hysteresis effects could in a first approximation be introduced by the restrictions it sets on the available MCE. Magnetic hysteresis can approximately be implemented from measured isothermal magnetization hysteresis loops, as done recently in Brey et al. [2014]. This method is supported by the findings in this thesis, since the accumulated magnetic hysteresis loss in a full AMR cycle equals that of the corresponding isothermal hysteresis loop. However, there is no account of thermal hysteresis, which can lead to problems in especially smaller magnetic fields where partial transitions occur.

A more consistent approach would be to couple the AMR system model and a Preisach type material model. As the Preisach model keeps track of the thermal and magnetic history, it provides correct values for all material parameters as a function of history, temperature, magnetic field and the changes in those. This implements thermal hysteresis effects and the heat production due to hysteresis during each transformation step into the system model. This opens up for a series of interesting problems:

- The influence of thermal hysteresis - This has not yet been implemented in any system models. Thermal hysteresis can reduce the maximum peak MCE and will reduce the width of the MCE peak. As first order materials already have a narrow MCE peak, layered regenerator beds are employed to maximize performance across the temperature range seen by the regenerator. Further decreasing the working range by thermal hysteresis could increase the needed amount of layers, which could easily lead to practical engineering problems.

- Heat production - The AMR-type cycles simulated in this work can be considered as a snapshot of just one volume element in a discrete system model. Here the heat production does not have much influence on the cycle itself, but on a macroscopic system scale the effects are not trivial to quantify. There is no doubt that the effects are negative, but how much heat generation can a given system handle? How much of the excess heat is effectively removed by the transfer fluid and how much remains in the material, continuously heating it up during each cycle. Such a material

heating will inadvertently shift the material away from its maximum MCE temperature.

These effects are difficult to quantify without a model, due to the complexity of the AMR system. But with a coupled Preisach type material model and AMR system model, the effects of hysteresis can be thoroughly investigated through parameter studies, where the hysteretic properties can be tuned and the critical values estimated. Such an approach would provide great insight. However, it does come with a computational cost. Transformations in Preisach models are not computationally light as one is required to keep track of the material history dependent state at all times. Each variation in temperature or field changes this state and the induced state changes themselves need to be calculated as well. These calculation need to happen at each temporal iteration step in the model, for each spatial discretized volume element of material. As the AMR system models are already computationally heavy, adding these calculations will require a thought out optimization process. However, it should by no means be impossible and such a detailed coupled systems model would be of great value to the magnetocaloric community.

Appendix A

Experimental investigation of the effect of thermal hysteresis in first order material MnFe(P,As) applied in an AMR device

INTERNATIONAL JOURNAL OF REFRIGERATION 37 (2014) 303–306

Available online at www.sciencedirect.com

SciVerse ScienceDirect

journal homepage: www.elsevier.com/locate/ijrefrig

Experimental investigation of the effect of thermal hysteresis in first order material MnFe(P,As) applied in an AMR device

L. von Moos, K.K. Nielsen, K. Engelbrecht, C.R.H. Bahl*

Technical University of Denmark, Department of Energy Conversion and Storage, Frederiksborgvej 399, 4000-DK Roskilde, Denmark

ARTICLE INFO

Article history:
Received 18 March 2013
Received in revised form
29 April 2013
Accepted 13 May 2013
Available online 23 May 2013

Keywords:
Magnetocaloric effect
First-order material
Hysteresis
Magnetic refrigeration
MnFe(P,As)

ABSTRACT

The magnetocaloric first order material MnFe(P,As) is a candidate for room temperature magnetic refrigeration. However, these materials have intrinsic hysteresis and the impact on the refrigeration performance has not yet been thoroughly investigated in the literature.

Here, the magnetocaloric effect (MCE) and the thermal hysteresis are studied using vibrating sample magnetometry. The influence on actual refrigeration performance is investigated with an established active magnetic regenerator (AMR) test device (Bahl et al., 2008), utilizing a flat plate regenerator of a single Curie temperature material.

We find that the MCE curves are shifted 1.5 K when comparing heating and cooling the material, while the maximum MCE remains constant. The width of the MCE curve peak is seen to increase 0.3 K when cooling compared to heating. These results are confirmed by experiments on the AMR test device.

Étude expérimentale sur l'effet de l'hystérésis thermique sur un matériau MnFe(P,As) de premier ordre, appliqués à un dispositif à régénération active magnétique

Mots clés : effet magnétocalorique ; matériau de premier ordre ; hysteresis ; froid magnétique ; MnFe(P,As)

1. Introduction

With the discovery of the giant magnetocaloric effect (Pecharsky and Gschneidner, 1997), magnetic refrigeration has become a potential environmentally friendly and efficient alternative to conventional vapor-compression refrigeration. During the last 15 years, a lot of research has been put into finding the optimal material for low priced household refrigeration devices, working around room temperature. One candidate is the first order material MnFe(P,As), having a magnetocaloric effect (MCE) comparable with other candidates working at room temperature (Tegus et al., 2002). The

* *Corresponding author*. Tel.: +45 51943481.
E-mail address: lmoo@dtu.dk (L. von Moos).
0140-7007/$ – see front matter © 2013 Elsevier Ltd and IIR. All rights reserved.
http://dx.doi.org/10.1016/j.ijrefrig.2013.05.005

Nomenclature

T_C	Curie temperature [K]
ΔS	adiabatic entropy change [J kg^{-1} K^{-1}]
T	Temperature [K]
M	magnetization [A m^2 kg^{-1}]
H	Magnetic field [A m^{-1}]
ΔS_{max}	Maximum adiabatic entropy change [J kg^{-1} K^{-1}]
T_p	Temperature of ΔS_{max} [K]
w	Full width at half maximum [K]
μ_0	Vacuum permeability [N A^{-2}]

Curie temperature can be tuned by changing the P/As ratio (Brück et al., 2005), making it customizable for specific application needs and for multilayered magnetocaloric regenerators. Due to the nature of first order phase transitions, the magnetic phase transition is coupled to a structural transition, giving rise a large MCE, but at the cost of hysteresis. The hysteretic behavior will introduce losses in each AMR cycle, which in a worst case scenario can nullify the MCE entirely (Tocado et al., 2006), and make the magnetocaloric properties dependent on the magnetic and thermal history. This is of great importance when designing a refrigeration device optimized for certain temperature conditions.

Here we investigate the thermal hysteresis of a MnFe(P,As) compound by Vibrating Sample Magnetometry (VSM) and measure how these properties influence the performance of an actual AMR test device.

2. Experiments

The material used is provided by BASF as a part of a series of MnFe(P,As) compounds with varying Curie temperatures. In these experiments a single of these materials is investigated. The material is bulk sintered and then cut into plates.

2.1. *Magnetization measurements*

In order to measure the magnetic entropy change, the magnetization was measured as a function of applied magnetic field and temperature, using the isofield method where temperature is varied point by point at constant applied magnetic field. The point by point method allows a 5 min settling period for the sample, to ensure thermal equilibrium of the 35 mg sample.

Initiating the measurements at temperatures far from T_C in each temperature run avoids complications due to mixed ferro- and paramagnetic states, as described by (Caron et al., 2009). These measurements were done on a commercial LakeShore 7407 VSM. The magnetization was measured under constant applied magnetic fields of 0.25, 0.50, 0.75, 1.00, 1.25 and 1.50 T, while the temperature range was 275–320 K in steps of 1 K for both heating and cooling at each field. From these results the entropy change was calculated by employing the Maxwell relation

$$\Delta S = \mu_0 \int_0^H \left.\frac{\partial M}{\partial T}\right|_H dH \tag{1}$$

The magnetization gradient for each field curve is numerically calculated for each temperature and then integrated over the different field values. The magnetization measurements and the corresponding calculated entropy changes are shown in Fig. 1.

Each entropy change curve fits well to a Lorentzian of the form,

$$\Delta S = \frac{\Delta S_{max}}{1 + \left(\frac{T - T_p}{(w/2)}\right)^2} \tag{2}$$

where ΔS_{max} is the maximum entropy change, T_p the transition peak temperature and w the full width at half maximum (FWHM).

In Fig. 2 the transition peak temperature is shown as a function of applied field. A clear thermal hysteresis is seen. The transition temperature is shifted by about 1.6 K depending on whether the sample is cooled or heated. The transition temperature increases linearly with about 2.4 K/T in both cases.

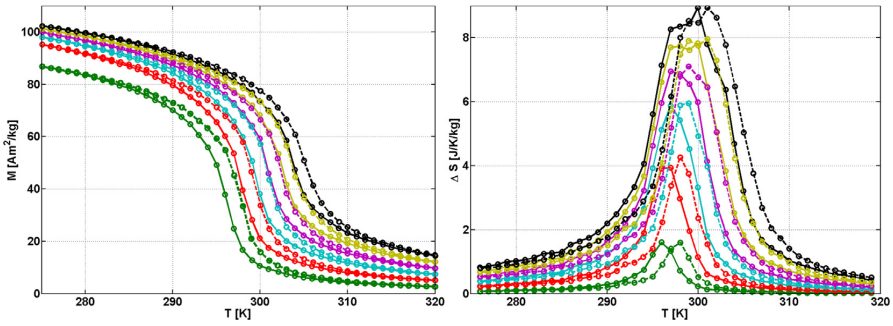

Fig. 1 – Measured magnetization (left) and integrated entropy change (right) curves with applied magnetic fields of 0.25, 0.50, 0.75, 1.00, 1.25 and 1.50 T. The solid and dashed lines represent cooling and heating conditions, respectively.

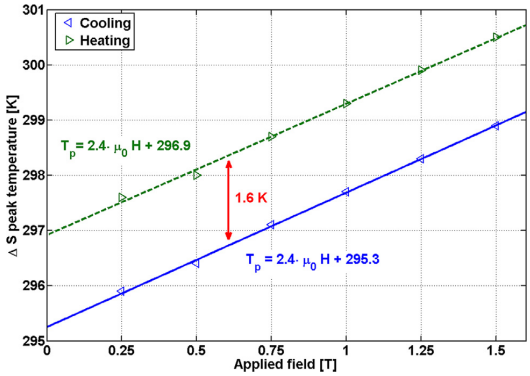

Fig. 2 – The magnetic phase transition temperature as a function of applied field measured in both heating and cooling conditions.

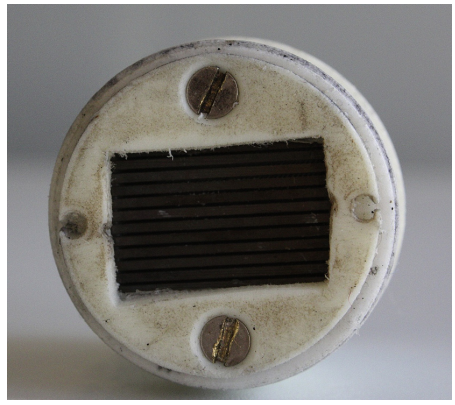

Fig. 4 – The stacked flat plates of MnFe(P,As). The plates are 36 mm long (into the page), 24 mm wide, 1 mm thick and have a separation of 0.6 mm.

However, it is noted that the linearity seems to deviate for fields below 0.5 T. This effect was also seen by (Zang et al., 2010), where it is attributed to the effects of the demagnetizing field and domains beginning to be significant in these low applied fields.

Fig. 3 shows ΔS_{max} and the FWHM of the entropy change peak for a given field. ΔS_{max} is seen to increase toward a saturation point, following a non-linear curve.

The FWHM of the entropy change peak increases linearly with field, when the field is larger than 0.5 T. For both heating and cooling the FWHM increases about 4.5 K/T across the entire range of fields. There is possibly minor thermal hysteresis between heating and cooling, where cooling consistently gives a 0.3 K wider peak.

2.2. *AMR test device*

In order to test the actual performance of the material and investigate if any thermal hysteresis effects are present, the MnFe(P,As) material was used in larger quantities as the refrigerant in an AMR device, described in (Bahl et al., 2008).

The regenerator is shown in Fig. 4. It consists of 12 stacked, flat plates; having length, width and thickness of 36 mm, 24 mm and 1 mm respectively. The plates are separated by 0.6 mm and have a total mass of 63 g. In cycles, the material is magnetized and demagnetized from 0 to 1 T by a permanent magnet, with an AMR frequency of about 0.2 Hz. The hot side of the regenerator is kept at constant temperature through a heat bath at a controlled temperature. The cycle is run for approximately 1 h (about 700 full AMR cycles), until thermal equilibrium of the experimental setup is reached and a stable temperature span across the regenerator is obtained. This was done for a range of hot side temperatures between 314 and 294 K. The regenerator was then cooled to 278 K and then the measurements were redone from 294 to 314 K.

Fig. 5 shows the results of the AMR test device experiments. The maximum temperature span is just below 5.5 K for both experiments and the peak performance temperature is about 302.5 K and 303.5 K when cooling and heating, respectively. These temperatures are higher than what is measured by magnetometry, since the material is submitted to a temperature gradient across the regenerator. When the two curves are shifted about 1.1 K across the entire temperature range it is noticed that the width of the heating curve is a bit narrower when heating compared to cooling. This is a minor compression of the peak width, but it is consistent for all measured temperatures and with the VSM measurements.

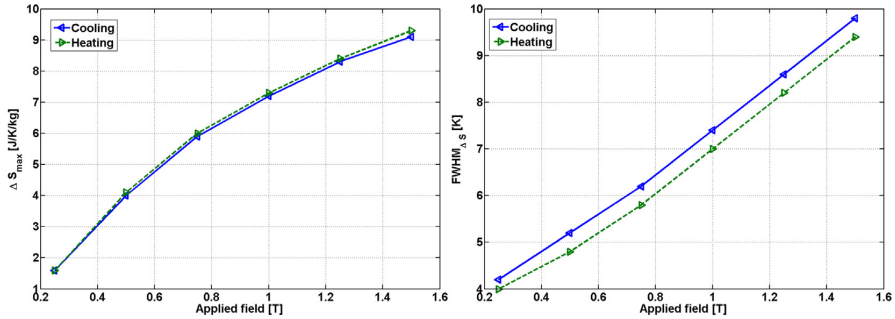

Fig. 3 – The peak maximum (left) and the full width at half maximum of the entropy change peaks (right) as a function of applied field.

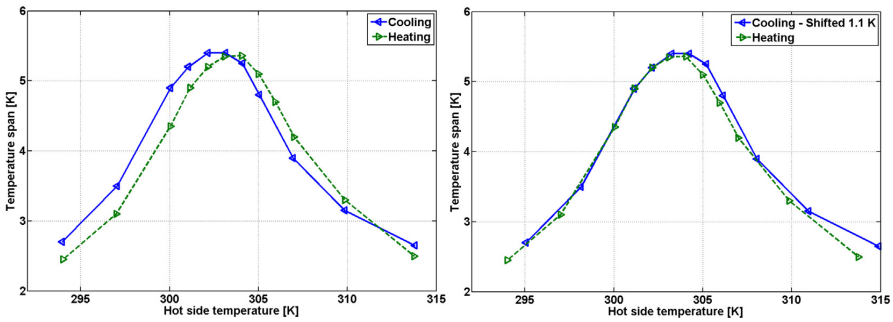

Fig. 5 – Measured temperature span between the hot and cold side of the AMR device as a function of the hot side temperature for both cooling and heating conditions (left). The right plot shows the results with the cooling curve temperature axis shifted by 1.1 K. The results were obtained using a regenerator consisting of a stack of 12 MnFe(P,As) flat plates, totaling 63 g, cycling between 0 and 1 T magnetic field with a frequency of 0.2 Hz.

When looking at the temperature span for the cooling curve at 314 K it seems higher than expected. However, this is the first measured point in the series of experiments. The regenerator was not heated up above 314 K prior to this measurement and the actual thermal history is unknown.

Four smaller AMR device control experiments were done around the peak temperature in order to check experimental consistency. All four experiments show the presence of thermal hysteresis.

Results from the AMR experiments generally show similar characteristics as the VSM measurements, but it should be noted that the similarities of the measured thermal hysteresis of 1.1 K and 1.6 K, respectively, might be a special case. The VSM measurements take the sample gradually around a full saturation loop in magnetization step by step. In the AMR experiments, the sample undergoes hundreds of minor magnetization loops to reach each temperature span. The coupling between these two scenarios is not obvious, and future investigations of materials with different hysteretic characteristics would be interesting. The findings of this paper do suggest that the material seems to partially stay in the originating magnetic phase during the experiments, regardless of the hundreds of magnetization and demagnetization cycles during the recording of each measurement.

3. Summary

Through VSM measurements it was found that the MnFe(P,As) material experiences clear thermal hysteresis. There is a thermal shift in peak entropy change temperature of 1.6 K. A similar effect is also observed during the application of the material in a device performing AMR cycles, where the peak performance temperature is shifted 1.1 K. VSM measurements also implied that the FWHM of the entropy change peak was 0.3 K wider when coming from the paramagnetic state, compared to originating in the ferromagnetic state. A similar broadening was also seen in the AMR experiments.

Acknowledgments

We thank BASF for the supply of materials. K.K. Nielsen wishes to thank The Danish Council for Independent Research | Technology and Production Sciences (Contract no. 10-092791) for financial support.

REFERENCES

Bahl, C.R.H., Petersen, T.F., Pryds, N., Smith, A., 2008. A versatile magnetic refrigeration test device. Rev. Sci. Instrum. 79.

Brück, E., Ilyn, M., Tishin, A.M., Tegus, O., 2005. Magnetocaloric effects in $MnFeP_{1-x}As_x$-based compounds. J. Magn. Magn. Mater., 290–291.

Caron, L., Ou, Z.Q., Nguyen, T.T., Cam Thanh, D.T., Tegus, O., Brück, E., 2009. On the determination of the magnetic entropy change in materials with first-order transitions. J. Magn. Magn. Mater. 321.

Pecharsky, V.K., Gschneidner, K.A., 1997. Giant magnetocaloric effect in $Gd5(Si_2Ge_2)$. Phys. Rev. Lett. 78.

Tegus, O., Brück, E., Buschow, K.H.J., de Boe, F.R., 2002. Transition-metal-based magnetic refrigerants for room-temperature applications. Nature 415.

Tocado, L., Palacios, T., Burriel, R., 2006. Adiabatic measurement of the giant magnetocaloric effect in MnAs. J. Therm. Analys. Cal. 84.

Zang, L., Vanasten, D., Seeler, F., Reesink, B., Brück, E., 2010. A fast method to evaluate magnetocaloric effect in first-order MnFe(P, As) compounds. In: 4. International Conference on Magnetic Refrigeration at Room Temperature, IIF/IIR, pp. 65–71.

Appendix B

A Preisach approach to modeling partial phase transitions in the first order magnetocaloric material MnFe(P,As)

Physica B 435 (2014) 144–147

Contents lists available at ScienceDirect

Physica B

journal homepage: www.elsevier.com/locate/physb

A Preisach approach to modeling partial phase transitions in the first order magnetocaloric material MnFe(P,As)

L. von Moos [a,*], C.R.H. Bahl [a], K.K. Nielsen [a], K. Engelbrecht [a], M. Küpferling [b], V. Basso [b]

[a] Department of Energy Conversion and Storage, Technical University of Denmark, 4000 Roskilde, Denmark
[b] Istituto Nazionale di Ricerca Metrologica, 10135 Torino, Italy

ARTICLE INFO

Available online 11 October 2013

Keywords:
Magnetocaloric effect
Magnetic refrigeration
First order material
Hysteresis
Preisach
MnFePAs

ABSTRACT

Magnetic refrigeration is an emerging technology that could provide energy efficient and environmentally friendly cooling. Magnetocaloric materials in which a structural phase transition is found concurrently with the magnetic phase transition are often termed first order magnetocaloric materials. Such materials are potential candidates for application in magnetic refrigeration devices. However, the first order materials often have adverse properties such as hysteresis, making actual performance troublesome to quantify, a subject not thoroughly studied within this field.

Here we investigate the behavior of MnFe(P,As) under partial phase transitions, which is similar to what materials experience in actual magnetic refrigeration devices. Partial phase transition curves, in the absence of a magnetic field, are measured using calorimetry and the experimental results are compared to simulations of a Preisach-type model. We show that this approach is applicable and discuss what experimental data is required to obtain a satisfactory material model.

1. Introduction

With the global focus on energy and new developments in room temperature magnetocaloric materials (MCM), the field of magnetic refrigeration has grown a lot within the last 15 years. Magnetic refrigeration utilizes the magnetocaloric effect (MCE), where a temperature change in the MCM is induced when a magnetic field is applied. Under adiabatic conditions, the total entropy remains constant and the decrease of magnetic entropy is balanced by an increase in lattice entropy and thus a temperature increase. The effect is completely reversible in the case of second order materials and a cooling effect is obtained upon removing the magnetic field.

The temperature increase is largest around the Curie temperature, T_C, but it is only of the order of a couple of degrees for an applied magnetic field of one tesla. In order to be useful in applications it must therefore be amplified through using Active Magnetic Regenerators (AMR), where the MCM undergoes thermodynamic cycles through magnetization, demagnetization and heat exchange with a fluid in order to cool a system. For a general review of magnetic refrigeration, see Smith et al. [1].

Many promising new materials are being researched, and some of these are the first order materials that have a coupled magnetic and structural phase transition, leading to a large entropy change during a transition. However, these materials have some degree of thermal and magnetic hysteresis, which is problematic in several ways. Hysteresis leads to heat production in the material during each cycle, which reduces the cooling capacity of the system. More importantly, the state variables, the magnetization M and the entropy s, become history dependent, making realistic predictions of performance and use of simple datasets in AMR modeling non-trivial. The characterization of the MCE is often done by mapping the complete phase transition through saturation loops. However, in an AMR cycle the MCM will rarely undergo a complete phase transition, but only cycle through minor loops. The trace of these minor loops depends on the specific, material dependent, properties of the phase transition and will influence the AMR performance.

Here we investigate the hysteresis properties of the partial first order phase transitions of the magnetocaloric material MnFe(P,As). The class of compounds MnFe(P,X), with X=As,Ge,Si is of high interest for application to magnetocaloric refrigeration because the phase transition temperature and hysteresis can be carefully tuned by changing the stoichiometry [2] and the raw materials are inexpensive compared to other MCMs.

For this study, a material composition with a small degree of hysteresis is chosen. The partial phase transitions are characterized by a differential scanning calorimeter (DSC) where the heat

* Corresponding author. Postal address: Frederiksborgvej 399, 4000 Roskilde, Denmark. Tel.: +45 51943481.
E-mail address: lmoo@dtu.dk (L. von Moos).

0921-4526/$ - see front matter © 2013 Elsevier B.V. All rights reserved.
http://dx.doi.org/10.1016/j.physb.2013.09.054

flux, q, needed to change the sample temperature at a given rate is measured. From this the entropy, s, is deduced and used as the material state variable. The experimental results are analyzed and compared to a Preisach-type thermodynamic model of the phase transition, suitable for out-of equilibrium phenomena [3].

2. A Preisach model approach

The modeling approach employed here is based on the idea of decomposing the hysteretic behavior of the system in terms of a superposition of a collection of bistable units.The output of each unit is the phase state, $x=\{0,1\}$, in our magnetic case corresponding to the paramagnetic (PM) and ferromagnetic (FM) phase states for the magnetocaloric material, respectively (Fig. 1). Each unit is characterized by two parameters $(g_u,\ g_c)$, which give the unit specific switching fields $Z_\beta=g_u+g_c$ and $Z_\alpha=g_u-g_c$ that determine when the unit is forced to be in either phase 0, $Z\le Z_\alpha$, or phase 1, $Z\ge Z_\beta$. The hysteretic behavior appears in the intermediate field region $Z_\alpha<Z<Z_\beta$, where the unit remains in its current phase. The energy landscape for an individual unit is shown in Fig. 1, from which the meaning of $(g_u,\ g_c)$ can be visualized.

The model input field, Z, that drives the unit transitions depends on the intensive variables, i.e. the magnetic field H and temperature T. Z is assumed the same for all units and is given by the difference in the Gibbs free energy of phase 0 and 1

$$Z(H,T)=\frac{g_0(H,T)-g_1(H,T)}{2}. \tag{1}$$

The functions $g_0(H,T)$ and $g_1(H,T)$ are the equilibrium Gibbs free energies of the two pure phases, far away from the transition. These are assumed single-valued functions of both H and T.

The total model output is determined by the collection of bistable units lying in the $(g_u,\ g_c)$-plane, the Preisach plane. The distribution of these units is given by the Preisach distribution $p(g_u,\ g_c)$. The Z-field then dictates which areas of the plane that are switched or maintained in their current phase and the time evolution of $Z(t)$ create the history dependent transition line $b(g_c)$, as illustrated in Fig. 2.

The current FM phase fraction is determined by integration in the Preisach plane

$$X=\int_0^{+\infty} dg_c \int_{-\infty}^{b(g_c)} p(g_u,g_c)dg_u. \tag{2}$$

The entropy of the mixed phase state is then given as

$$s=(1-X)s_0+Xs_1 \tag{3}$$

where s_0 and s_1 are the PM and FM pure phase entropies, respectively.

To model the phase transformation one has to know the pure phase Gibbs free energies, g_0 and g_1, and the Preisach distribution $p(g_u,\ g_c)$, which can be inferred from experiments, as shown in the following section.

In this paper this approach is tested by comparing the model to the measured hysteresis in s vs. T of MnFe(P,As) at the first order magnetoelastic phase transition.

3. Calorimetric measurements

For this study the first order material MnFe(P,As), provided by BASF Gmbh, has been used. It has a hexagonal Fe_2P structure and a magnetic phase transition between the low temperature FM state and the high temperature PM state [4]. The phase transition is magnetoelastic, coupling the magnetic transition with a structural transition. Around the transition temperature the lattice parameter ratio, c/a, of the hexagonal unit cell changes, while the volume remains approximately constant [2].

A 35 mg sample, measuring $2\times2\times1\ \mathrm{mm}^3$, with $T_C\approx297$ K was measured with a power compensation DSC. Each measurement was initiated with the sample being in the FM state by cooling it to 273 K. The measured data is the heat flux q absorbed by the sample in order to maintain a constant temperature-scanning rate of $\dot{T}=\pm2\ \mathrm{K\,min^{-1}}$, which corresponds to a scaled heat capacity

$$c=\frac{q}{\dot{T}}. \tag{4}$$

An example of the measured data is shown in Fig. 3. The results have been corrected for thermal lag, due to the heat transfer time between the sample and the sample chamber. Assuming a constant thermal contact resistance R between the sample and the chamber where the temperature is measured, this correction leads to a shift between the sample temperature T and the measured temperature T_m, $T=T_m-R\,q$. The resistance is determined by measuring q at different temperature rates and is estimated to $R=160\ \mathrm{K\,W^{-1}}$.

3.1. Modeling the material properties

Obtaining expressions for the pure phase properties of the material is done from the heat flux measured away from the phase transition. Fig. 3 shows data from the directly measured heat flux, where a thermal hysteresis of about 1.5 K is seen.

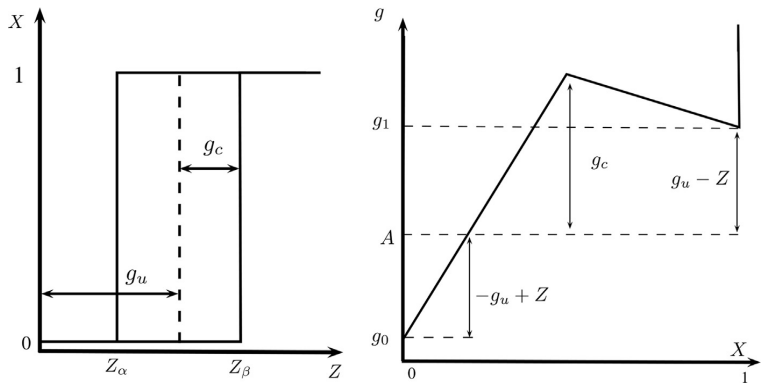

Fig. 1. (Left) A bistable hysteretic unit, defined by the parameters (g_u, g_c). (Right) The energy landscape of a unit in the presence of the Z-field.

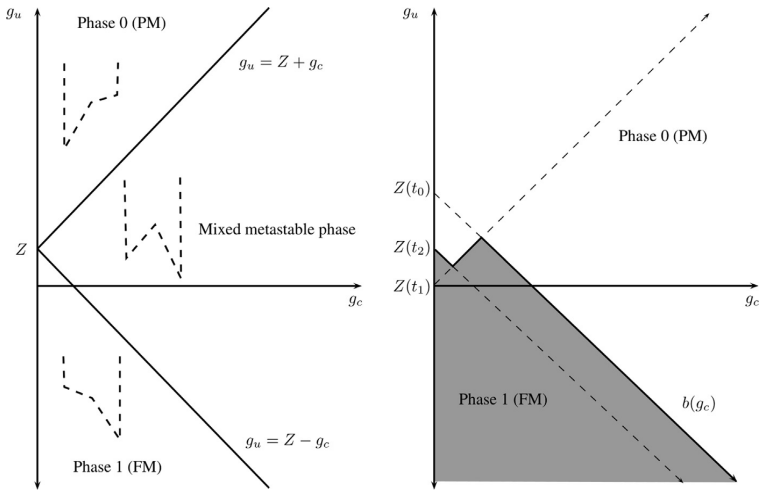

Fig. 2. (Left) The Preisach plane with the phase of each unit being determined by the thermodynamic field Z. (Right) An illustration of the time evolution of the Preisach plane driven by the time dependence of $Z(t)$.

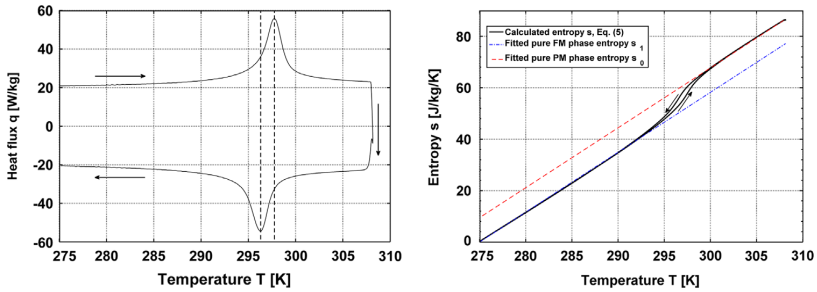

Fig. 3. (Left) Measurement of the heat flux to a 35 mg sample at a rate of ± 2 K/min. Arrows represent direction of measurement and the vertical lines the peak flux, showing thermal hysteresis of about 1.5 K. (Right) The entropy calculated from the measured heat flux (Eq. (5),) along with the fitted pure phase entropies (dashed lines).

The entropy change between the initial and final temperature, T_0 and T, is calculated from the heat flux, using Eq. (4) and $c = T(\partial s/\partial T)|_H$,

$$s(T) = \frac{1}{m}\int_{T_0}^{T} \frac{1}{T'}\frac{q}{T} dT' + s(T_0) \tag{5}$$

where we chose $s(T_0) = 0$. As seen in Fig. 3 the entropy, fitted away from the transition (below 293 K and above 300 K), is approximately linear in the pure phase states and is therefore simply modeled as

$$s_1(T) = \alpha(T - T_0), \quad s_0(T) = s_1(T) + \delta s. \tag{6}$$

The parameters $\alpha = 2.3\ \mathrm{J\,kg^{-1}\,K^{-2}}$ and $\delta s = 10.7\ \mathrm{J\,kg^{-1}\,K^{-1}}$ are obtained from fitting the data, and physically relate to the heat capacity and the entropy change of the phase transition, respectively. The initial temperature is set to $T_0 = 275$ K.

The pure phase entropies, s_i, determine the pure phase Gibbs free energies, g_i, driving the phase transition, through direct integration of $s_i = -\partial g_i/\partial T$.

In order to evaluate the phase state of the material at a given temperature, the FM phase fraction X is estimated from the calculated entropy, relative to the fitted pure phase entropies,

$$X_{est} = \frac{s - s_0}{s_1 - s_0}, \tag{7}$$

which can be directly compared to the results of the Preisach model, given by Eq. (2).

The Preisach distribution is assumed independent of temperature and magnetic field and consists of both an irreversible and a reversible contribution

$$p(g_u, g_c) = p_i(g_u, g_c) + p_r(g_u, 0). \tag{8}$$

The actual distribution for this material is unknown and in order to approximately describe the data, a combination of Gaussian and Lorentzian distribution functions is chosen. Both are commonly used in Preisach systems and the optimal combination of these varies with different materials [5].

The best fit to the measured data is a statistically independent combination of two Lorentzian distributions in (g_u, g_c) for the irreversible contribution

$$p_i(g_u, g_c) = A_i \frac{1}{1 + (g_u/\sigma_u)^2} \frac{1}{1 + ((g_c - g_{c,0})/\sigma_c)^2} \tag{9}$$

and a Gaussian distribution for the reversible part in g_u

$$p_r(g_u, 0) = A_r \exp\left(-\frac{g_u^2}{2\sigma_u^2}\right) \tag{10}$$

where $g_{c,0}$, σ_u, σ_c, A_i and A_r are fitting parameters. The shape of the distribution is given by $\{g_{c,0}, \sigma_u, \sigma_c\}$ and $\{A_i, A_r\}$ determines the ratio between the irreversible and reversible components of

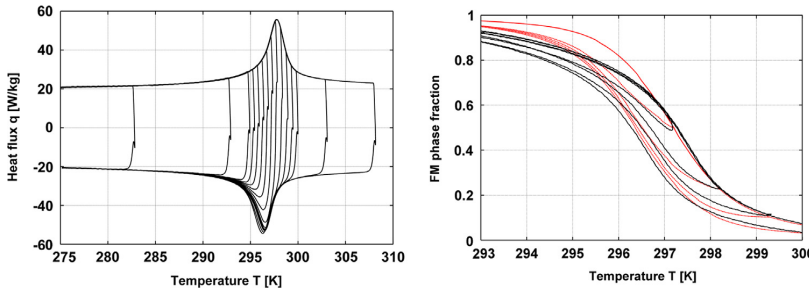

Fig. 4. (Left) Measured heat flux curves. (Right) Phase fraction from data, estimated from Eq. (7) (solid black curves) and simulated phase fraction (dashed red curves), Eq. (2), shown for a selection of reversal curves. (For interpretation of the references to color in this figure legend, the reader is referred to the web version of this article.)

the transition. The latter are chosen such that the total distribution function is normalized.

The parameters were fitted to make the simulated phase fraction curves, obtained from Eq. (2), reproduce the shapes of the measured phase fraction curves (as shown in Fig. 4). The parameters were found to be $g_{c,0} = 2.25\ \mathrm{J\,Kg^{-1}}$, $\sigma_u = 4.25\ \mathrm{J\,Kg^{-1}}$, $\sigma_c = 1.50\ \mathrm{J\,Kg^{-1}}$ and normalized such that the reversible part contributes to 30% of the total distribution.

3.2. Partial transitions

The partial transition measurements were carried out by: (1) cooling the sample to 273 K and letting it reach thermal equilibrium, (2) heating at a constant rate of $2\ \mathrm{K\,min^{-1}}$ until the desired maximum temperature is reached, and (3) cooling back to 273 K at the same rate without any equilibration time at the reversal point.

The measured reversal curves of the heat flux are shown in Fig. 4 along with the estimated FM phase fraction. Note that the temperature scales are different. The estimated phase fraction, Eq. (7), is shown as solid black curves, along with a model simulation of the experiment, shown in dashed red curves.

The heat flux oscillates around the reversal point, due to the PID control of the DSC heater, where it shortly after stabilizes again. This signal is not material related and has been filtered out when possible in the estimated phase fraction calculations. One should keep in mind that this leads to some uncertainty in the curve shapes immediately following the reversal points when comparing the data to the model.

4. Discussion

The model reproduces the measured phase fraction approximately well in most of the temperature range. This shows that the Preisach approach is definitely feasible to describe this kind of first order material. However, it is apparent that the simple, symmetric Preisach distribution applied here is not sufficient to completely represent the material. A clear asymmetry is seen in the phase fraction data, which stems from the fact that the gradient of q is slightly higher on the PM side, compared to the FM side.

When comparing the saturation curves, aside from the asymmetry, the simulations fit the data well. However, when comparing the reversal curves, the fit is not nearly as good. This illustrates two important points. The first is that even with a significant reversible contribution to the distribution, the irreversibility is still overestimated in the model, which emphasizes the need for a more advanced distribution. The second is that it is necessary to measure not only full saturation curves, but also minor reversal curves in order to correctly model the material; fitting saturation loops does not ensure correct minor loop behavior.

A clear separation of the reversible and irreversible parts of the transition plays an important role in realistic AMR modeling and is needed to understand the effect of hysteresis on cooling performance. Here we tested a material with relatively small hysteresis and chose a simple Preisach distribution, without any knowledge about the shape of the actual distribution. Some evident possibilities for future work could be to look at materials with larger degrees of hysteresis, which makes it easier to obtain detailed reversal curves reliably. Furthermore, the actual Preisach distribution could be measured in detail by the use of first order reversal curves (FORC), as described by Mayergoyz [6].

5. Conclusion

We have demonstrated that the Preisach approach to the out-of-equilibrium behavior of the first order magnetocaloric material MnFe(P,As) is feasible and can reproduce measured data approximately well based on simple material modeling. However, using simple Gaussian and Lorentzian Preisach distributions does not capture all the details of the transition, but generally work well.

It was shown that only using full saturation curves as characterization of the hysteretic material is not sufficient to separate the reversible and irreversible parts of the transition. Ideally, the actual distribution could be measured using the FORC technique. In other cases, at least some minor loop measurements should accompany the standard saturation loop data to realistically simulate material behavior in cycles such as an AMR.

Acknowledgments

We would like to thank BASF for providing the samples used in this work, INRIM for providing experimental equipment and expertise and Copenhagen Cleantech Cluster for financing part of this project.

References

[1] A. Smith, C.R.H. Bahl, R. Bjørk, K. Engelbrecht, K.K. Nielsen, N. Pryds, Advanced Energy Materials 2 (2012) 1288.
[2] N.H. Dūng (Ph.D. thesis), TU Delft 2012.
[3] V. Basso, C.P. Sasso, M. LoBue, Journal of Magnetism and Magnetic Materials 316 (2007) 262.
[4] O. Tegus, E. Brück, K.H.J. Buschow, F.R. de Boer, Nature 415 (2002) 150.
[5] P. Pruksanubal, A. Binner, K.H. Gonschorek, in: Proceedings of the 17th International Zurich Symposium on Electromagnetic Compatibility, 2006 pp. 258–261.
[6] I. Mayergoyz, IEEE Transactions on Magnetics 22 (1986) 603.

Appendix C

The influence of hysteresis on the determination of the magnetocaloric effect in $Gd_5Si_2Ge_2$

The influence of hysteresis on the determination of the magnetocaloric effect in $Gd_5Si_2Ge_2$

L. von Moos[1], C.R.H Bahl[1], K.K. Nielsen[1] and K. Engelbrecht[1]1
[1] *Technical University of Denmark, Department of Energy Conversion, Frederiksborgvej 399, 4000 Roskilde, Denmark*[a)]

We present a non-equilibrium Preisach-type hysteresis model based on the first order magnetocaloric material $Gd_5Si_2Ge_2$. The model is developed from isofield magnetization measurements and first order reversal curves, both of which constitute a new and detailed approach to characterizing and modelling magnetocaloric materials. It is shown that the model reproduces the magnetization data, directly measured adiabatic temperature changes and provides a good description of the material behavior under application conditions. We find that the material settles in an area of metastability under continuous magnetization cycles, which effectively limits the adiabatic temperature change by the amount of thermal hysteresis present. We suggest a straightforward method for realistic estimation of the magnetocaloric effect from indirect measurements.

I. INTRODUCTION

Magnetic cooling is a field that has experienced large growth in recent years due to the demand of energy-efficient technologies and the discovery of high performance, room temperature magnetocaloric materials (MCM)[1]. The magnetocaloric effect (MCE) originates from a coupling between the magnetic spins and the lattice, which causes a temperature change within the material when adiabatically magnetized or demagnetized. For conventional ferromagnetic materials the temperature is increased during magnetization and decreased during demagnetization, which is the case in this work, but an inverse MCE has also been observed[2]. The effect can be characterized by the adiabatic temperature change (ΔT_{ad}) and the isothermal entropy change (Δs), both of which can be inferred indirectly from magnetometric or calorimetric measurements. For cooling applications the MCM operates as an active magnetic regenerator (AMR), which typically undergoes a four step cycle: i) magnetization, ii) heat removal by fluid flow, iii) demagnetization, iv) heat absorption by fluid flow.

The $Gd_5Si_2Ge_2$ compound investigated here belongs to a class of MCMs experiencing a structural first order transition concurrently with a magnetic transition, which provides a large MCE due to the magneto-structural coupling[1,3]. However, these transitions are accompanied by hysteresis, which causes heat generation during each AMR cycle and makes material properties history dependent. Such heat generation is not desirable in a cooling application, but the effect in $Gd_5Si_2Ge_2$ is minimal and will not be the focus of this work[4,5]. However, we will demonstrate that the history dependence does play a significant role in determining the MCE of first order materials in working conditions, which is often approximated by imposing the equilibrium Maxwell relation on an inherently non-equilibrium problem.

In the following we present a non-equilibrium Preisach-type model based on magnetization measurements. Where earlier works have focused on covering a large magnetic field range with few isothermal measurements, we present here detailed data characterizing the material in the range up to 1.6 T, which is typical for permanent magnets that have been realized so far in magnetic refrigeration applications[6]. The material is primarily characterized by isofield measurements but is supplemented by a set of first order reversal magnetization curves, which provide information about the reversibility of the phase transition. The model is shown to approximately reproduce directly measured ΔT_{ad} values and material behavior under AMR-like conditions, from which we quantify the effect of hysteresis and discuss how it relates to the standard methods of characterizing the MCE.

II. METHOD

A. A Preisach approach

In order to accommodate the non-equilibrium nature of hysteresis we employ a Preisach-type model, in which magnetic phase coexistence and history dependence are accounted for. The general approach of this paper is a further development of earlier works[7–9] where more detailed descriptions can be found. A brief summary is given below.

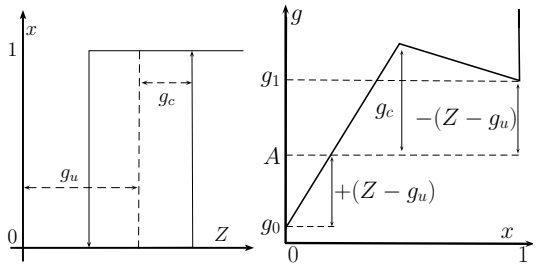

FIG. 1. Illustration of a bistable unit (left), which can be in either phase 0 or 1, and its energy landscape (right).

[a)]Electronic mail: lvmoos@gmail.com

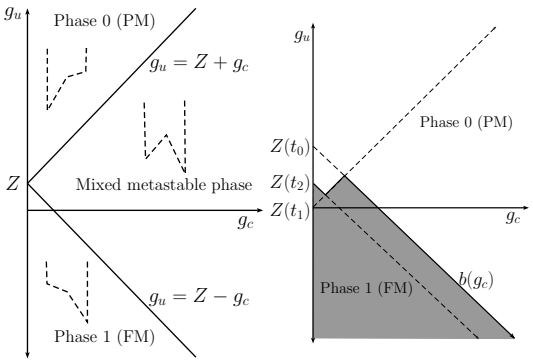

FIG. 2. (Left) Illustration of the (g_u, g_c)-plane of hysteretic units and their phase stability under the influence of the thermodynamic field Z. (Right) Generation of the history dependent state transition line $b(g_c)$ through variation of Z.

The hysteretic behavior of a bulk material is assumed to be a superposition of individual bistable, hysteretic units, as illustrated in Fig. 1. Each unit can be in either the purely paramagnetic (PM) or ferromagnetic (FM) state, represented throughout this paper by the phase state variable $x = \{0, 1\}$, respectively. Each state has an associated Gibbs free energy $g_x(H, T) = A \pm (Z - g_u)$, with $\pm$ corresponding to the subscripts $x = \{0, 1\}$, respectively. The Gibbs free energy is a function of the intensive variables: magnetic field H and temperature T. The mean free energy of the states is denoted $A = (g_1 + g_0)/2$, the difference in free energy driving the phase transition $Z = (g_1 - g_0)/2$, the unit energy shift g_u, and the dissipative energy barrier g_c, all of which are illustrated in Fig. 1. These definitions lead to the state conditions

$$x = \begin{cases} 0 & \text{if } Z \leq g_u - g_c \\ 1 & \text{if } Z \geq g_u + g_c \end{cases} \tag{1}$$

where hysteresis is introduced by the individual unit remaining in its current state in the intermediate region $g_u - g_c < Z < g_u + g_c$.

A material is modelled by assuming a statistical distribution p of these units, each with individual (g_u, g_c)-values,

$$p(g_u, g_c) \propto (1 - f_r)p_i(g_u, g_c) + f_r\delta(g_c)p_r(g_u)\,. \tag{2}$$

Here we assume both an irreversible p_i and a reversible contribution p_r, where the latter is often neglected. The distribution is normalized such that p_r constitutes the fraction f_r of the total distribution. The distribution is assumed independent of the intensive variables and is approximated by Lorentzian functions, described in detail in the appendix.

The variation of the external driving field $Z(t)$ will sweep out varying sections of the (g_u, g_c)-plane (Fig. 2) and define the history dependent state transition line $b(g_c)$. The history dependent FM phase fraction of the material is

$$X(H, T, b) = \int_0^\infty dg_c \int_{-\infty}^{b(g_c)} p(g_u, g_c)dg_u\,. \tag{3}$$

The resulting magnetization M and entropy s can be calculated from Eq. (3),

$$M = (1 - X)M_0 + XM_1 \tag{4}$$
$$s = (1 - X)s_0 + Xs_1\,, \tag{5}$$

where $M_{x=\{0,1\}}$ and $s_{x=\{0,1\}}$ are the pure phase material properties, which are obtained from experimental data.

B. Parameter estimation through experimental measurements

The estimation of model parameters is based on a series of isofield magnetization measurements, opposed to commonly used isothermal measurements, carried out on a Lakeshore 7407 vibrating sample magnetometer. The $Gd_5Si_2Ge_2$ sample is a solid rectangular piece of about 60 mg, provided by Ames Laboratory[10].

The magnetization was measured in consecutive heating and cooling modes in the temperature range 230-310 K under constant applied magnetic fields of $\mu_0 H = \{0.05, 0.10, 0.25, 0.50, 0.75, 1.00, 1.20, 1.40, 1.60\}$ T. The measurements were initiated at 230 K and done step-wise with a resolution of 1 K in the neighborhood of the phase transition, located around 270 K. The temperature PID control was carefully programmed to vary the temperature monotonically between consecutive set points in order to avoid any temperature overshooting, which would

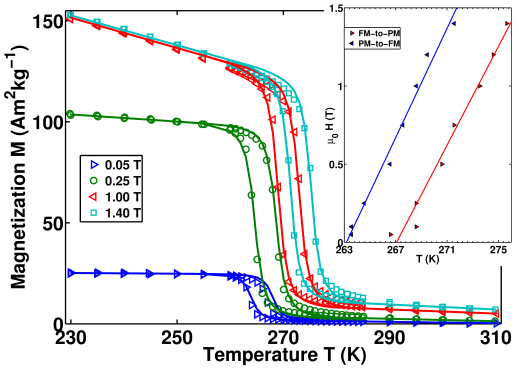

FIG. 3. Selection of isofield magnetization data shown for the magnetic field 0.05, 0.25, 1.00 and 1.40 T, as symbols. Solid lines show the Preisach model simulation of the experiment. (Inset) The estimated phase transition temperatures for each field, defined as the points of inflection on the magnetization curves.

cause a systematic underestimation of the hysteresis. A selection of these results (to avoid excessive overlapping) is shown in Fig. 3. The inset figure shows the approximated transition temperatures (defined as the point of inflection on the magnetization curves) for all the magnetic fields. The thermal hysteresis is nearly constant at 4 K across this field range and the transition temperature is shifted about $\delta T_p/\delta H_c \approx 6$ K/T as the magnetic field increases.

The temperature ranges 230-255 K and 290-310 K, where no hysteresis is present, characterize the pure phase behavior of the FM and PM states, respectively. This data is used to determine M_x, which is approximated as linear in temperature, with non-linear field dependent parameters (see the appendix)

$$M_x(H,T) = \left.\frac{\delta M_x}{\delta T}\right|_H (H)\,(T - T_{0,x}) + M_{0,x}(H)\,. \quad (6)$$

The Preisach distribution is determined by the characteristics of the transition in the intermediate temperature range. This is done in several steps in order to obtain meaningful parameters that do not suffer from unnecessary correlation. Firstly, the completely reversible contribution is determined from the cooling curves. These represent, to some extent, the anhysteretic magnetization curves, assuming the material is close to the global energy minimum at 310 K. Secondly, the irreversible parameters are determined from the full data set, having locked the reversible component.

Characterizing the magnetization by crossing both the FM and PM transition lines fully (inset of Fig. 3) will illustrate the full hysteresis of the material. However, this is not necessarily representative of realistic application scenarios where the available magnetic field is insufficient to force a complete transition. The material behavior under partial transitions can be visualized by first order reversal curves. Such curves are here measured in an applied magnetic field of 1.6 T. The measurements were carried out as described above, but instead of scanning the full temperature range, a set of reversal point temperatures T_r were chosen, resulting in temperature scanning profiles of the form $230\,\mathrm{K} \xrightarrow{\text{heating}} T_r \xrightarrow{\text{cooling}} 230\,\mathrm{K}$. The results are shown in Fig. 4.

These curves represent more appropriate material behavior under application conditions and also partly lift the degeneracy of the correlated distribution parameters. Combining all the available data, the final parameters are determined with minimal correlation. The experiments are modelled by using the experimental temperature profiles and the results are shown as solid lines in both Fig. 3 and 4. The influence of temperature and magnetic field on the magnetization is captured by the model across the entire measured range. More importantly, the partial transitions at 1.6 T are also well described by the model. Across the entire data set, the mean squared error between model and experiment is approximately 2 $\mathrm{Am^2kg^{-1}}$.

1. Pure phase entropy

The entropy of each phase s_x is governed by a magnetic contribution and a purely thermal component. The thermal contribution is determined by integration of the zero field heat capacity, which was measured utilizing a custom built differential scanning calorimeter[11]. The thermal contribution in each phase is found to be approximately linear in temperature, resulting in the total pure phase entropies

$$s_x(H,T) = \alpha_x(T - T_0) + \beta_x + \mu_0 \int_0^H \left.\frac{\partial M_x}{\partial T}\right|_{H'} dH'\,. \quad (7)$$

where T_0 is a chosen reference temperature. From this expression the pure phase free energies follow from $\partial g_x/\partial T = -s_x$, which is described in detail in the appendix.

III. RESULTS

The ΔT_{ad} of $Gd_5Si_2Ge_2$ was measured directly in order to compare with model predictions. The sample used for this experiment is from the same batch as was used for the magnetization measurements, on which the model is based. A type-E gauge bare-wire thermocouple was sandwiched between two separate sample pieces with a total mass of 90 mg, all held together by Arctic Silver thermal adhesive. The sample was placed in a vacuum chamber with $p < 10^{-5}$ mbar, which is low enough to eliminate convection and conduction in the surrounding air. The sample is in thermal contact with a brass cold-finger in order to mediate temperature control, though shielded by isolating material.

The setup is used to measure ΔT_{ad} values across a range of temperatures under AMR-like conditions, where the material undergoes a cycle of, i) magnetization from

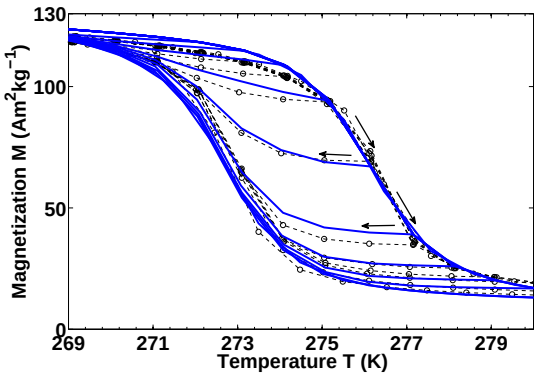

FIG. 4. First order reversal curves measured in an applied magnetic field of 1.6 T. Symbols represent the data and solid lines the model simulation of the experiment.

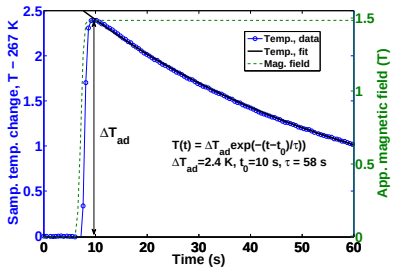

FIG. 5. Characteristic thermal response of the sample upon an applied magnetic field change of 1.5 T.

0 to 1.5 T at initial temperature T, ii) cooling back to T at constant field, iii) demagnetization from 1.5 T to 0 at initial temperature T, and iv) heating back to T in zero field.

A characteristic thermal response of the sample to a magnetic field change from 0 to 1.5 T, applied over approximately 2 s, is shown in Fig. 5. The sample response lags behind the magnetic field curve with about 1 s, which is attributed to the thermal resistance between the sample and the thermocouple. A standard exponential decay function fits the cooling curve and the characteristic sample cooling time is 58 s.

A. ΔT_{ad} in a continuous AMR cycle

Here we investigate the material behavior undergoing an ideal AMR cycle, as described above. The material is brought to the near transition temperature $T = 267$ K where the AMR-like cycle is run three consecutive times. The experiment is done in both a cooling and heating mode, where the sample is reset in the high temperature PM phase (by heating to 320 K) and the low temperature FM phase (by cooling to 230 K), respectively. The measured ΔT_{ad} values are listed in Table I, along with the corresponding model simulation of the experiments. When the sample is initiated in the PM state, an initially large ΔT_{ad} is measured during the first magnetization, whereafter it settles at a lower and constant value in the subsequent cycles. The demagnetization values remain constant during the three cycles. This is not observed when the sample is heated from the FM state. The ΔT_{ad} values are constant between all cycles, matching the stable values from the PM-reset experiment. This cyclic stabilization has been shown to exist in other first order magnetocaloric materials[12,13].

Both of these characteristics are qualitatively captured by the model. The discrepancy between the numerical ΔT_{ad} values is attributed to three factors. The non-perfect adiabatic conditions of the experiment are not accounted for in the model. From Fig. 5 the measured ΔT_{ad} values are expected to be underestimated, but only

TABLE I. Measured and modelled adiabatic temperature change during a triple magnetization cycle at 267 K with an applied magnetic field of 1.5 T, in both a heating and cooling mode. One cycle is given by i) magnetization (M), ii) thermal relaxation to 267 K, iii) demagnetization (DM), iv) thermal relaxation to 267 K, as illustrated in Fig. 6.

Cycle	Exp. ΔT_{ad} (K)		Model ΔT_{ad} (K)	
	Cooled to 267 K			
	M	DM	M	DM
1	4.5	-1.7	5.3	-1.6
2	2.3	-1.7	3.0	-1.6
3	2.3	-1.7	3.0	-1.6
	Heated to 267 K			
	M	DM	M	DM
1	2.4	-1.7	3.0	-1.6
2	2.4	-1.7	3.0	-1.6
3	2.4	-1.7	3.0	-1.6

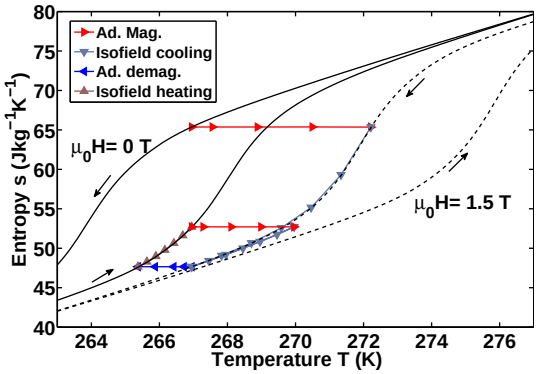

FIG. 6. Simulation of an AMR cycle initiated by cooling to 267 K from the PM state. The cycle is run three consecutive times with a field change of $\pm\mu_0 H = 1.5$ T. The cycle path (symbols) closes and settles after one cycle. The enveloping curves show the heating and cooling entropy curves at 0 and 1.5 T.

of the order 0.1 K. The more dominating factor arises from the applied simple Preisach distribution, which does not perfectly capture the hysteretic properties around the transition. Furthermore, the two different samples used for the model parameter estimation and the ΔT_{ad} experiments can result in different demagnetization effects within the samples.

The path taken by the material in the $(s,T)-$plane is illustrated through the model and shown in Fig. 6, where the direction is shown by the symbols. Superimposed on the figure are the complete isofield entropy heating and cooling curves one would obtain from heat capacity measurements at 0 and 1.5 T magnetic fields. The figure provides a qualitative interpretation of the data in Table I, namely that the material settles between the zero field heating and high field cooling entropy curves dur-

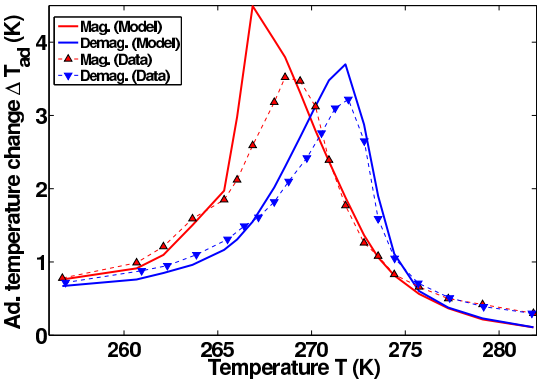

FIG. 7. Measured adiabatic temperature change in a cooling mode with an applied magnetic field of 1.5 T. Dashed line symbols represent the data and solid lines the simulation. Upward and downward symbols represent magnetization and demagnetization values, respectively.

ing continuous field cycling, regardless of its initial state. This behavior has been suggested in Ref.[13] and is also supported by Ref.[14], where estimating $\Delta T_{\rm ad}$ of first order material MnFe(P,As), from the zero field heating and high field cooling heat capacity curves approximately coincide with directly measured $\Delta T_{\rm ad}$ values.

A symmetric demagnetization experiment was carried out and simulated. Here the sample is reset in both the PM and FM states as previously described, but in an applied field of 1.5 T resulting in the cycling being initiated with a demagnetization step. In both cases an inverted behavior is observed. The initial demagnetization value of $\Delta T_{\rm ad}$ is high when the sample has been heated from the FM phase, whereafter it settles at a constant value. The $\Delta T_{\rm ad}$ values obtained from field cycling after the PM reset are constant and stable.

B. Direct $\Delta T_{\rm ad}$ measurements and model predictions

The temperature dependence of $\Delta T_{\rm ad}$ was measured during both magnetization and demagnetization in AMR-like conditions. This was accomplished by repeating the experiment described in the previous section for a range of temperatures. The experiment was done in a cooling mode, initiated at high temperature, where the system set point temperature is lowered after the AMR-cycle (As illustrated by the closed cycle in Fig. 6) has been run once at each temperature. The results are shown in Fig. 7. The maximum value is about 3.5 K at 1.5 T, which is in agreement with other direct measurements of $\Delta T_{\rm ad}$ in $Gd_5Si_2Ge_2$[15].

The experiment was simulated by using the experimentally measured temperature set points in the model and thus keeping the same temperature resolution between model and experiment. This is required to maintain a similar thermal history. The results are shown as solid lines in Fig. 7. The model captures the characteristic behavior of the material, but overestimates $\Delta T_{\rm ad}$ around the transition and underestimates it in both the high and low temperature range. The causes are the same as stated previously, namely a combination of i) non-perfect adiabatic conditions affecting primarily the larger $\Delta T_{\rm ad}$ values, ii) demagnetization field effects in the FM temperature range and iii) the simplicity of the Preisach distribution, which can affect the whole temperature range. It is noted that the magnetization curve is expected to be larger than the demagnetization curve, which is also seen experimentally. This is due to the non-monotonous temperature variations in the sample: as the sample is cooled to a new set point, the entropy state moves from the zero field heating curve to the zero field cooling curve. This reversal behavior is what the first order reversal curve measurements (Fig. 4) should describe, which is achieved qualitatively in the model but not quantitatively.

C. Correctly estimating the entropy change from indirect measurements

The general approach to characterizing the MCE is by obtaining the isothermal entropy change Δs indirectly. It is often deduced from magnetization curves, using the thermodynamic equilibrium Maxwell relation

$$\Delta s = \mu_0 \int_0^{H_f} \left.\frac{\partial M}{\partial T}\right|_H dH\,. \qquad (8)$$

This approach should be used with caution when applied to first order materials due to the non-equilibrium nature of the transition. Incorrect application of Eq. (8) can lead to spurious and artificially large Δs values[16]. The main concern is that the derivative of the magnetization is often not well defined since there is an internal variable of path dependence, which is generally not constant between magnetization curves. This is the case when measuring isothermal magnetization curves. Here the thermal and magnetic histories become completely convoluted between isotherms and the derivative is not well-defined. One can avoid this by thermally resetting the sample in the high temperature state between each magnetization measurement, as suggested in Ref.[16]. Then the magnetic history changes minimally between measurements, which is also the case when measuring the magnetization (or heat capacity) at constant field as done in this work. However, it is important to note that the Maxwell relation ignores the presence of hysteresis. As it is applied to either the set of isofield heating or cooling curves (or the magnetization or demagnetization curves in isothermal measurements) it effectively represents a reversible material.

Here a series of isothermal and isofield magnetization experiments are simulated by the Preisach model. Equation (8) is used to calculate Δs from the magnetization curves and these values are compared to the non-

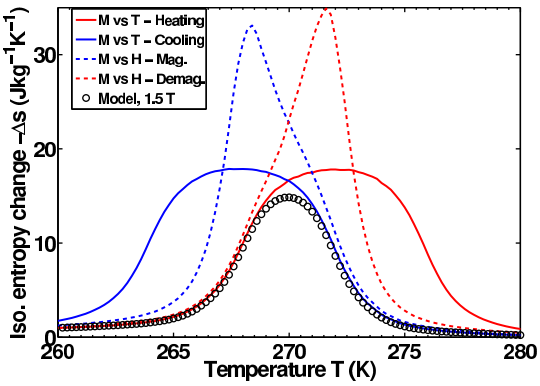

FIG. 8. Entropy change of $Gd_5Si_2Ge_2$ under an applied field change of 1.5 T by three different methods. Indirect calculations using the Maxwell relation are shown as lines, dashed and solid representing isothermal and isofield modes, respectively. The non-equilibrium values predicted by the model are shown as symbols.

equilibrium values predicted by the model. Figure 8 shows the four different curves representing Δs obtained from the simulated isothermal magnetization and demagnetization curves, the isofield magnetization heating and cooling curves and the model non-equilibrium predictions. The spurious peak effects from the isothermal calculations are noted. If the high temperature reset method is applied in the simulation, this effect completely disappears and the Δs values obtained from the isothermal magnetization curves become identical to those from the isofield cooling curves. The same holds for the isothermal demagnetization and isofield heating curves when the material is reset in the low temperature FM state under an applied field of 1.5 T. This suggests that the reset method should be used if the goal is to deduce the reversible Δs indirectly from the Maxwell relation. However, it is important to note that these estimates of Δs ignore any kind of hysteresis and are not obtainable in cyclic application conditions, as was demonstrated for $\Delta T_{\rm ad}$ in the previous section. This is taken into account by the Preisach model, which predicts that the realistically available Δs is bound by the minimum of the heating/cooling or magnetization/demagnetization(using the reset-methods) curves due to hysteresis.

IV. DISCUSSION

The results presented in this paper strongly suggest that in a cyclic application of hysteretic MCMs, the available $(s,T)-$space is bounded by the low field heating and high field cooling entropy curves. This result has several implications on inferring realistic MCM performance from indirect measurements. The Δs values obtained from the Maxwell relation represent either the $(s,T)-$space between the zero and high field heating or cooling curves. As our results suggest, only the overlapping area is realizable in an application scenario for a given magnetic field change, meaning that the available Δs^* is bounded by

$$\Delta s^* \leq \min\left(\Delta s^{\rm cool/mag}, \Delta s^{\rm heat/demag}\right). \qquad (9)$$

The equal sign will only apply in a situation where the magnetic field is large enough to traverse the temperature range over which the transition occurs *and* the thermal hysteresis gap. In the case of $Gd_5Si_2Ge_2$ a field of approximately 3.2 T would be needed to push across the transition (15 K) and the thermal hysteresis (4 K).

The $(s,T)-$space bound by the zero field heating and cooling curves will in practice be unavailable in any AMR-type cycle where the magnetization step follows a heating step, as the material will be on the zero field heating curve. However, the $(s,T)-$space bound by the high field heating and cooling curves is obtainable by increasing the magnetic field. Another way of stating this is that the Δs values calculated from the heating/demagnetization curves do not represent the MCE at the actually applied field H, but a higher field H^*. The field needs to be increased by an amount corresponding to the transition temperature being shifted by the thermal hysteresis,

$$H^* \approx H + \frac{\delta H_c}{\delta T_p}\Delta T_{\rm hyst}\,. \qquad (10)$$

In this case, a magnetic field of 2.2 T would be needed to practically realize the Δs values obtained at 1.5 T using the Maxwell relation on heating/demagnetization curves.

Considering a total cooling capacity, here defined as the integral of $\Delta s(T)$, the curves obtained from Eq. (8) overestimate the value by 77%, compared to the model predictions. As the magnetic field is increased, the relative overestimate will decrease and the hysteresis effects will not be as significant. However, for smaller magnetic fields in the permanent magnet range, the corrections lead to severe performance reductions.

V. CONCLUSION

We have provided a detailed non-equilibrium Preisach-type model that is able to reproduce both magnetization and directly measured $\Delta T_{\rm ad}$ data obtained from $Gd_5Si_2Ge_2$. The model predicts that the available $(s,T)-$space is limited by the zero field heating and the high field cooling entropy curves under AMR-like conditions. The maximum value of $\Delta T_{\rm ad}$ and the width of the Δs curve are by that effectively reduced by the thermal hysteresis, compared to an otherwise equivalent reversible material. It is demonstrated that Δs can be realistically estimated by only considering the minimum of the Δs values obtained from the Maxwell relation, when applied to isofield heating and cooling data or isothermal magnetization and demagnetization data.

VI. ACKNOWLEDGEMENTS

We would like to thank Copenhagen Cleantech Cluster for sponsoring part of this project and profs. K.A. Gschneidner Jr. and V. Pecharsky at Ames Laboratory for providing the sample.

Appendix: Model parameters

The Preisach distribution is modelled by Lorentzian functions

$$p(g_u, g_c) \propto \frac{1-f_r}{\left[1+\left(\frac{g_u}{\sigma_u}\right)^2\right]\cdot\left[1+\left(\frac{g_c-g_{c,0}}{\sigma_c}\right)^2\right]} + \quad \text{(A.1)}$$

$$\delta(g_c)\frac{f_r}{1+\left(\frac{g_u}{\sigma_{u,r}}\right)^2} \quad \text{(A.2)}$$

which provide a longer tail compared to often used Gaussian functions. This fit well with the experimental data, which shows the transition and the hysteretic behavior spans a wide temperature range of roughly 15 K. The reversible fraction f_r is found to be about 6%, and the remaining Preisach distribution parameters, all in units of Jkg^{-1}, are fitted to $\sigma_{u,r} = 9.1$, $\sigma_u = 6.9$, $\sigma_c = 4.2$, $g_{0,c} = 19.2$.

In the following the applied magnetic field is denoted $h = \mu_0 H$ and given in units of tesla to avoid cluttering. The pure phase magnetization M_x, with $x = \{0, 1\}$ respectively representing the PM and FM phases, are approximated with a linear temperature dependence as

$$M_x(h,T) = \left.\frac{\delta M_x}{\delta T}\right|_h (T - T_{0,x}) + M_{0,x} \quad \text{(A.3)}$$

with a field dependent reference magnetization $M_{0,x}$ at temperature $T_{0,x}$ given by

$$M_{0,1}(h) = M_s \tanh(\gamma\, h) + \chi_1\, h \quad \text{and} \quad \text{(A.4)}$$

$$M_{0,0}(h) = \chi_0\, h\,, \quad \text{(A.5)}$$

The magnetization gradients with respect to temperature are modelled by the following smoothly connected linear functions

$$\frac{\delta M_x}{\delta T} = \frac{1}{2}\left[1 - \tanh\left(\frac{h - H_{0,x}}{w_x}\right)\right](a_{1,x}\, h) + \frac{1}{2}\left[1 + \tanh\left(\frac{h - H_{0,x}}{w_x}\right)\right](a_{2,x}\, h + b_{2,x}) \quad \text{(A.6)}$$

All parameters are fitted from the magnetization data, part of which is shown in in Fig. 3, and have the following values: $T_{0,1} = 230$ K, $M_s = 150$ $\mathrm{Am^2kg^{-1}}$, $\gamma = 3.4$ $\mathrm{T^{-1}}$, $\chi_1 = 2.1$ $\mathrm{Am^2kg^{-1}T^{-1}}$, $T_{0,0} = 310$ K, $\chi_0 = 5.1$ $\mathrm{Am^2kg^{-1}T^{-1}}$, $a_{1,1} = -0.17$ $\mathrm{Am^2kg^{-1}K^{-1}T^{-1}}$, $a_{2,1} = 0.029$ $\mathrm{Am^2kg^{-1}K^{-1}T^{-1}}$, $b_{2,1} = -0.78$ $\mathrm{Am^2kg^{-1}K^{-1}}$, $w_1 = 0.14$ T, $H_{0,1} = 0.35$ T, $a_{1,0} = -0.30$ $\mathrm{Am^2kg^{-1}K^{-1}T^{-1}}$, $a_{2,0} = -0.056$ $\mathrm{Am^2kg^{-1}K^{-1}T^{-1}}$, $b_{2,0} = -0.045$ $\mathrm{Am^2kg^{-1}K^{-1}}$, $w_0 = 0.20$ T, $H_{0,0} = 0$ T.

The pure phase entropies are assumed to consist of a thermal and a magnetic contribution,

$$s_x(H,T) = \alpha_x(T - T_0) + \beta_x + \mu_0 \int_0^H \left.\frac{dM_x}{dT}\right|_{H'} dH'. \quad \text{(A.7)}$$

In the FM phase the thermal contribution is based on the measured heat capacity, which is around $\bar{c} \sim 300$ $\mathrm{Jkg^{-1}K^{-1}}$ away from the transition. This leads to the entropy being approximately linear in temperature with $T_0 = 230$ K , $\alpha \approx \bar{c}/T_0 = 1.3$ $\mathrm{Jkg^{-1}K^{-2}}$ and $\beta_1 = 0$. The thermal component in the PM phase is assumed identical, but shifted by the entropy change of the transition $\beta_0 \approx L/T_0 = -18$ $\mathrm{Jkg^{-1}K^{-1}}$, L being the measured heat of the transformation. From these expressions the free energy follows through $\partial g_x/\partial T = -s_x$ along with Z. The temperature dependent part is here linearized around the material transition temperature $T_p = 270$ K,

$$Z(H,T) = \frac{1}{2}\left(\beta_0(T - T_p) + \epsilon + \mu_0 \int_0^H (M_0 - M_1) dH'\right). \quad \text{(A.8)}$$

with $\epsilon = -75$ $\mathrm{Jkg^{-1}K^{-1}}$.

[1] Pecharsky VK, Gschneidner KA. Giant magnetocaloric effect in $Gd_5(Si_2Ge_2)$. Physical Review Letters. 1997;78(23):4494–4497.

[2] Krenke T, Duman E, Acet M, Wassermann EF, Moya X, Maosa L, et al. Inverse magnetocaloric effect in ferromagnetic NiMnSn alloys. Nature Materials. 2005;4:450–454.

[3] Tegus O, Brück E, Buschow KHJ, de Boer FR. Transition-metal-based magnetic refrigerants for room-temperature applications. Nature. 2002;415:150–152.

[4] Basso V, Sasso CP, Bertotti G, LoBue M, Morellon L, Magen C. Predictions of AMR refrigeration cycles on Gd-Si-Ge alloys. Refrigeration Science and technology proceedings. 2007;p. 35593566.

[5] Basso V, Küpferling M, Sasso CP, Giudici L. A Peltier cell calorimeter for the direct measurement of the isothermal entropy change in magnetic materials. Review of Scientific Instruments. 2008;79(6):–. Available from: `http://scitation.aip.org/content/aip/journal/rsi/79/6/10.1063/1.2940218`.

[6] Bjørk R, Bahl CRH, Smith A, Pryds N. Comparison of adjustable permanent magnetic field sources. Journal of Magnetism and Magnetic Materials. 2010;322.

[7] Basso V, LoBue M, Sasso CP, Bertotti G. Thermodynamic aspects of magnetic-field-driven phase transformations in Gd-Si-Ge alloys. Journal of Applied Physics. 2006;99(8).

[8] Basso V, Sasso CP, LoBue M. Thermodynamic aspects of first-order phase transformations with hysteresis in magnetic materials. Journal of Magnetism and Magnetic Materials. 2007;316(2):262 – 268. Available from: `http://www.sciencedirect.com/science/article/pii/S0304885307005264`.

[9] von Moos L, Bahl CRH, Nielsen KK, Engelbrecht K, Küpferling M, Basso V. A Preisach approach to modeling partial phase transitions in the first order magnetocaloric material MnFe(P,As). Physica B: Condensed Matter. 2014;435(0):144 – 147. Available from: `http://www.sciencedirect.com/science/article/pii/S0921452613006054`.

[10] Pecharsky AO, Gschneidner KA, Pecharsky VK. The giant magnetocaloric effect of optimally prepared $Gd_5Si_2Ge_2$. Journal of Applied Physics. 2003;93:4722–4728.

[11] Jeppesen S, Linderoth S, Pryds N, Kuhn LT, Jensen JB. Indirect measurement of the magnetocaloric effect using a novel differential scanning calorimeter with magnetic field. Review of Scientific Instruments. 2008;79(8):–. Available from: `http://scitation.aip.org/content/aip/journal/rsi/79/8/10.1063/1.2957611`.

[12]Liu J, Gottschall T, Skokov KP, Moore JD, Gutfleisch O. Giant magnetocaloric effect driven by structural transitions. Nature Materials. 2012;11:620626.

[13]Skokov KP, Müller KH, Moore JD, Liu J, Karpenkov AY, Krautz M, et al. Influence of thermal hysteresis and field cycling on the magnetocaloric effect in $LaFe_{11.6}Si_{1.4}$. Journal of Alloys and Compounds. 2013;552(0):310 – 317. Available from: http://www.sciencedirect.com/science/article/pii/S0925838812017586.

[14]Engelbrecht K, Nielsen KK, Bahl CRH, Carroll CP, van Asten D. Material properties and modeling characteristics for $MnFeP_{1x}As_x$ materials for application in magnetic refrigeration. Journal of Applied Physics. 2013;113(17):–. Available from: http://scitation.aip.org/content/aip/journal/jap/113/17/10.1063/1.4803495.

[15]Giguère A, Foldeaki M, Ravi Gopal B, Chahine R, Bose TK, Frydman A, et al. Direct Measurement of the "Giant" Adiabatic Temperature Change in $Gd_5Si_2Ge_2$. Phys Rev Lett. 1999 Sep;83:2262–2265. Available from: http://link.aps.org/doi/10.1103/PhysRevLett.83.2262.

[16]Caron L, Ou ZQ, Nguyen TT, Thanh DTC, Tegus O, Brück E. On the determination of the magnetic entropy change in materials with first-order transitions. Journal of Magnetism and Magnetic Materials. 2009;321(21):3559 – 3566. Available from: http://www.sciencedirect.com/science/article/pii/S0304885309006787.

Appendix D

Quantification of the effect of hysteresis on the magnetocaloric effect in first order $Gd_5Si_2Ge_2$

6th IIF-IIR International Conference on Magnetic Refrigeration
Victoria, BC, 7-10 September 2014

QUANTIFICATION OF THE EFFECT OF HYSTERESIS ON THE MAGNETOCALORIC EFFECT IN FIRST ORDER $Gd_5Si_2Ge_2$

L. von Moos, C.R.H. Bahl, K.K. Nielsen, K. Engelbrect
Department of Energy Conversion and Storage, Technical University of Denmark
Roskilde, Denmark, lmoo@dtu.dk, chrb@dtu.dk, kaki@dtu.dk, kuen@dtu.dk

ABSTRACT — We quantify the effect of hysteresis on the performance of the magnetocaloric first order material $Gd_5Si_2Ge_2$ undergoing an ideal active magnetic regenerator (AMR) cycle. The material is carefully characterized through magnetometry (VSM) and calorimetry (DSC) in order to enable an accurate model description of the phase transition at varying magnetic fields and temperatures. Using detailed experimental property data, a Preisach type model is used to describe the thermal hysteresis effects and simulate the material under realistic working conditions. We find that the magnetocaloric effect is limited by a significant fraction of the thermal hysteresis.

1. INTRODUCTION

Magnetocaloric first order materials have a coupled magnetic and structural transition, giving rise to both magnetic and thermal hysteresis in the characteristic material properties, i.e. magnetization and heat capacity. Hysteresis causes some degree of entropy production in each cycle, but more importantly also makes the material properties history dependent and thus non-single valued functions of both magnetic field and temperature. This makes determination of the adiabatic temperature change (ΔT_{ad}) non-trivial. In order to account for the material history dependence we employ a non-equilibrium Preisach-type model.

2. METHODS

Experimental characterization of $Gd_5Si_2Ge_2$

The material used for this work is the first order magnetocaloric material $Gd_5Si_2Ge_2$. The sample is a solid rectangular piece of about 60 mg, provided by Ames Laboratory [1].

The data to be modelled was obtained through isothermal magnetization measurements. Each isotherm was obtained by the standard procedure of starting at the lowest temperature (250 K) and measuring magnetization and demagnetization curves with a maximum applied field of $\mu_0 H = 1.6$ T. The temperature is varied by chosen steps (1 K around the transition) and the procedure is repeated until the maximum temperature is reached (300 K). A selection of the measured isotherms is shown in Fig. 1 (symbols). Measurements were performed with a careful temperature control and a low field ramp rate of 0.05 T/min, in order to avoid temperature overshooting and the MCE affecting the measurements, which was unfortunately not achieved, as seen at $T = 272$ K.

Furthermore, the sample was characterized by a zero field DSC scan from 240 K – 310 K to obtain a baseline for the heat capacity (and entropy) in the model. The heat capacity is approximately constant, $c_p \approx 300$ J/kg/K, away from the phase transition.

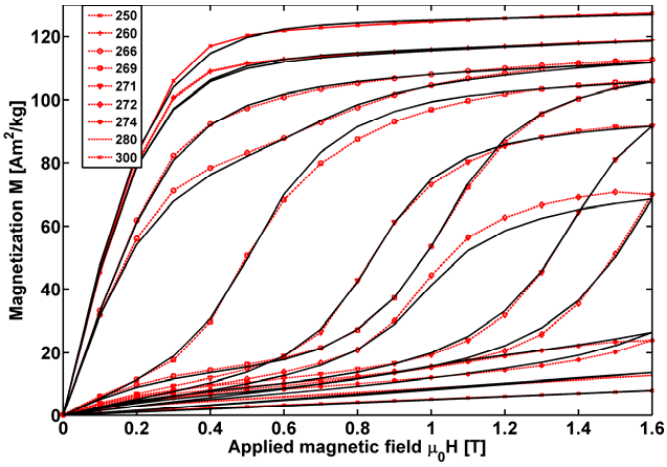

Fig. 1. Isothermal magnetization measurements on $Gd_5Si_2Ge_2$ (dashed symbols) and the corresponding Preisach model simulations (solid lines).

The Preisach model

A Preisach-type model is employed to describe the out-of-equilibrium aspects of the first order material. The Preisach approach to magnetic modelling utilizes a superposition of hysteretic bistable units, each characterized by two fields, switching the unit state between the purely ferromagnetic (FM) and paramagnetic (PM) phases. A detailed description of the applied Preisach model can be found in [1, 2]. In short, the magnetization M and entropy s are given as

$$M(H,T) = X \cdot M_{fm}(H,T) + (1-X) \cdot M_{pm}(H,T), \qquad s(H,T) = X \cdot s_{fm}(H,T) + (1-X) \cdot s_{pm}(H,T), \qquad (1)$$

where the path dependent ferromagnetic phase fraction, X, is the main output of the Preisach model. The pure phase magnetization behavior, $M_{fm/pm}$, is approximated from the non-hysteretic low and high temperature magnetization data (Fig. 1). The field independent part of the pure phase entropy, $s_{fm/pm}$, is obtained from the DSC data and the magnetic contribution calculated from $M_{fm/pm}$. The solid lines in Fig. 1 show the Preisach simulation of the magnetization experiment. The material behavior is well captured across the temperature range, including the partial transformations around 271 K.

3. RESULTS

The Preisach model is applied to investigate the material behavior in an ideal AMR-cycle: adiabatic magnetization at $T_i \rightarrow$ isofield cooling back to $T_i \rightarrow$ adiabatic demagnetization at $T_i \rightarrow$ isofield heating back to T_i. The hysteretic path dependence is taken into account, but the entropy production is ignored.

An example of such a cycle is shown in Fig. 2(inset), where the path is denoted by the triangular markers. Starting at 267 K, the magnetization from 0 – 1.6 T results in ΔT_{ad} = 4.4 K. The enveloping entropy curves show the full transition from the pure FM to PM state and back, by scanning temperature, in an applied magnetic field of 0 and 1.6 T. It is noted that the maximum hysteresis loss during a magnetization cycle is about 50 J/kg (maximum (*M*,*H*)-loop area in Fig. 1), resulting in an approximate temperature increase of 0.1 K during a half cycle, making it a small correction ΔT_{ad}.

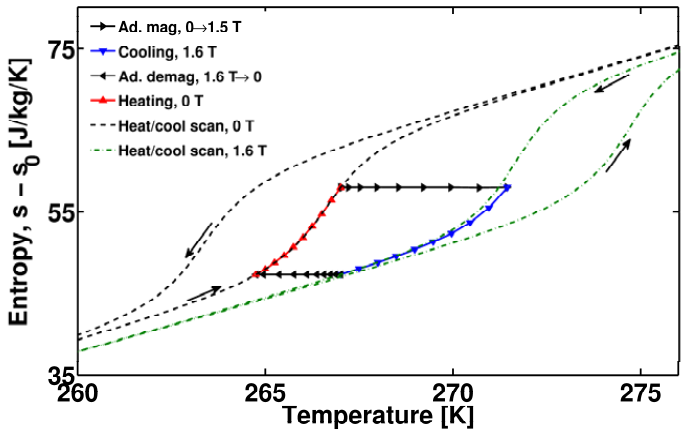

Fig. 2. A simulation of an ideal AMR-like cycle at 267 K, with max field of 1.6 T.

The available *s*-*T* space is limited by the thermal hysteresis regions and thus bound by the zero field heating and high field cooling curves. This should be compared to the *s*-*T* spaces obtained indirectly through the often used Maxwell relation, which are given by the areas enclosed by the zero and high field cooling-cooling or heating-heating curves, when applied to the isothermal magnetization or demagnetization curves, respectively.

4. CONCLUSION

These results show that the *s*-*T* space available under realistic application conditions is limited by if the thermal hysteresis and is bound by the zero field heating and high field cooling entropy curves.

We would like to thank profs. Gschneidner and Pecharsky for supplying the sample and the Copenhagen Cleantech Cluster for funding part of this project.

REFERENCES

[1] A.O. Pecharsky, K.A. Gschneidner, V.K. Pecharsky, "The giant magnetocaloric effect of optimally prepared $Gd_5Si_2Ge_2$", J. Appl. Phys, Vol. 93, 2003

[2] L. von Moos, C.R.H. Bahl, K.K. Nielsen, K. Engelbrecht, M. Küpferling, V. Basso, "A Preisach approach to modeling partial phase transitions in the first order magnetocaloric material MnFe(P,As)", Physica B: Condensed Matter, Volume 435, 2013

[3] V. Basso, C.P. Sasso, G. Bertotti, M . Lobue, L Morellon, C. Magen, "Predictions of AMR refrigeration cycles on Gd-Si-Ge alloys", IRR/IFF, 2007

Appendix E

Direct measurements of the magnetocaloric effect

6th IIF-IIR International Conference on Magnetic Refrigeration
Victoria, BC, 7-10 September 2014

DIRECT MEASUREMENTS OF THE MAGNETOCALORIC EFFECT

K.K. Nielsen, C.R.H. Bahl, H.N. Bez, R. Bjørk, L. von Moos, D. Eriksen
Technical University of Denmark, DTU Energy Conversion and Storage, kaki@dtu.dk

ABSTRACT — We present an experimental setup recently developed at DTU Energy Conversion for measuring specific heat and direct isothermal entropy change in a varying magnetic field (DSC device) using calorimetry. The device operates in high vacuum (~1e-6 mbar) and measurements are fully automated with respect to magnetic field and temperature control. A magnetic field source comprised of two concentric Halbach type magnets that are fixed with respect to each other through a mechanical gear supply the applied magnetic field. The applied field range is 0.001 to 1.57 T with a minimum field step size smaller than 0.01 T. The magnet control is fully integrated in software allowing measurement scans to be automated. This device is an upgrade of an existing device where it is now possible to install a sample and then run temperature scans at different magnetic fields (specific heat measurement) as well as magnetic field scans under isothermal conditions (direct isothermal entropy change measurements).

1. INTRODUCTION

The specific heat of magnetocaloric materials is of crucial importance for characterization, evaluation and generation of property data sets applied in active magnetic regenerator (AMR) models. Having specific heat data as a function of temperature and constant applied magnetic field it is possible to generate entropy curves of a material. This enables the calculation of the magnetocaloric properties, i.e. isothermal entropy change and adiabatic temperature change. Furthermore, in hysteretic materials, heating and cooling specific heat curves are very important for proper handling of the hysteresis in a magnetocaloric context [1].

Differential scanning calorimetry (DSC) is an established technique for measuring specific heat. However, measurements under applied field typically demand custom-built devices [2],[3],[4]. The custom DSC with magnetic field at DTU has been upgraded so it is fully automatic and also a mode for measuring the isothermal entropy change, ΔS, has been added. In the following we present the details and the first isothermal entropy change measurements.

2. EXPERIMENTAL

The DSC principle relies on two heat flux sensors that are, in principle, identical. These are intimately connected to a thermal reservoir and through this a constant temperature ramp rate may be applied. Placing a sample on one of the heat flux sensors and measuring the difference between the two sensors essentially provides the heat flux through the sample. In practice, we apply Peltier cells where the voltage measured across the cell is proportional to the heat flux through the cell. The key hardware specifics are given in Table I and a schematic of the device is given in Fig. 1.

TABLE I. SPECIFICATIONS OF THE DEVICE. THE THERMAL RESISTANCE IS DERIVED FROM SPECIFICATIONS FROM THE MANUFACTURER.

Hardware	Specification
Heat flux sensors	3.25x4.88 mm Peltier elements OT08,11,F1,0305,11,W2.25, Optotec Thermal resistance approx. 130 K/W
Hall probe	2.5x4x1 mm Arepoc HHP-NU
Temperature measurement	PT-100 elements
Atmosphere	High vacuum (~10^{-6} mbar)
Temperature	-40 to +55 °C
Magnetic field range	0.001 to 1.57 T

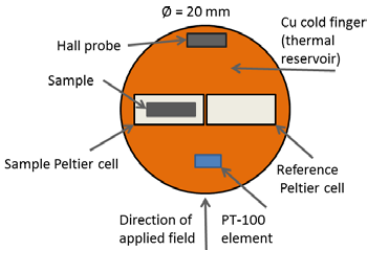

Fig. 1. Schematic of the top of the DSC/direct ΔS measurement device.

In any DSC system there will be instrumental hysteresis induced by the lag in temperature between the sample and the thermal reservoir, which in turn is caused by the finite heat transfer across the Peltier cell. Separation of the heating and cooling curves is therefore a (nearly linear) function of temperature ramp rate. This has been calibrated by measuring a standard Ga sample with a melting point at 29.76 °C at different ramp rates and extrapolating to zero ramp rate. We find that at a ramp rate of 1K/min the separation of the curves due to temperature lag is of the order 1 K (device hysteresis). The temperature measurements are corrected for the device hysteresis. Any splitting in peak temperature after this correction is interpreted as intrinsic material hysteresis. In order to convert the measured differential voltage signal to heat flux (and thus either specific heat or entropy change depending on the experiment mode) we use 99.999 wt.% pure Cu as a reference.

The magnetic field source consists of two concentric Halbach-type magnets with the field concentrated in a central axial bore [4]. The magnets are mechanically connected with a gear so that they counter-rotate with exactly the same angular frequency. The direction of the applied field is thus constant while the field magnitude is varied from 0.001 to 1.57 T.

3. Conclusion

The direct measurement of the isothermal entropy change of a sample of $La_{0.67}Ca_{0.33}MnO_3$ is shown in Fig. 2 and compared to entropy data based on magnetization measured in a vibrating sample magnetometer (VSM), i.e. relying on the Maxwell relation. From these first results it is apparent that the two methods are in agreement. Specific heat measurements show an intrinsic thermal hysteresis of 0.7 K, as discussed in [6].

Our custom made DSC was presented in terms of the recently implemented upgrades. The first results presented show that the method applied to measure direct ΔS gives results comparable to those obtained via magnetometry. The advantage of this approach is twofold: i) The same sample may be mounted and specific heat and isothermal entropy change found in one series of experiments and ii) any measurement issues related to the indirect method of using magnetometry may be circumvented by the direct calorimetric method. The latter advantage may prove to be of great importance when studying, e.g., hysteretic effects in magnetocaloric materials especially with a 1st order transition.

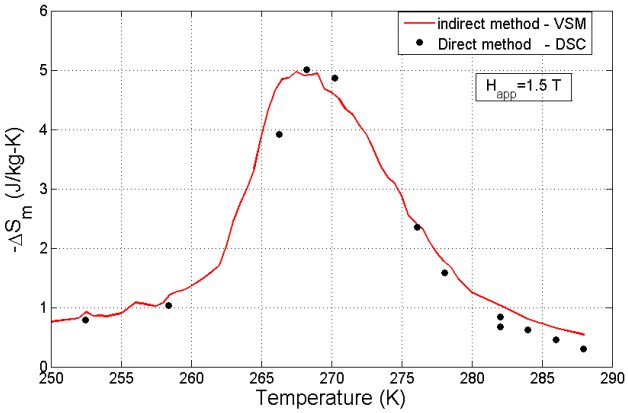

Fig. 2. Direct ΔS measurements (symbols) and indirect measurements from magnetization measurements on a sample of $La_{0.67}Ca_{0.33}MnO_3$. Details about the sample may be found in Ref. [5].

References

[1] L. von Moos, C.R.H. Bahl, K.K. Nielsen, K. Engelbrecht, "Quantification of the effect of hysteresis on the adiabatic temperature change in magnetocaloric materials", in proc. Thermag IV, 2014.

[2] S. Jeppesen, S. Linderoth, N. Pryds, L. Theil Kuhn, J. Buch Jensen, "Indirect measurements of the magnetocaloric effect using a novel differential scanning calorimeter with magnetic field", Rev. Sci. Instrum. 79, 083901, 2008.

[3] V. Basso, C.P. Sasso, M. Kuepferling, "A peltier cells differential calorimeter with kinetic correction for the measurement of cp(H,T) and deltaS(H,T) of magnetocaloric materials", 81, 113904, 2010.

[4] M. Kuepferling, C.P. Sasso, V. Basso, L. Giudici, "An isothermal Peltier cell Calorimeter for measuring the magnetocaloric effect", IEEE Trans. Magn., 43 (6), 2764-2766, 2007

[5] R. Bjørk, C.R.H. Bahl, A. Smith, N. Pryds, "Comparison of adjustable permanent magnetic field sources", J. Magn. Magn. Mater. 322, 3664-3671, 2010.

[6] H.N. Bez, K.K. Nielsen, A. Smith, C.R.H. Bahl, "Thermal hysteretic behavior of La-manganite", in proc. Thermag VI, 2014.

Appendix F

Delft Days 2013

Partial phase transitions in magnetocaloric material MnFe(P,As)

Lars von Moos[a], **Vittorio Basso**[b], **Michaela Küpferling**[b]

[a] *Department of Energy Conversion and Storage, Technical University of Denmark, Denmark*

[b] *Istituto Nazionale di Ricerca Metrologica, Italy*

Introduction

The field of magnetic refrigeration has grown a lot with the discovery of room temperature 1st order Magnetocaloric Materials (MCM), experiencing a large Magnetocaloric Effect (MCE). MCM are applied in Active Magnetic Regenerators (AMR), where they undergo thermodynamic cycles in order to heat or cool a system. This process has previously been modeled for 2nd order materials, but there is a general lack of detailed modeling of 1st order materials, where hysteresis is present [Nielsen et al.,2011].

We investigate how thermal hysteresis affects the heat capacity of the 1st order material MnFe(P,As) under partial phase transitions through Differential Scanning Calorimetry (DSC) and compare to a Preisach-type model.

Magnetocaloric materials and magnetic refrigeration

The magnetocaloric effect can be measured as the adiabatic temperature change in magnetic material when a magnetic field is applied. Under adiabatic conditions the total entropy remains constant and the decrease of magnetic entropy is balanced by an increase in lattice entropy and a temperature increase. See Smith et al., 2011 for a review.

$$\Delta T_{ad}(T,H) = -\int_{H_0}^{H_1} \frac{T}{c(T,H)}\left|\frac{\partial M(T,H)}{\partial T}\right|_H \Big|_H dH$$

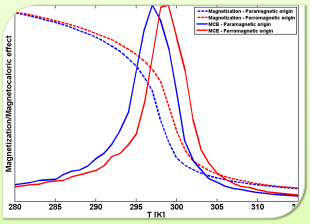

The magnetic refrigeration cycle

The MCE can be magnified by applying MCM in thermodynamic cycles, analogous to gas vapor-compression.

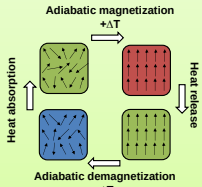

1st order materials

- Coupled structural and magnetic transition
- Large MCE! Wanted!
- Hysteresis… not wanted.

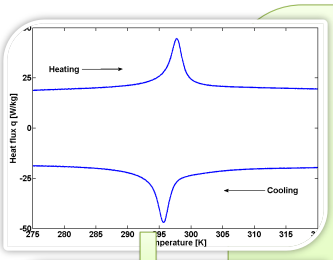

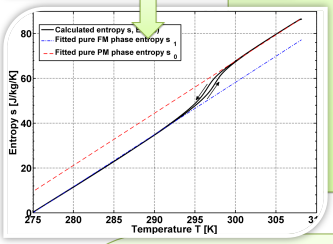

Material modeling

Setting the scale

The entropy is estimated through heat flux measurements,

$$s(T) = \frac{1}{m}\int_{T_0}^{T}\frac{1}{T'}\frac{q}{T'}dT' + s(T_0)$$

where the Gibbs free energy follows from

$$\frac{\partial g}{\partial T} = -s$$

The pure phase entropies are seen to be approximately linear

$s_0(T) = c_b(T - T_{min}),$ $\quad s_1(T) = s_0(T) + \delta s$

The right mix of hysteretic units

The Preisach distribution is assumed to have both a reversible and irreversible component

$$p_r(g_u,0) \propto \exp\left(-\frac{{g_u}^2}{2\sigma_u{}^2}\right)$$

$$p_i(g_u,g_c) \propto \frac{1}{1+\left(\frac{g_u}{\sigma_u}\right)^2}\frac{1}{1+\left(\frac{g_c - g_{c,0}}{\sigma_c}\right)^2}$$

with $g_{u,0}$, $g_{c,0}$, σ_u and σ_c being material fitting parameters.

MnFe(P,As)

- 1st order material with a hexagonal Fe_2P structure.
- Phase transition between the low temperature ferromagnetic state and the high temperature paramagnetic state.
- The phase transition is magnetoelastic: at the transition temperature the c/a ratio of the hexagonal unit cell changes while the volume basically does not change [Dũng, 2012].

The Preisach-model

MCM behavior is often described by a set of *M(T,H)* and *c(T,H)* measurements. However, the applicability of such measurements in models is not straightforward when hysteresis is present.

Here we apply a Preisach-type model that is appropriate to describe the out-of-equilibrium thermodynamic aspects of hysteresis [Basso et al., 2007].

Modeling hysteretic behavior

- A distribution, $p(g_u, g_c)$, of bistable hysteretic units, which can be either in phase 1 (ferromagnetic) or 0 (paramagnetic).
- Each unit is represented by parameters (g_u, g_c) which determine the critical phase switching fields

$$Z_\alpha = g_u - g_c\,, \qquad Z_\beta = g_u + g_c$$

- The difference in the Gibbs potential between phase 0 and 1 is the driving force in the transition

$$Z(T,H) = \frac{g_0(T,H) - g_1(T,H)}{2}$$

- History of *Z*-field determines the transition line $b(g_c)$, which gives the current ferromagnetic phase fraction

$$X_1 = \int_0^{+\infty} dg_c \int_{-\infty}^{b(g_c)} p(g_u,g_c)\,dg_u$$

- The phase fraction gives the relevant thermodynamic quantities of the mixed phase state, utilizing the pure phase material properties, e.g. entropy and heat flux

$$s = (1 - X_1)s_0 + X_1 s_1\,, \qquad q = T\frac{\partial T}{\partial t}\frac{\partial s}{\partial T}$$

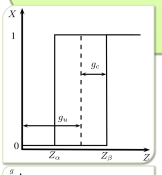

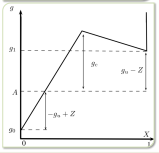

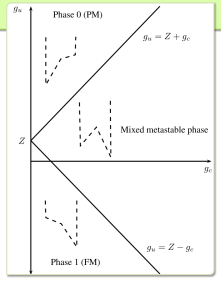

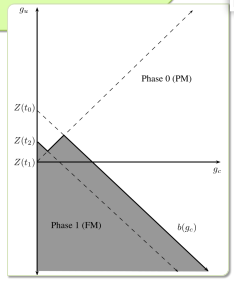

DSC measurements and model simulations

A 35 mg sample of MnFe(P,As) with T_C=296 K was measured with a commercial PerkinElmer Diamond DSC in 0 T magnetic field. The data is given as the heat flux *q* absorbed by the sample to maintain a constant temperature rate of ±2 K/min.

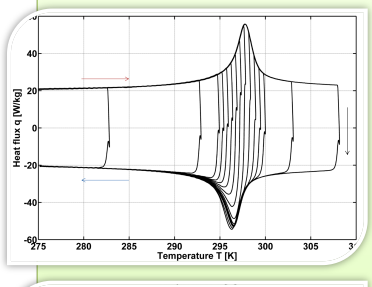

Measurements were performed with the sample originating in the FM phase. The sample was heated to a number of set temperatures, after which it was cooled again, resulting in partial phase transitions as shown in the figure.

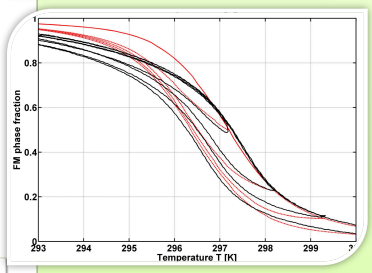

The experimental FM phase fraction is obtained from the data as

$$X_{est}(T) = \frac{s - s_0}{s_1 - s_0}$$

and is shown as the solid black curve.

The experimental procedure was simulated with the Preisach model and the calculated FM phase fraction X_1 is shown as the dashed red curve

Results

- Model simulations generally fit well with complete transitions curves
- Transition not completely symmetric
- Model predictions of partial transitions lack detail and overestimate hysteresis → more detailed Preisach distribution
- Experimental data on partial phase transitions is needed to realistically model 1st order materials and the effect of hysteresis in AMR cycles

Acknowledgements

BASF for providing the samples used in this work, INRIM for providing experimental equipment and expertise and Copenhagen Cleantech Cluster for financing part of this project.

References

K. K. Nielsen et al., Int. J. Refrig. 34 (2011).
A. Smith et al., Adv. Energy Mater. 2 (2012).
V. Basso et al., J. Magn. Magn. Mater. 316 (2007).
N. H. Dũng, PhD thesis, TU Delft (2012)

DTU Energy Conversion
Department of Energy Conversion and Storage

Appendix G

Pure phase parameters

Isofield pure phase magnetization is modelled by

$$M_x(H,T) = \left.\frac{\delta M_x}{\delta T}\right|_H (H)\,(T - T_{0,x}) + M_{0,x}(H)\,. \tag{G.1}$$

In the following the parameters to each material are shown. To avoid cluttering we define $h = \mu_0 H$.

High hysteresis MnFe(P,As)

Reference magnetization

$$M_{0,0}(h) = \chi_0 h \tag{G.2}$$

$$M_{0,1}(h) = M_s \tanh(\gamma h) + \chi_1\, h \tag{G.3}$$

Magnetization gradient with temperature

$$\left.\frac{\delta M_0}{\delta T}\right|_h (h) = A_0\, h \tag{G.4}$$

$$\left.\frac{\delta M_1}{\delta T}\right|_h (h) = A_1\big[1 - \exp(B_1\, h)\big] \tag{G.5}$$

Parameter	Value	Unit
α	2.3	$\mathrm{J/kg/K^2}$
δs	-11	J/kg/K
χ_0	9.8	$\mathrm{Am^2kg^{-1}T^{-1}}$
M_s	93.1	$\mathrm{Am^2kg^{-1}}$
γ	6.3	$\mathrm{T^{-1}}$
χ_1	6.7	$\mathrm{Am^2kg^{-1}T^{-1}}$
A_0	-0.4	$\mathrm{Am^2kg^{-1}K^{-1}T^{-1}}$
A_1	-0.6	$\mathrm{Am^2kg^{-1}K^{-1}}$
B_1	-13.2	$\mathrm{T^{-1}}$
ϵ	-11	J/kg
σ_u	10	J/kg
σ_c	4	J/kg
$g_{c,0}$	4	J/kg
f_r	-	-
$\sigma_{u,r}$	-	-

Table G.1: Model parameters describing the high hysteresis MnFe(P,As) material

Low hysteresis MnFe(P,As)

Field dependence of pure phase magnetization

$$M_0(h) = a_{1,0}h \,. M_1(h) = a_{1,1}\tanh(a_{2,1}h) + a_{3,1}h \tag{G.6}$$

with temperature dependent parameters, fitted by a 2. order polynomial

$$a_{i,x}(T) = A_{i,x}T^2 + B_{i,x}T + C_{i,x}\,. \tag{G.7}$$

Parameter	Value	Unit
α	2.0	J/kg/K^2
δs	-10.3	J/kg/K
$A_{1,0}$	$6.1{\cdot}10^{-3}$	
$B_{1,0}$	-4.1	
$C_{1,0}$	$6.9{\cdot}10^{2}$	
$A_{2,0}$	2.9	
$B_{2,0}$	$1.2{\cdot}10^{-2}$	
$A_{1,1}$	$-9.7{\cdot}10^{-3}$	
$B_{1,1}$	4.7	
$C_{1,1}$	$-4.8{\cdot}10^{2}$	
$A_{2,1}$	$-2.2{\cdot}10^{-4}$	
$B_{2,1}$	$1.3{\cdot}10^{-1}$	
$C_{2,1}$	$-1.3{\cdot}10^{1}$	
$A_{3,1}$	0	
$B_{3,1}$	$3.9{\cdot}10^{-2}$	
$C_{3,1}$	-4.5	
ϵ	-59.9	J/kg
σ_u	4	J/kg
σ_c	4	J/kg
$g_{c,0}$	-1	J/kg
f_r	0.73	-
$\sigma_{u,r}$	6.8	J/kg

$\mathbf{Gd_5Si_2Ge_2}$

Reference magnetization

$$M_{0,0}(H) = \chi_0\,\mu_0 H$$
$$M_{0,1}(H) = M_s\,\tanh(\gamma\,\mu_0 H) + \chi_1\,\mu_0 H$$

Magnetization gradient with temperature

$$\frac{\delta M_x}{\delta T} = \frac{1}{2}\left[1 - \tanh\left(\frac{h - H_x}{w_i}\right)\right](a_x\,h) + \frac{1}{2}\left[1 + \tanh\left(\frac{h - H_x}{w_x}\right)\right](b_x\,h + c_x) \tag{G.8}$$

Parameter	Value	Unit
α	1.3	J/kg/K^2
δs	18.6	J/kg/K
H_0	0	
w_0	0.20	
a_0	-0.30	
b_0	-0.056	
c_0	-0.045	
χ_0	5.05	
M_s	149.8	
γ	3.38	
χ_1	2.05	
H_1	0.35	
w_1	0.14	
a_1	-0.17	
b_1	0.029	
c_1	-0.78	
ϵ	-75.3	J/kg
σ_u	6.9	J/kg
σ_c	4.2	J/kg
$g_{c,0}$	19.2	J/kg
f_r	0.06	-
$\sigma_{u,r}$	9.1	J/kg

Bibliography

A. Aharoni. Demagnetizing factors for rectangular ferromagnetic prisms. *Journal of Applied Physics*, 83(6):3432–3434, 1998. URL http://scitation.aip.org/content/aip/journal/jap/83/6/10.1063/1.367113.

M. Bacmann, J.-L. Soubeyroux, R. Barrett, D. Fruchart, R. Zach, S. Niziol, and R. Fruchart. Magnetoelastic transition and antiferro-ferromagnetic ordering in the system $MnFeP_{1-y}As_y$. *Journal of Magnetism and Magnetic Materials*, 134(1):59 – 67, 1994. ISSN 0304-8853. URL http://www.sciencedirect.com/science/article/pii/0304885394900736.

C. Bahl, R. Bjørk, A. Smith, and K. Nielsen. Properties of magnetocaloric materials with a distribution of curie temperatures. *Journal of Magnetism and Magnetic Materials*, 324(4):564 – 568, 2012. ISSN 0304-8853. URL http://www.sciencedirect.com/science/article/pii/S0304885311006202.

C. R. H. Bahl, T. F. Petersen, N. Pryds, and A. Smith. A versatile magnetic refrigeration test device. *Review of Scientific Instruments*, 79(9):–, 2008. URL http://scitation.aip.org/content/aip/journal/rsi/79/9/10.1063/1.2981692.

J. Barclay and W. Steyert. Active magnetic regenerator, June 1 1982. URL http://www.google.com/patents/US4332135. US Patent 4,332,135.

V. Basso, G. Bertotti, M. LoBue, and C. Sasso. Theoretical approach to the magnetocaloric effect with hysteresis. *Journal of Magnetism and Magnetic Materials*, 290–291, Part 1(0):654 – 657, 2005. ISSN 0304-8853. URL http://www.sciencedirect.com/science/article/pii/S0304885304015549. Proceedings of the Joint European Magnetic Symposia (JEMS' 04).

V. Basso, M. LoBue, C. P. Sasso, and G. Bertotti. Thermodynamic aspects of magnetic-field-driven phase transformations in Gd-Si-Ge alloys. *Journal of Applied Physics*, 99(8):–, 2006a. URL http://scitation.aip.org/content/aip/journal/jap/99/8/10.1063/1.2163836.

V. Basso, C. P. Sasso, G. Bertotti, and M. LoBue. Effect of material hysteresis in magnetic refrigeration cycles. *International Journal of Refrigeration*, 29(8): 1358 – 1365, 2006b. ISSN 0140-7007. URL http://www.sciencedirect.com/science/article/pii/S0140700706001666. Magnetic Refrigeration at Room Temperature.

V. Basso, C. Sasso, G. Bertotti, M. LoBue, L. Morellon, and C. Magen. Predictions of AMR refrigeration cycles on Gd-Si-Ge alloys. *Refrigeration Science and technology proceedings*, 2007a.

V. Basso, C. P. Sasso, and M. LoBue. Thermodynamic aspects of first-order phase transformations with hysteresis in magnetic materials. *Journal of Magnetism and Magnetic Materials*, 316(2):262 – 268, 2007b. ISSN 0304-8853. URL http://www.sciencedirect.com/science/article/pii/S0304885307005264.

V. Basso, M. Küpferling, C. P. Sasso, and L. Giudici. A peltier cell calorimeter for the direct measurement of the isothermal entropy change in magnetic materials. *Review of Scientific Instruments*, 79(6):–, 2008a. URL http://scitation.aip.org/content/aip/journal/rsi/79/6/10.1063/1.2940218.

V. Basso, C. P. Küpferling, M. nd Sasso, and M. LoBue. Modeling hysteresis of first-order magneto-structural phase transformations. *IEEE Transactions on Magnetics*, 44(11):3177–3180, 2008b.

V. Basso, C. Sasso, G. Bertotti, and M. LoBue. Instabilities in adiabatic transformations of first-order phase transitions in a model with bistable units. *Physica B: Condensed Matter*, 403(2-3):312 – 315, 2008c. ISSN 0921-4526. URL http://www.sciencedirect.com/science/article/pii/S0921452607005789.

V. Basso, C. P. Sasso, and M. Küpferling. A peltier cells differential calorimeter with kinetic correction for the measurement of $c_p(H,T)$ and $\Delta s(H,T)$ of magnetocaloric materials. *Review of Scientific Instruments*, 81(11):–, 2010. URL http://scitation.aip.org/content/aip/journal/rsi/81/11/10.1063/1.3499253.

K. Belov, E. Talalaeva, L. Chernikova, A. Andreenko, and V. Ivanovskii. Observation of the magnetic compensation point in the spinel ferrites $MnFe_{2-x}Cr_xO_4$. *Sov. Phys. JETP.*, 39:316–318, 1974.

G. Bertotti. Energetic and thermodynamic aspects of hysteresis. *Phys. Rev. Lett.*, 76:1739–1742, 1996. URL http://link.aps.org/doi/10.1103/PhysRevLett.76.1739.

G. Bertotti. *Hysteresis in Magnetism - For Physicists, Materials Scientists, and Engineers*. Academic Press, 1998.

R. Bjørk, C. Bahl, A. Smith, and N. Pryds. Comparison of adjustable permanent magnetic field sources. *Journal of Magnetism and Magnetic Materials*, 322(22): 3664 – 3671, 2010a. ISSN 0304-8853. URL http://www.sciencedirect.com/science/article/pii/S0304885310004865.

R. Bjørk, C. R. H. Bahl, and M. Katter. Magnetocaloric properties of $LaFe_{13-x-y}Co_xSi_y$ and commercial grade Gd. *Journal of Magnetism and Magnetic Materials*, 322(24):3882 – 3888, 2010b. ISSN 0304-8853. URL http://www.sciencedirect.com/science/article/pii/S0304885310005391.

S. Blundell. *Magnetism in Condensed Matter*. Oxford University Press, 2001.

M. Bratko, K. Morrison, A. de Campos, S. Gama, L. F. Cohen, and K. G. Sandeman. History dependence of directly observed magnetocaloric effects in (Mn, Fe)As. *Applied Physics Letters*, 100(25):–, 2012. URL http://scitation.aip.org/content/aip/journal/apl/100/25/10.1063/1.4729893.

E. Brück, M. Ilyn, A. Tishin, and O. Tegus. Magnetocaloric effects in $MnFeP_{1-x}As_x$-based compounds. *Journal of Magnetism and Magnetic Materials*, 290–291, Part 1(0):8 – 13, 2005. ISSN 0304-8853. URL http://www.sciencedirect.com/science/article/pii/S0304885304013927. Proceedings of the Joint European Magnetic Symposia (JEMS' 04).

W. Brey, G. Nellis, and S. Klein. Thermodynamic modeling of magnetic hysteresis in AMRR cycles. *International Journal of Refrigeration*, 47:85–97, 2014. ISSN 0140-7007. URL http://www.sciencedirect.com/science/article/pii/S0140700714001911.

G. V. Brown. Magnetic heat pumping near room temperature. *Journal of Applied Physics*, 47(8):3673–3680, 1976. URL http://scitation.aip.org/content/aip/journal/jap/47/8/10.1063/1.323176.

L. Caron, Z. Q. Ou, T. T. Nguyen, D. T. C. Thanh, O. Tegus, and E. Brück. On the determination of the magnetic entropy change in materials with first-order transitions. *Journal of Magnetism and Magnetic Materials*, 321(21):3559 – 3566, 2009. ISSN 0304-8853. URL http://www.sciencedirect.com/science/article/pii/S0304885309006787.

S. Das, J. S. Amaral, and V. S. Amaral. Prediction of realistic entropy behavior from mixed state magnetization data for first order phase transition materials. *Journal of Applied Physics*, 107(9):–, 2010. URL http://scitation.aip.org/content/aip/journal/jap/107/9/10.1063/1.3356007.

N. H. Dung. *Moment formation and giant magnetocaloric effects in hexagonal Mn-Fe-P-Si compounds.* PhD thesis, Delft University of Technology, 2012.

M. D. Dyar, D. G. Agresti, M. W. Schaefer, C. A. Grant, and E. C. Sklute. Mössbauer spectroscopy of earth and planetary materials. *Annu. Rev. Earth Planet. Sci.*, 34:83–125, 2006.

K. Engelbrecht, K. K. Nielsen, C. R. H. Bahl, C. P. Carroll, and D. van Asten. Material properties and modeling characteristics for $MnFeP_{1-x}As_x$ materials for application in magnetic refrigeration. *Journal of Applied Physics*, 113(17): –, 2013. URL http://scitation.aip.org/content/aip/journal/jap/113/17/10.1063/1.4803495.

V. Franco, J. S. Blázquez, and A. Conde. Field dependence of the magnetocaloric effect in materials with a second order phase transition: A master curve for the magnetic entropy change. *Applied Physics Letters*, 89(22):–, 2006. URL http://scitation.aip.org/content/aip/journal/apl/89/22/10.1063/1.2399361.

A. Giguère, M. Foldeaki, B. Ravi Gopal, R. Chahine, T. K. Bose, A. Frydman, and J. A. Barclay. Direct measurement of the "giant" adiabatic temperature change in $Gd_5Si_2Ge_2$. *Phys. Rev. Lett.*, 83:2262–2265, Sep 1999. URL http://link.aps.org/doi/10.1103/PhysRevLett.83.2262.

K. Gschneidner Jr. and V. Pecharsky. Magnetocaloric materials. *Annu. Rev. Mater. Sci*, 30:387–429, 2000.

B. R. Hansen, C. R. H. Bahl, L. T. Kuhn, A. Smith, K. A. Gschneidner, and V. K. Pecharsky. Consequences of the magnetocaloric effect on magnetometry measurements. *Journal of Applied Physics*, 108(4):–, 2010. URL http://scitation.aip.org/content/aip/journal/jap/108/4/10.1063/1.3466977.

R. P. Hermann, O. Tegus, E. Brück, K. H. J. Buschow, F. R. de Boer, G. J. Long, and F. Grandjean. Mössbauer spectral study of the magnetocaloric $FeMnP_{1-x}As_x$ compounds. *Phys. Rev. B*, 70:214425, Dec 2004. URL http://link.aps.org/doi/10.1103/PhysRevB.70.214425.

G. Höhne, W. Hemminger, and H.-J. Flammersheim. *Differential Scanning Calorimetry.* Springer, 2003.

S. Jeppesen. *Magnetocaloric materials*. PhD thesis, University of Copenhagen, 2008.

S. Jeppesen, S. Linderoth, N. Pryds, L. T. Kuhn, and J. B. Jensen. Indirect measurement of the magnetocaloric effect using a novel differential scanning calorimeter with magnetic field. *Review of Scientific Instruments*, 79(8):–, 2008. URL `http://scitation.aip.org/content/aip/journal/rsi/79/8/10.1063/1.2957611`.

K. Koyama, T. Kanomata, T. Matsukawa, and K. Watanabe. Magnetic field effect on structural property of $MnFeP_{0.5}As_{0.5}$. *MATERIALS TRANSACTIONS*, 46 (8):1753–1756, 2005. ISSN 13459678, 13475320. doi: 10.2320/matertrans.46.1753.

M. A. Krasnosel'skii and A. V. Pokrovskii. *Systems with Hysteresis*. Nauka, 1983.

T. Krenke, E. Duman, M. Acet, E. F. Wassermann, X. Moya, L. Manosa, and A. Planes. Inverse magnetocaloric effect in ferromagnetic Ni-Mn-Sn alloys. *Nature Materials*, 4:450 – 454, 2005. ISSN 1476-1122. URL `http://dx.doi.org/10.1038/nmat1395`.

M. Küpferling, V. Basso, C. Sasso, L. Giudici, J. Moore, K. Morrison, and L. Cohen. Hall imaging of the history dependence of the magnetocaloric effect in $Gd_5Si_{2.09}Ge_{1.91}$. *Magnetics, IEEE Transactions on*, 44(11):3233–3236, 2008. ISSN 0018-9464.

G. J. Liu, J. R. Sun, J. Shen, B. Gao, H. W. Zhang, F. X. Hu, and B. G. Shen. Determination of the entropy changes in the compounds with a first-order magnetic transition. *Applied Physics Letters*, 90(3):–, 2007. URL `http://scitation.aip.org/content/aip/journal/apl/90/3/10.1063/1.2425033`.

J. Liu, T. Gottschall, K. P. Skokov, J. D. Moore, and O. Gutfleisch. Giant magnetocaloric effect driven by structural transitions. *Nature Materials*, 11: 620–626, 2012.

M. LoBue, V. Basso, C. P. Sasso, and G. Bertotti. Entropy and entropy production in magnetic systems with hysteresis. *Journal of Applied Physics*, 97(10):–, 2005. URL `http://scitation.aip.org/content/aip/journal/jap/97/10/10.1063/1.1852321`.

I. Mayergoyz. *Mathematical Models of Hysteresis and Their Applications*. Academic Press, 2003.

I. D. Mayergoyz. Hysteresis models from the mathematical and control theory points of view. *Journal of Applied Physics*, 57(8):3803–3805, 1985. URL `http://scitation.aip.org/content/aip/journal/jap/57/8/10.1063/1.334925`.

J. D. Moore, K. Morrison, K. G. Sandeman, M. Katter, and L. F. Cohen. Reducing extrinsic hysteresis in first-order La(Fe,Co,Si)$_{13}$ magnetocaloric systems. *Applied Physics Letters*, 95(25):–, 2009. URL http://scitation.aip.org/content/aip/journal/apl/95/25/10.1063/1.3276565.

S. Mørup. Mössbauer spectroscopy and its applications in materials science, 2004. Course notes.

S. Mørup and B. H. Rosendahl. Guide to experimental mössbauer spectroscopy, 2004. Course notes.

K. K. Nielsen, C. R. H. Bahl, H. N. Bez, R. Bjørk, L. von Moos, and D. Eriksen. Direct measurements of the magnetocaloric effect. In *6th IIF-IIR International Conference on Magnetic Refrigeration*, 2014.

H. Oesterreicher and F. T. Parker. Magnetic cooling near curie temperatures above 300 k. *Journal of Applied Physics*, 55(12):4334–4338, 1984. URL http://scitation.aip.org/content/aip/journal/jap/55/12/10.1063/1.333046.

A. O. Pecharsky, K. A. Gschneidner, and V. K. Pecharsky. The giant magnetocaloric effect of optimally prepared $Gd_5Si_2Ge_2$. *Journal of Applied Physics*, 93(8):4722–4728, 2003. URL http://scitation.aip.org/content/aip/journal/jap/93/8/10.1063/1.1558210.

V. Pecharsky and K. Gschneidner. Giant magnetocaloric effect in Gd5(Si2Ge2). *Physical Review Letters*, 78(23):4494–4497, 1997. ISSN 00319007, 10797114.

V. K. Pecharsky, K. A. Gschneidner, A. O. Pecharsky, and A. M. Tishin. Thermodynamics of the magnetocaloric effect. *Phys. Rev. B*, 64:144406, Sep 2001. doi: 10.1103/PhysRevB.64.144406. URL http://link.aps.org/doi/10.1103/PhysRevB.64.144406.

F. Preisach. Über die magnetische nachwirkung. *Zeitschrift für Physik*, 94(5-6):277–302, 1935. ISSN 0044-3328. URL http://dx.doi.org/10.1007/BF01349418.

P. Pruksanubal, A. Binner, and K. H. Gonschorek. Determination of distribution functions and parameters for the preisach hysteresis model. *17th International Zurich Symposium on Electromagnetic Compatibility, 2006*, pages 258 – 261, 2006. doi: 10.1109/EMCZUR.2006.214919.

F. Reif. *Fundamentals of Statistical and Thermal Physics*. McGraw-Hill, 1965.

K. Skokov, K.-H. Müller, J. Moore, J. Liu, A. Karpenkov, M. Krautz, and O. Gutfleisch. Influence of thermal hysteresis and field cycling on the magnetocaloric effect in $LaFe_{11.6}Si_{1.4}$. *Journal of Alloys and Compounds*, 552(0):310 – 317, 2013.

ISSN 0925-8388. URL http://www.sciencedirect.com/science/article/pii/S0925838812017586.

A. Smith, C. R. Bahl, R. Bjørk, K. Engelbrecht, K. K. Nielsen, and N. Pryds. Materials challenges for high performance magnetocaloric refrigeration devices. *Advanced Energy Materials*, 2(11):1288–1318, 2012. ISSN 1614-6840. URL http://dx.doi.org/10.1002/aenm.201200167.

E. C. Stoner and E. P. Wohlfarth. A mechanism of magnetic hysteresis in heterogeneous alloys. *Philosophical Transactions of the Royal Society of London. Series A, Mathematical and Physical Sciences*, 240(826):599–642, 1948. URL http://www.jstor.org/stable/91421.

O. Tegus, E. Brück, K. H. J. Buschow, and F. R. de Boer. Transition-metal-based magnetic refrigerants for room-temperature applications. *Nature*, 415:150–152, 2002.

L. Tocado, E. Palacios, and R. Burriel. Adiabatic measurement of the giant magnetocaloric effect in MnAs. *Journal of Thermal Analysis and Calorimetry*, 84:213–217, 2006. URL http://www.akademiai.com/content/N603K328472744K2.

L. Tocado, E. Palacios, and R. Burriel. Entropy determinations and magnetocaloric parameters in systems with first-order transitions: Study of MnAs. *Journal of Applied Physics*, 105(9):–, 2009. URL http://scitation.aip.org/content/aip/journal/jap/105/9/10.1063/1.3093880.

L. von Moos, C. Bahl, K. Nielsen, K. Engelbrecht, M. Küpferling, and V. Basso. A preisach approach to modeling partial phase transitions in the first order magnetocaloric material MnFe(P,As). *Physica B: Condensed Matter*, 435(0): 144 – 147, 2014a. ISSN 0921-4526. URL http://www.sciencedirect.com/science/article/pii/S0921452613006054.

L. von Moos, C. R. H. Bahl, K. K. Nielsen, and K. Engelbrecht. The influence of hysteresis on the determination of the magnetocaloric effect in $Gd_5Si_2Ge_2$. *Journal of Physics D: Applied Physics*, In print, 2014b.

L. von Moos, C. R. H. Bahl, K. K. Nielsen, and K. Engelbrecht. Quantification of the effect of hysteresis on the magnetocaloric effect in first order $Gd_5Si_2Ge_2$. In *6th IIF-IIR International Conference on Magnetic Refrigeration*, 2014c.

L. von Moos, K. Nielsen, K. Engelbrecht, and C. Bahl. Experimental investigation of the effect of thermal hysteresis in first order material MnFe(P,As) applied in an AMR device. *International Journal of Refrigeration*, 37(-):303 – 306, 2014d. ISSN 0140-7007. URL http://www.sciencedirect.com/science/article/pii/S0140700713001163.

H. Wada and Y. Tanabe. Giant magnetocaloric effect of $MnAs_{1-x}Sb_x$. *Applied Physics Letters*, 79(20):3302–3304, 2001. URL http://scitation.aip.org/content/aip/journal/apl/79/20/10.1063/1.1419048.

G. Wang. *Magnetic and calorimetric study of the magnetocaloric effect in intermetallics exhibiting first-order magnetostructural transitions*. PhD thesis, Universidad Zaragoza, 2012.

G. K. White and S. J. Collocott. Heat capacity of reference materials: Cu and W. *Journal of Physical and Chemical Reference Data*, 13(4):1251–1257, 1984. URL http://scitation.aip.org/content/aip/journal/jpcrd/13/4/10.1063/1.555728.

L. Zang, D. Vanasten, F. Seeler, B. Reesink, and E. Brück. A fast method to evaluate magnetocaloric effect in first-order MnFe(P,As) compounds, 4. In *International Conference on Magnetic Refrigeration at Room Temperature*, pages 65–71, 2010.